

ISSN 1980-9743

Soils and Rocks

An International Journal of Geotechnical
and Geoenvironmental Engineering

AB
—
MS



Special Issue: Unsaturated Soils
Guest editors:
G.F.N. Gitirana Jr. & D.G. Fredlund

Volume 39, N. 1
January-April 2016

**Soils and Rocks is an International Journal of Geotechnical and
Geoenvironmental Engineering published by**

**ABMS - Brazilian Association for Soil Mechanics and Geotechnical Engineering
Av. Queiroz Filho, 1700 - Torre A Sky, Sala 106 - Vila Hamburguesa
05319-000, São Paulo, SP
Brazil**

**SPG - Portuguese Geotechnical Society
LNEC, Avenida do Brasil, 101
1700-066 Lisboa
Portugal**



Issue Date: April 2016

Issue: 400 copies and 800 online-distributed copies

Manuscript Submission: For review criteria and manuscript submission information, see *Instructions for Authors at the end.*

Disclaimer: The opinions and statements published in this journal are solely the author's and not necessarily reflect the views or opinions of the publishers (ABMS and SPG). The publishers do not accept any liability arising in any way from the opinions, statements and use of the information presented.

Copyright: Authors and ABMS-Brazilian Society for Soil Mechanics and Geotechnical Engineering

SOILS and ROCKS

An International Journal of Geotechnical and Geoenvironmental Engineering

Editor Waldemar Coelho Hachich - University of São Paulo, Brazil

Co-editor Manuel Matos Fernandes - University of Porto, Portugal

Special Issue: Unsaturated Soils

Guest-editors: G.F.N. Gitirana Jr. - Universidade Federal de Goiás

D.G. Fredlund - Golder Associates Ltd.

Executive Board

Alberto Sayão

Pontifical Catholic University of Rio de Janeiro, Brazil

Jorge Almeida e Sousa

University of Coimbra, Portugal

Ian Schumann Martins

Federal University of Rio de Janeiro, Brazil

João Maranhã

LNEC, Portugal

Associate Editors

H. Einstein

MIT, USA

John A. Hudson

Imperial College, UK

Kenji Ishihara

University of Tokyo, Japan

Michele Jamiolkowski

Studio Geotecnico Italiano, Italy

Willy A. Lacerda

COPPE/UFRJ, Brazil

E. Maranhã das Neves

Lisbon Technical University, Portugal

Nielen van der Merve

University of Pretoria, South Africa

Paul Marinou

NTUA, Greece

James K. Mitchell

Virginia Tech., USA

Lars Persson

SGU, Sweden

Harry G. Poulos

University of Sidney, Australia

Niek Rengers

ITC, The Netherlands

Fumio Tatsuoka

Tokyo University of Science, Japan

Luiuz González de Vallejo

UCM, Spain

Roger Frank

ENPC-Cermes, France

Editorial Board Members

Roberto F. Azevedo

Federal University of Viçosa, Brazil

Milton Kanji

University of São Paulo, Brazil

Antonio M.S. Oliveira

University of Guarulhos, Brazil

Omar Y. Bitar

IPT, Brazil

Lázaro V. Zuquette

University of São Paulo, Brazil

Fabio Taioli

University of São Paulo, Brazil

Tarcisio Celestino

University of São Paulo-SC, Brazil

Roberto Q. Coutinho

Federal Univ. of Pernambuco, Brazil

Nilo C. Consoli

Federal Univ. Rio Grande do Sul, Brazil

Sandro S. Sandroni

Consultant, Brazil

Sérgio A.B. Fontoura

Pontifical Catholic University, Brazil

Ennio M. Palmeira

University of Brasília, Brazil

Luciano Décourt

Consultant, Brazil

Faiçal Massad

University of São Paulo, Brazil

Marcus Pacheco

University of the State of Rio de Janeiro, Brazil

Paulo Maia

University of Northern Rio de Janeiro, Brazil

Renato Cunha

University of Brasília, Brazil

Orencio Monje Vilar

University of São Paulo at São Carlos, Brazil

Maria Eugenia Boscov

University of São Paulo, Brazil

Eda Freitas de Quadros

BGTECH, Brazil

Tácio de Campos

Pontifical Catholic University of Rio de Janeiro, Brazil

Richard J. Bathurst

Royal Military College of Canada

Robert Mair

University of Cambridge, UK

Serge Leroueil

University of Laval, Canada

Mario Manassero

Politécnico di Torino, Italy

Luis Valenzuela

Consultant, Chile

Jorge G. Zornberg

University of Texas/Austin, USA

Andrew Whittle

MIT, USA

Pierre Bérest

LCPC, France

Peter Kaiser

Laurentian University, Canada

He Manchao

CUMT, China

Teruo Nakai

Nagoya Inst. Technology, Japan

Claudio Olalla

CEDEX, Spain

Frederick Baynes

Baynes Geologic Ltd., Australia

R. Kerry Rowe

Queen's University, Canada

R. Jonathan Fannin

University of British Columbia, Canada

Laura Caldeira

LNEC, Portugal

António S. Cardoso

University of Porto, Portugal

José D. Rodrigues

Consultant, Portugal

António G. Coelho

Consultant, Portugal

Luís R. Sousa

University of Porto, Portugal

Rui M. Correia

LNEC, Portugal

João Marcelino

LNEC, Portugal

António C. Mineiro

University of Lisbon, Portugal

António P. Cunha

LNEC, Portugal New

António G. Correia

University of Minho, Portugal

Carlos D. Gama

Lisbon Technical University, Portugal

José V. Lemos

LNEC, Portugal

Nuno Grossmann

LNEC, Portugal

Luís L. Lemos

University of Coimbra, Portugal

Ricardo Oliveira

COBA, Portugal

“Ad hoc” Reviewers (2014-2015)

Ana Cristina Sieira <i>UERJ, Brazil</i>	Edmundo Rogério Esquível <i>USP-S. Carlos, Brazil</i>	Luís Valenzuela <i>Arcadis, Chile</i>
André Luís Brasil Cavalcante <i>UnB, Brazil</i>	Eurípedes Vargas <i>PUC-RJ, Brazil</i>	Marc Vinches <i>Ecole des Mines d'Alès, France</i>
Antonio Airton Bortolucci <i>USP-S. Carlos, Brazil</i>	Fernando Antonio Medeiros Marinho <i>USP-Poli, Brazil</i>	Marcia Maria dos Anjos Mascarenhas <i>UFG, Brazil</i>
Arsenio Negro Jr. <i>Bureau, Brazil</i>	Fernando Olavo Franciss <i>Progeo, Brazil</i>	Maria Cláudia Barbosa <i>UFRJ, Brazil</i>
Bernadete Ragoni Danziger <i>UERJ, Brazil</i>	Francisco Chagas da Silva Filho <i>UFC, Brazil</i>	Maurício Ehrlich <i>UFRJ, Brazil</i>
Carlos Medeiros Silva <i>Embre, Brazil</i>	Francisco de Rezende Lopes <i>UFRJ, Brazil</i>	Nelson Aoki <i>USP-S. Carlos, Brazil</i>
Claudio Fernando Mahler <i>UFRJ, Brazil</i>	Frederico Falconi <i>ZF, Brazil</i>	Paulo Scarano Hemi <i>ITA, Brazil</i>
Claudio Michael Wolle <i>USP-Poli, Brazil</i>	Isabel Lopes <i>IST, Portugal</i>	Renato Pinto da Cunha <i>UnB, Brazil</i>
David Martins Geraldo Taborda <i>Imperial College, UK</i>	João Manuel Marcelino Mateus da Silva <i>LNEC, Portugal</i>	Sussumu Niyama <i>Tecnum, Brazil</i>
Denise Gerscovich <i>UERJ, Brazil</i>	José Camapum de Carvalho <i>UnB, Brazil</i>	Tácio Campos <i>PUC-RJ, Brazil</i>
Eda Quadros <i>BGTECH, Brazil</i>	José Renato Baptista de Lima <i>USP-Poli</i>	Tiago Miranda <i>Univ. do Minho, Portugal</i>
Edgar Odebrecht <i>Geoforma, Brazil</i>	Kátia Bicalho <i>UFES, Brazil</i>	Waldyr Lopes de Oliveira Filho <i>UFOP, Brazil</i>
Edgard Poiate <i>Petrobrás, Brazil</i>	Leonardo Becker <i>UFRJ, Brazil</i>	

Soils and Rocks publishes papers in English in the broad fields of Geotechnical Engineering, Engineering Geology and Geo-environmental Engineering. The Journal is published in April, August and December. Subscription price is US\$ 90.00 per year. The journal, with the name “Solos e Rochas”, was first published in 1978 by the Graduate School of Engineering, Federal University of Rio de Janeiro (COPPE-UFRJ). In 1980 it became the official magazine of the Brazilian Association for Soil Mechanics and Geotechnical Engineering (ABMS), acquiring the national character that had been the intention of its founders. In 1986 it also became the official Journal of the Brazilian Association for Engineering Geology and the Environment (ABGE) and in 1999 became the Latin American Geotechnical Journal, following the support of Latin-American representatives gathered for the Pan-American Conference of Guadalajara (1996). In 2007 the journal acquired the status of an international journal under the name of *Soils and Rocks*, published by the Brazilian Association for Soil Mechanics and Geotechnical Engineering (ABMS), Brazilian Association for Engineering Geology and the Environment (ABGE) and Portuguese Geotechnical Society (SPG). In 2010, ABGE decided to publish its own journal and left the partnership.

Soils and Rocks

1978,	1 (1, 2)
1979,	1 (3), 2 (1,2)
1980-1983,	3-6 (1, 2, 3)
1984,	7 (single number)
1985-1987,	8-10 (1, 2, 3)
1988-1990,	11-13 (single number)
1991-1992,	14-15 (1, 2)
1993,	16 (1, 2, 3, 4)
1994-2010,	17-33 (1, 2, 3)
2011,	34 (1, 2, 3, 4)
2012-2015,	35-38 (1, 2, 3)
2016,	39 (1,

ISSN 1980-9743

CDU 624.131.1

SOILS and ROCKS

An International Journal of Geotechnical and Geoenvironmental Engineering

Publication of**ABMS - Brazilian Association for Soil Mechanics and Geotechnical Engineering****SPG - Portuguese Geotechnical Society****Volume 39, N. 1, January-April 2015****Table of Contents***ARTICLES*

<i>State Variables in Saturated-Unsaturated Soil Mechanics</i> D.G. Fredlund	3
<i>Numerical and Experimental Analysis of Horizontal Stress Changes and Soil Collapse During Chemical Dissolution in a Modified Oedometer Cell</i> C. Lins, N. Silva, L. Guimarães, A. Lima, I. Gomes	19
<i>Alternative Method for Analysing Hydromechanical Behaviour of Unsaturated Soils</i> M.M.A. Mascarenha, M.P. Cordão Neto, M.T.M.G. Silva	29
<i>Recent Developments and Limitations of the SFG Model</i> D. Sheng	41
<i>Effectiveness of Capillary Barrier and Vegetative Slope Covers in Maintaining Soil Suction</i> H. Rahardjo, S. Krisnanto, E.C. Leong	51
<i>Influence of Poisson's Ratio on the Stress vs. Settlement Behavior of Shallow Foundations in Unsaturated Fine-Grained Soils</i> W.T. Oh, S.K. Vanapalli	71
<i>Statistical Assessment of Hydraulic Properties of Unsaturated Soils</i> G.F.N. Gitirana Jr., D.G. Fredlund	81
<i>Numerical Modeling of Unsaturated Soils Problems</i> M.D. Fredlund	97

Articles

Soils and Rocks
v. 39, n. 1

State Variables in Saturated-Unsaturated Soil Mechanics

D.G. Fredlund

Abstract. The description of the stress state in soils is the foundational point around which an applied science should be built for engineering practice. The stress state description has proven to be pivotal for saturated soil mechanics and the same should be true for unsaturated soil mechanics. Continuum mechanics sets forth a series of principles upon which a common science base can be developed for a wide range of materials. The principles require that there be a clear distinction between state variables and constitutive relations. Constitutive relations relate state variables and incorporate material properties. State variables, on the other hand, are independent of the material properties. It has been possible to maintain a clear distinction between variables of state and constitutive relations in the development of saturated soil mechanics and the same should be true for unsaturated soil mechanics. This paper presents a description of the source and character of stress state variables for saturated and unsaturated soils. The descriptions are consistent with the principles of multiphase continuum mechanics and provide an understanding of the source and importance of stress state variables.

Keywords: state variables, soil suction, constitutive relations, continuum mechanics.

1. Introduction

Karl Terzaghi (1883-1963) is recognized as the “Father of Soil Mechanics”. He defined the term “effective stress” as the variable around which the physical behaviour of a saturated soil can be described. Effective stress was defined as $(\sigma - u_w)$ where σ was total stress and u_w was the pore-water pressure. The recognition of effective stress as the state variable controlling the equilibrium of the soil structure of a saturated soil elevated saturated soil mechanics from an art to a science. Effective stress provided a means whereby the physical behaviour of a saturated soil could be described. The effective stress variable was independent of the properties of the soil. The effective stress variable has become the rallying point and the unifying variable for understanding volume change, distortion, shear strength, seepage and other physical process in saturated soils. The use of the effective stress variable in saturated soil mechanics was clearly illustrated for various soil mechanics problems in Terzaghi’s first textbook, “Theoretical Soil Mechanics” published in 1943.

This paper revisits issues relevant to the description of the stress state of particulate materials; in particular, saturated and unsaturated soils. The fundamental basis for use of stress state variables in soil mechanics is explained. The fundamental basis for the use of effective stress for saturated soils is presented first followed by a similar description of the stress state variables for unsaturated soils. The emphasis is on state variables associated with stresses; however, it is recognized that there are also other state variables such as those required for mapping deformations and distortions of particulate, multiphase systems. These are referred to as deformation state variables but their description is outside the scope of this paper.

2. Terzaghi’s Description of Effective Stress

In 1936, Terzaghi described and justified the use of the effective stress variable for saturated soils as follows. Terzaghi (1936) wrote, “The stresses in any point of a section through a mass of soil can be computed from the total principal stresses, $\sigma_1, \sigma_2, \sigma_3$, which act at this point. If the voids of the soil are filled with water under a stress, u_w , the total principal stresses consist of two parts. One part, u_w , acts in the water and in the solid in every direction with equal intensity (emphasis added). It is called the neutral (or pore-water) pressure. The balance $\sigma_1' = \sigma_1 - u_w, \sigma_2' = \sigma_2 - u_w, \sigma_3' = \sigma_3 - u_w$ represent an excess over the neutral stress, u_w , and has its seat exclusively in the solid phase of the soil (emphasis added). All the measurable effects of a change in shearing resistance are exclusively due to changes in the effective stress, $\sigma_1', \sigma_2', \sigma_3'$ ”

The above paragraph sets forth the meaning of the effective stress variable. Effective stress is the difference between the total stresses and pore-water pressure in three orthogonal directions. The three principal directions arise from the Cartesian coordinate system associated with three-dimensional space. Stresses in three directions can be combined to form a stress tensor that defines the stress state at a point in saturated soil. The stress tensor with components, $(\sigma_1 - u_w), (\sigma_2 - u_w),$ and $(\sigma_3 - u_w),$ form the variables that control the equilibrium of the soil structure. The words “soil structure” is used in the sense of referring to the arrangement of the soil solids. The effective stress variables are associated with equilibrium conditions and can therefore be used to describe the behaviour of the soil structure of a saturated soil. Stated another way, the effective stress variables can be used to describe changes from the equilibrium state in a saturated soil.

There are two statements in Terzaghi's description of effective stress that are noteworthy because of their consistency with the principles of multiphase continuum mechanics. The first statement notes that the water pressure "acts in the water and in the solid in every direction with equal intensity". This statement is consistent with the concept of superposition of equilibrium stress fields in multiphase continuum mechanics (Fung, 1965). The second statement notes that the difference between the total stress and pore-water pressure "has its seat exclusively in the solid phase of the soil". In other words, the effective stress variable is linked to the soil structure (or the arrangement of soil solids). It is also noteworthy that while these statements are consistent with continuum mechanics principles, Terzaghi wrote these statements when continuum mechanics was still in a formative stage.

Terzaghi's statement describing effective stress remains consistent with the principles of multiphase continuum mechanics attesting to the wisdom of his original description.

3. What is Effective Stress?

- History has shown that even though the original definition of effective stress was presented with clarity, the term "effective stress" has still suffered considerable misunderstanding. As a teacher of soil mechanics, students have sometimes inquired of the author as to the physical meaning and source of "effective stress". Effective stress has been highly esteemed and almost treated as a sacrament within geotechnical engineering but the questions remains, "What is the source and physical meaning of effective stress?" Effective stress has been described in numerous ways; some descriptions being inaccurate while others are reasonable and acceptable. Listed below are some of the descriptive terms associated with effective stress along with a brief description of how each term is used.
- 1) *Is effective stress an equation?* It can be argued that "effective stress" is an equation because it has an equal sign. However, it can also be argued the effective stress symbol is simply the difference between two variables; that difference being called effective stress. The dictionary defined an equation as "a statement that the values of two mathematical expressions are equal" (Wikipedia, 2013). The use of the word *equation* for the effective stress variable may have led geotechnical engineers to think there is additional physical meaning behind the use of the term "effective stress". The use of the word, "*equation*" may have fuelled the search for refinements to the equation for both saturated and unsaturated soils.
- 2) *Is effective stress a law?* This question could also be presented in a slightly different manner as, "Should *effective stress* strictly be referred to as a physical law?" And if *effective stress* is a law, then what is the physical process behind the law. Maybe the word *law* once again

elevates the term *effective stress* to a perceived level that is not justifiable. Or is the only law involved behind the term *effective stress*, the summation or equilibrium of forces associated with Newtonian mechanics?

- 3) *Is effective stress a constitutive equation?* The word *constitutive* implies the incorporation of one or more soil properties. Consequently, it would seem clear to come to the conclusion that effective stress should not be referred to as a constitutive equation. However, the history of soil mechanics shows that there have been attempts to bring soil properties into the description of effective stress. It is important to remember that variables associated with *state* cannot be constitutive in character.
- 4) *Is effective stress a concept?* The concept could be stated as follows, "If one changes effective stress, it should be anticipated that something might happen to the equilibrium of the soil structure". For example, it is anticipated that there may be a change in volume of the saturated soil. On the converse, if effective stress is not changed there should not be a change in volume. The linkage between changes in stress state and changes in equilibrium of the soil structure can be referred to as the effective stress concept. Stated another way, the equilibrium of the soil structure is perturbed when 'effective stresses' in a saturated soil are changed.
- 5) *Is effective stress a principle?* The principle of effective stress could also be described in a manner similar to that used for the concept of effective stress. The principle of effective stress would state, "If effective stresses are changed, something should happen to the equilibrium of the soil structure and if effective stresses are not changed, there should be no change in the equilibrium of the soil structure of a saturated soil". Changes in the saturated soil structure may be small but equilibrium conditions have been perturbed when the stress state is changed.
- 6) *Is effective stress a stress state variable?* State variables should be defined independent of material properties (*i.e.*, non-material based variables). In this sense "effective stress" qualifies as a stress state variable. It can also be reasoned that effective stress applies in each of the Cartesian coordinate directions since equilibrium conditions must be satisfied in all three orthogonal directions.
- 7) *Is effective stress a tensor?* A tensor is a 3 by 3 matrix which arises out of consideration of three orthogonal directions. The three-dimensions define space. Effective stress can also be visualized as having three principal directions where there are only normal stresses and no shear stresses. The stress tensor contains effective stress variables along the trace and as such, effective stress has three spatial components.
- 8) *Is effective stress only for saturated soils?* The term effective stress was initially defined solely for saturated soils. As shown later in this paper, effective stress does not qualify as an adequate term to describe the stress

state of an unsaturated soil. However, the principles of continuum mechanics allow for the use of more than one tensor (or combination of state variables) for the description of stress state.

The following responses to the above-mentioned questions should apply to the use of the words, “effective stress”, if the strict definitions from continuum mechanics are applied.

- 1) *Is effective stress an equation?* No
- 2) *Is effective stress a law?* No
- 3) *Is effective stress a constitutive equation?* No
- 4) *Is effective stress a concept?* Yes
- 5) *Is effective stress a principle?* Yes
- 6) *Is effective stress a stress state variable?* Yes
- 7) *Is effective stress a tensor?* Yes
- 8) *Is effective stress only for saturated soils?* Yes

There may be some room for debate regarding the usage of some of the effective stress terms; however, as far as possible it would appear to be best to remain consistent with continuum mechanics’ terminology and definitions.

The question might rightfully be asked, “Where does effective stress come from and does it have a physical basis?” There would appear to be a sound continuum mechanics basis for the “effective stress” variable for saturated soil but that will be presented later in the paper. The same continuum mechanics principles and definitions can also be applied to unsaturated soils and the result is the realization that more than one independent state variable is required to describe the stress state of an unsaturated soil.

4. Definition of Key Technical Terms from Continuum Mechanics

There are several technical terms and definitions that are well accepted within continuum mechanics that need to be described in order to understand the characteristics of state variables (Fung, 1965; 1977). Continuum mechanics has attempted to define a consistent set of terms that can be applied to all types of material behaviour. The terminology applies to single and multiphase particulate media. It applies to solids as well as fluids. It applies to elastic behaviour, plastic behaviour and viscous behaviour. The key variables that need to be defined are as follows:

State Variables: Are variables independent of material properties required for the characterization of a system (*e.g.*, pressure, temperature, volume, time, etc.). These variables are defined independent of the physical properties of the material.

Stress State Variables: Are independent of material properties required for the characterization of force (or stress) equilibrium conditions.

Deformation State Variables: Are independent of material properties variables required for the description of deformations, distortions and deviations from an initial state.

Constitutive Relations: Single-valued equations expressing the relationship between state variables. Constitutive relations incorporate the physical properties of a material corresponding to a particular process to be simulated.

5. The Search for an Equation

The original definition of effective stress for saturated soil behaviour has been the single most important concept behind the development of saturated soil mechanics. While the original description of effective stress by Terzaghi (1936) is clear, there is a subtle variation of the definition that has been included in virtually every soil mechanics textbook. The variation arises out of an attempt to describe the meaning of effective stress. The variations are often put in the context of a “refinement” to the effective stress equation; however, the revisions to the effective stress equations would appear to constitute a step away from the concepts associated with continuum mechanics and an accurate application of soil mechanics. One of the suggested revisions to the effective stress equation involved the use of a wavy plane passed through the points of contact in a saturated particulate medium.

Most soil mechanics’ textbooks have a figure that shows a particulate media with a wavy plane passed between the contact points between particles (Fig. 1). The figures common to most soil mechanics textbooks portray what is referred to as the “wavy plane” concept. A portion of the wavy plane is shown to pass through the contact points between particles while the remainder of the plane passes through water in the voids. The common explanations suggest that static equilibrium can be applied across the wavy plane over a unit area. This figure is then treated as a free-body diagram and forces are summed in the vertical direction across the wavy plane.

The analysis usually goes on to justify the form of the effective stress equation and suggests that an area correction should be applied to the effective stress equation to make it more refined and accurate. It is also often suggested that the area correction in the effective stress equation is small and its usage is not necessary. It is important to fur-

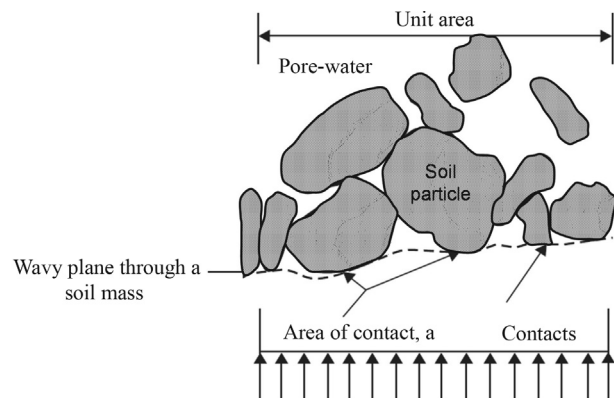


Figure 1 - Illustration of the use of the wavy plane concept.

ther investigate the wavy plane analysis to ascertain whether the wavy plane analysis is fundamentally flawed.

There appears to be a fundamental flaw with the above-mentioned analysis in the sense that a wavy plane passed through a soil mass does not represent a legitimate free-body diagram (Fung, 1977). Even the use of a linear plane surface passed through a continuum does not represent a legitimate free-body diagram. In order to qualify as an acceptable free-body diagram in static mechanics, the free-body must have spatial variation (Fung, 1977). If a wavy plane does not constitute an acceptable free-body diagram then any subsequent mathematical manipulations that may be undertaken are unacceptable.

6. Steps Taken in the Wavy Plane Analysis

The mathematical steps that are adhered to in the wavy plane analysis are presented in detail in order to examine aspects of the analysis that are unacceptable. The examination of the wavy plane analysis is important because of the significant impact that this analysis has had on attempting to understand and define the stress state for unsaturated soils.

Forces are summed in the vertical direction, over a unit area with the understanding that the sum of the forces of the parts must equal the total force (Fig. 1).

$$a \sigma_i + (1 - a) u_w = \sigma \quad (1)$$

where a = area of contact, σ_i = inter-particle (or inter-granular) stress, u_w = pore-water pressure, and σ = total stress,

Multiplying out the terms in Eq. 1 gives,

$$a \sigma_i + u_w - a u_w = \sigma \quad (2)$$

The term effective stress is assumed to be equivalent to the inter-granular stress multiplied by the area of contact giving,

$$a \sigma_i = \sigma' \quad (3)$$

The “ a ” variable is a ratio of areas but it is also a material property. The above-mentioned conversion has changed a force to a stress. Rearranging the above equation gives the effective stress equation with an area of contact term.

$$\sigma' = (\sigma - u_w) + a u_w \quad (4)$$

The effective stress equation can be written as follows provided it is assumed that the area of contact is small.

$$\sigma' = (\sigma - u_w) \quad (5)$$

At this point it is important to re-visit the above-mentioned steps and identify the shortcomings of such an analysis.

7. Inherent Limitations Associated with the Wavy Plane Analysis

There are a number of inherent limitations associated with the wavy plane analysis. The first question that might be asked is, “Why is a (wavy) plane not an acceptable free-body diagram?” In response to this question, let us consider the simple case of a ladder leaning against a wall as shown in Fig. 2.

The central diagram showing the forces on the leaning ladder is an acceptable free-body diagram. However, it is not possible to draw a free-body diagram of the plane where the ladder touches the wall. It is possible to state that “action” is equal to “reaction” of the point where the ladder touches the wall but is not possible to apply Newton’s second law of statics. It is important to recall Newton’s three laws of statics and the reason why an independent law of “action” is equal to “reaction” was needed.

First Law: Bodies in motion will remain in motion unless it is acted upon by an external force.

Second Law: The acceleration of an object is dependent upon the net force acting upon the object and the mass of the object. Consequently, when an object is in static equilibrium the summation of forces and moments are equal to zero.

Third Law: For every action there must be an equal and opposite reaction.

Newton’s third law can be applied to stresses on a plane passed through an object or when one object interacts with another object. Newton’s third law constitutes a statement of equivalence when applied to a plane. It is not possible to use the third law as a basis for a static equilibrium proof. Rather, it is simply possible to let one condition be equal to another condition. The wavy plane passed through a multiphase system such as soil cannot be used as a static equilibrium proof (*i.e.*, Newton’s second law), because there is no spatial variation of forces.

The second question to address is, “Why is a wavy plane unacceptable?” A wavy plane builds bias into the analysis. Using a wavy plane goes contrary to the basic definition of a continuum. Any plane passed through a multiphase material must be unbiased (Truesdell, 1966; Fung, 1969; 1977). The definition of a continuum requires that the porosity of a multiphase material must be equal with re-

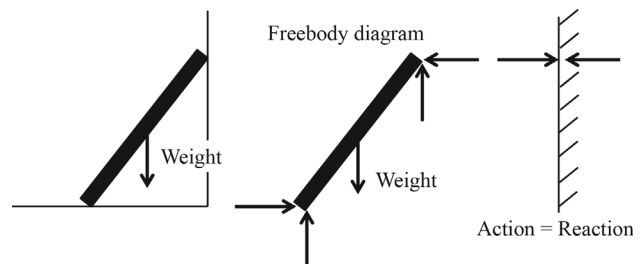


Figure 2 - Free-body diagram of a ladder leaning against a wall.

spect to volume porosity (of a representative elemental volume, REV), and area porosity (*i.e.*, the sides of the REV). The definition of a continuum is described in terms of the density function with respect to each phase of a multiphase system being constant. A wavy plane creates a problem in that it builds bias into the analysis and contradicts the definition of a continuum.

The definition of a continuum requires that the sum of the components of a multiphase system must be the same on a volume and area basis. A saturated soil consists of solids and water with the sum of the parts equal to the whole, both in terms of volume and area. Therefore, the plane cannot be biased.

$$V_s + V_w = V_r \text{ (by volume)} \quad (6)$$

$$a_s + n_w = 1 \text{ (by area)} \quad (7)$$

where V_s = volume of solids, V_w = volume of water, a_s = area of solids, and n_w = porosity.

The equilibrium of two-dimensional (or three-dimensional) stress fields can be used to verify the acceptability of the effective stress variable for saturated soils. The multi-dimensional force equilibrium analysis illustrates that there is no need to apply an area of contact correction to the effective stress variable.

There have also been other attempts to refine Terzaghi's original effective stress variable; however, in each case, a soil property has been incorporated into the stress variable. In so doing the stress variable has become "constitutive" in nature and no longer rigorously qualifies as a state variable.

8. Acceptable Stress Fields for the Verification of the Stress State of Multiphase Systems

There are two types of stress fields that can be placed on a representative elemental volume, REV, of a continuum; namely, i) body forces per unit volume, and ii) surface tractions. Each phase of a multiphase system has an independent stress field. The stress fields can be viewed as being superimposed when several phases are involved (Truesdell, 1966). The continuum mechanics representation of stress fields for a one phase solid will first be presented followed by consideration of a saturated soil (*i.e.*, a two phase system). And finally, consideration will be given to the stress fields for an unsaturated soil system.

9. Representation of Stress Fields for a One Phase Continuum

A stress field acting in a particular direction can be represented mathematically as a linearly varying field across a REV as shown in Fig. 3 (Truesdell, 1966). When forces are summed in the vertical direction, equilibrium is maintained since the variation of the stress field in the y -direction is taken into consideration. It can also be seen that a

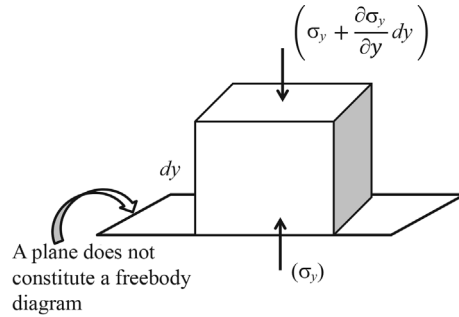


Figure 3 - Illustration of a multi-dimensional free-body diagram showing a stress field.

plane through the bottom surface of the REV cannot be used to satisfy equilibrium considerations. The same equilibrium analysis can be extended to the three coordinate directions as shown in Fig. 4.

Equilibrium equations for a one phase solid can be written by summing forces in each of the Cartesian coordinate directions (Fung, 1969; 1977). The equilibrium equations for the x -, y -, and z -directions, respectively, are:

$$\left(\frac{\partial \sigma_x}{\partial x} + \frac{\partial \tau_{yx}}{\partial y} + \frac{\partial \tau_{zx}}{\partial z} \right) dx dy dz = 0 \quad (8)$$

$$\left(\frac{\partial \tau_{xy}}{\partial x} + \frac{\partial \sigma_y}{\partial y} + \frac{\partial \tau_{zy}}{\partial z} + \rho g \right) dx dy dz = 0 \quad (9)$$

$$\left(\frac{\partial \tau_{xz}}{\partial x} + \frac{\partial \tau_{yz}}{\partial y} + \frac{\partial \sigma_z}{\partial z} \right) dx dy dz = 0 \quad (10)$$

where σ_x = total normal stress in the x -direction, σ_y = total normal stress in the y -direction, σ_z = total normal stress in the z -direction, τ_{yx} = shear stress on the y -plane in the x -direction, τ_{xy} = shear stress on the x -plane in the y -direction, τ_{zy} = shear stress on the z -plane in the y -direction, τ_{yz} = shear stress on the y -plane in the z -direction, τ_{zx} = shear stress on the x -plane in the z -direction, and τ_{xz} = shear stress on the z -plane in the x -direction.

The surface tractions found in the equilibrium equation can be extracted to form a 3 by 3 matrix, (*i.e.*, a tensor) as shown in Eq. 11. The tensor represents the stress state at a point in any one phase solid.

$$\begin{bmatrix} \sigma_x & \tau_{yx} & \tau_{zx} \\ \tau_{xy} & \sigma_y & \tau_{zy} \\ \tau_{xz} & \tau_{yz} & \sigma_z \end{bmatrix} \quad (11)$$

The stress tensor can also be plotted on a cube as a representation of the stress state in the one phase solid (Fig. 5). A one phase solid could consist of any material ranging from steel to cheese. The form of the stress state variables is dictated largely by the number of phases involved.

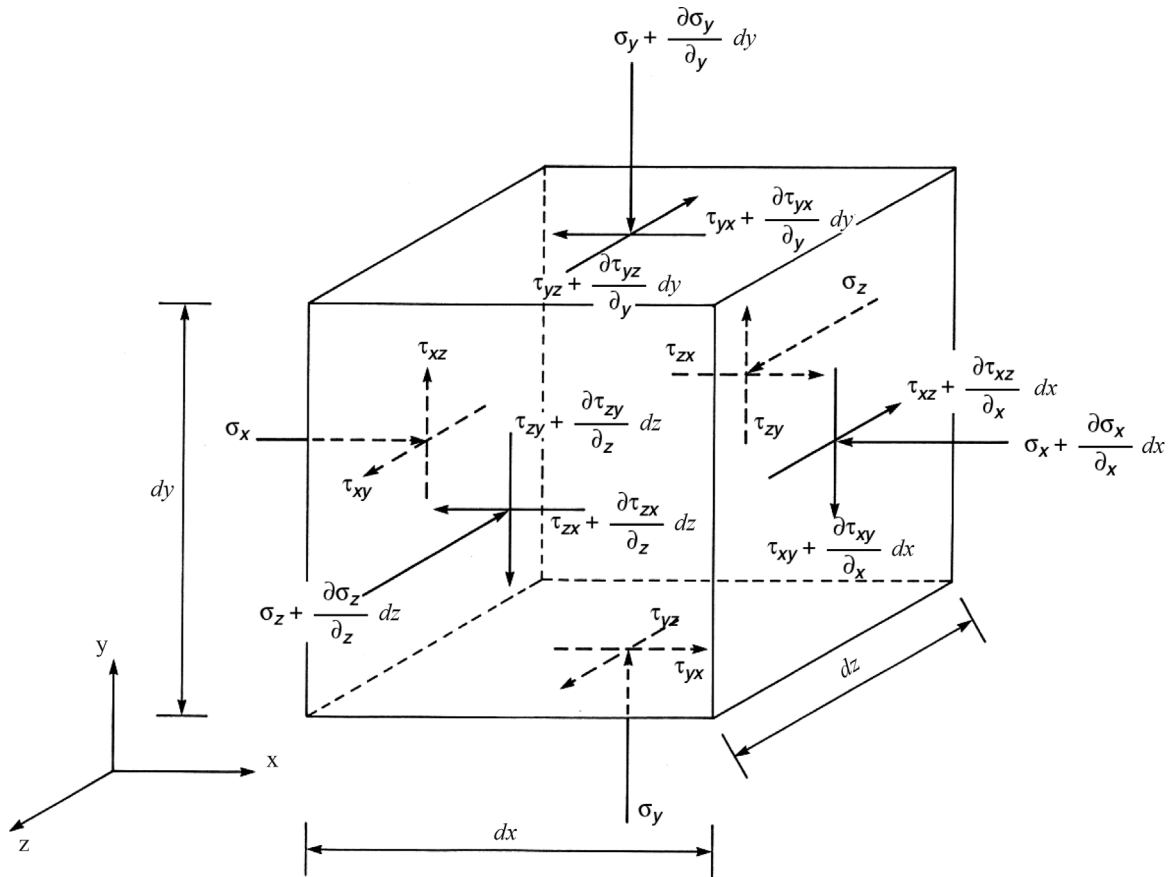


Figure 4 - Equilibrium stress fields in three Cartesian coordinate directions for a one phase solid.

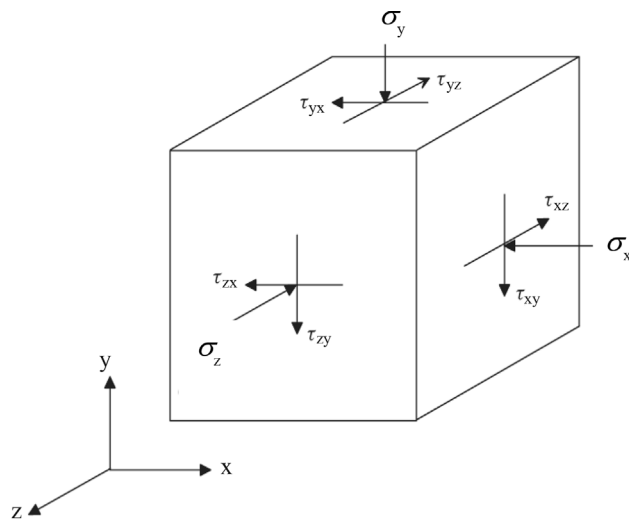


Figure 5 - Stress state at a point in a one phase solid.

10. Stress Fields for the Verification of Effective Stress for a Saturated Soil

A stress field exists for each phase of a multiphase system. A saturated soil has a stress field associated with the water phase. Terzaghi (1936) clearly explained that the water

phase stress field acts in the water and through the solid phase. The solid phase consisting of an arrangement of particles also has an independent stress field. In fact, it is the stress field associated with the soil solids that represents the equilibrium of soil structure. Unfortunately, the stress field associated with the soil structure cannot be directly measured. On the other hand, it is possible to write a stress field that represents the summation of all the individual stress fields. This stress field can be referred to as the overall stress field or the total stress field. The total stress field has the same form as the stress field equation written for a one phase solid. The summation of the superimposed coincident, equilibrium stress fields associated for each phase of a multiphase system form the overall equilibrium stress field.

The stress field equation (Eq. 12), for the water phase is illustrated by the free-body diagram shown in Fig. 6 for the y-direction. The free-body diagram for the water phase must also have two added body forces. One body force is for the gravity force associated with water, $n_w \rho_w g$, while the other body force is the seepage force, F_{sy}^w , which must be taken into consideration when the water phase is separated from the soil solids phase.

$$\frac{n_w \partial u_w}{\partial y} + n_w \rho_w g + F_{sy}^w = 0 \tag{12}$$

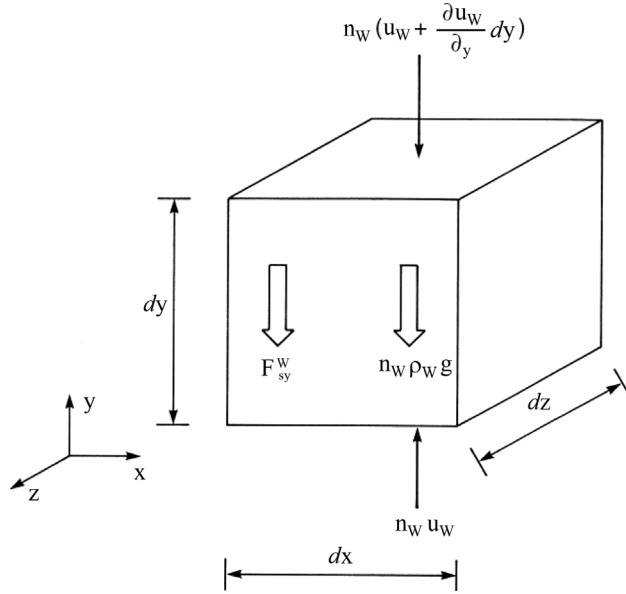


Figure 6 - Equilibrium stress field associate with the water phase of a saturated soil.

Equilibrium equations for the x - and z -directions can be written in a similar manner.

Since the sum of the individual stress fields must be equal to the overall stress field, it is possible to write the equilibrium stress field for the soil solids phase as the difference between the overall stress field and the water phase stress field. These equations are shown for the x -, y -, and z -directions, respectively, are shown in Eqs. 13, 14, and 15.

$$\frac{\partial(\sigma_x - u_w)}{\partial x} + \frac{\partial\tau_{yx}}{\partial y} + \frac{\partial\tau_{zx}}{\partial z} + \frac{n_s \partial u_w}{\partial x} + n_s \rho_s g + F_{sx}^w = 0 \quad (13)$$

$$\frac{\partial\tau_{xu}}{\partial x} + \frac{\partial(\sigma_y - u_w)}{\partial y} + \frac{\partial\tau_{zy}}{\partial z} + \frac{n_s \partial u_w}{\partial y} + n_s \rho_s g + F_{sy}^w = 0 \quad (14)$$

$$\frac{\partial\tau_{xz}}{\partial x} + \frac{\partial\tau_{yz}}{\partial y} + \frac{\partial(\sigma_z - u_w)}{\partial z} + \frac{n_s \partial u_w}{\partial z} + n_s \rho_s g + F_{sz}^w = 0 \quad (15)$$

The surface tractions found in the equilibrium equation can be extracted to form a 3 by 3 matrix, (*i.e.*, a tensor) as shown in Eq. 16. The tensor represents the stress state of the soil structure at a point in the two phase material such as a saturated soil.

$$\begin{bmatrix} (\sigma_x - u_w) & \tau_{yx} & \tau_{zx} \\ \tau_{xy} & (\sigma_y - u_w) & \tau_{zy} \\ \tau_{xz} & \tau_{yz} & (\sigma_z - u_w) \end{bmatrix} \quad (16)$$

A stress tensor can also be plotted on a cube to represent the soil solids stress state for a saturated soil (Fig. 7). The stress tensor should represent the stress state variables controlling the solid phase of a two phase system.

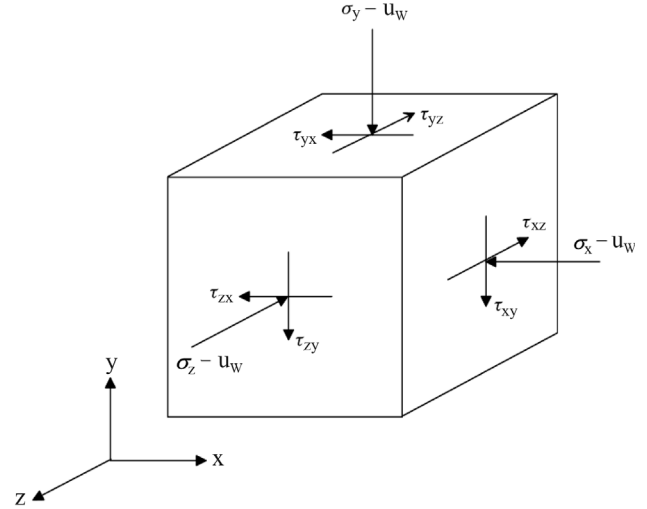


Figure 7 - Stress state at a point for the solids phase of a two phase saturated soil.

11. Stress Fields for a Dry Soil

Equilibrium equations can also be written for a completely dry soil with a pore-air pressure, u_a . In this case the soil structure equilibrium equations are the same as Eqs. 13, 14 and 15 with the exception that pore-air pressure is substituted for pore-water pressure. The stress tensor for the dry soil is shown as Eq. 17 and the stress state at a point is shown in Fig. 8. Even in the case of a highly compressible pore fluid, the description of the stress state is independent of the properties of the pore fluid.

$$\begin{bmatrix} (\sigma_x - u_a) & \tau_{yx} & \tau_{zx} \\ \tau_{xy} & (\sigma_y - u_a) & \tau_{zy} \\ \tau_{xz} & \tau_{yz} & (\sigma_z - u_a) \end{bmatrix} \quad (17)$$

The superposition of independent, coincident equilibrium stress fields can also be applied to multiphase systems with more than two phases, for example, a four phase system such as an unsaturated soil (Fredlund, 1973). A review of the research literature shows that historical, fundamental studies of unsaturated soil behaviour were primarily interested in finding an equation that could be used to describe the physical behaviour of an unsaturated soil. The search seemed to be for a single-valued equation rather than a search for independent stress state variables.

12. The Search for an Effective Stress Equation for Unsaturated Soils

Effective stress equations proposed for unsaturated soils shows the primary focus of a variety of researchers. The search started in the late 1950s and has continued to the present. The earliest proposed equation, and the best known of all equations is Bishop's effective stress equation (1959).

$$\sigma' = (\sigma - u_a) + \chi(u_a - u_w) \quad (18)$$

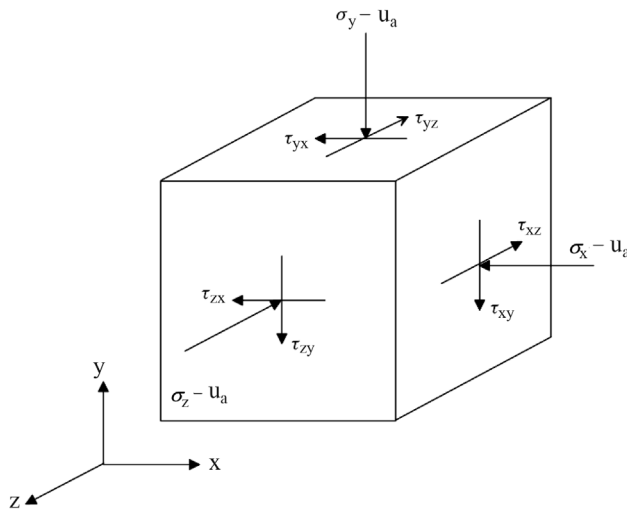


Figure 8 - Stress state for the soil structure of a completely dry particulate medium.

where σ = effective stress, σ = total stress, u_w = pore-water pressure, u_a = pore-air pressure, and χ = soil parameter related to the degree of saturation of the soil, ranging from zero to 1.0

Other effective stress equations have also been proposed (Croney *et al.*, 1958; Jennings 1961; Aitchison, 1961). All of the proposed equations are similar in form and become equal when the pore-air pressure is atmospheric. Also common to all equations is the incorporation of a soil property into the description of the stress state of an unsaturated soil. The soil property makes all equations take on the character of a constitutive equation; thus violating the fundamental separation of state variables and constitutive behaviour.

With time the degree of saturation, S , of the soil has often been used in place of the χ soil parameter, and the equations have been written in a tensor form (Jommi, 2000). In so doing, the degree of saturation has become an approximation for the χ parameter but the equation still has a constitutive nature.

Wavy planes have also been passed through an unsaturated soil in an attempt to justify the so-called effective stress equations for an unsaturated soil. The fallacy of such an approach is the same as explained above for a saturated soil.

Over the same period of time when effective stress equations have been proposed for unsaturated soils, there have also been researchers who have maintained that the stress variables, $(\sigma - u_a)$ and $(u_a - u_w)$ should be treated as independent stress state variables and used as such to form constitutive equations that are then used in theoretical formulations. As early as 1941, Biot used the stress state variables in an independent manner in his formulation of the theory of consolidation of an unsaturated soil. Coleman (1962), Matyas & Radakrishna (1968), and Fredlund &

Morgenstern (1977) advocated the use of independent stress state variables.

12.1. Examination of the wavy plane analysis for an unsaturated soil

A wavy plane passed through an unsaturated soil will pass through the air and water phases in addition to the soil-to-soil points of contact as shown in Fig. 9. Once again, the wavy plane does not constitute a legitimate free-body diagram and is therefore unacceptable for verification purposes. However, let us follow the steps common to this derivation to observe the fallacies associated with the wavy plane analysis.

The wavy plane analysis does not even qualify as an approximation of the physics behind the stress state of an unsaturated soil. Rather, the wavy plane analysis is a violation of statics at its most fundamental level. The rationale; however, is as follows. The attempt to sum forces in the vertical direction across a plane yields the following equation.

$$\sigma = \sigma_i a + u_w(1 - a - a_a) + u_a(1 - a - a_w) \tag{19}$$

where a = area of contact between particles along the wavy plane, a_w = portion of the unit area that is in water, and a_a = portion of the unit area that is in air.

Multiplying out the terms in Eq. 19, collecting terms and setting σ' equal to $\sigma_i a$ gives the following equation.

$$\sigma = \sigma' + u_w - a_a u_w + u_a - a_w u_a + a u_w - a u_a \tag{20}$$

The terms in Eq. 20 can be collected and solved for the effective stress term after making the assumption that the area of contact between solid particles approaches zero.

$$\sigma' = (\sigma - u_a) + a_w u_a + (a_a - 1)u_w \tag{21}$$

A further collection of terms gives.

$$\sigma' = (\sigma - u_a) + a_w(u_a - u_w) \tag{22}$$

Setting the area of the plane passing through water equal to the degree of saturation of the soil gives an equa-

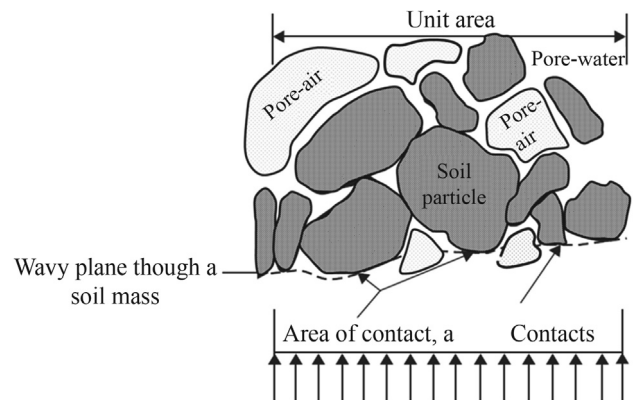


Figure 9 - Wavy plane passed through an unsaturated soil.

tion that is similar in character to the Bishop (1959) equation.

$$\sigma' = (\sigma - u_a) + S(u_a - u_w) \quad (23)$$

The question remains, “Can a wavy plane analysis be used as a proof for an effective stress equation?” The answer would appear to be “no” because a plane, (and particularly a wavy plane), does not constitute a legitimate free-body diagram. Or it can be stated that a wavy plane does not incorporate spatial variation and as a result it cannot be considered to be a legitimate free-body diagram.

The superposition of coincident equilibrium stress fields associated with the independent phases of a multiphase medium would appear to provide a more convincing explanation for the selection of independent stress state variables for multiphase materials.

12.2. What is the fundamental difficulty associated with the use of an equation to describe the stress state for an unsaturated soils?

The term, effective stress, $(\sigma - u_w)$, was originally defined for a saturated soil and became part of a stress tensor that described the stress state for the soil structure. Attempts to generate a so-called effective stress equation for an unsaturated soil have always resulted in the incorporation of a soil property into the attempt to describe the stress state. Soil properties are unacceptable in the description of stress state based on the fundamental principles of continuum mechanics.

Incorporating soil properties into the description of stress state also imposes serious inflexibility with respect to the development of a range of required constitutive equations and subsequent formulations. This is particularly true when attempting to account for behavioural effects such as nonlinearity and hysteresis. Geotechnical engineers must decide whether or not it is important to adhere to the fundamental principles of continuum mechanics or strike off on another course of action. In this sense, the decision becomes philosophical in nature.

Morgenstern (1979) in his comments titled, Properties of Compacted Soils, published in the proceedings of the 6th Pan-American Conference on Soil Mechanics and Foundation Engineering in Lima, Peru, explained his concerns about the use of an equation containing soil properties to describe the stress state of an unsaturated soil. He pointed out that Bishop’s effective stress equation has “proved to have little impact on practice. The parameter, χ , when determined for volume change behaviour was found to differ when determined for shear strength. While originally thought to be a function of degree of saturation and hence bounded by 0 and 1, experiments were conducted in which χ was found to go beyond these bounds. The effective stress is a stress variable and hence related to equilibrium considerations alone”. Morgenstern went on to explain that Bishop’s effective stress equation “contains the parameter, χ ,

that bears on constitutive behaviour. This parameter is found by assuming that the behaviour of a soil can be expressed uniquely in terms of a single effective stress variable and by matching unsaturated soil behaviour with saturated soil behaviour in order to calculate χ . Normally, we link equilibrium considerations to deformations through constitutive behaviour and do not introduce constitutive behaviour into the stress state”.

Once the effective stress equation becomes constitutive in character, it must be faced with the rigorous tests of uniqueness for usage in engineering practice. It would appear that the need for an effective stress equation can easily be replaced through use of independent stress tensors containing stress state variables. However, there continues to be ongoing attempts to revert to the usage of an effective stress equation. The use of an effective stress equation for unsaturated soils violates the basic assumptions inherent in classical continuum mechanics and places serious constraints on subsequent formulations. These concerns can be circumvented through the use of independent stress state variables for the proposal of shear strength, volume change and other constitutive relations for the practice of unsaturated soil mechanics (Fredlund & Rahardjo, 1993; Fredlund *et al.*, 2012).

It would appear that the issues related to the description of the stress state in an unsaturated soil can only be resolved through an understanding and acceptance of the independent roles of state variables and constitutive behaviour within the context of continuum mechanics. The basis for stress state variables for an unsaturated soil is the same as those explained for a saturated soil. In other words, consideration of force equilibrium for each phase of an unsaturated soil provides the basis for the selection of appropriate independent stress state variables. The important equations that must be given consideration are Newton’s equilibrium equations in three coordinate directions. The search needs to focus on variable(s) that qualify as state variables. These variables need to be placed into the tensor form and in so doing will provide a strong science basis for the formulation of unsaturated soil mechanics theories.

13. Theoretical Basis for Independent Stress State Variables

Fredlund & Morgenstern (1977) provided a theoretical justification for independent stress state variables based on a continuum mechanics approach. The independent stress state variables were then used in the formulation of constitutive models for all the classic application areas of unsaturated soil mechanics. Engineering problems were solved based on constitutive models and theoretical derivations that utilized independent stress state variables. This information was subsequently synthesized in two books on unsaturated soil mechanics; namely, Soil Mechanics for Unsaturated Soils (1993) by D.G. Fredlund & H. Rahardjo,

and Unsaturated Soil Mechanics in Engineering Practice (2012) by D.G. Fredlund *et al.*

It would appear that fundamentally, “state variables” are embedded within the conservative laws of physics. The conservation of mass dictates the form and number of “deformation state variables” required to map the movement of independent phases of a multiphase system. The conservation of energy (or momentum) dictates the form and number of “stress state variables” and “thermal state variables” required for equilibrium considerations of a multiphase system (*e.g.*, an unsaturated soil).

The general procedure outlined for the determination of the stress tensor for the soil structure of a saturated soil can also be used for consideration of an unsaturated soil. While the saturated soil constituted a two phase system, an unsaturated soil needs to be considered as a four phase system. In addition to the soil solids (*i.e.*, soil structure), water phase and air phase, the contractile skin needs to be recognized as a fourth independent phase (Wang & Fredlund, 2003). The need for the contractile skin to be recognized as a fourth phase can be visualized by observing the changes in volume that can occur (*i.e.*, changes in the volume defined by the soil structure), as a soil is dried under conditions where total stresses remain constant. Under this condition, volume changes are due to the shrinkage imposed by the air-water interface. The air-water interface is commonly referred to as the contractile skin.

An unsaturated soil can be visualized as having two phases that behave as solids; namely, the soil solids and the contractile skin (Wang & Fredlund, 2003). These phases qualify as solids within the continuum mechanics sense since they can come to equilibrium under the application of a stress gradient. The unsaturated soil also has two phases that qualify as fluids; namely, water and air. These phases qualify as fluids in the sense that they do not come to equilibrium under the application of a stress gradient.

An unsaturated soil has four phases and as a result, four independent equilibrium equations can be written. An equilibrium equation can also be written for the overall combination of the four phases and it will take the form of Eqs. 8, 9, and 10. There are only four independent equations that can be written. Equilibrium equations can also be formed through the combination of one or more phases as illustrated by Fredlund & Morgenstern (1977). Fredlund (1973) also showed that the equations describing the equilibrium of the soil structure were yielded the same stress state variables for the equilibrium of the contractile skin. In other words, the stress state variables that produce equilibrium for the soil solids (*i.e.*, soil structure) also produce equilibrium for the contractile skin.

13.1. Equilibrium of soil structure for an unsaturated soil element

The equilibrium of the soil structure in the y -direction can be written as the difference between the total equilib-

rium equation and the sum of the water, air and contractile skin equilibrium equations. The following equation is obtained when using the air phase as a reference phase during the derivation of the equilibrium equation for the soil structure.

$$\begin{aligned} \frac{\partial \tau_{xy}}{\partial x} + \frac{\partial(\sigma_y - u_a)}{\partial y} + (n_w + n_c f^*) \frac{\partial(u_a - u_w)}{\partial y} + \\ \frac{\partial \tau_{zy}}{\partial z} + (n_c + n_s) \frac{\partial u_a}{\partial y} + n_s \rho_s g - \\ F_{sy}^w - F_{sy}^a + n_c (u_a - u_w) \frac{\partial f^*}{\partial y} = 0 \end{aligned} \quad (24)$$

where n_a = porosity with respect to the air phase, n_w = porosity with respect to the water phase, n_c = porosity with respect to the contractile skin, f^* = interaction function between the contractile skin and the soil structure, F_{sy}^a = interaction body force between the solids and the air phase in the y -direction, and F_{sy}^w = interaction body force between the solids and the water phase in the y -direction.

Similar equations can be written for the x - and z -directions, respectively:

$$\begin{aligned} \frac{\partial(\sigma_x - u_a) \tau_{xy}}{\partial x} + (n_w + n_c f^*) \frac{\partial(u_a - u_w)}{\partial x} + \frac{\partial \tau_{yx}}{\partial y} + \\ \frac{\partial \tau_{zx}}{\partial z} + (n_c + n_s) \frac{\partial u_a}{\partial x} - F_{sx}^w - F_{sx}^a + \\ n_c (u_a - u_w) \frac{\partial f^*}{\partial x} = 0 \end{aligned} \quad (25)$$

where F_{sx}^a = interaction body force between the solids and the air phase in the x -direction, and F_{sx}^w = interaction body force between the solids and the water phase in the x -direction.

$$\begin{aligned} \frac{\partial \tau_{xz}}{\partial x} + \frac{\partial \tau_{yz}}{\partial y} + \frac{\partial(\sigma_z - u_a)}{\partial z} + (n_w + n_c f^*) \frac{\partial(u_a - u_w)}{\partial z} + \\ (n_c + n_s) \frac{\partial u_a}{\partial z} - F_{sz}^w - F_{sz}^a + n_c (u_a - u_w) \frac{\partial f^*}{\partial z} = 0 \end{aligned} \quad (26)$$

where F_{sz}^a = interaction body force between the solids and the air phase in the z -direction, and F_{sz}^w = interaction body force between the solids and the water phase in the z -direction.

The stress variables controlling the equilibrium of the soil structure are the stress state variables that control the mechanical behavior of soils. There are three independent sets of normal stresses, (*i.e.*, surface tractions) that can be extracted from the equilibrium equations for the soil structure to form the stress state variables. The three stress state variables are: $(\sigma - u_a)$, $(u_a - u_w)$, and (u_c) . The stress variable, u_a , is also a stress state variable but can be eliminated if the soil particles are assumed to be incompressible. Therefore,

the stress state variables for the soil structure and the contractile skin in an unsaturated soil are $(\sigma - u_a)$ and $(u_a - u_w)$.

The stress state variables act in three Cartesian coordinate directions and the variables can be collected to form two independent stress tensors. The two independent stress tensors can be written as the stress state at a point in an unsaturated soil.

$$\begin{bmatrix} (\sigma_x - u_a) & \tau_{yx} & \tau_{zx} \\ \tau_{xy} & (\sigma_y - u_a) & \tau_{zy} \\ \tau_{xz} & \tau_{yz} & (\sigma_z - u_a) \end{bmatrix} \quad (27)$$

$$\begin{bmatrix} (u_a - u_w) & 0 & 0 \\ 0 & (u_a - u_w) & 0 \\ 0 & 0 & (u_a - u_w) \end{bmatrix} \quad (28)$$

Equation 27 is referred to as the net normal stress tensor and Eq. 28 is referred to as the matric suction (or soil suction) tensor. The pore-air pressure appears in both stress tensors; however, it is the difference between stress components that allows the two tensors to qualify as independent stress state variables. The stress variables in Eqs. 27 and 28 can be placed on the surface of a cube to give the stress state at a point as shown in Fig. 10.

As an unsaturated soil approaches saturation, the degree of saturation, S , approaches 100%. The pore-water pressure, u_w , approaches the pore-air pressure, u_a , and the matric suction term, $(u_a - u_w)$, goes towards zero. The second stress tensors for the unsaturated soil disappear because the matric suction, $(u_a - u_w)$, becomes zero. It should be noted that it is not necessary for the pore-water pressure to go to zero in order for the soil to behave as a saturated soil. Rather, it is necessary for the pore-water pressure to increase until it becomes equal to the pore-air pressure and then the soil behaves as a saturated soil.

Only the first stress tensor is left to represent the stress state for a saturated soil once the pore-water pressure is equal to pore-air pressure. The pore-air pressure term in the first stress tensor becomes equal to the pore-water pres-

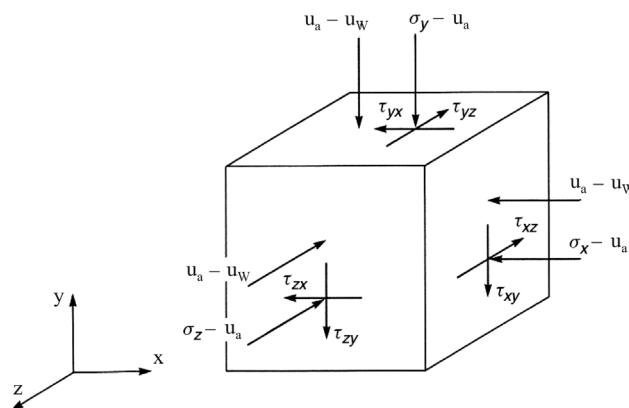


Figure 10 - Stress state at a point for the soil structure and the contractile skin in an unsaturated soil.

sure, u_w , as the soil becomes saturated. The stress state at a point in a saturated soil was illustrated in Fig. 7. The stress tensor for a saturated soil is consistent with that presented by Terzaghi (1936) as the effective stress variable, $(\sigma - u_w)$.

13.2. Other combinations of stress state variables

The soil structure equilibrium equations can have three different forms depending upon the reference phase used during the derivation of the equilibrium equations. Equations 24, 25, and 26 are the resulting equations when using the air phase as the reference phase during the derivation. Other forms of the derivation can use the water phase or else the total stress field as a reference. Each form of the equilibrium equations contains a combination of two stress state variables. In other words, any two of three possible stress variables, (*i.e.*, $(\sigma - u_a)$, $(\sigma - u_w)$, and $(u_a - u_w)$), can be used to describe the stress state for the soil structure and contractile skin in an unsaturated soil.

14. The Principle or Concept Associated with Stress State Variables

The principle or concept associated with stress state variables can be stated as follows: “If one or more of the stress state variables are changed, the equilibrium of the system is disturbed and changes in the system can be anticipated, and vice versa”. The same principle applies to both the soil structure and the contractile skin.

15. Visualization of the World of Soil Mechanics Based on Stress State Variables

Figure 11 illustrates the transition in the description of the stress state when moving from a saturated soil to an unsaturated soil (and vice versa), (Fredlund, 1994). The transition is shown to occur at the water table or the point at which the pore-water pressures change from a positive value to a negative value. There is a zone immediately above the water table referred to as the capillary zone. This zone may be essentially saturated; however, it is suggested

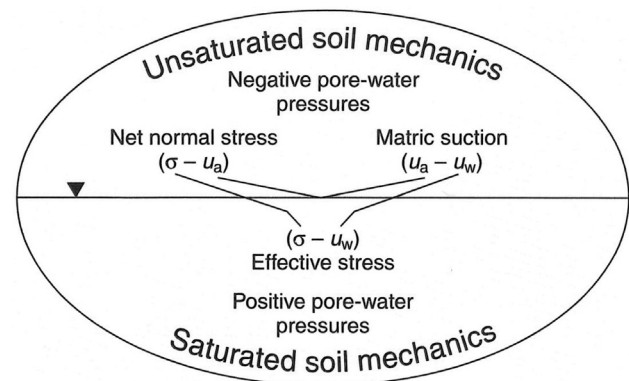


Figure 11 - Visualization of the world of soil mechanics in terms of the description of the stress state for saturated and unsaturated soils (Fredlund, 1996).

that the transition between saturated soil mechanics and unsaturated soil mechanics is best based on whether the pore-water pressures are positive or negative.

Numerous problems in soil mechanics are analyzed using a one-dimensional analysis with total stresses being changed in the vertical direction. Consequently, an increase in stresses in the vertical direction produces a tendency for deformation in the horizontal direction as well as the (downward) vertical direction. On the other hand, a decrease in the pore-water pressure will produce a tendency for shrinkage in all three directions. Only under isotropic total stress conditions will the deformation directions be similar for total stress and pore-water pressure changes. Consequently, it would appear to be reasonable to acknowledge the independent behaviour of changes in the total stress field from that of the pore-water pressure field when moving above the water table. The above conceptual picture is a reminder that changes in total stresses and changes in pore-water pressures can produce different deformation fields in an unsaturated soil. Therefore, the net normal stress variable needs to be considered as being independent of the matric suction variable for analytical purposes. Also, the magnitude of deformations associated with changes in net total stress may be different from the magnitude of deformations associated with changes in matric suction. Fig-

ure 12 provides a visualization tool that illustrates the difference in the stress state at a point when the soil is saturated and unsaturated.

16. Recommendations for the Ongoing Development of Unsaturated Soil Mechanics

Following are a series of suggested recommendations for the development of a continuum mechanics based approach to the development of unsaturated soil mechanics.

- 1) That the term “effective stress” should be limited to the original definition described by Terzaghi (1936) for saturated soils.
- 2) The concepts of stress state variables as defined in continuum mechanics should be adopted as the science basis for unsaturated soil mechanics.
- 3) Stress state variables for any soil should be kept independent of the material properties.
- 4) There can be multiple stress state variables (and deformation state variables) for a multiphase material.
- 5) Temperature and time should also be considered as state variables, in addition to deformation state variables.

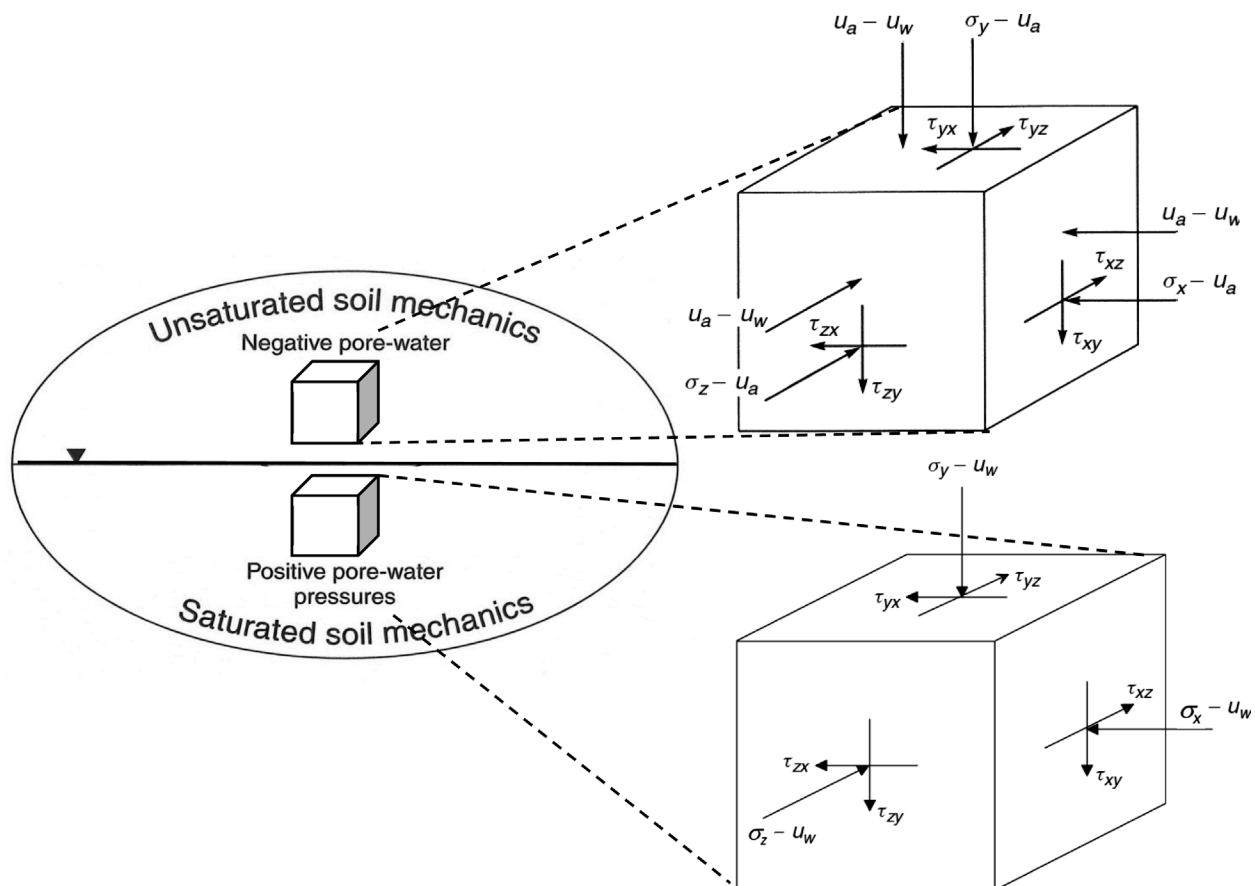


Figure 12 - Visualization of the stress state at a point for saturated and unsaturated soils (Fredlund, 1996).

17. Incorporation of Soil Properties into the Definition of Stress State

Skempton (1961) felt that it was of “philosophical interest to examine the fundamental principles of effective stress, since it would seem improbable that an expression of the form” proposed by Terzaghi, “is strictly true.” He went on to say, “We may therefore anticipate that, even for fully saturated porous materials, the general expression for effective stress is more complex, and that Terzaghi’s equation has the status of an excellent approximation in the special case of saturated soils.” He goes on to say that “the effective stress is actually the intergranular stress acting between the particles” and the effective stress should be corrected for the area of contact between the particles.

Skempton’s (1961) statements did not recognize the need for multiple stress state variables in some situations (*e.g.*, the case of a saturated soil with compressible soil particles). His search opened the way for introducing material properties into the description of stress state. The so-called refinement associated with the “area of contact” between soil particles did not have a significant impact in saturated soil mechanics but it set the stage for other considerations related to effective stress for volume change and shear strength of saturated and unsaturated soils.

Nur & Byerlee (1971) went through a similar exercise in attempting to develop an “exact effective stress law for elastic deformation of rock with fluids”. In coming to the conclusion that Terzaghi’s equation “is an excellent approximation”, they failed to realize the need for multiple stress state variables for the situation involving compressible materials.

17.1. Soil properties in effective stress equations for saturated soils

Consideration of the area of contact between soil particles set the stage for suggestions that there was a “more correct expression” for effective stress equation that could be written for analyzing shear strength problems. Equation 29 was suggested as the effective stress equation for “fully saturated materials” (Skempton, 1961).

$$\sigma' = \sigma - \left(1 - \frac{a \tan \Psi}{\tan \varphi'} \right) u_w \quad (29)$$

where a = area of contact between particles, Ψ = angle of intrinsic friction of the solid particles, and φ' = angle of internal friction between the soil particles.

An independent effective stress equation was suggested for the analysis of volume change problems involving saturated soils (Skempton, 1961).

$$\sigma' = \sigma - \left(1 - \frac{C_s}{C} \right) u_w \quad (30)$$

where C_s = compressibility of the solids, and C = compressibility of the porous material or the soil structure.

Laughton (1955) performed experiments on materials with compressible particles. The results can be interpreted as showing the need for a second independent state variable (*i.e.*, u_w), when dealing with compressible materials.

The need for separate effective stress equations when analyzing shear strength and volume change problems would appear to be surprising if the equations are truly a description of “stress state”. The volume change analysis of materials with compressible solids can be analyzed without the need for a new effective stress equation if it is realized that two independent stress state variables are required; namely, the Terzaghi effective stress variable ($\sigma - u_w$) and pore-water pressure, (u_w). There is no need for two effective stress equations (*i.e.*, one for shear strength and another for volume change). All material properties must be incorporated at the constitutive behaviour level of formulations that describe soil behaviour.

Nur & Byerlee (1971) incorporated the compressibility properties into their attempt to develop a more “exact expression for an effective stress law” for the study of elastic deformations of rock materials. Their statement that “there is a great deal of disagreement on the theoretical accuracy and validity of Terzaghi’s relation” would appear to be an overstatement. Bringing compressibility values into the effective stress equation is not necessary if it is recognized that a compressible particulate soil or rock requires an independent stress state variable in this situation; namely, an isotropic pore-water pressure tensor.

A summary of so-called proposed refinements to Terzaghi’s effective stress equation has been given by Gens (2005). The proposed refinements are not repeated herein because there appears to be no fundamental reason to accept soil properties into the description of stress state.

17.2. Soil properties in effective stress equations for unsaturated soils

With a history of incorporating soil properties into effective stress equations for saturated soils, it is not that surprising that soil properties should find their way into an effective stress equation for unsaturated soils. Bishop (1959) introduced the χ parameter into his proposed effective stress equation for unsaturated soils. The χ parameter was found to generally be a nonlinear function of degree of saturation. Later, the degree of saturation variable, S , was substituted for the χ parameter by some researchers Bishop’s (1959) equation became referred to as the average skeleton stress.

$$\sigma' = (\sigma - u_a) + S(u_a - u_w) \quad (31)$$

The history of various forms for the effective stress for an unsaturated soil has been summarized by Gens (2005) and is not repeated herein.

Khalili & Khabbaz (1998) suggested that the χ parameter could be related to the air-entry value for an unsaturated soil. The soil-water characteristic curve, SWCC, for desorption of a soil was set as a demarcation between saturated and unsaturated soil behaviour. Unsaturated soil behaviour was related to degree of saturation through use of a second soil parameter, m , which was set to 0.55.

It is apparent that the search for an effective stress equation for unsaturated soil behavior had its origin in the incorporation of soil properties into Terzaghi's effective stress equation. This constitutes a fundamental deviation from the context of continuum mechanics.

There have been several researchers who have proposed and advocated the use of independent stress state variables. Fredlund & Morgenstern (1977) used equilibrium considerations of a multiphase system to illustrate the source for acceptable, independent stress state variables. Null type laboratory tests were also used to confirm the suitability of two independent stress state variables for unsaturated soils. There are other researchers who previously suggested using independent stress state variables. Biot's (1941), in his proposed theory of consolidation advocated the use of two independent stress variables for unsaturated soils. Others who supported this approach are Coleman (1962) and Matyas & Radhakrishna (1968). Bishop & Blight (1963) also presented laboratory measured constitutive data using two independent stress state variables.

In his notes on effective stresses Gens (2005) concludes, "The description of the behaviour of unsaturated soils requires the use of two independent stress variables". The author agrees with the direction advocated and would add that there ought to not be an ongoing search for a universal effective stress expression for unsaturated soils. Such a search appears to always lead to the inclusion of soil properties, making the stress state expressions "constitutive" in character.

Theoretical formulations for unsaturated soils problems have been proposed that maintained the separation of state variables and constitutive equations. These formulations have also been solved for a variety of saturated-unsaturated soils problems common to geotechnical engineering (Fredlund & Rahardjo (1993) and Fredlund *et al.* (2012)). The solutions have been used extensively in solving geotechnical engineering problems. It is the soil-water characteristic curves, SWCCs, (*i.e.*, desorption and adsorption branches) that have proved to provide the primary unsaturated soils information required for each of the formulations. Sheng *et al.* (2008) also demonstrated that it was possible to formulate a critical state model for unsaturated soils while maintaining the separation of state variables and constitutive behaviour.

18. Grounds for a Connection Between the Two Approaches to Formulating Unsaturated Soil Mechanics

It is of interest to examine the possible grounds for a compromise between the two procedures that have been proposed for formulating unsaturated soil mechanics problems. The relationship between the two approaches can be viewed as follows from an elementary standpoint.

Let us start with the use of two independent stress state variables for an unsaturated soil and then try to formulate an acceptable constitutive relationship. Let us consider the volume change of an unsaturated soil where the difference in behaviour associated with changing net total stress and matric suction is uniquely related to the degree of saturation of the soil. It would then be possible to write the following general volume change equation with constant, linear soil properties.

$$dv = m_i^s(\sigma - u_a) + m_i^s S(u_a - u_w) \quad (32)$$

where dv = soil structure volume change, $(\sigma - u_a)$ = net total stress state variable, $(u_a - u_w)$ = matric suction variable, m_i^s = compressibility of the soil structure with respect to the $(\sigma - u_a)$ stress state variable, and S = degree of saturation of the soil.

Equation 32 states that the relationship between changing the net total stress and the matric suction variables can be approximated through use of the degree of saturation variable. Equation 32 is an acceptable form for a constitutive relationship. However, it may not be sufficiently general to embrace all unsaturated soil behaviour. Consequently, the use of such an equation may prove to be too restrictive in engineering practice.

Equation 32 also suggests that the degree of saturation is known at all times when simulating a particular process. However, in reality, an independent analysis is generally required to predict water movement in or out of the soil. A transient seepage analysis also requires two nonlinear soil properties for its solution; namely, the hydraulic conductivity and the water storage function. The hydraulic properties in turn may or may not be affected by both stress state variables. It should also be noted that the overall volume and the volume of water in the soil must both be known in order to compute the degree of saturation.

A similar equation can be written for the characterization of shear strength but once again the form may prove to be not sufficiently general for engineering practice. There are also other physical relationships such as the water content constitutive relationship (*i.e.*, the soil-water characteristic curve, SWCC), that does not have a unique response to the degree of saturation.

In general, it would appear to be better to separate state variables from constitutive behaviour in order to provide the greatest flexibility and accuracy in defining unsaturated soil behaviour.

References

- Aitchison, G.D. (1961). Relationship of moisture and effective stress functions in unsaturated soils. Proc. Pore Pressure and Suction in Soils Conference, Butterworths, London, pp. 47-52.
- Biot, M.A. (1941). General theory for three-dimensional consolidation. *Journal of Applied Physics*, 12(2):155-164.
- Bishop, A.W. (1959). The principle of effective stress. *Teknisk Ukeblad, Norwegian Geotechnical Institute*, 106(39):859-863 (Lecture delivered in 1955).
- Bishop, A.W. & Blight, G. E. (1963). Some aspects of effective stress in saturated and unsaturated soils. *Geotechnique*, 13(3):177-197.
- Crone, D.; Coleman, J.D. & Black, W.P.M. (1958). Movement and distribution of water in soil in relation to highway design and performance. In: *Water and Its Conduction in Soils*, Highway Research Board, Special Report, Washington, DC, No. 40, pp. 226-252.
- Coleman, J.D. (1962). Stress/strain relations for partly saturated soils. *Geotechnique*, 12(4):348-350.
- Fredlund, D.G. (1973). Volume Change Behaviour of Unsaturated Soils. PhD Thesis, Department of Civil Engineering, University of Alberta, Edmonton.
- Fredlund, D. G. & Rahardjo, H. (1993). *Soil Mechanics for Unsaturated Soils*. John Wiley & Sons, New York, 507 p.
- Fredlund, D.G. (1994). Visualization of the world of soil mechanics. Proceedings of the Sino-Canadian Symposium on Unsaturated/Expansive Soils, Wuhan, China, pp. 1-21.
- Fredlund, D.G. & Morgenstern, N.R. (1977). Stress state variables for unsaturated soils. *Journal of Geotechnical Engineering Division, ASCE*, 103(GT5):447-466.
- Fredlund, D.G.; Rahardjo, H. & Fredlund, M.D. (2012). *Unsaturated Soil Mechanics in Engineering Practice*. John Wiley & Sons, New York, 926 p.
- Fung, Y.C. (1965). *Foundations of Solid Mechanics*. Prentice-Hall, Englewood Cliffs, 525 p.
- Fung, Y.C. (1977). *A First Course in Continuum Mechanics*. Second Edition. Prentice-Hall, Englewood Cliffs, 311 p.
- Gens, A. (2005). Effective stresses. First MUSE School, (Mechanics of Unsaturated Soils for Engineering), Fundamentals of Unsaturated Soils, (PowerPoint), Universitat Politècnica de Catalunya, Barcelona.
- Jennings, J.E. (1961). A revised effective stress law for use in the prediction of the behaviour of unsaturated soils. Proc. Conference on Pore Pressure and Suction in Soils, London, England, pp. 26-30.
- Jommi, C. (2000). Remarks on the constitutive modeling of unsaturated soils. In: *Experimental Evidence and Theoretical Approaches in Unsaturated Soils*, A. Tarantino, and C. Mancuso (eds), Rotterdam, Balkema, pp. 139-153.
- Khalili, N. & Khabbaz, M.H. (1998). A unique relationship for χ for the determination of the shear strength of unsaturated soils. *Geotechnique*, 48(5):681-687.
- Laughton, A.S. (1955). *The Compaction of Ocean Sediments*. PhD Thesis, University of Cambridge, Cambridge, U.K.
- Matyas, E.L. & Radhakrishna, H.S. (1968). Volume change characteristics of partially saturated soils. *Geotechnique*, 18(4):432-448.
- Morgenstern, N.R. (1979). Properties of compacted soils. Proc. Sixth Pan-American Conference on Soil Mechanics and Foundation Engineering, Lima, Peru, v. 3, pp. 349-354.
- Nur, A. & Byerlee, J.D. (1971). An exact effective stress law for elastic deformation of rock with fluids. *Journal of Geophysical Research*, 76(26):6414-6419.
- Sheng, D.; Fredlund, D.G. & Gens, A. (2008). A new modelling approach for unsaturated soils using independent stress variables. *Canadian Geotechnical Journal*, 45(4):511-534.
- Skempton, A.W. (1961). Effective stress in soils, concrete and rocks. Proc. Conference on Pore Pressure and Suction in Soils, Butterworths, London, pp. 4-16.
- Terzaghi, K. (1936). The shear strength of saturated soils. Proc. First International Conference on Soil Mechanics and Foundation Engineering, Cambridge, v. 1, pp. 54-56.
- Terzaghi, K. (1943). *Theoretical Soil Mechanics*. John Wiley & Sons, New York, 528 p.
- Truesdell, C. (1966). *The Elements of Continuum Mechanics*, Springer-Verlag, New York, 280 p.
- Wang, Y.H. & Fredlund, D.G. (2003.) Towards a better understanding of the role of the contractile skin. Proc. Second Asian Conference on Unsaturated Soils, UNSAT-ASIA 2003, Osaka, Japan, pp. 419-424.

Numerical and Experimental Analysis of Horizontal Stress Changes and Soil Collapse During Chemical Dissolution in a Modified Oedometer Cell

C. Lins, N. Silva, L. Guimarães, A. Lima, I. Gomes

Abstract - . The purpose of this paper is to investigate the horizontal stress evolution and soil collapse during the cement dissolution process using a combination of experimental and numerical methods. The experimental procedure was carried out using a modified oedometer cell with horizontal stress measurements and synthetic samples in order to simulate simultaneous cement dissolution, stress changes and sample deformation. The samples were loaded at a constant vertical stress and exposed to a reactive fluid which dissolved the cementation of the artificial soil. During the dissolution process, sample volume decreased and horizontal stress changes were observed. Initially the horizontal stress decreased due to grain mass loss and then increased due to solid matrix rearrangement. Numerical simulation of these coupled chemical and mechanical processes was performed using a general purpose finite element code capable of performing numerical analysis of engineering problems. The constitutive model adopted to reproduce the soil behavior is an extension of the Barcelona Basic Model for unsaturated soils including the cement mineral concentration as state variable. Some new features were incorporated to the original elasto-plastic model in order to represent the results observed in the experiments. In this paper a good agreement between experimental and numerical results was achieved.

Keywords: modified oedometer cell, soil collapse, horizontal stress changes, chemical dissolution, coupled simulation, elasto-plastic model.

1. Introduction

The recent development of experimental techniques, where measurements of variables of different nature (thermal, hydraulic, mechanical and chemical) can be performed simultaneously in the same experiment, allowed the incorporation of new variables and equations to the numerical procedures used to reproduce the behavior of soils and rocks. In geotechnical engineering, such models are mainly related to the effects of partial saturation and consequences of chemical actions on the porous media, where suctions (matric and osmotic) and chemical concentrations were included as state variables of the mechanical problem (Alonso *et al.*, 1990; Castellanza & Nova, 2004; Gens & Nova, 1993; Guimarães *et al.*, 2013).

Some geotechnical problems that are likely to require new approaches or, at least, extension of the classical ones are as follows: collapse and swelling of active soils, subsidence due to oil and gas extraction, dissolution, degradation and weathering of soils and rocks and CO₂ sequestration (Gens, 2010).

For instance, the large-scale injection of CO₂ and other gases into geological formations may induce complex interaction of multiphase flow, diffusion, convection, mineral and gas dissolution, mineral precipitation, and other

chemical reactions. Depending on the composition of the rock and fluids and CO₂ injection strategy, the rock-fluid interactions may have a significant impact on safety and reservoir storage capacity (Lins, 2012).

The injection and extraction of fluids cause mineral dissolution, changes of pressure, temperature and saturation that affect the state of stress resulting in deformations of the reservoir rock, as well as changes of the porosity and permeability. Therefore, this is a coupled problem where the fluid flow in the reservoir rock and the rock geomechanical and geochemical behavior are correlated (Guimarães *et al.*, 2009).

Mineral dissolution has been used to explain artificial and natural chemical weathering of rocks as a result of geological or engineering processes such as stimulation of petroleum reservoirs, mining degradation, geological sequestration of carbon dioxide, diagenesis, and dissolution/formation of hydrates (Chen *et al.*, 2009). Some consequences of the mineral dissolution are changes of porosity and permeability, chemically induced reservoir compaction and decreasing of shear strength. In the area of Reservoir Geomechanics, the term “reservoir compaction” is referred to all mechanisms which result in decreasing of rock volume due to pore collapse.

Cecilia Lins, PhD., Centro de Ciências e Tecnologia, Universidade Católica de Pernambuco, Recife, PE, Brazil. e-mail: cecilia.lins@gmail.com.

Nayra Silva, PhD., Centro de Tecnologia, Universidade Federal de Alagoas, Maceió, AL, Brazil. e-mail: nayvicente@gmail.com.

Leonardo Guimarães, PhD., Departamento de Engenharia Civil, Universidade Federal de Pernambuco, Recife, PE, Brazil. e-mail: leojnguiamaraes@gmail.com.

Analice Lima, PhD., Departamento de Engenharia Civil, Universidade Federal de Pernambuco, Recife, PE, Brazil. e-mail: analicelima@hotmail.com.

Igor Gomes, PhD., Departamento de Engenharia Civil, Universidade Federal de Pernambuco, Recife, PE, Brazil. e-mail: gomes@ufpe.br.

Invited Article, no discussion.

So, in the case of the chemically induced reservoir compaction, it is observed the decreasing of rock volume under constant mechanical boundary conditions when a reactive fluid is injected into the geological formation. From the pore scale point of view, the injection of aggressive fluids causes cement dissolution, weakening of bounds between inert minerals and finally pore collapse. It is observed also a decreasing of shear strength and stiffness. This phenomenon is known as water-weakening of the rock (Korsnes *et al.*, 2008; Silva, 2012).

Nowadays, the analysis of geomechanical effects on deformable soils and rocks induced by chemical dissolution is an open field. The knowledge of the coefficient of earth pressure at rest (K_0) is a key parameter for many subsurface applications of Civil, Petroleum and Mining Engineering. For instance, K_0 is fundamental to verify the stability of well perforations and underground excavations such as tunnels and galleries. Its value reflects the soil characteristics and stress history.

Despite its importance on the evolution of K_0 during the formation history of the rock, such as changes of chemical and mechanical conditions, is very limited (Shin & Santamarina, 2009). At laboratory scale, it is also not easy to determine K_0 when the soil or rock is simultaneously loaded and exposed to reactive fluids in the attempt to simulate diagenetic or weathering processes. In this area, authors such as Shin and Santamarina (2009) and Castellanza and Nova (2004) have given some insights into this complex behavior of cemented soils and rocks. They developed modified oedometer cells to evaluate changes of horizontal stress caused by mineral dissolution. Performing tests using these modified apparatus, they were able to determine the complete stress path during rock exposure to a reactive fluid at constant vertical stress.

This paper describes tests performed with an oedometer cell similar to those proposed by Castellanza & Nova (2004) and Shin & Santamarina (2009) using an artificial soil proposed by Shin & Santamarina (2009), composed of glass beads as the inert mineral and sodium chlorite as the cement at different concentrations (12% and 20%). The reactive fluid is distilled water, which will dissolve the sodium chlorite.

Based on the framework proposed by Gens & Nova (1993), Castellanza & Nova (2004) also proposed a constitutive model able to reproduce the stress path observed in carbonatic soft rocks subjected to acid injection. In Gens & Nova (1993), the basic conceptual requirements for constitutive models for bonded soils and weak rocks are discussed within the framework of hardening plasticity. A reference model for unbonded material is used as a start point and it is modified according to the magnitude of bonding. Finally, material degradation is simulated by a reduction of degree of bonding caused by mechanical and chemical actions. The model incorporates bonding to the

material behavior in a similar way of suction, as both confer an additional strength and stiffness to the material.

In the elasto-plastic model proposed by Castellanza & Nova (2004), the reference model for the unbonded material is based on the Critical State Theory and a new state variable to represent bonding is proposed. This new variable affects the shear strength (cohesion) and pre-consolidation stress of the material and its evolution is a result of imposed mechanical and chemical loads. The model is also able to simulate irreversible (plastic) strain due to material degradation, by modifying the hardening law which relates evolution of the pre-consolidation stress and volumetric plastic strain. It is proposed in this paper a modification of Castellanza & Nova (2004) model to include deformations and changes of stresses due to solid mass loss in the elastic part of the model.

The model was implemented in a general purpose finite element code (Olivella *et al.*, 1994 and Guimarães *et al.*, 2007) capable of performing coupled thermo-hydro-mechanical and chemical (THMC) analysis of engineering problems. The model was implemented as an extension of the Barcelona Basic Model (BBM) for unsaturated soils, now incorporating bonding effects. The chemical variable selected to affect the bonding of the material is the concentration of the cement, represented in the chemical model (reactive transport problem) as a precipitated mineral. Experimental evidence is still necessary to validate the model when both effects of no saturation and chemical changes take place simultaneously.

In the validation exercise presented here, only the chemical part of the model is validated for a previously saturated soil. Coupled hydro-mechanical and chemical (HMC) analysis of the modified oedometer tests was performed in order to reproduce the most significant aspects of the observed behavior of the sample subjected to simultaneous mechanical and chemical loads. The experimental procedure was carried out using a modified oedometer cell with horizontal stress measurements and synthetic samples in order to simulate simultaneous cement dissolution, stress changes and sample deformation. The samples were loaded at a constant vertical stress and exposed to a reactive fluid which dissolved the cementation of the artificial soil. In this analysis, the mass balance equations for water and all chemical species (flow and reactive transport problems) and the balance equation for momentum (mechanical problem) are solved together in a fully coupled way according to Guimarães *et al.* (2007).

2. Experimental Programme

2.1. Experimental setup - Soft oedometer cell

Figure 1 shows the scheme of the modified soft oedometer cell used to perform the tests. The equipment was developed and instrumented based on specifications outlined by Castellanza & Nova (2004) and Shin & Santamarina

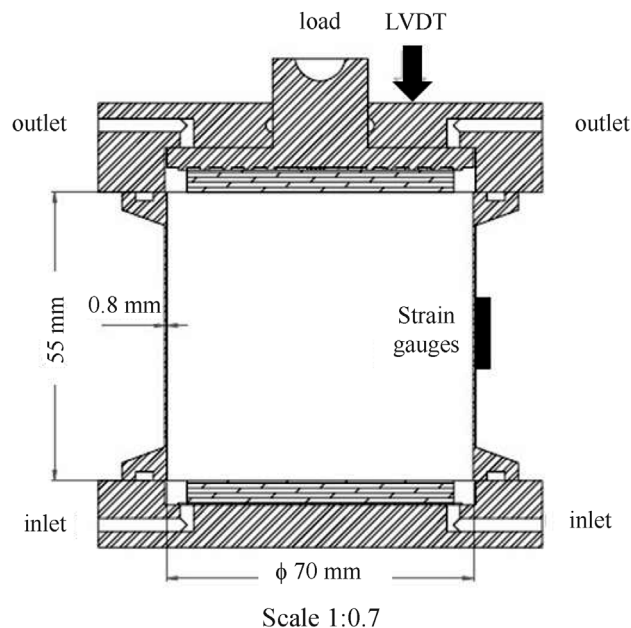


Figure 1 - Scheme of modified soft oedometer cell.

(2009), specifically designed to measure the horizontal stress.

This cell is composed by an aluminum-bronze alloy using a ring with 70 mm in diameter, 55 mm in height and 0.8 mm thickness. A thin ring is used allowing very small horizontal strain (quasi-oedometric conditions) measured by strain gages attached to the ring wall. Strain gages are calibrated in order to directly correlate wall deformation and horizontal stress. The four strain gauges installed are used to reach two different objectives: two of them to measure horizontal stress and the other two to correct temperature influence.

The sample is placed inside the ring between two porous stones and the whole set is fixed by top and bottom caps. The inlet and outlet water valves are connected in the caps. The vertical displacements are measured using Linear Variable Differential Transformers (LVDT). Before performing the tests, the different transducers were carefully calibrated. The vertical displacements and horizontal stress measurements during the tests were stored using a data acquisition program specifically designed for this equipment.

2.2. Test protocol

The experimental tests were carried out using synthetic samples proposed by Shin & Santamarina (2009). The samples consist of a mixture of glass beads and sodium chloride (NaCl) with diameter of 2 mm. The synthetic samples were used in order to represent and understand the chemical phenomena during dissolution processes and the impact on hydraulic and mechanical properties on natural porous materials, with the aim to simulate the chemical effects on geological formations subjected to fluid injection,

such as rock reservoirs. The test protocol was carried out in two stages: (1) to obtain the yield stress and (2) to obtain the time evolution of volumetric strain and horizontal stress during chemical dissolution.

Initially, glass beads and NaCl were mixed under a salt-saturated brine to prevent NaCl dissolution and placed in the oedometer cell. In the first protocol tests, the samples were loaded/unloaded (up to 150 kPa) in order to obtain the yield stress. In the second protocol tests, an initial vertical stress of 5 kPa was applied to ensure the contact between the sample and the loading system, after that the vertical stress was increased to 25 kPa. A constant backpressure of 8 kPa was applied using distilled water with the aim to dissolve the NaCl of the sample. During this stage, the top valve was maintained open and the water permeability and electrical conductivity were measured. The tests ended when the vertical displacement reading was constant and the electric conductivity reached values close to 3 mS/cm, indicating the complete dissolution of NaCl.

Several tests were carried out at controlled temperature room at 22 °C and this experimental protocol was repeated for different concentrations of NaCl (12% and 20% in weight).

2.3. Experimental results

Figure 2a shows the step-loading/unloading curves in terms of void ratio (e) and vertical stress (σ_v) and Fig. 2b shows the same curve in terms of specific volume (v) and mean stress (p) for NaCl concentration of 12%. According to this result, the initial void ratio is $e_0 = 0.43$ and the preconsolidation stress is approximately = 20 kPa. Values for compression index (C_c) of 0.017 and recompression index (C_r) of 0.003 were determined from the curves in Fig. 2a.

Figures 3a shows the time evolution of volumetric strain for loading and NaCl dissolution stages for different NaCl concentrations. During step-loading and NaCl dissolution stages, the samples were consolidated and the volumetric strain decreases to 8 and 17% for NaCl concentrations of 12 and 20%, respectively. So, samples with higher NaCl concentrations achieved larger values of volumetric strains due to grain mass loss during the NaCl dissolution. The same behavior was observed in the tests performed by Shin & Santamarina (2009), where the volumetric strains obtained were about of 2, 4, and 6% for NaCl concentrations of 5, 10 and 15%, respectively.

Figures 3b presents the time evolution of horizontal effective stress at different NaCl concentrations. During the step-loading stage, the horizontal effective stress increases to about 26 kPa for different NaCl concentrations. During the NaCl dissolution, at first, a pronounced horizontal effective stress drop was observed due to the grain mass loss. After that, a rise in the horizontal effective stress is observed due to rearrangement of internal granular structure (development of plastic strains). Increasing of horizontal

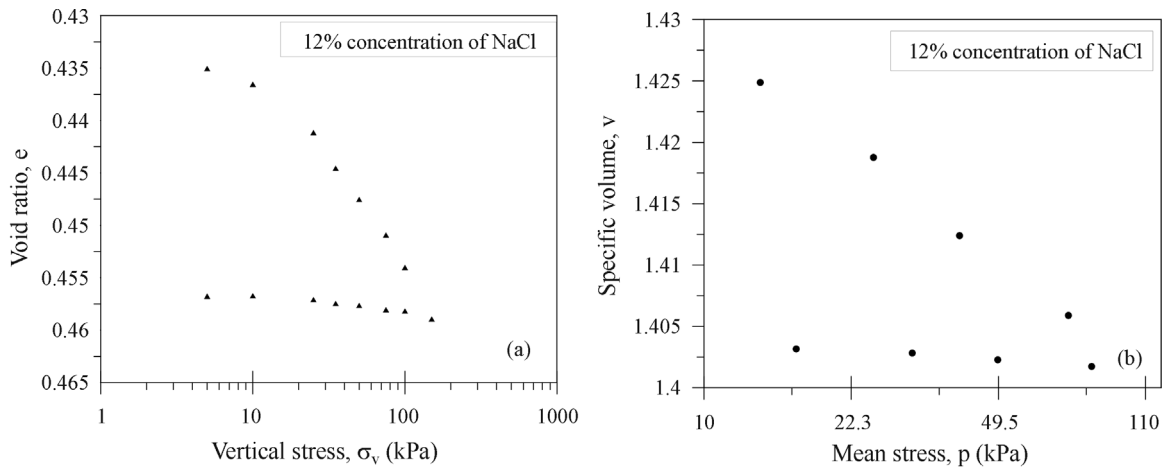


Figure 2 - Step-loading/unloading paths with 12% of NaCl concentration in terms of (a) void ratio vs. vertical stress and (b) specific volume and mean stress.

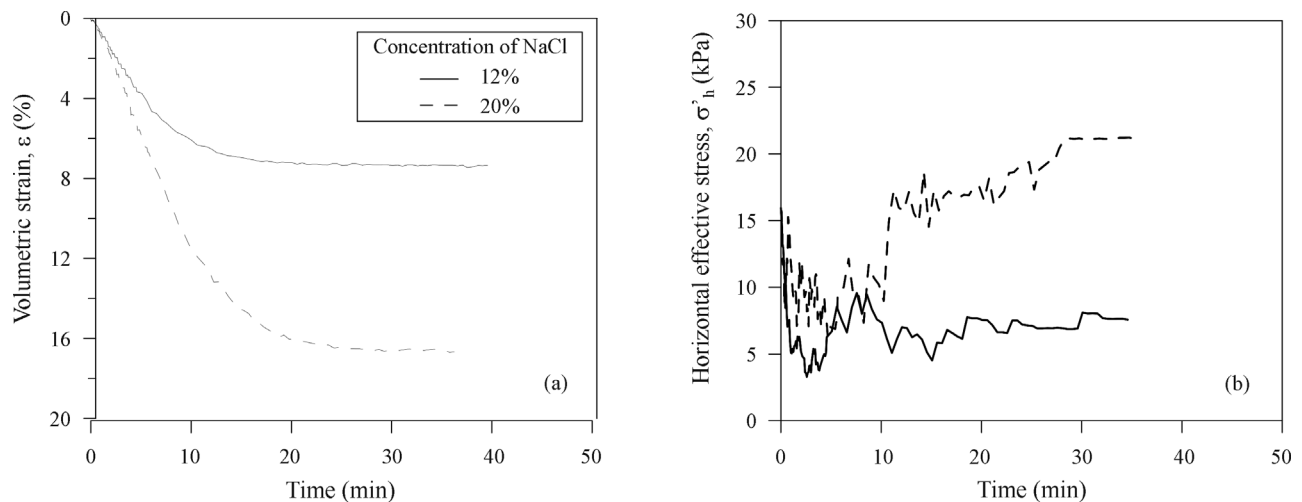


Figure 3 - Time evolution of volumetric strain and horizontal effective stress for NaCl, concentration of 12% and 20%.

effective stress can be only explained by development of compressive horizontal elastic strain. At oedometric conditions (sample is not allowed to deform horizontally) this is also directly related to development of expansive horizontal plastic strain, as it will be shown in the next sections. However, Pereira & Fredlund (2002) used the concept of stress-induced anisotropy to interpret the changes in horizontal stresses during collapse.

Increasing of horizontal effective stress was more strongly observed in the tests with the NaCl concentration of 20%. At the end of the test its value was lower than the initial horizontal effective stress observed for samples with NaCl concentrations of 12%. But for the sample with NaCl concentration of 20%, the final horizontal effective stress is higher than the initial value.

Therefore, the results showed in this paper had a similar behavior with the results presented by Shin & Santamarina (2009). Initially, when water injection begins, hori-

zontal stress decreases due to the loss of sodium chlorite mass. After some minutes of fluid injection, horizontal stress begins to increase due to rearrangement of the internal granular structure. During the entire test, vertical stress is maintained constant and sample volume decreases (compressive vertical strains were observed and horizontal strains were prevented).

Figure 4 presents the time evolution of electrical conductivity during NaCl dissolution for different NaCl concentrations of 12 and 20%. In this figure, a reduction in the electrical conductivity caused by the NaCl dissolution was observed. Initially, the electrical conductivity decreases faster for all NaCl concentrations. However, a faster reduction of electrical conductivity in samples with a lower NaCl concentration was also observed, due to the lower amount of NaCl in the sample. Basically, the dissolution test ended after about 40 min for NaCl concentration of 12 and 20%, when the electrical conductivity reaches values below 3 mS/cm.

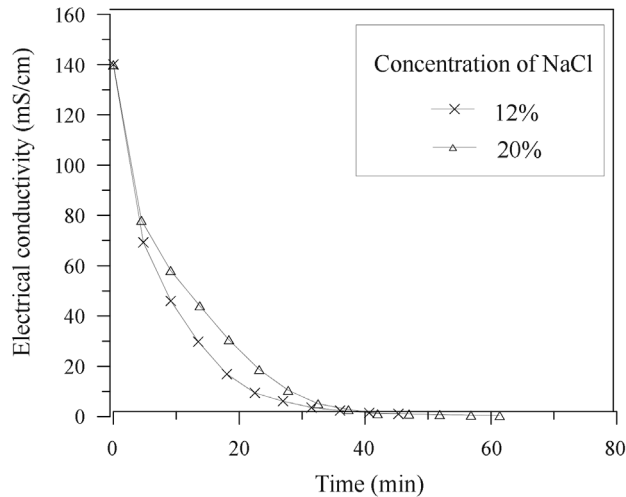


Figure 4 - Time evolution of electrical conductivity for NaCl concentrations of 12 and 20%.

The average permeability obtained during dissolution tests for different concentrations was about 2.6×10^{-5} m/s. Significant variation of the permeability between the different NaCl concentrations was not observed.

3. Mathematical Formulation

In this section the constitutive model proposed by Castellanza & Nova (2004) for bonded materials is described and a modification to include strain and stress changes due to grain mass loss is proposed. The constitutive model was implemented as an extension of the Barcelona Basic Model (BBM) (Alonso *et al.*, 1990) for unsaturated soils, including the cement concentration as a new chemical state variable for the mechanical behavior.

3.1. Constitutive model for bonded materials

The BBM model considers two independent stress variables to describe the behavior of unsaturated soils. They are the net stress ($\sigma' = \sigma - u_a I$) and suction ($s = u_a - u_w$), obtained as a function of total stress and air and water pressures (u_a, u_w). It consists in a hardening elastoplastic model with a yield surface defined as function of net mean stress p , deviatoric stress q and suction s in a three-dimensional space (Alonso *et al.*, 1990).

In order to consider the effect of artificial or natural weathering a modification of BBM is adopted, based on the model proposed by Castellanza & Nova (2004). In this case, the yield function also depends on history variables related to plastic strain and bonding. The yield surface is expressed as:

$$f = f(p, q, s, \varepsilon_v^p, X_d) = q^2 - M^2 (p + p_s)(p_0 - p) = 0 \quad (1)$$

with

$$p = \sigma_m - \max(p_a, p_l); \quad \sigma_m = \frac{\sigma_1 + \sigma_2 + \sigma_3}{3} \quad (2)$$

$$q = \sigma_1 - \sigma_3 \quad (3)$$

where σ_1, σ_2 and σ_3 are the total principal stress, σ_m is the mean stress, ε_v^p is the plastic volumetric strain, M is the slope of the critical state and, p_s is related to shear strength material as function of the suction and chemical weathering. X_d is a scalar index that gives the degree of chemical degradation. Equation 1 gives the shape of the elastic domain (Fig. 5).

In Fig. 5, the two yield surfaces represent the soil under bonded and unsaturated conditions (F_B) and the soil under unbonded (degraded) and saturated conditions (F_A). Herein, the Modified Cam-Clay model was adopted as the reference model to reproduce the unbonded saturated soil behavior. In the proposed model, p_0 is the apparent isotropic preconsolidation stress for the unsaturated and bonded conditions, which is related to suction, saturated unbonded preconsolidation stress, and the chemical weathering expressed by addition of the bonding variable p_m . The relationship is expressed as:

$$p_0 = p \left(\frac{p_0^*}{p^c} \right)^{\frac{\lambda(0) - \kappa}{\lambda(s) - \kappa}} + p_m \quad (4)$$

where p^c is a reference stress, κ is the elastic stiffness parameter, $\lambda(0)$ is the slope of the virgin consolidation line on saturated and isotropic conditions, $\lambda(s)$ is the slope of the virgin consolidation line for isotropic loading at constant suction.

The variable $\lambda(s)$ is expressed as:

$$\lambda(s) = \lambda(0)[(1 - r) \exp(-\beta_s s) + r] \quad (5)$$

where r is the limiting value of soil stiffness for high suction and β_s controls the rate stiffness increase with suction.

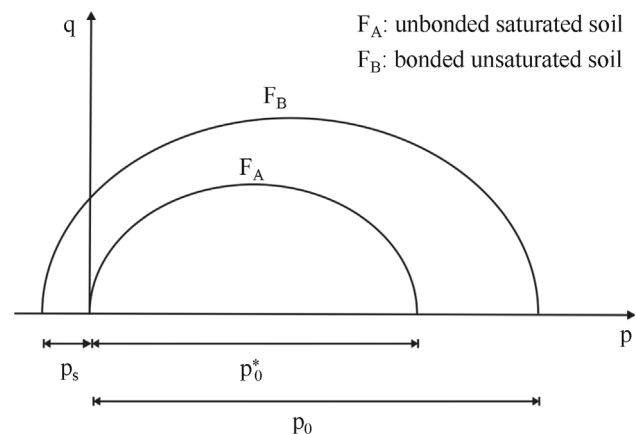


Figure 5 - Yield surfaces for bonded and unbonded soils in p - q plane.

In Eq. 4, the term $p \left(\frac{p_0^*}{p^c} \right)^{\frac{\lambda(0)-\kappa}{\lambda(s)-\kappa}}$ is related to unsatu-

rated condition of porous media (suction) to the apparent preconsolidation stress (Alonso *et al.*, 1990). The variable p_m , which is related to bonding, is given by:

$$p_m = \beta p_t \quad (6)$$

where β is a constant and p_t is an internal variable which controls the bond strength through chemical weathering.

The other important internal variable p_s is related to the increasing of shear strength (cohesion) of the material due to its unsaturation or bonding. It is defined by suction and chemical weathering variable p_i :

$$p_s = k_s + p_t \quad (7)$$

where k describes the increase of the apparent cohesion with suction s .

The variables p_s , p_0^* , p_m and p_t govern the size of the elastic domain. The last two (p_m and p_t) are related to bonding and they are affected by both plastic degradation (induced by stress changes) and chemical weathering (Castellanza & Nova, 2004).

The variable p_t changes due to mechanical and chemical actions and can be expressed as:

$$\dot{p}_t = p_t \left[-\rho_t \left| \dot{\epsilon}_v^p \right| + \frac{\dot{Y}}{Y(X_d)} \right] \quad (8)$$

where ρ_t controls the rate of mechanical degradation, and $Y(X_d)$ is a function which controls the decrease of p_t with the degree of chemical degradation X_d .

$$Y(X_d) = (1 - X_d)^2 \quad (9)$$

When X_d increases mineral precipitation takes place and when it decreases the result is mineral dissolution. As proposed by Castellanza & Nova (2004), X_d ranges from 0 (bonded material) to 1 (totally unbonded material). X_d is directly related to the cement concentration and represents the degree of bonding of the material. Cement concentration is an important variable for this problem as it gives the degree of degradation (weathering) of the bonded soil. In present paper it is proposed a linear correlation between the degree of chemical degradation X_d and the cement mineral concentration C , given by:

$$X_d = \frac{C_0 - C}{C_0} \quad (10)$$

where C_0 is the initial mineral concentration. The variable C is the mineral concentration for a time t of the degradation process and comes from the reactive transport problem, solved simultaneously with the fluid flow and mechanical problems.

The hardening/softening law that relates changes of to volumetric plastic strain is given by the same law for

BBM and Modified Cam-Clay model, based on the Critical State Theory:

$$\frac{dp_0^*}{p_0^*} = d\epsilon_v^p \frac{v}{\lambda(0) - \kappa} \quad (11)$$

where $v = 1 + e$ is the specific volume and e is the void ratio.

Another important element of this formulation is the model for the elastic behavior of the material. Here, the elastic strains is related to changes in stress, suction and chemical degradation as follows:

$$d\epsilon^e = \frac{\kappa}{v} \frac{dp}{p} + \frac{1}{3G} dq + \frac{\kappa_s}{v} \frac{ds}{(s + p_{atm})} + \frac{\alpha \kappa}{v} \frac{dX_d}{p} \quad (12)$$

where G is the shear modulus, κ_s is the elastic stiffness related to suction, p_{atm} is the atmospheric pressure and α is a chemo-elastic parameter. In the present paper, a term related to changes of X_d was introduced in Eq. 12 with the objective to reproduce soil contraction due to mineral mass loss.

3.2. Model validation

A preliminary validation of the proposed model was performed using the results from the experimental program presented in Section 2. The simulations of the oedometer tests were performed with NaCl concentrations of 12 and 20%, mixed with the glass beads. In order to validate the constitutive model a uniform mineral dissolution was imposed along the sample. In the numerical simulations a one-dimensional finite element mesh of 20 elements was adopted. The boundary conditions for the mechanical problem are: applied load at the top of the sample and no displacement is allowed at the bottom. These geometry and boundary conditions presume that the cell is rigid and the friction between the cell and the sample is negligible.

The material parameters used in the simulations are presented in Table 1. Typical values for sands (granular soils) were adopted for Poisson's ratio (ν), friction angle (ϕ) and slope of the critical state line (M). The values of

Table 1 - Material parameters for HMQ analysis.

Parameters	Sample
Slope of the unloading-reloading line, κ	$1.4e^{-3}$
Slope of virgin consolidation line, λ	$7.2e^{-3}$
Preconsolidation stress	20 kPa
Poisson's ratio, ν	0.40
Permeability, k	2.6×10^{-5} m/s
Friction angle, ϕ	30°
Slope of the critical state line, M	1.00
Internal variable related to the strength of bonds, p_t	0.010
Harding parameter of mechanical degradation, ρ_t	10.0

preconsolidation stress, slope of the unloading-reloading line (κ), slope of virgin consolidation line (λ) and the water permeability (k) were calibrated from the tests results.

Figures 6a and 7a show the time evolution of volumetric strain of experimental and predicted results for different NaCl concentrations of 12 and 20%, respectively. Figures 6b and 7b display the corresponding time evolutions of horizontal stress (experimental and predicted results). In these figures, it can be seen that the simulated and experimental results showed a good agreement in both volumetric strain and horizontal stress evolutions for 12 and 20% of NaCl concentrations. During the NaCl dissolution, it can be observed that the numerical results could represent the pronounced horizontal effective stress drop as well as decreases of volumetric strain due to a grain mass loss. The model was also able to represent a rise in the horizontal stress due to solid matrix rearrangement, as observed in the

experimental results. However, it can be seen in Fig. 7b (NaCl concentration of 20%) that the model does not fit perfectly the experimental data, where higher values of horizontal stress were measured. Improvements of the numerical model are necessary in order to achieve higher values of horizontal stress, which are related to the plastic behaviour of the material.

A good representation of the volumetric strain was obtained for the values adopted for the chemo-elastic coefficient α (Eq. 12). The calibration of model for the two artificial soils gave the values of 0.07 and 0.165 for NaCl concentrations of 12 and 20%, respectively.

Figure 8a and 8b show the evolution of hardening variables for NaCl concentrations of 12 and 20%, respectively. In these figures, it can be observed that the samples (NaCl concentrations of 12 and 20%) show similar behavior with respect to hardening variables during mineral dis-

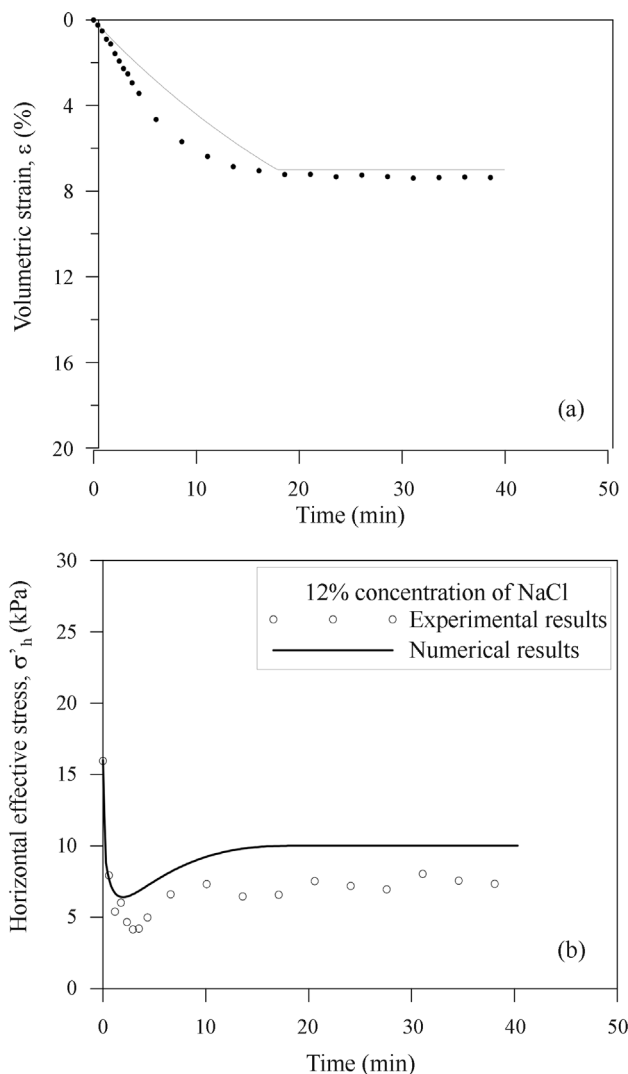


Figure 6 - Time evolution of volumetric strain and horizontal effective stress of experimental and numerical results for NaCl concentration of 12%.

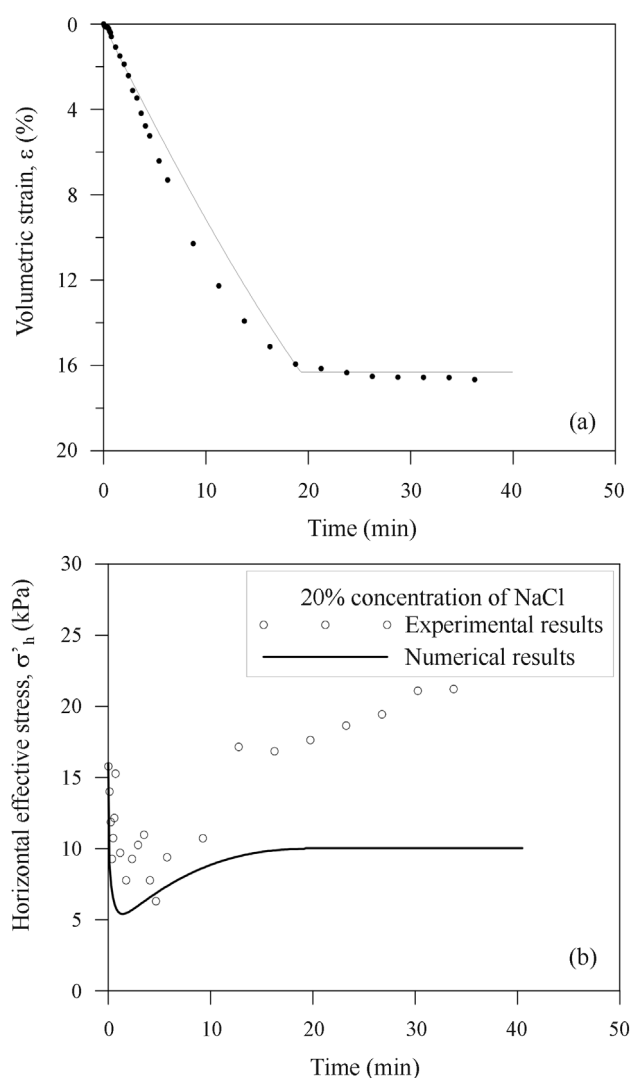


Figure 7 - Time evolution of volumetric strain and horizontal effective stress of experimental and numerical results for NaCl concentration of 20%.

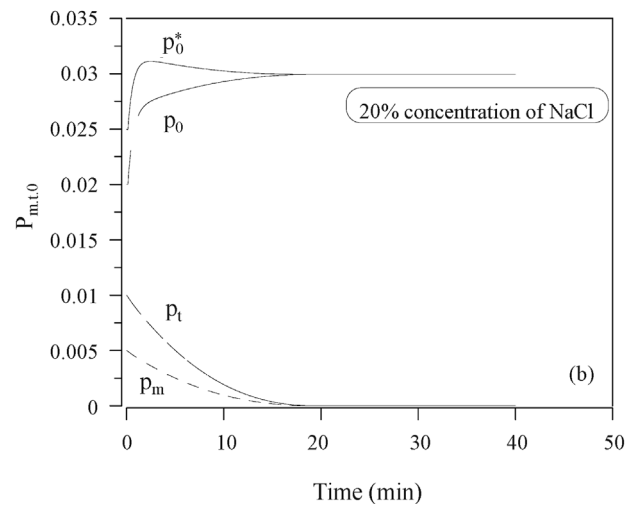
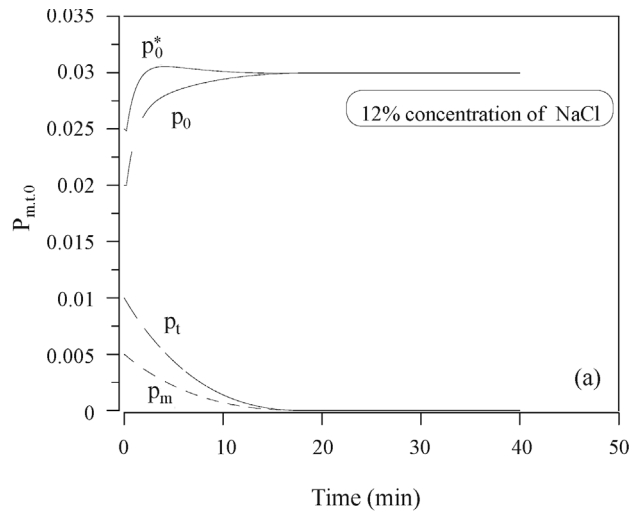


Figure 8 - Evolution of hardening variables during mineral dissolution for NaCl concentrations of 12 and 20%.

solution. As expected, the parameters p_m and p_t decrease when chemical degradation takes place. As the artificial soil is close to the normally consolidated state, a hardening of the material is also observed, where increases as a result of the development of compressive volumetric plastic strain (as described by Eq. 11).

Figures 9a and 9b show the evolution of horizontal strains during mineral dissolution. In both tests it is observed the evolution of negative horizontal plastic strain, which (swelling) is related to irreversible solid matrix rearrangement. As total horizontal strain is not allowed in the oedometer test, positive horizontal elastic strain (compression) takes place to maintain the equilibrium, which results in a more compressive state of stress as the horizontal stress increases. The value of the horizontal plastic strain is equal in module to the values of horizontal elastic strain, so, .

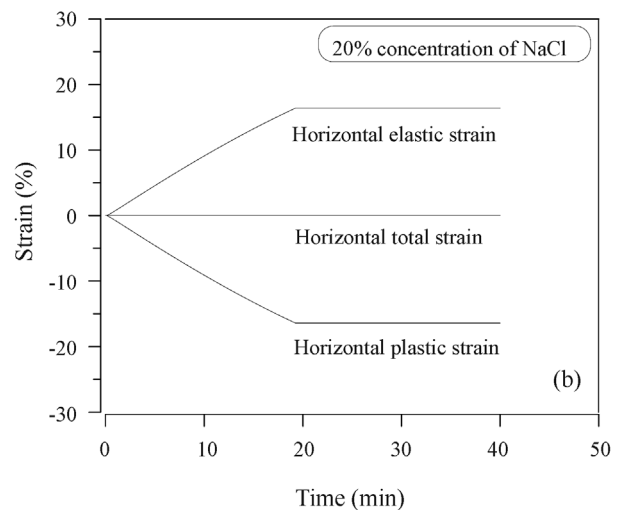
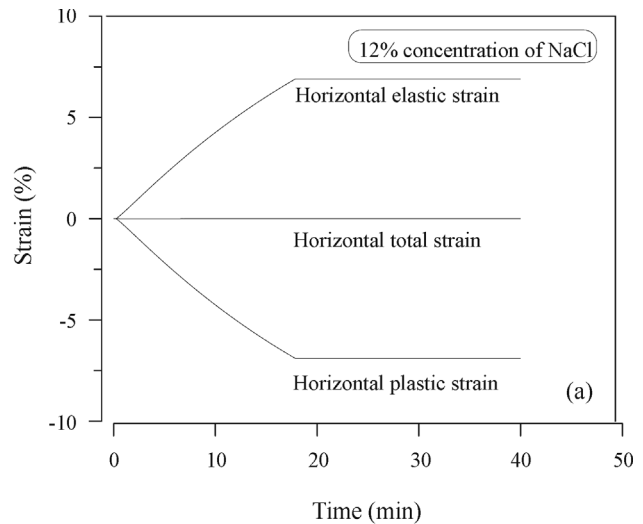


Figure 9 - Evolution of elastic and plastic horizontal strains during mineral dissolution for NaCl concentrations of 12 and 20%.

4. Conclusions

A series of tests along step-loading/unloading and NaCl dissolution paths were performed to study the geomechanical effects caused in the porous medium during mineral dissolution. The tests were carried out in a fully-instrumented oedometer cell with LVDT and strain gauges, specially constructed to measure horizontal stress.

Results of a comprehensive experimental programme on synthetic samples (mixture of glass beads and NaCl) at different NaCl concentrations were presented and discussed in terms of the simultaneous measurements of volumetric strains and horizontal stresses during the dissolution tests.

During NaCl dissolution stage, sample volume decreases. Samples with higher NaCl concentrations achieved larger values of volumetric strains. A pronounced horizontal effective stress drop was observed and

then it starts to increase. This behavior was observed for the different NaCl concentrations but it was more pronounced in the tests with the NaCl concentration of 20%. The K_0 values were affected by the mineral dissolution process, as a result of chemically induced pore collapse and solid matrix rearrangement.

Encouraging agreement has been found concerning the validation of the proposed formulation. During the NaCl dissolution, numerical simulation could represent the pronounced drop of sample volume. The model was also able to reproduce the changes of horizontal stress observed in the experiments. For the sample with higher NaCl concentration (20%), numerical results of horizontal stress did not reach the experimental values, but they were in qualitative agreement.

Acknowledgments

The authors acknowledge the financial support from PETROBRAS, CNPq (Brazilian National Research Council) and Foundation CMG (Chair on Reservoir Simulation at UFPE).

References

- Alonso *et al.* (1990). A constitutive model for partially saturated soils. *Geotechnique*, 40(3):405-430.
- Alonso, E.E. & Gens, A. (1993). On the mechanical behavior of arid soils. *Proc. 1st International Symposium on Engineering Characteristics of Arid Soils*, London, England, v. 1, pp. 173-205.
- Castellanza, R. & Nova, R. (2004). Oedometric tests on artificially weathered carbonatic soft rocks. *J. Geotech. & Geoenviron. Eng.*, 130(7):728-739.
- Chen *et al.* (2009). Effects of mechanical dispersion on the morphological evolution of a chemical dissolution front in a fluid-saturated porous medium. *J. of Hydrology*, 373(1-2):96-102.
- Costa *et al.* (2008). Numerical modelling of hydro-mechanical behaviour of collapsible soils. *Communications in Numerical Methods in Engineering*, 24(12):1839-1852.
- Fogler, H.S. & Rege, S.D. (1989). Competition among flow, dissolution, and precipitation in porous media. *AIChE J.*, 35(7):1117-1185.
- Gens, A. (2010). Soil-environment interactions in geotechnical engineering. *Geotechnique*, 60(1):3-74.
- Gens, A. & Nova, R. (1993). Conceptual bases for a constitutive model for bonded soils and weak rocks. *Proc. International Symposium On Geomechanical Engineering of Hard Soils and Soft Rocks*, Athens, v. 1, pp. 485-494.
- Gouze *et al.* (2001). Computing permeability change in sedimentary reservoirs including clays: application to the Bray fault zone (Paris Basin). *B. Soc. Geol.*, 172(4):427-436.
- Guimarães *et al.* (2006). THM and reactive transport analysis of expansive clay barrier in radioactive waste isolation. *Communications in Numerical Methods in Engineering*, 22(8):849-859.
- Guimarães *et al.* (2007). Coupled thermo-hydro mechanical and chemical analysis of expansive clay subjected to heating and hydration. *Transport in Porous Media*, 66(3):341-372.
- Guimarães *et al.* (2009). Influence of mechanical constitutive model on the coupled hydro-geomechanical analysis of fault reactivation. In: *Reservoir Simulation Symposium - Society of Petroleum Engineers SPE*, The Woodlands, Texas, SPE-119168-PP(CD-ROM).
- Guimarães *et al.* (2013). A chemo-mechanical constitutive model accounting for cation exchange in expansive clays. *Geotechnique*, 63(3):221-234.
- Korsnes *et al.* (2008). Enhanced chemical weakening of chalk due to injection of CO₂ enriched water. In: *International Symposium of The Society of Core Analysts*, Abu Dhabi, October 29-November 2 2008, v.1, pp. 1-12.
- Lins *et al.* (2012). Analysis of the carbon dioxide (CO₂) injection in carbonate rocks. *Cientec.*, 4(2):84-91.
- Melo *et al.* (2013). Análise numérico-experimental de rochas carbonáticas sintéticas submetidas à injeção de um fluido reativo. In: *2 °Congresso Brasileiro de CO2 na Indústria de Petróleo, Gás e Biocombustíveis*. (CD-ROM).
- Navarro *et al.* (2010). A constitutive model for porous rock including effects of bond strength degradation and partial saturation. *International Journal of Rock Mechanics & Mining Sciences*, 47(8):1330-1338.
- Olivella *et al.* (1994). Nonisothermal multiphase flow of brine and gas through saline media. *Transport in Porous Media*, 15(3):271-293.
- Pereira, J.H.F. & Fredlund, D.G. (2000). Volume change behavior of collapsible compacted gneiss soil. *J. Geotech. Geoenviron. Eng.*, 128(2):184-185.
- Shin, H. & Santamarina, J.C. (2009). Mineral dissolution and the evolution of K_0 . *J. of Geotech. & Geoenviron. Eng.*, 135(8):1141-1147.
- Silva, N.V.S. (2012). Modeling the Phenomenon of Capillary and Chemical Compaction in Petroleum Reservoirs. PhD Dissertation, Department of Civil Engineering, Federal University of Pernambuco, 136 p.
- Uchaipichat, A. (2011). An elasto-plastic model for cemented soils under unsaturated condition. *European Journal of Scientific Research*, 60(2):231-236.

Alternative Method for Analysing Hydromechanical Behaviour of Unsaturated Soils

M.M.A. Mascarenha, M.P. Cordão Neto, M.T.M.G. Silva

Abstract. The suction-control techniques commonly used for laboratory studies of mechanical behaviour of unsaturated soils are much more time consuming than standard soil mechanics tests. In addition, few laboratories have the required apparatus for testing unsaturated soils. This paper proposes an alternative method of analysing hydromechanical behaviour of unsaturated soils with high-porosity. The method is divided in three tasks: 1) verification of the effect of void ratio changes on the water retention curve using filter paper; 2) determining water content changes by evaporation under the same test conditions; and 3) performing saturated and unsaturated consolidation tests. Unsaturated tests make use of samples that are less than 100% saturated and there is no suction control during the test. Therefore, only initial water content is known. Significant suction changes take place due to void closure and evaporation while testing. The results obtained using the proposed methodology showed the stress and suction path and enhance the understanding of the hydromechanical behaviour of unsaturated soils. The results also showed that analyses of water content alone cannot explain some unexpected results, such as: 20% initial water content samples present less deformation than 16% samples.

Keywords: unsaturated soil, hydromechanical behaviour, water content control test, filter paper method.

1. Introduction

The study of unsaturated soil mechanics has shown great progress in recent decades due to the need to solve practical engineering problems such as designing and maintaining foundations, pavements, dams, embankments, and canals subject to varying degrees of saturation during construction as well as during the design lifetime.

Paradigms have changed significantly. It was natural that first approaches considered mechanical and hydraulic behaviour uncoupled (Bishop, 1959; Matyas & Radhakrishna, 1968; and Fredlund *et al.*, 1978). Afterwards, several more recent papers have examined their interaction, *i.e.*, mechanical and hydraulic behaviour coupled (Vaunat *et al.*, 2000; Wheeler *et al.*, 2003; Sheng *et al.*, 2004, Della Vecchia, *et al.*, 2012).

Modern testing techniques for characterization of soil microstructure have led to studies of hydromechanical behaviour of unsaturated soils based on microstructural characterization and constitutive models coupling these three aspects (Gens & Alonso, 1992, Alonso *et al.*, 1999 and Alonso *et al.*, 2011, Alonso *et al.*, 2013).

Currently, characterizing and obtaining constitutive parameters of unsaturated soils is time-consuming and therefore testing and acquisition of equipment with suction control techniques, using advanced technology that is not available at most geotechnical laboratories, can be costly.

Accordingly, developing a methodology to evaluate the influence of suction on the mechanical behaviour of soils using basic tests in common use would be a significant

contribution for the technical community since unsaturated soil concepts could then be used in geotechnical engineering practice.

In this context, this paper proposes an alternative method of measuring suction using the filter paper technique combined with gravimetric water-content control test.

2. Methodology

This section describes the soil used, sample preparation procedure and details of the gravimetric water content control test.

2.1. Material

The soil used in this study is a lateritic residual soil consisting of sandy red clay with over 50% porosity in its natural state extracted from the experimental field of the Post-graduation program of Geotechnics of the University of Brasília at 2 m depth. Kaolin is the predominant clay mineral however high levels of iron and aluminium oxide are also present (Cardoso, 1995; Araki, 1997).

Another particular feature of this soil is the high volumetric collapse produced by increasing the degree of saturation, even with loading held constant; hence the soil is sometimes referred to as a metastable soil.

Additionally, structural analysis showed that the soil consists of micro and macropores (Camapum de Carvalho *et al.*, 1994). The existence of micro and macropores results in a bimodal water retention curve with two air-entry values

Márcia Maria dos Anjos Márcia Maria dos Anjos Mascarenha, DSc., Escola de Engenharia Civil e Ambiental, Universidade Federal de Goiás, Goiânia, GO, Brazil. e-mail: marciamascarenha@gmail.com.
Manoel Porfírio Cordão Neto, DSc., Departamento de Engenharia Civil e Ambiental, Universidade Federal de Brasília, Brasília, DF, Brazil. e-mail: mporfirio76@gmail.com.
Tâmara de Moraes Guimarães Silva, MSc., Instituto Federal de Goiás, Anápolis, GO., Brazil. e-mail: mtamaramgs@gmail.com.
Invited Article, no discussion.

(AEV), one for the microstructure and the other for the macrostructure (Camapum de Carvalho & Leroueil, 2000). The soil continues to show bimodal structure and to maintain a high void ratio even when it is subjected to compaction (Otálvaro, 2013).

Table 1 shows specific gravity (G_s), consistency index (w_L and w_p), water content for compaction (w_{com}) and void ratio (e) of this soil.

Figure 1 shows two distinct particle size distribution curves of this very soil, where the solid line represents the curve when using a dispersing agent and the dashed line represents the curve when no dispersant agent is used. The soil is classified as a silt with low plasticity (ML) (Unified Classification System). However, it does not show hydraulic and mechanical behaviour consistent with this classification. Indeed, the hydraulic and mechanical behaviours are associated with the high content of clay, found in clusters which are strongly responsible for the hydromechanic responses, and may be observed when using dispersant agent.

The interpretation of results from mechanical tests, such as the direct shear test, requires particular care for this type of soil due to the fact that clay clusters control the soil mechanical response. The clay clusters are heavily affected when there is a change in the degree of saturation or stress state. Thus, samples of the same soil with different stress state and degree of saturation may behave as dense sand or normally consolidated clay.

2.2. Preparing samples

Semi-statically compacted samples were obtained to eliminate the natural heterogeneity found in soil samples. Camapum de Carvalho *et al.* (1987) asserted that the use of

Table 1 - Basic soil characterization (Silva, 2009).

w_L (%)	w_p (%)	w_{com} (%)	G_s	e
36	26	24	2.74	1.16

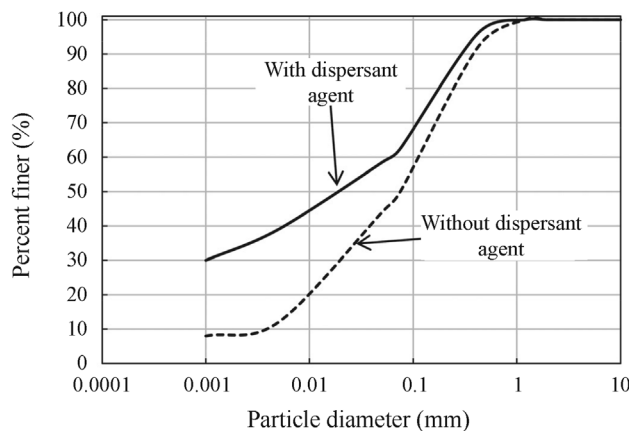


Figure 1 - Particle size distribution curves (Guimarães, 2002).

static compaction ensures more repeatability of soil properties and is also in agreement with the behaviour of compacted soils in the field.

The initial idea was to statically compact the sample with the void ratio and water content values found in the field, which were obtained by Silva (2007). However moulding in this state was not possible since the sample fragmented. Such behaviour is related to the fact that the natural soil contains bonding (iron and aluminium oxides) which allows the highly porous structure to exist. However, the process of preparing soil for the compaction test destroys the bonding, thus the same structure cannot be reproduced in laboratory.

For this study, the samples were compacted with the same water content as in the field ($w = 20\%$). The compaction energy was below Standard Proctor resulting in samples with dry unit weight close to the soil in its natural state, as shown in Fig. 2.

Figure 3 shows the void ratio distribution for samples used by Silva (2009) for direct shear and consolidation tests. The methodology used proved to be efficient since void ratios of natural samples ranged from 1.08 to 1.23 with average of 1.16, which was the target void ratio. In addition, the coefficient of variation (COV) was 3.5%.

2.3. Tests performed

Water content control test, filter paper, and consolidation tests were performed for this study. Detailed descriptions of tests and conditions in which they were performed are found in this section.

Soil samples obtained as above described in section 2.2 were subjected to consolidation tests in accordance with NBR 12007 (ABNT, 1990). There were two different testing objectives: one was to assess soil compressibility in different initial water content conditions; the other was to obtain the void ratios at which retention curves would be performed.

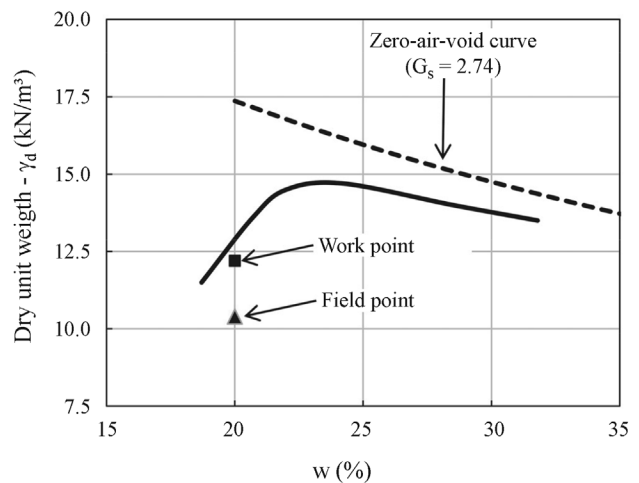


Figure 2 - Compaction Curve - Standard Proctor Energy (Silva, 2009).

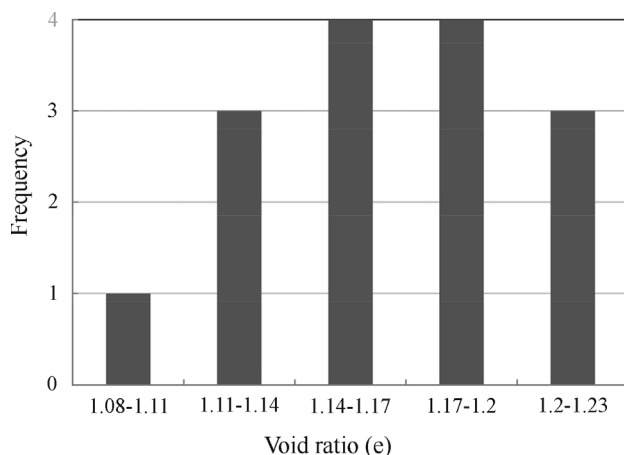


Figure 3 - Range of samples' void ratios.

In order to evaluate the effect of suction on soil compressibility, tests were carried out with different initial water contents (16%, 18%, 20%, 22%, and 24%) and in the saturated state. Samples at water content levels below the compaction water content ($w = 20\%$) were air-dried to the required value. Samples at water content levels greater than the compaction water content were wetted, after the air-drying stage, by dripping water up to their required water content. The latter samples required 24 h to reach equilibrium. For the saturated state, the sample underwent saturation for 12 h before the test. To verify the collapse potential, the 22% and 24% water content samples were flooded, after stabilization of deformability readings were reached, at a vertical load of 1000 kPa.

When consolidation tests are performed under unsaturated conditions with no suction control, it is a general agreement to say that these tests were performed under constant water content. However, there is some natural loss of water content in the course of testing. Therefore, in order to determine water content values during testing, the followed methodology was proposed.

A soil sample was compacted in the conditions mentioned in the section 2.2. Specimens were then moulded from this sample in a similar way of those prepared for standard consolidation tests. Then, the soil specimens were held inside the oedometric cell within the moulding ring, with filter paper and porous stones at its upper and lower faces in order to simulate the conditions for the consolidation tests. Testing took place over a period of 24 h during which the weights of the soil specimen and temperature at the time of weighing were recorded simultaneously thus, the evolution of loss of water content to the environment could be determined.

Water evaporation rate is known to be related to soil water content; therefore ideally this test would ideally be conducted in samples with different initial water content values. However, as discussed in section 3.1, errors due to

the use of a model obtained from a single water content value is irrelevant.

Moreover, in addition to the variation in water content, there is the effect of void ratio variation on suction values. Therefore, to determine suction values throughout the consolidation tests, not only the variations of water content (determined by water content loss tests) should be known, but the effects of the void ratios on the retention curve are also required. Thus, water retention curves for three different void ratios were determined.

In order to determine the void ratios at which retention curves would be performed, Silva (2009) carried out the previously mentioned consolidation tests for both saturated and unsaturated conditions and the results are shown in Fig. 4. Thus, water retention curves were determined for three different void ratios: compacted sample, (point A); unsaturated condition after loading and unloading cycle (point B) and saturated condition after loading and unloading cycle (point C).

The filter paper technique procedure proposed by Marinho (1994) was used to obtain the water retention curves. Whatman No. 42 filter paper, which has the calibration curves previously determined, was used for the tests. Note that the tests were performed both in wetting and drying (mixed) paths.

3. Results and Discussion

This section presents and analyses the results used to obtain soil parameters for the unsaturated condition. Subsequently, from these parameters, the stress-strain curves of soil are analysed with different initial water contents emphasizing the effects of initial water content and variation of suction during the test.

3.1. Time dependence of water content

As previously mentioned, it is normally assumed that water content remains constant during consolidation tests

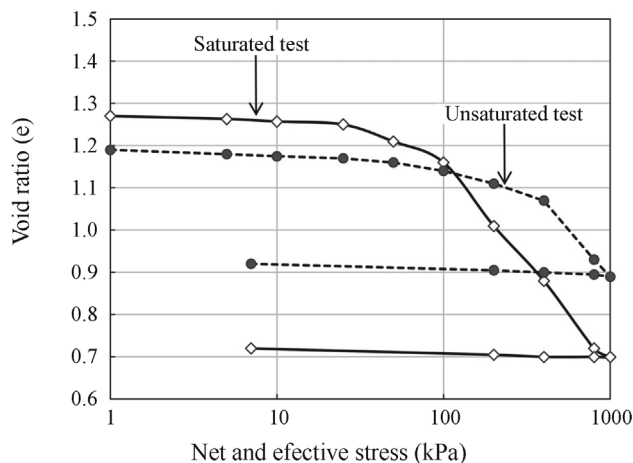


Figure 4 - Determination of points for retention curve tests (Silva, 2009).

with initial water content known, thus sample suction may thereafter be evaluated. However, samples tend to lose water to the environment during testing. In order to measure the amount of water lost, the water content control test described in the previous item was used.

The results for variation of water content over time are shown in Fig. 5. From this figure, empirical equations may be obtained to calculate sample water content for any given time t after start of testing. Two ratios are used - one for times of less than 240 min (6 h) and the other for over 240 min. Equations 1 and 2 below show these ratios.

$$w_c = w_i - 0.0035t \text{ for } t < 240 \text{ min} \quad (1)$$

$$w_c = w_k - 0.0017(t - 240) \text{ for } t > 240 \text{ min} \quad (2)$$

where w_c - corrected water content; w_i - initial water content; w_k - corrected water content for time 240 min and t - time elapsed from start of testing.

To demonstrate the potential of this technique, Table 2 shows that water content measurements for the samples subjected to consolidation tests are in good agreement with those predicted by Eqs. 1 and 2. Since the 22% and 24% initial water content samples were flooded at the end, it was not possible to check whether the values estimate for variation of water content over time were consistent with actual values. Due to the good results obtained for samples with less than 20% water content, the same is expected for samples at higher levels of water content.

Due to water content and void ratio variations, suction changes in the course of the consolidation test per-

Table 2 - Mean water content measured in tests and estimated from equations.

Sample	$w_{measured}$ (%)	$w_{estimated}$ (%)
16%	13.8	13.4
18%	15.8	15.4
20%	16.7	16.1

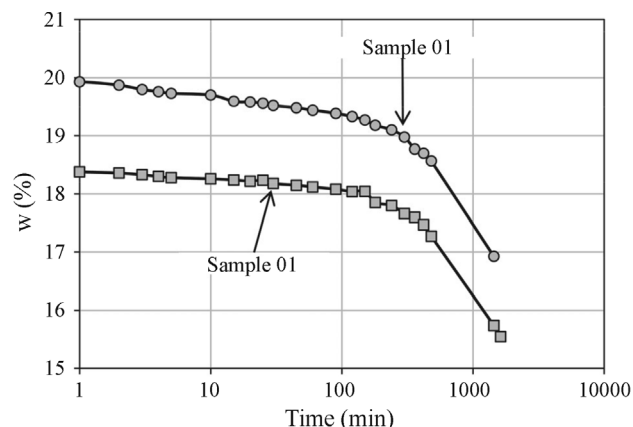


Figure 5 - Water content and time relationship.

formed. A key requirement to obtain suction values during testing is to know how the water retention curve is affected by the void ratio, which is discussed in the next item.

3.2. Modelling the water retention curve

Figure 6 shows the retention curves obtained by Silva (2009) for different void ratios (0.77, 0.97 and 1.16) in relation to soil water content ($e_w = Se$). It is also shown the water retention curves data for void ratio of 1.6 obtained by Guimarães (2002) and Silva (2007) using undisturbed sample from a depth of 2 m.

According to Romero & Vaunat (2000), water present in the soil may be stored in two ways: in the macrostructure, in the form of free and meniscus water, in which active suction is related to capillarity; and in the microstructure, as adsorbed water; suction under these conditions is governed by physicochemical bonds. Thus, soil water content is the sum of two factors, namely macroscopic (w^M) and microscopic water content (w^m). This fact is clearly seen in soil water retention curves (Fig. 6).

In this way, Fig. 6 shows experimental data coinciding in terms of suction values for water content (e_w) below 0.44, which corresponds to the water found in the micropores. On the other hand, void ratio variations only affect the retention curve behaviour at values below 100 kPa (corresponding to $e_w > 0.44$), in other words, significant on the macrostructural level.

The equation used for mathematical representation of the water retention curve of experimental data was proposed by Durner (1994), who modified the van Genuchten (1980) equation in order to extend its use to bimodal curves, typical of tropical soils as shown as following.

$$e_w = e_{wL} \left[\frac{1}{1 + (\alpha_L (u_a - u_w))^{n_L}} \right]^{m_L} + e_{wS} \left[\frac{1}{1 + (\alpha_S (u_a - u_w))^{n_S}} \right]^{m_S} \quad (3)$$

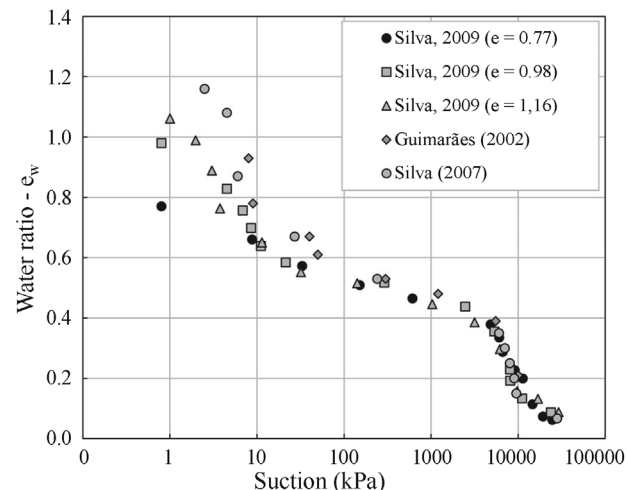


Figure 6 - Retention curves as a function of soil water content.

where e_w is the soil water content, and e_{wL} is the macropore void ratio; α_L is related to the air-entry value for macropores, n_L is the slope of the line that relates macropore water content and suction; m_L is the slope of the line that relates water content and suction in the transition region, and e_{wS} is the micropore void ratio; α_S is related to air entry value for micropores; n_S is the slope of the line that relates micropore water content and suction, and m_S is the slope of the line that relates water content and suction after hygroscopic soil water content value. Note that parameters m_L and m_S are obtained from n_L and n_S as follows:

$$m_L = 1 - \frac{1}{n_L} \tag{4}$$

$$m_S = 1 - \frac{1}{n_S} \tag{5}$$

Figure 7 show the relationship between Pore Size Density (PSD) and Water Retention Curve (WRC). It also shows the relationship between the Air Entry Value for the micropores (AEVs) and the dominant micro pore size α_S is determined. The PSD and WRC correlation helps to understand the modelling process of WRC for different void ratios.

Likewise, as previously mentioned, the parameters e_{wS} and n_S are related to the distribution of pores in the microstructure. Thus, as Romero & Vaunat (2000) showed, the microstructure is the part of the soil not affected by loading paths, these values are constant for all samples studied, even with different void ratios and moulding processes since compaction only alters the macrostructural level of soil structure. Findings showing microstructure pore distribution remaining unchanged with loading paths have been reported by Simms & Yanful (2002), Romero *et al.* (2005), Buenfil (2007), and Mascarenha (2008).

In the macrostructure, on the other hand, the reduction of void ratio causes the closure of the macropores, hence reduction of the values of e_{wL} and n_L . Moreover, this reduction leads to the increase of the macropore air-entry

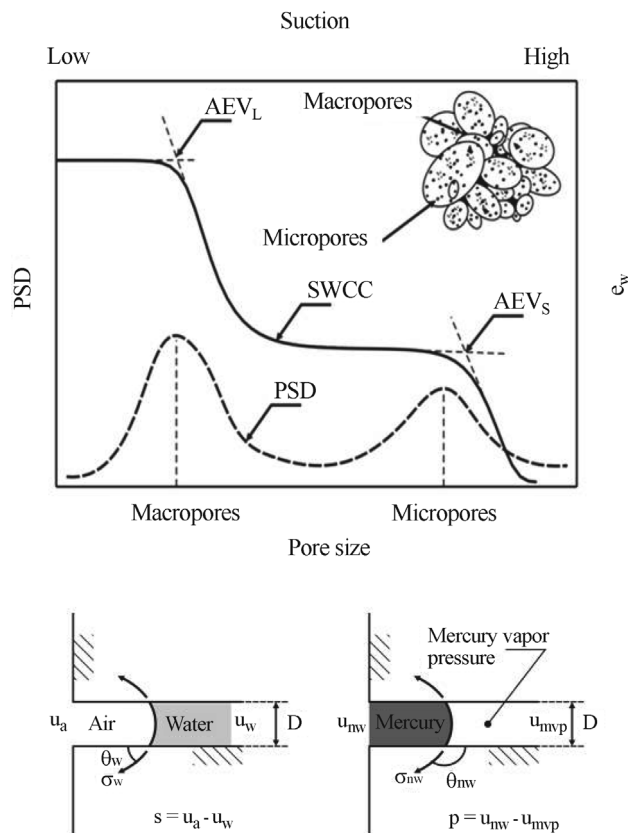


Figure 7 - Analogy between pore size density (PSD) and water retention curve (WRC) (modified from Otálvaro, 2013).

values (AEV_L) and reduction of the values of α_L . Based on these points, experimental data of water retention curves and respective fitting curves are shown in Fig. 8. The fitting parameters used are presented in Table 3.

Figure 9 shows the values of the parameters e_{wL} , α_L e n_L as functions of the void ratios from experimental data of Silva (2009). Note that for the void ratio interval shown, there is a clear correlation between the parameters associated with the macrostructure and the global void ratio. Fur-

Table 3 - Retention curve fitting parameters.

Parameters	Silva 2009			Silva 2007	Guimarães 2002
	$e = 1.16$	$e = 0.98$	$e = 0.77$	$e = 1.57$	$e = 1.60$
Macrostructure					
e_{wL}	0.72	0.54	0.33	1.14	1.14
α_L	0.55	0.35	0.19	0.35	0.35
n_L	1.80	1.70	1.50	1.70	1.70
m_L	0.44	0.41	0.33	0.41	0.41
Microstructure					
e_{wS}	0.44	0.44	0.44	0.44	0.44
α_S	1.5×10^{-4}				
n_S	2.5	2.5	2.5	2.5	2.5
m_S	0.6	0.6	0.6	0.6	0.6

thermore, for this interval, the correlation is linear for all parameters, as seen in the Eqs. 6 to 8.

It is worth mentioning that no experimental data from Silva (2007) and Guimarães (2002) were used in the fittings, since these water retention curves were obtained from undisturbed soil samples in which bonding agents lead to a pore size distribution at microstructural level different from that of the compacted sample.

$$ew = (1.00e - 0.44) \left[\frac{1}{1 + ((0.92e - 0.53)(u_a - u_w))^{0.77e + 0.92}} \right]^{\frac{0.77e - 0.08}{0.77e + 0.92}} + 0.44 \left[\frac{1}{1 + (0.00015(u_a - u_w))^{2.5}} \right]^{0.6} \quad (9)$$

Once the relationships between suction, water content and void ratio are known they may be used to determine the suction path during the tests.

3.3. Stress-strain relation in unsaturated soil

Figure 10 shows compression curves for the samples tested with different initial water content values. Generally,

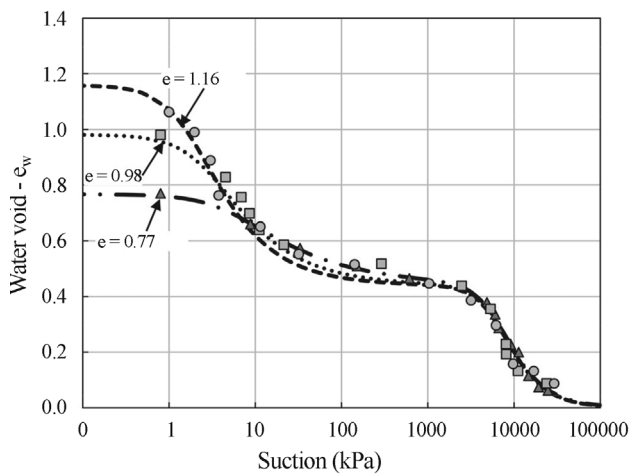


Figure 8 - Retention curve fittings as a function of soil water content.

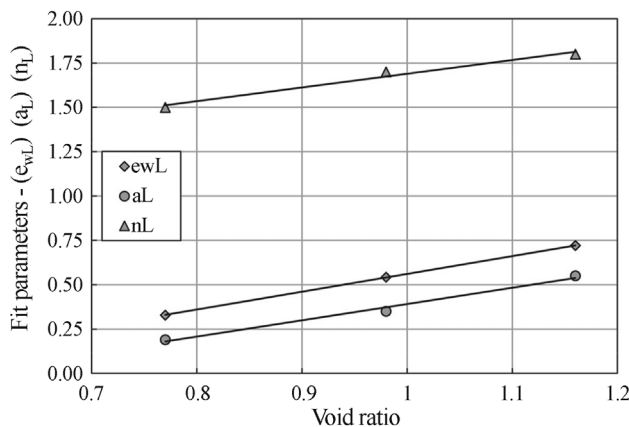


Figure 9 - Retention curve fitting parameters as a function of void ratio.

$$e_{wL} = 1.00e - 0.44 \quad (6)$$

$$a_L = 0.92e - 0.53 \quad (7)$$

$$n_L = 0.77e + 0.92 \quad (8)$$

Using Eqs. 6 to 8 combined with Eqs. 3 to 5, modeling of the retention curve may be completed. Table 3 shows the parameters associated with microstructure and the final equation is given by:

the results are as expected with deformability rising as initial soil water content rises. The only exception to this is seen in the results from the sample at 16% initial water content, which will be analysed in detail in this section.

All samples have two loading components related to the increase of vertical stress and suction changes. In this case, suction changes arise from both the sample water content and void ratio decreasing in the course of testing. Fig-

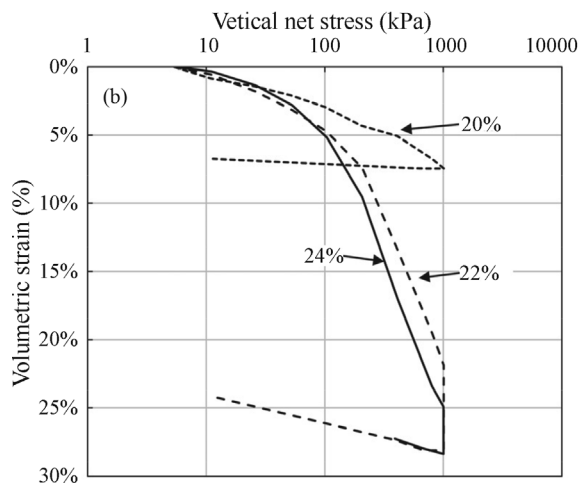
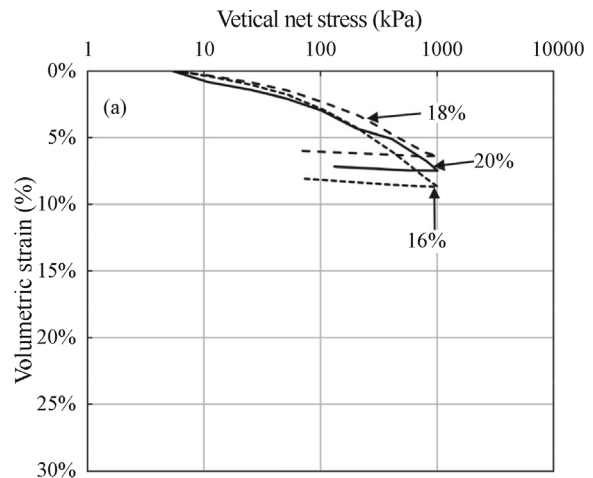


Figure 10 - Volumetric deformations of the consolidation test (a) 16, 18 and 20% initial water content samples (b) 20, 22, and 24% initial water content samples.

ure 11 shows water content and suction variation for each sample during the test. Furthermore, these paths are compared with the water retention curves, which allow understanding particular aspects to be discussed along this section. The paths shown in Fig. 11 were obtained using Eqs. 1, 2 and 9.

An analysis of Fig. 11 shows that although the samples have the same structure, the effect of water content variation is different in each case. For example, in the higher (22% and 24%) water content samples there is outflow of water from soil macrostructure, while in the lower water content (16%) sample, water flows out of the microstructure.

This factor helps to explain two aspects observed in the soil behaviour shown in Fig. 10: different behaviour for samples with different water content and the fact that the 16% water content sample showed larger volumetric deformations than the 18% and 20% water content samples.

On the other hand, the higher water content samples (24% and 22%) show low suction values throughout the test: for the 24% water content sample suction ranges from 7 to 30 kPa and for 22% from 11 to 78 kPa. Despite the short range of suction values, the samples experiences accentuated collapse due to saturation, as seen in Fig. 10, which is associated with the pore-size distribution, as explained in the following.

When suction is reduced to zero by saturating the 22 and 24% initial water content samples, its effect are experienced by the macropores range as shown in Fig. 11. Thus suction plays a key role in the soil structural stability, since its reduction leads to closing macropores and therefore volumetric collapse.

Figure 12 shows the distribution of pores in the soil obtained by indirect measurements using the methodology reported by Mascarenha (2008) and Otálvaro (2013) for different void ratios. Note that the PSD also helps to explain why the suction value associated with macropore air-entry (AEV_l) for this soil is so low.

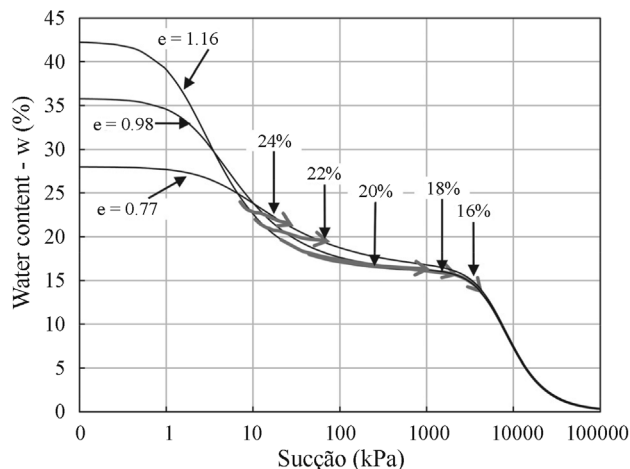


Figure 11 - Water retention curve - water content against suction.

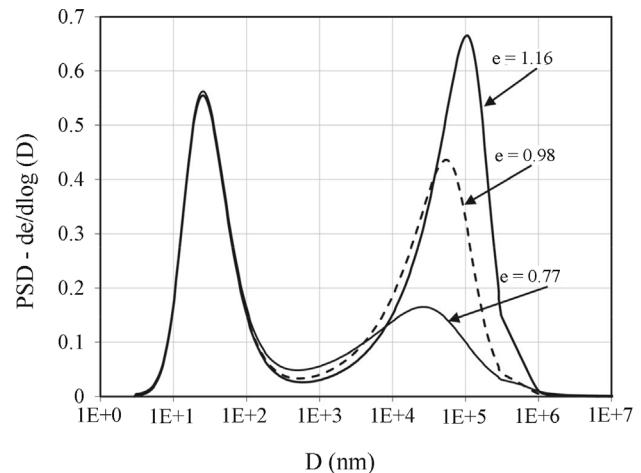


Figure 12 - Changes in pore size density functions of a collapsible soil.

It is worth noting that Figs. 11 and 12 justify what was said previously about the effect of loading being significant only for the macropores range while the microstructure remains constant after different types of loading.

The other aspect to be considered is that the process of water outlet for the 16% water content sample starts at the micropores level. Suction values for this sample ranged from 1480 to 4445 kPa. The high suction value associated to this sample should increase soil stiffness, as described in several studies such as Alonso *et al.* (1990). However, since these suction values led to outflow of water from the micropores, another phenomenon should be considered - the contraction of the clay clusters that form the microstructure.

Alonso *et al.* (1999) mentioned that soil macrostructural response is strongly influenced by microstructural behaviour. A simpler way of evaluating the influence of the macrostructural response caused by microstructure variation will be presented, through a formulation, and subsequently discussed.

Other aspects for interpretation of the results in Fig. 10 are seen in Fig. 13, which shows net vertical stress and suction paths for all samples. The data shows that although all the samples have similar variations in water content (about 0.05), the effect on suction values depends on whether this variation takes place in the soil microstructure or macrostructure as mentioned previously.

An uncertain point in relation to obtaining suction values from the methodology presented is that the water retention curves were carried out on mixed (wetting and drying) paths. The water retention curves obtained by Otálvaro (2013) for a soil from Brasilia with similar physical and mineralogical characteristics of the soil studied in this paper showed hysteresis. The present study ignored hysteresis effect and therefore if this behaviour is present in the soil studied it was not taken into account when determining its compressibility parameters.

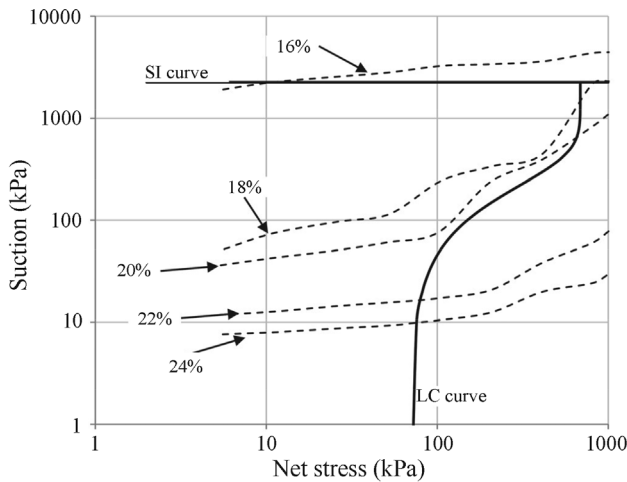


Figure 13 - Variation of suction values during consolidation tests for samples with different water contents.

3.4. Obtaining constitutive parameters

Figure 14 shows the void ratio-effective stress curve for the saturated condition. In this case, all volumetric change is associated with vertical loading. Therefore the following parameters associated with constitutive models such as Cam-clay or Barcelona Basic Model (Alonso *et al.*, 1990) may be obtained: pre-consolidation stress for saturated conditions (p_0^*), elastic stiffness parameter (k), and plastic stiffness parameter for saturated condition (λ_0).

However, the results shown in Fig. 10, in which there is no direct suction control, in principle, cannot be used to define constitutive model parameters, but may be used to enhance interpretation of soil behaviour.

The volumetric strain found for consolidation testing of the 16% initial water content sample was larger than that of samples with 18 and 20% initial water content. The rea-

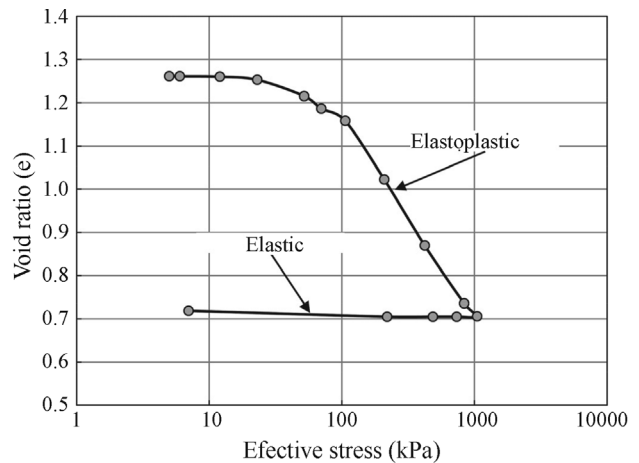


Figure 14 - Consolidation curve for a saturated sample.

son for this is associated with suction changes leading to contraction of microstructure, as discussed previously.

In order to separate strain due to loading from that due to contraction of the 16% water content sample microstructure, it will be assumed there is no plastic deformation due to loading, only elastic deformations, whereas suction changes produces elastic and plastic deformations (Fig. 15).

Although the hypothesis cannot be proven from the results presented in this paper, it will reveal helpful in understanding soil behaviour and obtaining a set of parameters to simulate the paths used.

Figure 15a shows the variation of the sample void ratio due to suction change alone, in accordance with the above assumption. Based on this curve, the Barcelona Basic Model constitutive parameters for suction changes may be obtained (Alonso *et al.*, 1990): hardening parameter (s_0),

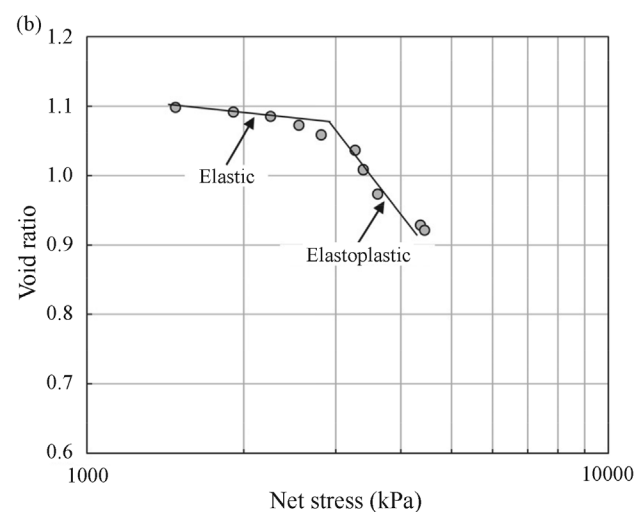
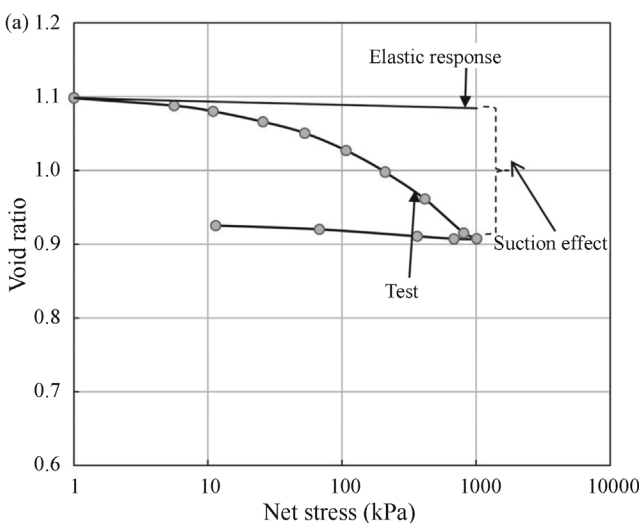


Figure 15 - Consolidation tests -sample at 16% water content: a) Variation of void ratio with net stress; b) Variation of void ratio with suction.

Table 4 - Barcelona Basic Model (BBM) parameters.

Author	Stress			Elastic		Plastic volumetric compressibility			
	p_c (kPa)	p_0^* (kPa)	s_0 (kPa)	κ	κ_s	λ_0	λ_s	r	β (kPa ⁻¹)
Present study	7.5	70	2250	0.002	0.02	0.20	0.20	0.50	0.007
Peixoto (1999)	20	50	-	0.02	-	0.32	-	0.50	0.01

elastic stiffness parameter for change in suction (k_s) and plastic stiffness parameter for change in suction (λ_s).

All parameters required by the Barcelona Basic Model to reproduce the paths shown in Fig. 10 are presented in Table 4. The parameters obtained by Peixoto (1999) for the same soil in its natural (or undisturbed) state are also shown. The values match quite well, particularly given the fact that the samples used were in different conditions.

Figure 13 shows hypothetical LC (loading-collapse) and SI (suction increase) yield surfaces obtained using parameters from Table 4. This figure clearly shows that 16% initial water content sample would be yielding by reaching the SI. In contrast, 22% and 24% initial water content samples would quickly reach LC and be deformed by vertical stress alone. The 18% initial water content sample only reaches LC and SI for high stress levels and the 20% initial water content sample does not touch SI and is always tangential to LC, although it does reach LC at high levels of loading, with strain occurring due to vertical stress.

In order to validate the model parameters shown in Table 4, test simulations were performed to obtain the results shown in Figs. 16 to 18. In general, the results obtained with the parameters match experimental results quite well. Furthermore, in the 16% and 18% initial water content samples there are two inflection points in the fittings of the consolidation curve. This is due to a fact that loading stabilization times were not constant, thus causing different variations of suction in the course of the test.

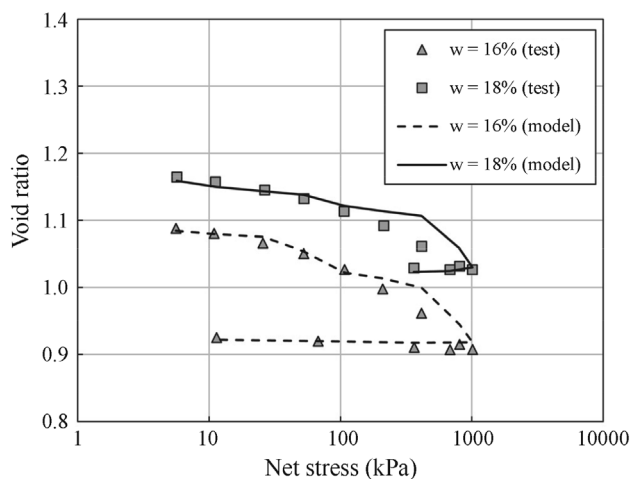


Figure 16 - Experimental results from consolidation tests and model simulations 16% and 18% initial water content samples.

Another problem observed in the fittings was that the 22% initial water content sample showed less collapse than the simulation.

A point to note is that if the variation of suction values in the course of the consolidation test were not taken into account, a consistent fitting could not be obtained for two reasons. One is that, although the 16% initial water content sample has a higher initial suction value, it shows more strain than the 18% and 20% initial water content samples,

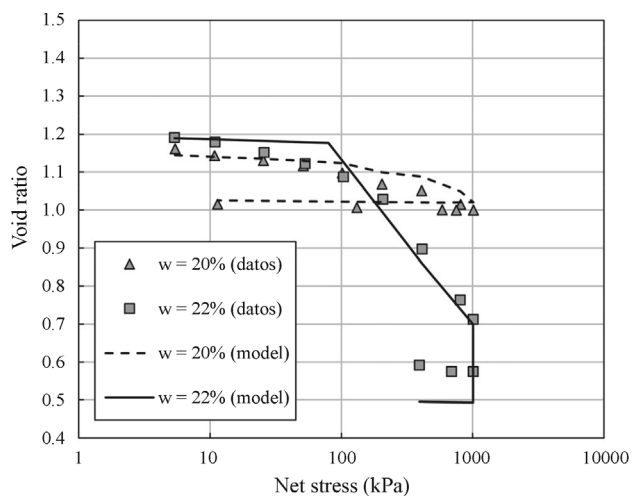


Figure 17 - Experimental results from consolidation tests and model simulations -20% and 22% initial water content samples.

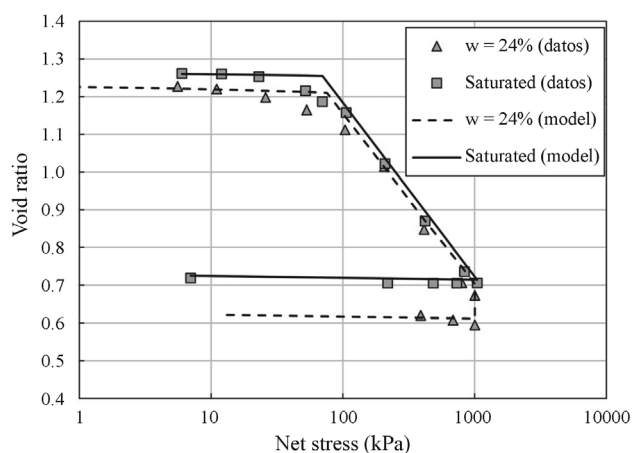


Figure 18 - Experimental results from consolidation tests and model simulations - 24% and saturated initial water content samples.

which was due to the large variation in suction during testing and these strains occurring in the microstructure, resulting in permanent deformations.

The second reason is that, the collapse due to flooding under 1000 kPa stress in the 22% and 24% initial water content samples would be underestimated, since both samples present initial suction of around 10 kPa, but reached 78 and 30 kPa of suction respectively before flooding, due to decrease of water content. Note that the underestimation of collapse due to assuming constant water content is greater than from the use of retention curve in mixed (wetting and drying) paths to estimate suction values in the course of consolidation tests.

4. Conclusions

In the consolidation tests performed assuming constant water content, suction change due to evaporation of water and reduction of voids is not considered. Thus, soil shrinking due to increased suction is associated with the increase of vertical stress. In some cases, this may be wrongly reflected in the value of the compressibility coefficient.

The water content control test described in this paper proved to be efficient at obtaining water content values over the test period, and values estimated by the method proposed were similar to those measured at the end of the test.

Additionally, a water retention curve could be obtained for different void ratios showing that the variation of void ratio affecting soil suction values is only significant in the soil macrostructure.

Suction changes due to water evaporation rate and reduced voids was incorporated in the estimation of constitutive parameters and proved quite adequate, which was confirmed by simulations of the experimental data.

The evaporation rate for the 22% and 24% initial water content samples must be higher than for a 20% sample, which means that soil water content before flooding the sample was smaller than the estimated value. Additionally, the water retention curve used to estimate suction was obtained from a wetting path, whereas in the consolidation tests they were estimated from a drying path. Both factors combined result in estimated suction lower than actual suction, which would lead to underestimating collapse.

Finally, it is important to note that these parameters were obtained by means of simple testing: filter paper, water content control test and consolidation tests.

References

ABNT (1990). Consolidation Test - NBR 12007. Rio de Janeiro, Brazil, 13 p.

Alonso, E.; Gens, A. & Josa, A. (1990). A constitutive model for partially saturated soils. *Géotechnique*, 40(3):405-430.

Alonso, E.; Vaunat, J. & Gens, A. (1999). Modelling the mechanical behaviour of expansive clays. *Engineering Geology*, 54(1):173-183.

Alonso, E.; Romero, E. & Hoffmann, C. (2011). Hydro-mechanical behaviour of compacted granular expansive mixtures: experimental and constitutive study. *Géotechnique*, 61(4):329-344.

Alonso, E.E.; Pinyol, N.M. & Gens, A. (2013). Compacted soil behaviour: initial state, structure and constitutive modelling. *Géotechnique*, 63(6):463-478.

Araki, M.S. (1997). Aspects Related to Collapsible and Porous Soils of Federal District. Dissertation G.DM-040A/957, Department of Civil Engineering, University of Brasília, Brasília, 121 pp.

Bishop, A.W. (1959). The principle of effective stress. lecture delivered in Oslo, Norway in 1995. *Teknisk Ukeblad*, 106(39):859-863.

Buenfil, C.M.B. (2007). Hydromechanical Behavior of Compacted Clay. Doctoral Thesis, Department of Geotechnics and Cartography Engenharia, Politécnica University of Catalonia, 466 pp.

Camapum de Carvalho, J.; Crispel, J.J.; Mieussens, C. & Nardone, A. (1987). Reconstitution of Samples Laboratory - Theory and Practice. Research Report, LPC No. 145, Regional Laboratory of Toulouse, Toulouse, 88 p.

Camapum de Carvalho, J.; Mortari, D.; Araki, M.S. & Palmeira, E.M. (1994). Behavior of collapsible and porous clay of Brasília, Distrito Federal. Proc. X Brazilian Congress on Soil Mechanics and Foundation Engineering, Foz do Iguaçu, v. 3, pp. 1157-1163.

Camapum de Carvalho, J. & Leroueil, S. (2000). Normalized characteristic curve. 32nd Annual Paving Conference, Brasília, v. 1, pp. 96-106.

Cardoso, F.B.F. (1995). Chemical, Mineralogical and Micromorphological Analysis of Collapsible Tropical Soils and Study of the Dynamics of Collapse. Dissertation G.DM-026A/95, Department of Civil Engineering, University of Brasília, Brasília, 140 p.

Della Vecchia, G.; Jommi, C. & Romero, E. (2012). A fully-coupled elastic-plastic hydromechanical model for compacted soils accounting for clay activity. *International Journal for Numerical and Analytical Methods in Geomechanics*, 37(5):503-535.

Durner, W. (1994). Hydraulic conductivity estimation for soils with heterogeneous pore structure. *Water Resources Res.*, 30(2):211-223.

Fredlund, D.G.; Morgenstern, N.R. & Widger, R.A. (1978). The shear strength of unsaturated soils. *Canadian Geotechnical Journal*, 15(3):313-321.

Gens, A. & Alonso, E. (1992). A framework for the behaviour of unsaturated expansive clays. *Canadian Geotechnical Journal*, 29(6):1013-1032.

Guimarães, R.C. (2002). Lateritic Soil Profile Behavior Applied to the Study of Bored Piles Performance. Dissertation G.DM-091A/02, Department of Civil and En-

- vironmental Engineering, University of Brasilia, Brasilia, 183 p.
- Marinho, F.A.M. (1994). Filter paper method to measure suction. Proc. X Brazilian Congress on Soil Mechanics and Foundation Engineering, Foz do Iguaçu, v. 2, pp. 515-522.
- Matyas, E.L. & Radhakrishna, H.S. (1968). Volume change characteristics of partially saturated soils. *Geotechnique*, 18(4):432-448.
- Mascarenha, M.M.A. (2008). Influence of Microstructure on Hydro-Mechanical Behavior of a Silty Clay Unsaturated. Doctoral Thesis, Publication G.TD-056/08, Department of Civil Engineering, University of Brasília, Brasília, 158 p.
- Otálvaro, I.F.C. (2013). Hydromechanical Behavior of a Compacted Soil Tropical. Doctoral Thesis, Graduate Program in Geotechnical Engineering, Department of Civil and Environmental Engineering, Faculty of Technology, University of Brasilia, 122 p.
- Peixoto, R.J. (1999). Modeling Constitutive of Collapsible and Porous Clay Behavior of Federal District. Dissertation, Department of Civil and Environmental Engineering, University of Brasilia, Brasilia, 191 pp.
- Romero, E.; Hoffmann, C.; Castellanos, E.; Suriol, J. & Lloret, A. (2005). Microstructural changes of compacted bentonite induced by hydro-mechanical actions. *Advances in Understanding Engineered Clay Barriers*, E.E., Alonso & A. Ledesma (eds.) Taylor & Francis Group, London, pp. 193-202.
- Romero, E. & Vaunat, J. (2000). Retention curves of deformable clays. Tarantino & Mancuso (eds), *Experimental Evidence and Theoretical Approaches in Unsaturated Soils*, Balkema, Rotterdam, pp. 91-106.
- Sheng, D.; Sloan, S.W. & Gens, A. (2004). A constitutive model for unsaturated soils: thermomechanical and computational aspects. *Computational Mechanics Journal*, 33(6): 453-465.
- Silva, J.P. (2007). Preliminary Studies for the Infiltration Trenches Implementation. Dissertation G.DM-154A/07, Department of Civil and Environmental Engineering, University of Brasilia, Brasilia, 183 p.
- Silva, M.T.M.G. (2009). Methodology for Determination of Unsaturated Soils Parameters Using Tests with Known Humidity. Dissertation, Department of Civil Engineering, University of Brasília, Brasília, 98 p.
- Simms, P.H. & Yanful, E.K. (2002). Predicting soil-water characteristic curves of compacted plastic soils from measured pore-size distributions. *Géotechnique*, 52(4):269-278.
- Van Genuchten, M.Th. (1980). A closed-form equation for predicting the hydraulic conductivity of unsaturated soils. *Soil Science Society of America Journal*, 44(5):892-898.
- Vaunat, J.; Romero, E. & Jommi, C. (2000). An elastoplastic hydromechanical model for unsaturated soils. Tarantino & Mancuso (eds), *Experimental Evidence and Theoretical Approaches in Unsaturated Soils*, Balkema, Rotterdam, pp. 121-138.
- Wheeler, S.J.; Sharma, R.S. & Buisson, M.S.R. (2003). Coupling of hydraulic hysteresis and stress-strain behaviour in unsaturated soils. *Géotechnique*, 53(1):41-54.

List of Symbols

- AEV: air entry values
 COV: coefficient of variation
 e : void ratio
 e_w : soil water content
 e_{wL} : macropore void ratio
 e_{wS} : micropore void ratio
 G_s : specific gravity
 k : elastic stiffness parameter
 k_s : elastic stiffness parameter for change in suction
 m_L : slope of the line that relates transition water content and suction
 m_S : slope of the line that relates water content and suction after hygroscopic soil water content value
 n_L : slope of the line that relates macropore water content and suction
 n_S : slope of the line that relates macropore water content and suction
 p_c : reference stress
 p_0^* : pre-consolidation stress for saturated conditions
 PSD: Pore Size Density
 r : parameter defining the maximum soil stiffness
 s_0 : hardening parameter
 t : time elapsed from start of testing
 w : water content
 w_c : corrected water content
 w_{com} : compaction water content
 w_i : initial water content
 w_k : corrected water content for time 240 min
 w_L : liquid limit index
 w^M : macroscopic water content
 w^m : microscopic water content
 w_p : plastic limit index
 α_L : parameter related to air-entry value for macropores
 α_S : parameter related to air-entry value for micropores
 β : parameter controlling the rate of increase of soil stiffness with suction
 λ_0 : plastic stiffness parameter for saturated condition
 λ_s : plastic stiffness parameter for change in suction

Recent Developments and Limitations of the SFG Model

D. Sheng

Abstract. The SFG model was proposed in attempt to provide a consistent description of the stress-strain behaviour of unsaturated soils, including compacted soils and soils dried from slurry. It differs from existing models mainly through two aspects: a consistent description of volume change, yield stress and shear strength behaviour of unsaturated soils and a smooth and natural transition between saturated and unsaturated states. The model has attracted significant attention since it was first proposed and has been extended to cover coupled hydro-mechanical behaviour, hysteretic water retention behaviour and density-dependency. This paper presents a summary of the latest developments of the model, as well as the aspects that require further refinements.

Keywords: SFG model, unsaturated soils, volume change, shear strength, hydro-mechanical coupling.

1. Introduction

The SFG model proposed by Sheng *et al.* (2008a) attempts to provide a consistent and unified description of volume change, yield stress, shear strength and hydraulic behaviour of unsaturated soils, including compacted soils and soils dried from slurry. It is established in the space of the independent stress variables, namely net stress and matric suction. However, unlike models using similar stress variables, the SFG model provides a smooth and natural transition between saturated and unsaturated states. The model has attracted significant attention since it was proposed in 2008. It has been further extended to cover soil behaviour such as hydro-mechanical interaction, hysteretic water retention, and density dependency. However, this model also has a number of limitations that require further improvements. This paper presents a summary of the latest developments of the SFG model and the areas where the model falls short of real soil behaviour.

2. The SFG Model

The essential ingredient of the SFG model is its volume change equation. According to the model, the volume change of a soil can be caused by a change of net stress or a change of suction. For normally consolidated soils under isotropic stress states, the volume change equation takes the following form:

$$dv = -\lambda_{vp} \frac{d\bar{p}}{\bar{p} + f(s)} - \lambda_{vs}(s) \frac{ds}{\bar{p} + f(s)} \quad (1)$$

where v is the specific volume and $v = 1 + e$, e is the void ratio, \bar{p} is the mean net stress and $\bar{p} = p - u_a$, p is the mean stress, u_a is the pore air pressure, u_w is the pore water pressure, s is the soil suction and $s = u_a - u_w$, λ_{vp} is the soil compressibility in terms of stress changes, and λ_{vs} is the soil compressibility in

terms of suction changes. The function $f(s)$ represents the interaction between stress and suction and was simply set to s in the original SFG model (Sheng *et al.*, 2008a). However, more advanced forms could be used, as suggested by Sheng (2011).

The parameter λ_{vp} can be determined from normal compression lines (NCL) for $s = 0$. It is the same as the slope (λ) of NCL in e - $\ln p$ plots that are commonly used for saturated soils. In its simplest form this parameter can be treated as a constant for one soil, but more realistically it should be a function of suction. The parameter λ_{vs} is a function of suction. Its initial value is the same as λ_{vp} for suctions below the transition value between saturated and unsaturated states, but it approaches zero as suction increases to infinite. The following simple equation was used in Sheng *et al.* (2008b):

$$\lambda_{vs} = \begin{cases} \lambda_{vp} & s < s_{sa} \\ \lambda_{vp} \frac{s_{sa}}{s} & s \geq s_{sa} \end{cases} \quad (2)$$

where s_{sa} is the transition suction and its definition is slightly different from the air entry value (see Sheng *et al.*, 2008a).

The volume change model defined by Eqs. 1 and 2 is the foundation of the SFG model. Zhou & Sheng (2009) provided a systematic validation of the volume change equation for compacted and air-dry soils. The yield stress and shear strength criteria in the SFG model are all based on this volumetric model. The yield stress function for a slurry soil can be derived from the volume change equation (assuming that the plastic volumetric strain is only hardening variable) and it also defines the apparent tensile strength of the soil:

Daichao Sheng, Professor, School of Engineering, The University of Newcastle, NSW 2308, Australia, and School of Civil Engineering, Central South University, Changsha, 410072, China. e-mail: daichao.sheng@gmail.com.
Invited Article, no discussion.

$$\bar{p}_0 = \begin{cases} -s & s < s_{sa} \\ -s_{sa} - s_{sa} \ln \frac{s}{s_{sa}} & s \geq s_{sa} \end{cases} \quad (3)$$

The loading-collapse equation for collapsible soils (e.g. compacted soils) can also be derived from the volume change equation:

$$\bar{p}_c = \begin{cases} \bar{p}_{cn0} - s & s \leq s_{sa} \\ \bar{p}_{cn0} \left(\frac{\bar{p}_{c0}}{\bar{p}_{c0} + f(s) - s_{sa} - s_{sa} \ln \frac{s}{s_{sa}}} \right) & s > s_{sa} \end{cases} \quad (4)$$

where \bar{p}_c is the yield stress at an arbitrary suction, \bar{p}_{cn0} is the yield stress at zero suction, \bar{p}_{c0} is a constant.

Note that there is no ‘suction-increase’ or ‘suction-decrease’ yield surface in the SFG model. The plastic volumetric strain caused by drying a soil to historically high suction is automatically covered in the apparent tensile strength function \bar{p}_c .

The apparent tensile strength function and the load-ing-collapse function can be incorporated into existing constitutive models for saturated soils. For example, if the modified Cam clay model is used for saturated soil behaviour, the yield function can be generalised to unsaturated states along the suction axis:

$$f = q^2 - M^2 (\bar{p} - \bar{p}_0)(\bar{p}_c - \bar{p}) \equiv 0 \quad (5)$$

where f is the yield function in the stress space, q is the deviator stress, M is the slope of the critical state line in $q - \bar{p}$ space, and \bar{p}_0 and \bar{p}_c are defined above.

Using the shear strength criterion proposed by Fredlund *et al.* (1978):

$$\tau = [c' + (\sigma_n - u_a) \tan \phi'] + [(u_a - u_w) \tan \phi^b] \quad (6)$$

The friction angle due to suction in the SFG model can be derived from the apparent tensile strength equation and is given by

$$\tan \phi^b = \begin{cases} \tan \phi' & s < s_{sa} \\ \tan \phi' \left(\frac{s_{sa}}{s} + \frac{s_{sa}}{s} \ln \frac{s}{s_{sa}} \right) & s \geq s_{sa} \end{cases} \quad (7)$$

In the equations above, τ is the shear strength, σ_n is the normal stress on the failure plane, ϕ' is the effective friction angle of the soil, and ϕ^b is the frictional angle due to suction. Equation 7 can be used to predict the change of the shear strength against suction.

In the original SFG model, hydro-mechanical coupling was only considered from the aspect that suction affects the stress-strain behaviour. This was extended to consider the effect of stress on the water retention behaviour by Sheng & Zhou (2011) by incorporating the following constitutive equation:

$$dS_r = Eds + \frac{S_r}{n} (1 - S_r)^m \frac{\lambda_{vp}}{\bar{p} + f(s)} d\bar{p} \quad (8)$$

where S_r is the degree of saturation, n is the porosity, and m is a fitting parameter. Function E in Eq. 8 refers to the gradient of the soil-water characteristic curve (SWCC, $dS_r = Eds$) and may also be multi-valued in a piece-wise equation, dependent on the suction path. Because Eq. 8 is in an incremental form, integration of the equation requires one specific SWCC that corresponds to a reference initial void ratio. In other words, the conventional SWCC equation is only used for the reference initial void ratio and the new SWCC for a new initial void ratio is obtained by integration of Eq. 8. Sheng & Zhou (2011) gives the details on how to use an existing SWCC equation for different initial void ratios.

We note that replacing Eq. 1 into Eq. 8 leads to:

$$dS_r = \left(E - \frac{\lambda_{vs}}{\bar{p} + f(s)} \frac{S_r}{n} (1 - S_r)^m \right) ds - \frac{S_r}{e} (1 - S_r)^m de \quad (9)$$

The above equation clearly indicates that the $S_r - s$ relationship for constant void ratio ($de = 0$) is not the same as the SWCC equation ($dS_r = Eds$). Equations 8 and 9 are equivalent and interchangeable.

Equations 1-9 are the main equations of the SFG model. These equations sufficiently define the volume change, yield stress, shear strength and coupled hydro-mechanical behaviour of unsaturated soils. In the following, we will first discuss what the SFG model can do and then outline where it falls short.

3. Predictions of the SFG Model

The main advantage of the SFG model is that it is based on a simple volume change equation and is able to provide a consistent framework for volume change, shear strength and coupled hydro-mechanical behaviour of unsaturated soils.

3.1. Volume change behaviour

The volume change caused by suction increase (drying) can be predicted by Eqs. 1 and 2 directly. Figure 1 shows the SFG prediction compared with experimental of Mariho *et al.* (1995). There are three parameters involved in the prediction: the compressibility of saturated soil (κ_{vp} and λ_{vp}) and the transition suction (air entry value in this case). The figure shows that the SFG model is capable of capturing the volume change during drying.

The volume change caused by stress change can also be predicted by Eq. 1. Figure 2 compares the SFG predictions with the experimental data of Thu *et al.* (2007). The data were obtained from isotropic compression tests under constant suctions on compacted Kaolin. The predicted results match very well the experimental data, indicating that

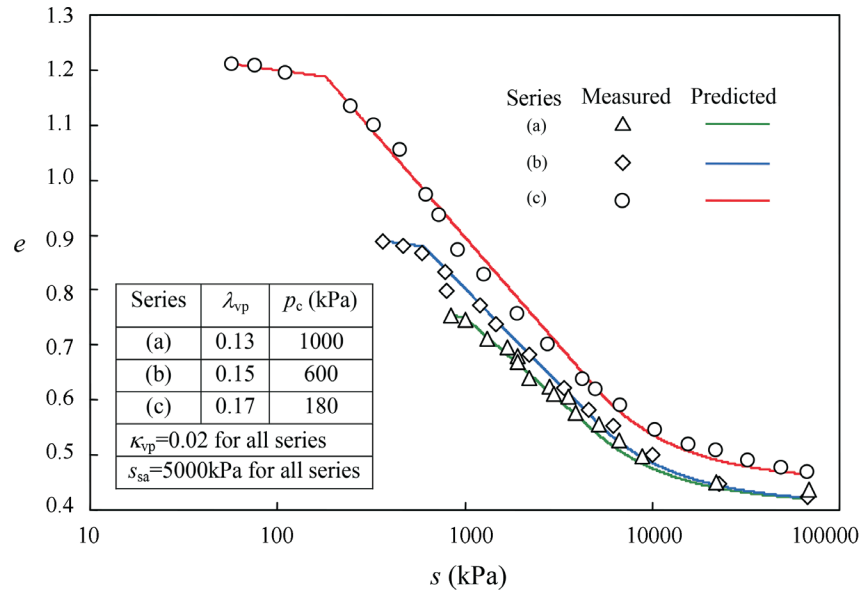


Figure 1 - Volume change during drying for Brown London Clay (data of Marinho, *et al.*, 1995).

Material parameters used in the prediction

	s , kPa	λ_{vp}	κ_{vp}	\bar{p}_c	Data	Predictions
(a)	0	0.058	0.018	25kPa	•	—
(b)	50	0.058	0.018	35 kPa	□	—
(c)	100	0.058	0.018	25 kPa	△	—
(d)	150	0.058	0.018	35 kPa	◇	—

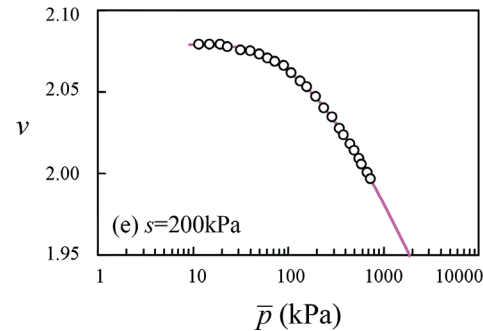
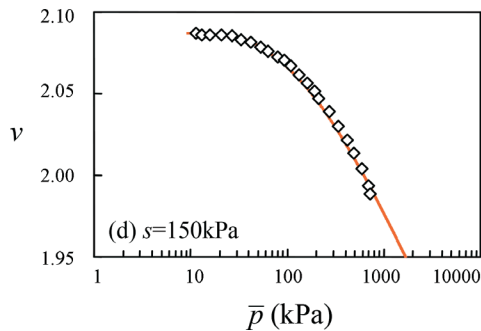
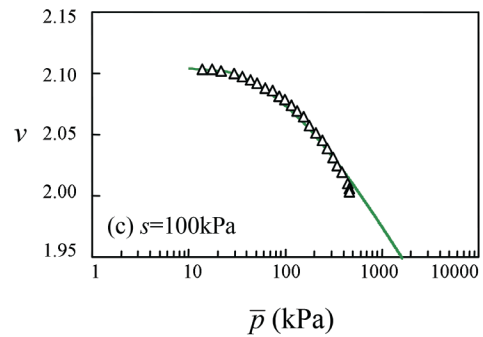
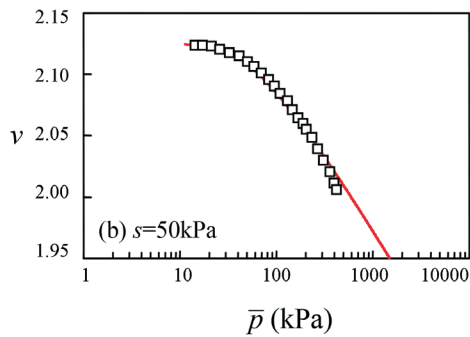
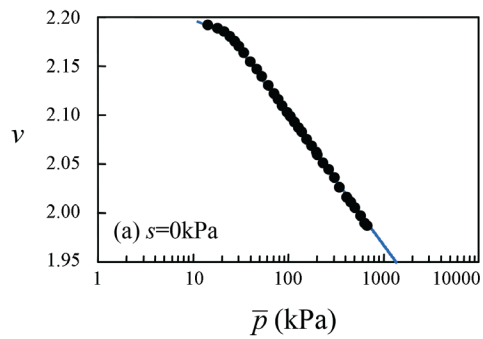


Figure 2 - Predictions of isotropic compression curves for compacted kaolin specimen (data by Thu *et al.*, 2007).

the SFG model is capable of predicting the volume change caused by stress change.

The volume change during wetting is more complex. It may involve the expansion of the loading-collapse yield surface, or so-called hardening. In this case, a complete constitutive model is needed to predict the volume change. Figure 3 was taken out from Sheng *et al.* (2008a) and shows the predicted volume collapse during wetting of compacted Pearl clay. The compacted sample (point A in Fig. 3) was first dried to a constant suction (point B) and then compressed to different stress levels (Points D, E, F, G, H, I), followed by wetting under constant net mean stresses full saturation (Points D', E', F', G', H', I'). Figure 3 shows that the predicted collapse volume depends on the stress level where the wetting takes place. The prediction was not compared with experimental data due to the lack of detailed soil parameters. However, the experimental data was shown on the lower left corner, to indicate the qualitative agreement between the prediction and the experimental data.

3.2. Shear strength

In the SFG model, the shear strength behaviour is a natural outcome of the volume change equations and does

not need any additional definition or material parameters. Nevertheless, the model is capable to predict the shear strength variation with suction to a reasonable degree. Figure 4 shows the predicted shear strength variation with suction, compared with the experimental data by Vanapalli *et al.* (1996). The tests and predictions are for direct shear tests. Figure 5 compares the predictions with experimental data from triaxial tests. The results in both figures indicate that the SFG model provides a reasonable prediction of unsaturated soil shear strength.

3.3. Hydro-mechanical coupling

The extended SFG model by Sheng & Zhou (2011) and Zhou *et al.* (2012a) provides a complete coupling mechanism for the interaction between stress-strain and water retention behaviour. The effects of suction and degree of saturation on stress-strain and strength behaviour have already been demonstrated above. The effects of stress on water retention behaviour are demonstrated below.

Considering the soil water characteristic curves (or SWCC) under constant stresses, the effect of stress is primarily reflected through its effect on the initial soil density

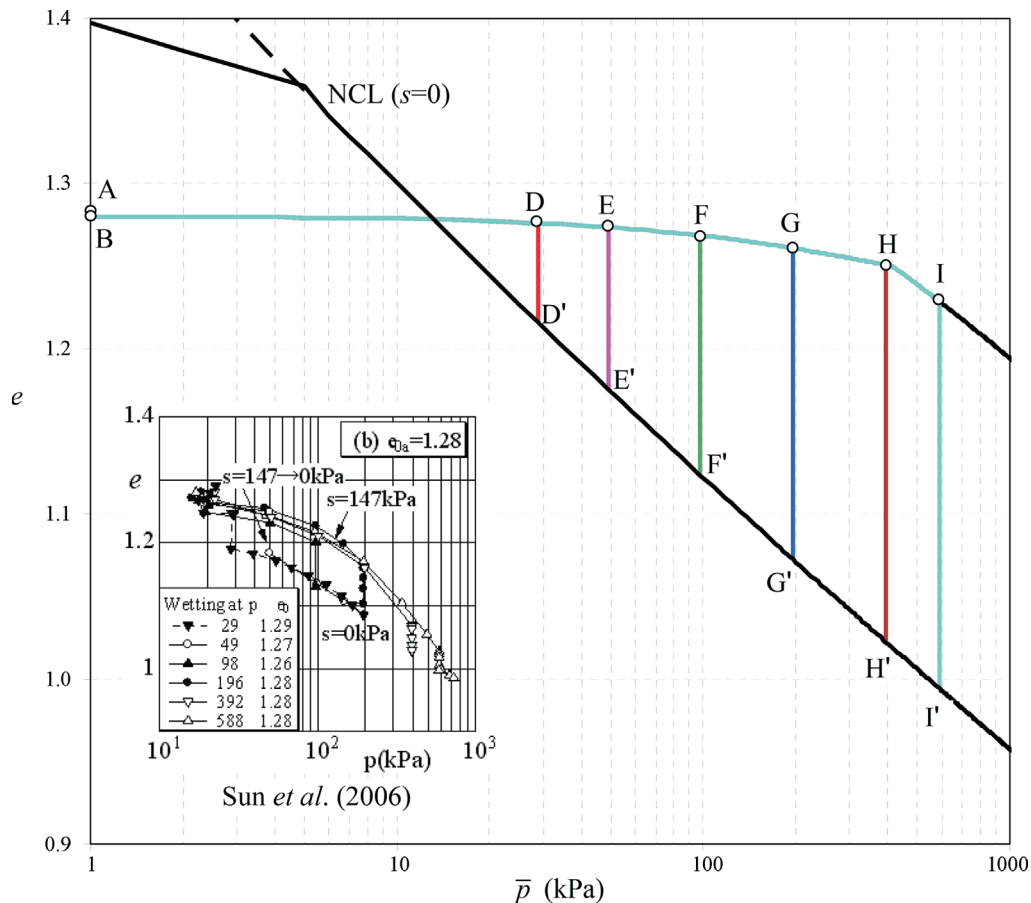


Figure 3 - Predicted volume collapse during the final wetting paths (experimental results of Sun *et al.* (2007) shown on the lower left corner).

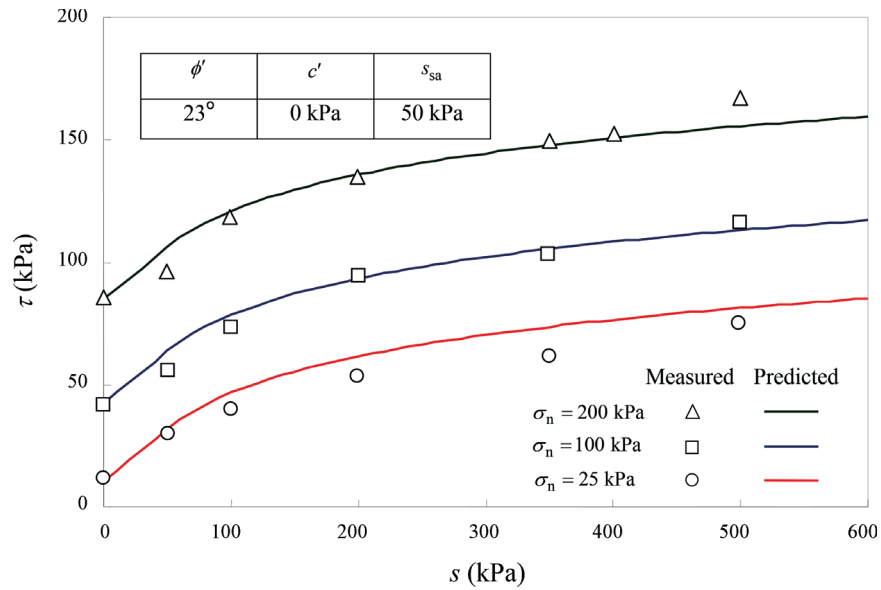


Figure 4 - Shear strength vs. suction during direct shear tests (data by Vanapalli *et al.*, 1996).

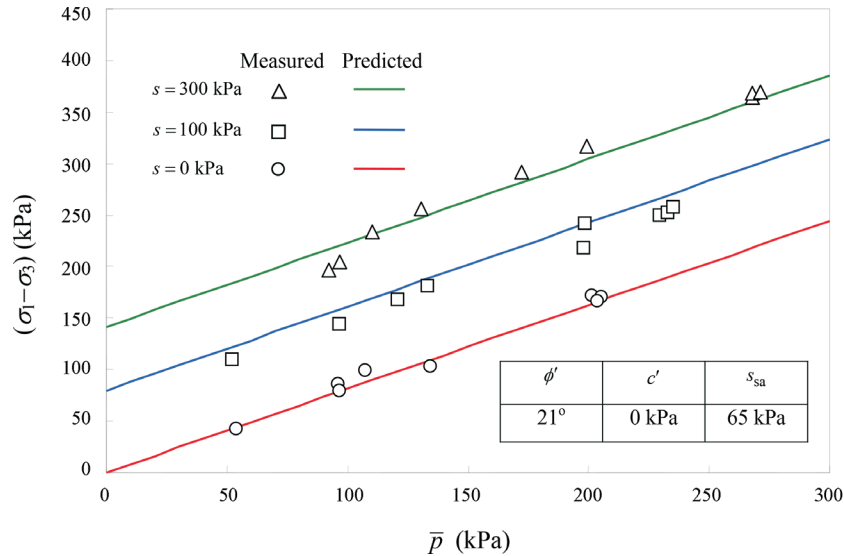


Figure 5 - Shear strength vs. suction during triaxial compression tests (data by Wheeler & Sivakumar, 2000).

or initial soil void ratio. Figure 6 shows the predicted and measured SWCCs for soils compacted to different initial void ratios. The predicted SWCCs are shown as solid curves. The fitting parameter m in Eq. 8 is set to 0.03. The SWCC for initial ratio of 0.517 was obtained using van Genuchten equation with fitting parameters given in Sheng & Zhou (2011). The predicted SWCCs compares very well with the measured data, indicating that the proposed model can capture the shift of SWCC with initial void ratio.

Figure 7 further demonstrates the capability of the SFG model in predicting the effects of initial void ratio on the water retention behaviour. The soil tested was a silty sand from a Saskatchewan Department of Highway borrow pit (Huang *et al.*, 1998). The air-dried silty sand was mixed with distilled water to prepare slurry specimens for the ex-

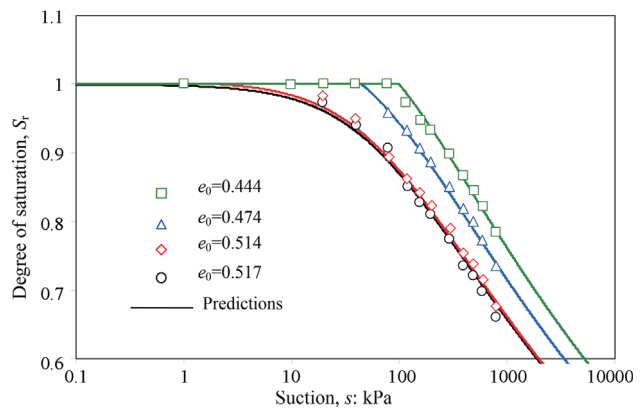


Figure 6 - Measured and predicted SWCCs (data after Vanapalli *et al.*, 1999).

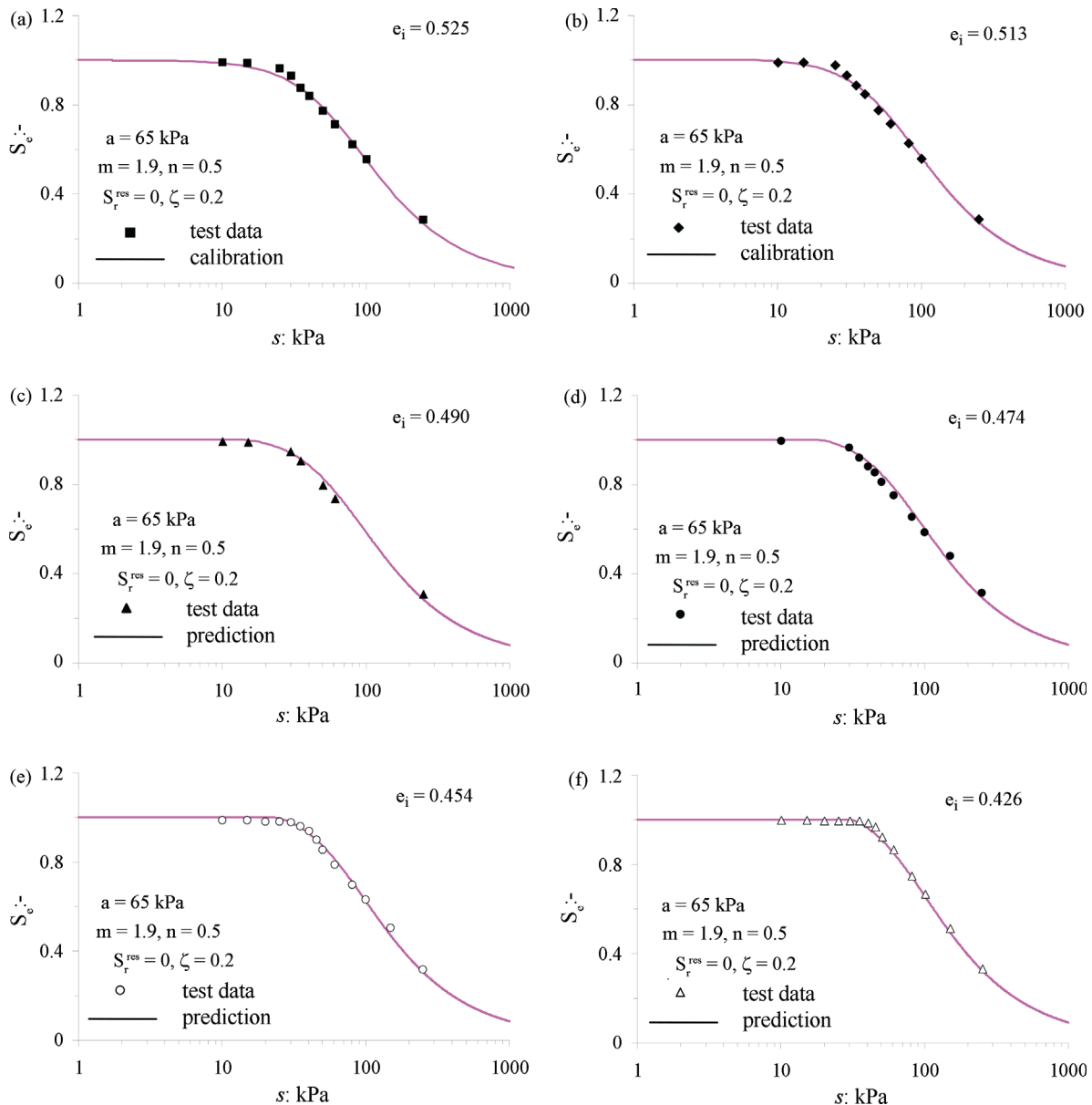


Figure 7 - Measured and predicted SWCCs for a silty sand with different initial void ratios (data after Huang *et al.*, 1998).

perimental program. Six initially slurry specimens were one-dimensionally preconsolidated under different pressures to obtain different initial void ratios for the water retention tests. The test results are replotted in the $S_w - s$ plane together with the predictions of Eq. 8, as shown in Fig. 7. The water retention test data for an initial void ratio 0.525 were used to calibrate the reference van Genuchten SWCC equation (Zhou *et al.*, 2012a). The fitting parameter m in Eq. 8 was set to 0.2. As shown in Figure 7, the predicted SWCCs agree very well with the experimental SWCCs. The shifting of the SWCC due to changes in the initial density is well portrayed by the SFG model.

4. Limitations of the SFG Model

4.1. Loading collapse surface for coupled hydro-mechanical formulation

One common limitation of models defined in the stress - suction space is related to the coupling between water retention and stress-strain behaviour. The SFG model is no exception for this shortcoming.

It is commonly accepted that the water retention curve of a soil depends on the stress level and the initial state (such as initial density) of the soil. Under the same stress level, the main drying curve shifts towards higher suction region with decreasing initial void ratio (Fig. 6). For the

same soil, the main drying curve shifts towards higher suction region when the stress level applied to the soil increases. That means the air entry suction is not constant for the same soil, but depends on the initial void ratio of the soil and the stress level applied to the soil. On the other hand, the loading-collapse yield curve experiences a curvature change around the transition suction such as the air entry value, which means the shape of the loading-collapse curve depends on the air entry value. Because of the dependency of the air entry value on the stress level and initial condition of the soil, the shape of the load-collapse curve would then depend on the stress level and initial condition of the soil, which is not acceptable for the definition of a yield surface. The yield surface must be independent of the stress states it encloses.

This limitation is common to all models defined in the stress - suction space, irrespective of the stress variables used (Fig. 8). It should also be noted that the transition suction appears implicitly in all models, even though some models set it to zero (such as in BBM of Alonso *et al.*, 1990). As mentioned in Sheng (2011), different degrees of saturation are only states of the soil and the transition from saturated to unsaturated states (for example, a change of pore water pressure from 10 kPa to -10 kPa) should always be allowed in a model. Therefore it is not possible to get rid of the transition suction. The conclusion is then that the

loading-collapse yield surface becomes meaningless in the stress - suction space if the water retention behaviour is considered to depend on stress level or initial condition of the soil.

A possible solution to the above shortcoming is to define the loading-collapse curve in terms of a variable alternative of suction. In the model by Wheeler *et al.* (2003), the loading-collapse curve is defined in the space of effective stress *vs.* modified suction, where it does not have an inflection point (Fig. 9a). Such a definition essentially implies that the water retention curve when plotted in terms of modified suction and degree of saturation is independent of stress levels or initial density of the soil. This implication remains to be further validated experimentally. In the model of Zhou *et al.* (2012b, 2012c), the loading-collapse curve is defined in the space of effective stress *vs.* degree of saturation and there is no inflection point along the loading-collapse curve in this space (Figure 9b). The loading-collapse curves in these models are then independent of the stress or suction path within the loading-collapse curves and are hence more meaningful.

4.2. Compression under constant suction

The current version of the SFG model predicts typical normal compression curves under constant suctions as shown in Fig. 10. In reality, compression under constant

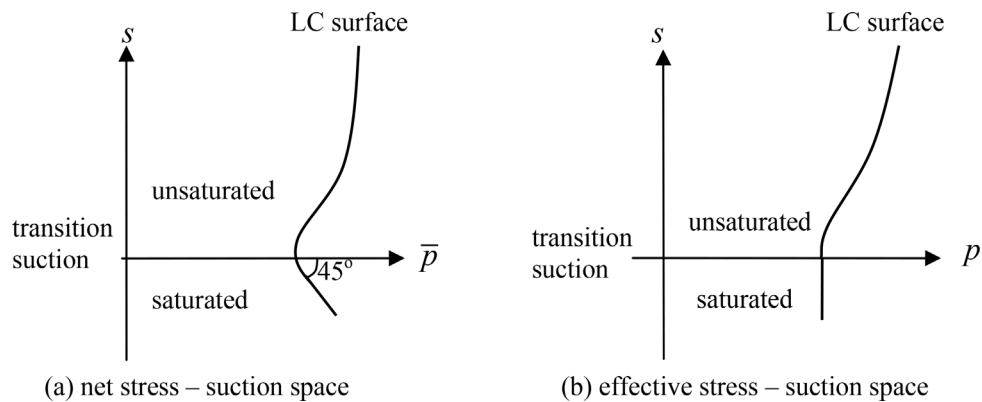


Figure 8 - Loading-collapse yield surface in suction-stress space.

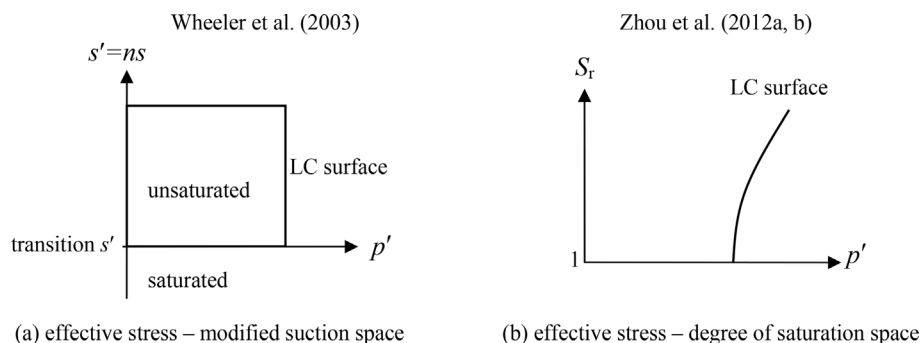


Figure 9 - Loading-collapse yield surface defined in alternative spaces.

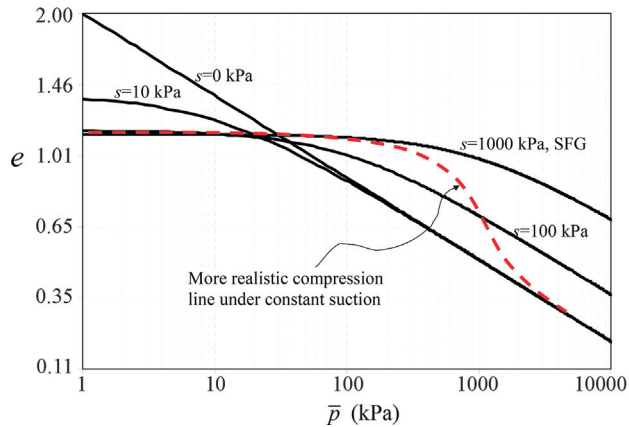


Figure 10 - SFG normal compression lines at different suctions ($N = 3$, $\lambda_{vp} = 0.1$, $s_{sa} = 10$ kPa).

suction, especially under a low suction, results in increase of degree of saturation. In other words, it is possible to compress an unsaturated soil under constant suction to full saturation. A more realistic compression curve for constant suction should then converge to the saturated normal compression line, as shown by the dashed curve in Fig. 10.

This limitation can in theory be overcome by using a compressibility parameter (λ_{vp}) that increases with increasing suction. However, such a modification would significantly complicate the integration of incremental equations in the SFG model. In addition, it would not provide a smooth convergence to full saturation. A better solution is, as suggested in Zhou *et al.* (2012b), that the compressibility parameter is assumed to decrease with decreasing degree of saturation. With such an assumption, compression under constant suction would result in increase in the degree of saturation and hence decrease in the soil compressibility. However, as pointed out in Sheng (2011), it should be avoided to have both suction and degree of saturation in the volume change equation, due to the hysteretic relationship of the two variables. Introducing the degree of saturation into the volume change equation would require the elimination of suction from it. The effects of suction have then to be considered through the stress variable - effective stress. This is the fundamental reason why Zhou *et al.* establish their model in the space of effective stress *vs.* the degree of saturation.

Other limitations of the SFG model include the non-conservative behaviour of the elastic zone, the difficulty of using a more advanced function $f(s)$ in Eq. 1, and the non-convexity of the elastic zone, as discussed in Sheng (2011). However, these limitations are not unique to the SFG model and the measures for dealing with them have been discussed in detail in Sheng (2011).

5. Summary

The SFG model provides a consistent and unified framework for describing volume change, yield stress,

shear strength and coupled hydro-mechanical behaviour of unsaturated soils. It is established in the space of the independent stress variables, namely net stress and matric suction. It provides a smooth and natural transition between saturated and unsaturated states. The model has been further extended to cover soil behaviour such as hydro-mechanical interaction, hysteretic water retention, and density dependency. However, this model also has a number of limitations that require further improvements. One of the most significant limitations is related to the definition of the loading-collapse yield surface when the coupled hydro-mechanical behaviour is considered. This paper has presented a summary of the latest developments of the SFG model and the areas where the model falls short of real soil behaviour.

References

- Alonso, E.E.; Gens, A. & Josa, A. (1990). A constitutive model for partially saturated soils. *Geotechnique*, 40(3):405-430.
- Fredlund, D.G.; Morgenstern, N.R. & Widger, A. (1978). Shear strength of unsaturated soils. *Canadian Geotechnical Journal*, 15(3):313-321.
- Huang, S.; Barbour, S.L. & Fredlund, D.G. (1998). Development and verification of a coefficient of permeability function for a deformable unsaturated soil. *Canadian Geotechnical Journal*, 35(3):411-425.
- Marinho, F.A.M.; Chandler, R.J.; & Crilly, M.S. (1995). Stiffness measurements on an unsaturated high plasticity clay using bender elements. In *Proceedings of the 1st International Conference on Unsaturated Soils*, September 1995. Paris. A.A. Balkema, Rotterdam, v. 2, pp. 535-539.
- Sheng, D. (2011). Review of fundamental principles in modelling unsaturated soil behaviour. *Computers and Geotechnics*, 38:757-776.
- Sheng, D.; Fredlund, D.G. & Gens, A. (2008a). A new modelling approach for unsaturated soils using independent stress variables. *Canadian Geotechnical Journal*, 45(5):511-534.
- Sheng, D.; Gens, A.; Fredlund, D.G. & Sloan, S.W. (2008b). Unsaturated soils: From constitutive modelling to numerical algorithms. *Computers & Geotechnics*, 35:810-824.
- Sheng, D. & Zhou, A.N. (2011). Coupling hydraulic with mechanical models for unsaturated soils, *Canadian Geotechnical Journal*, 48(5):826-840.
- Sun, D.A.; Sheng, D. & Xu, X.F. (2007). Collapse behaviour of unsaturated compacted soil. *Canadian Geotechnical Journal*, 44(6):673-686.
- Thu, T.M.; Rahardjo, H. & Leong, E.C. (2007). Soil water characteristic curve and consolidation behaviour of a compacted silt. *Canadian Geotechnical Journal*, 44(3):266-275.

- Vanapalli, S.K.; Fredlund, D.G.; Pufahl, D.E. & Clifton, A.W. (1996). Model for the prediction of shear strength with respect to soil suction. *Canadian Geotechnical Journal*, 33(3):379-392.
- Vanapalli, S.K.; Fredlund, D.G. & Pufahl, D.E. (1999). The influence of soil structure and stress history on soil-water characteristics of a compacted till. *Géotechnique*, 49(2):143-159.
- Wheeler, S.J.; Sharma, R.S. & Buisson, M.S.R. (2003). Coupling of hydraulic hysteresis and stress-strain behaviour in unsaturated soils. *Géotechnique*, 53(1):41-54.
- Wheeler, S.J. and Sivakumar, V. (2000). Influence of compaction procedure on the mechanical behaviour of an unsaturated compacted clay. Part 2: Shearing and constitutive modelling. *Géotechnique*, 50(4):369-376.
- Zhou, A.N. & Sheng, D. (2009). Yield stress, volume change and shear strength behaviour of unsaturated soils: Validation of the SFG model. *Canadian Geotechnical Journal*, 46(8):1034-1045.
- Zhou, A.N.; Sheng, D. & Carter, J.P. (2012a). Modelling the effect of initial density on soil water characteristic curves, *Géotechnique*, 62(8):669-680.
- Zhou, A.N.; Sheng, D.; Sloan, S.W. & Gens, A. (2012b). Interpretation of unsaturated soil behaviour in the stress - saturation space, I: Volume change and water retention behaviour. *Computers and Geotechnics*, 43:178-187.
- Zhou, A.N.; Sheng, D.; Sloan, S.W. & Gens, A. (2012c). Interpretation of unsaturated soil behaviour in the stress - saturation space, II: Constitutive relationships and validations. *Computers and Geotechnics*, 43:111-123.

Effectiveness of Capillary Barrier and Vegetative Slope Covers in Maintaining Soil Suction

H. Rahardjo, S. Krisnanto, E.C. Leong

Abstract. Capillary barrier and vegetative slope covers can be used to improve slope stability during rainfall by maintaining matric suction in the slope. A study was performed to investigate the effectiveness of capillary barrier system (CBS) and vegetative slope covers (Orange Jasmine and Vetiver grass) in maintaining soil suction. Performance of slopes with and without slope covers was investigated using field instrumentations and numerical analyses. Laboratory tests were performed to measure hydraulic and shear strength properties of the soil, the soils with Orange Jasmine and Vetiver grass root, and CBS materials. Numerical analyses were performed to investigate the variation of pore-water pressure profiles at a selected location and factor of safety during low, high, and maximum rainfall intensities. Pore-water pressures measured in the field were used to calibrate the numerical models. Laboratory test results showed that the presence of root increased the shear strength of soil. Numerical analyses and field monitoring results showed that the slope with covers can maintain negative pore-water pressure better than the original slope. Performance of Orange Jasmine, Vetiver grass, and CBS in maintaining matric suction in the slope is essentially similar during low, high, and maximum rainfall intensities.

Keywords: slope covers, stability, soil suction, infiltration, instrumentation.

1. Introduction

Residual soils commonly exist in many tropical areas. These soils are often in the unsaturated condition with negative pore-water pressure (matric suction). The presence of matric suction increases shear strength of the soil. Therefore, the presence of matric suction is a favorable condition for slope stability. However, rainfall infiltration into slope will increase pore-water pressure or decrease matric suction in soil, resulting in a decrease in shear strength of the soil. The decrease of shear strength causes the slope to become more prone to failure that is commonly referred to as rainfall-induced slope failure (Pitts 1985; Tan *et al.*, 1987; Brand 1992; Gasmol *et al.*, 2000; Tsaparas *et al.*, 2002).

Capillary barrier system (CBS) is a two-layer system of soil cover that is designed based on unsaturated soil mechanics principles. CBS consists of a fine-grained soil layer placed on top of a coarse-grained soil layer. The contrast in soil-water characteristic curve (SWCC) and permeability function between these two layers is utilized to create a barrier to minimize water infiltration into the underlying soil.

Capillary barrier system (CBS) can be used to mitigate rainfall-induced slope failures (Ross 1990; Steenhuis *et al.*, 1991; Morel-Seytoux 1993, 1994; Stormont 1996; Morris & Stormont 1997a, 1997b; Khire *et al.*, 2000; Tami *et al.*, 2004a, 2004b; Yang *et al.*, 2004b; Krisdani *et al.*, 2008). CBS consists of two different soil layers with a significant difference in their soil-water characteristic curves

(SWCC) and permeability functions that serves to minimize water seepage into the underlying layers.

Besides CBS, vegetative cover can also be used to mitigate rainfall-induced slope failure (*e.g.* Grimshaw 1994; Thruong & Gawander 1996; World Bank 1995; National Research Council 1993). The presence of root can increase shear strength of soil (Styczen & Morgan 1995). Orange Jasmine, *Murraya exotica L.*, and Vetiver grass, *Chrysopogon zizanioides*, are evergreen vegetations that can be planted in a tropical area like Singapore. They can adapt to variation in weather conditions and require minimum maintenance. Because of these characteristics, Orange Jasmine and Vetiver grass are potential vegetations to be used as soil covers to overcome rainfall-induced failure problems in the tropics.

Each slope cover may perform differently in maintaining matric suction. In addition, the performance of slope cover may differ under different rainfall intensities. Therefore, there is a need to investigate the effectiveness of capillary barrier and vegetative slope covers in maintaining soil suction.

The objective of this study is to compare the performance of Orange Jasmine and Vetiver grass slope covers and CBS in maintaining matric suction through field measurements and numerical analyses. The effect of Orange Jasmine and Vetiver grass roots on soil shear strength is also investigated through laboratory tests.

H. Rahardjo, Professor, School of Civil & Environmental Engineering, Nanyang Technological University, Blk N1, #1B-36, 50 Nanyang Avenue, 639798, Singapore. e-mail: chrahardjo@ntu.edu.sg.

S. Krisnanto, Lecturer, Geotechnical Engineering Research Division, Faculty of Civil & Environmental Engineering, Bandung Institute of Technology, Soil Mechanics Laboratory, CIBE Building, Jalan Ganesha No. 10, Bandung 40132, Indonesia. e-mail: sugeng.krisnanto@ftsl.itb.ac.id.

E.C. Leong, Associate Professor, School of Civil & Environmental Engineering, Nanyang Technological University, Blk N1, #1C-80, 50 Nanyang Avenue, 639798, Singapore. e-mail: cecleong@ntu.edu.sg.

Invited Article, no discussion.

2. Site Overview

The geology of Singapore consists of Old Alluvium in the eastern and northeastern regions, the sedimentary Jurong Formation in the western region, and Bukit Timah Granite in the center and northwestern regions.

A slope consists of soil from the Old Alluvium was selected for this study. The slope has a height of 8.21 m, a length of 22.55 m, and a slope angle of 20°. The slope was divided into three sections: the first section was the original slope covered with cow grass, the second section was covered with Orange Jasmine, the third section was covered with Vetiver grass, and the fourth section was covered with CBS. Layout of the slope is shown in Fig. 1. Based on soil investigation and laboratory tests, it was found that the slope consists of two layers of residual soils, named as layer 1 and layer 2. A relatively thin sub layer with saturated permeability lower than those of layers 1 and 2 was found within layer 1. Schematic diagrams of each section of the slope are shown in Fig. 2.

3. Design of Slopes and Field Instrumentation

The original slope was covered by cow grass surrounded by trench (Fig. 1). The original slope was instrumented with three Casagrande piezometers and three tensiometers (Fig. 2(a)). The piezometers were installed at near the crest, middle and near the toe of the slope. The tensiometers were labelled as TA3, TB3, and TD3 with a spacing of 0.5 m and insertion depths of 0.67 m, 1.29 m, and 1.84 m, respectively (Fig. 2(a)). Polyvinyl chloride (PVC) casings were installed at the locations of tensiometers and piezometers for installing the instruments.

Schematic diagram of the slope covered with Orange Jasmine and Vetiver grass is shown in Fig. 2(b). Orange Jasmine and Vetiver grass were planted in June and Sep-

tember 2009, respectively. In this study, only direct rainfall infiltration onto the covered slope had to be observed. Therefore, the lateral water flow from the surrounding soil into the vegetated area must be prevented. To achieve this condition, the vegetated areas were surrounded by a trench and impermeable metal sheets that were installed to 600 mm depth from the slope surface (Fig. 2(b)). PVC casings for tensiometers were installed at the planned locations of tensiometers. Before planting the vegetations, erosion blanket was laid on the slope surface to protect the slope within the study area from erosion during rainfall. Orange Jasmine was planted with lateral and down slope spacing of 450 mm whereas Vetiver grass was planted with lateral spacing of 250 mm and down slope spacing of 450 mm to avoid overlapping roots between adjacent vegetations. In the slope with Orange Jasmine, three tensiometers were installed. The installed tensiometers were labelled as TE4, TA4, and TB4 with a spacing of 0.5 m and insertion depths of 0.4 m, 0.66 m, and 1.21 m, respectively. In the slope with Vetiver grass, three tensiometers were also installed. The installed tensiometers were labelled as TE5, TA5, and TB5 with a spacing of 0.5 m and insertion depths of 0.4 m, 0.67 m, and 1.24 m, respectively.

Schematic diagram of the slope covered with CBS is shown in Fig. 2(c). To construct the CBS, the slope surface was excavated to 540 mm depth below the slope surface. Similar to the slope sections with vegetations, the CBS area was also surrounded by trench and impermeable metal sheets. A 6.5 mm thick layer of a geosynthetic drainage system (Secudrain) was used as a separator between the fine-grained layer and the original soil. J-pins of 75 cm and 115 cm in length penetrating 54 cm and 75 cm into the ground, respectively, were installed. PVC casings for tensiometers were installed at the planned locations of tensiometers. Geocells were laid on top of the secudrain for con-

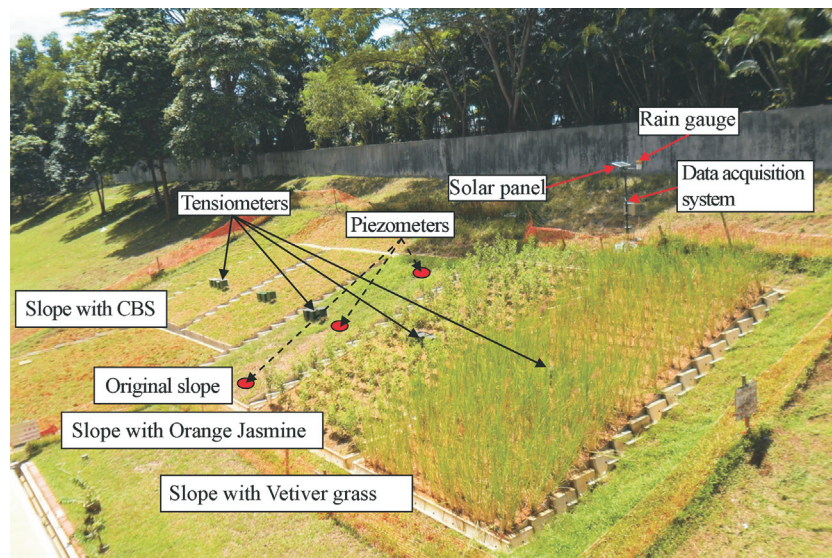


Figure 1 - Layout of the investigated slope.

taining the coarse-grained layer secured by the 75 cm long J-pins. Recycled concrete aggregate (RCA) as the coarse-grained layer was backfilled into the geocells and compacted to a relative density (D_r) between 70%-90% or to the required dry density (ρ_d) of 1.80 g/cm³. A nonwoven geotextile TS 80 (TenCate 2011) was used in the capillary barrier as a separator between the coarse- and fine-grained lay-

ers. Geocells for containing the fine-grained layer were laid on top of the nonwoven geotextile secured by the 115 cm length J-pins. Fine sand for the fine-grained layer was backfilled into the geocells and compacted to a relative density (D_r) between 70%-90% or to the required dry density (ρ_d) of 1.65 g/cm³. Perforated PVC pipes (diameter 15 mm) wrapped with the nonwoven geotextile TS 20 (TenCate

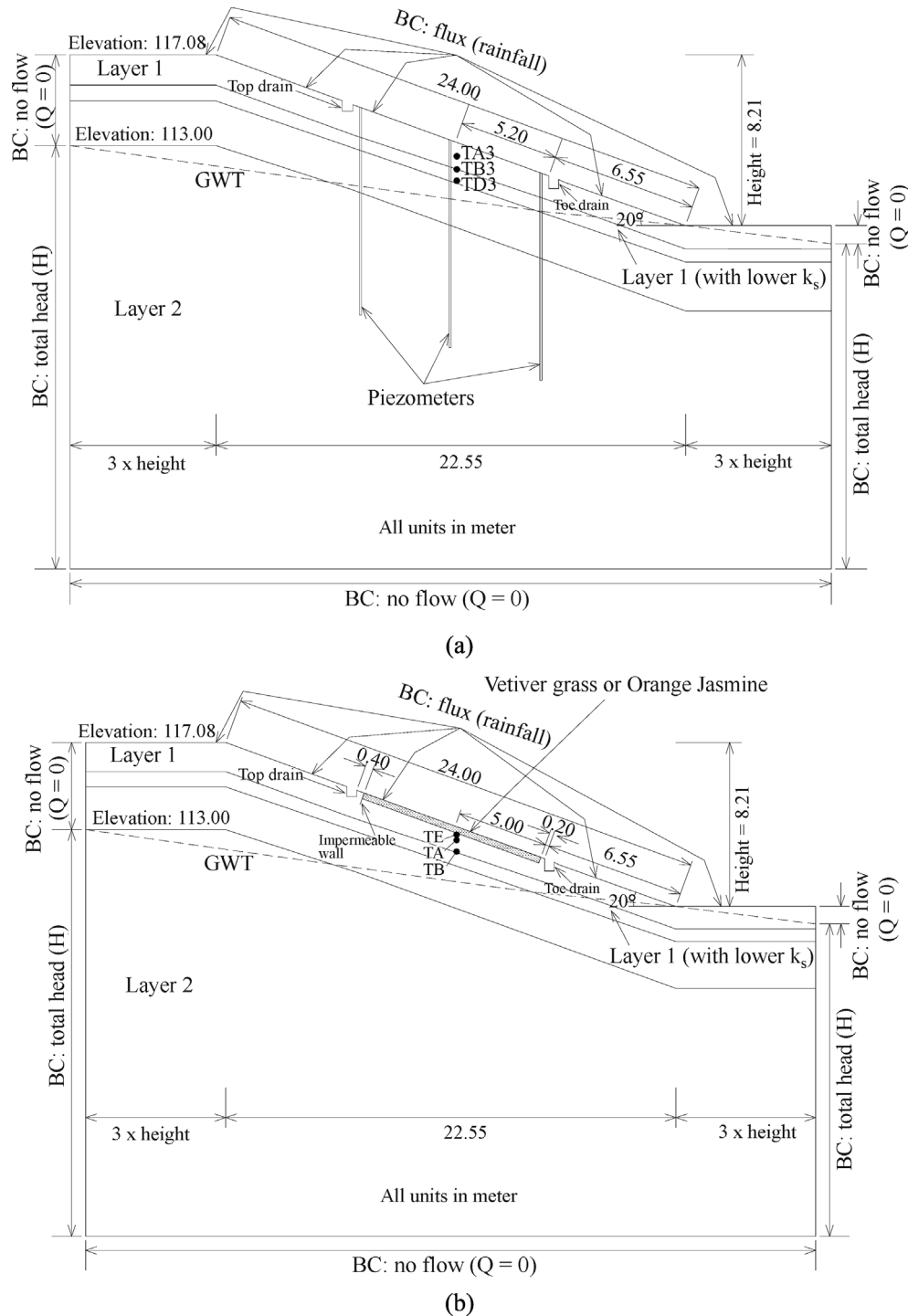


Figure 2 - Schematic diagram of slope with vegetation and CBS: (a) original slope, (b) slope with Orange Jasmine and Vetiver grass.

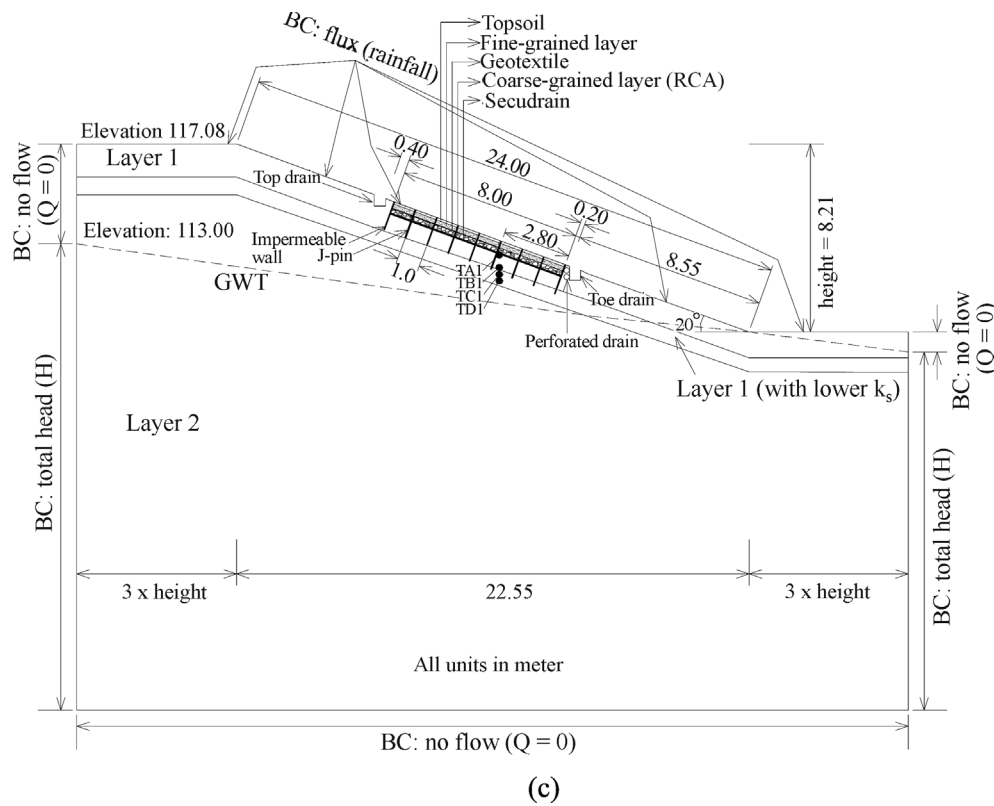


Figure 2 (cont) - (c) slope with CBS with recycled concrete as the coarse-grained layer.

2011) were installed at the toe of the slope for collecting water that flowed through the coarse- and the fine-grained layers to the toe of the slope. The erosion control blanket mat was placed below the top soil to prevent the erosion of fine-grained soil during heavy rainfall. The slope was then backfilled and compacted to the slope surface with top soil. In the slope with CBS, four tensiometers were installed. The installed tensiometers were labelled as TA1, TB1, TC1, and TD1 with a spacing of 0.5 m and insertion depths of 0.63, 1.18, 1.48, and 1.76 m, respectively (Fig. 2(c)).

A tipping bucket rain gauge was used to determine the amount of rainfall at the site (Fig. 1). A photovoltaic power supply system consisting of one module of solar panel and several reserve batteries was installed on the crest of the slope (Fig. 1). The tensiometers, piezometers, and

rain gauge were connected to the same power supply and data logger to obtain the readings in real time which can be accessed on-line.

4. Laboratory Test and Soil Properties

Laboratory tests were carried out to determine saturated and unsaturated properties of layer 1, layer 2, soil with Orange Jasmine roots, soil with Vetiver grass roots, fine- and coarse-grained materials of the CBS. Index and engineering properties tests were carried out to obtain index properties, soil-water characteristic curve (SWCC), saturated and unsaturated permeability, and shear strength of the soils. The basic soil properties are summarized in Tables 1 to 3.

Table 1 - Basic properties of the soils without vegetation.

Description	Soil		
	Layer 1	Layer 1 (with lower k_s)	Layer 2
USCS	SP	SP	SP
Specific gravity, G_s	2.66	2.66	2.61
Water content, w (%)	21.1	16.8	25.8
Saturated coefficient of permeability, k_s (m/s)	8.7×10^{-8}	6.4×10^{-10}	5.0×10^{-8}
Organic content at 440 °C (%)	0	0	0
Organic content at 750 °C (%)	0	0	0

Table 2 - Basic properties of the soils with vegetation.

Description	Soil with Orange Jasmine Root			Soil with Vetiver Grass Root		
	29 Jul 2010	18 Nov 2010	28 Feb 2011	29 Jul 2010	18 Nov 2010	28 Feb 2011
USCS	SP	SP	SP	SP	SP	SP
Specific gravity, G_s	2.64	2.71	2.71	2.32	2.65	2.64
Water content, w (%)	18.0	17.3	22.6	23.4	23.4	17.2
Saturated coefficient of permeability, k_s (m/s)	5.5×10^{-8}	1.0×10^{-7}	2.4×10^{-8}	7.1×10^{-8}	5.0×10^{-8}	3.9×10^{-8}
Organic content at 440 °C (%)	1.1	3.1	2.9	1.2	2.1	5.4
Organic content at 750 °C (%)	3.9	5.1	6.1	1.9	4.4	9.2

Table 3 - Basic properties of CBS.

Description	Fine-grained layer	Coarse-grained layer (RCA)
USCS	SP	GP
Specific gravity, G_s	2.65	2.66
Gravel content (>4.75 mm; %)	0	100
Sand (%)	100	0
Fines (<0.075 mm; %)	0	0
Grain-size distribution:		
D_{60} (mm)	0.52	10.6
D_{30} (mm)	0.32	10.3
D_{10} (mm)	0.20	9.5
Coefficient of uniformity, C_u	2.60	1.12
Coefficient of curvature, C_c	0.98	1.05
Dry density, ρ_d (g/cm ³)	1.58	1.53
Void ratio, e	0.70	0.66
Saturated coefficient of permeability, k_s (m/s)	2.7×10^{-4}	7.5×10^{-3}

The SWCCs were determined by combining the results from Tempe cell tests (for matric suction up to 100 kPa) and pressure plate tests (for matric suction up to 1500 kPa). SWCCs were measured for both drying and wetting processes. The measured SWCCs were best-fitted using the Fredlund & Xing (1994) equation with the correction factor taken as 1 as suggested by Leong & Rahardjo (1997). SWCCs were obtained for both drying and wetting for several specimens of soil with vegetation. However, for some soil specimens, only drying SWCC was obtained. In the absence of wetting SWCC data, the wetting SWCC was predicted from the drying SWCC. The scaling method (Pham *et al.*, 2005) was used for estimating the wetting SWCC from the drying SWCC. The SWCCs of the soils used in this study are shown in Fig. 3 whereas the fitting parameters are shown in Tables 4 to 6.

Table 4 - Hydraulic properties of the soils without vegetation.

Description	Symbol (unit)	Soil	
		Layer 1	Layer 2
Drying curve			
Saturated volumetric water content	θ_s	0.25	0.42
Air-entry value	Ψ_a (kPa)	1	12
Residual matric suction	Ψ_r (kPa)	9	600
Residual volumetric water content	θ_r	0.11	0.34
Fredlund & Xing (1994)	a (kPa)	1.55	16.6
Fitting parameters	n	4.42	1.02
	m	0.31	0.19
Wetting curve			
Water-entry value	Ψ_w (kPa)	30	600
Volumetric water content at Ψ_w	θ_w	0.1	0.33
Fredlund & Xing (1994)	a (kPa)	3.41	7.47
Fitting parameters	n	2.20	1.41
	m	0.28	0.09

The saturated permeability for layer 1, layer 2, soil with Orange Jasmine, soil with Vetiver grass, fine- and coarse-grained materials of the CBS are shown in Tables 1 to 3. Permeability functions were estimated using the statistical method (Fredlund & Rahardjo 1993) by utilizing SWCC and saturated permeability data. Permeability functions of the soils used in this study are shown in Fig. 4.

It can be observed from Fig. 3 and Table 5 that the saturated water content and the air-entry value (AEV) increased as time of observation increased. This occurred for soils with Vetiver grass (Fig. 3a and Table 5) as well as soils with Orange Jasmine (Fig. 3b and Table 5). Table 2 shows that as time of observation increased, organic content also increased. The increase in organic content indicated that there was an increase in the volume of roots in

Table 5 - Hydraulic properties of the soils with vegetations.

Description	Symbol (unit)	Soil with Orange Jasmine root			Soil with Vetiver Grass root		
		29 Jul 2010	18 Nov 2010	28 Feb 2011	29 Jul 2010	18 Nov 2010	28 Feb 2011
Drying curve							
Saturated volumetric water content	θ_s	0.32	0.37	0.41	0.27	0.28	0.30
Air-entry value	Ψ_a (kPa)	1.3	2.0	4.0	2.2	4.1	4.6
Residual matric suction	Ψ_r (kPa)	553	734	859	7118	7716	9684
Residual volumetric water content	θ_r	0.14	0.16	0.17	0.18	0.19	0.19
Fredlund & Xing (1994)	a (kPa)	5.61	7.90	13.05	8.43	14.00	17.20
Fitting parameters	n	0.98	1.05	1.20	1.01	1.11	1.04
	m	0.55	0.53	0.51	0.21	0.21	0.24
Wetting curve							
Water-entry value	Ψ_w (kPa)	770	1263	1511	8796	24364	55064
Volumetric water content at Ψ_w	θ_w	0.12	0.15	0.16	0.18	0.17	0.18
Fredlund & Xing (1994)	a (kPa)	3.52	2.50	4.13	3.41	4.43	5.44
Fitting parameters	n	0.81	0.70	0.79	2.20	0.80	0.70
	m	0.53	0.53	0.51	0.28	0.21	0.24

Table 6 - Hydraulic properties of CBS.

Description	Symbol (unit)	Soil		Secudrain
		Fine-grained layer	RCA	
Drying curve				
Saturated volumetric water content	θ_s	0.41	0.47	0.69
Air-entry value	Ψ_a (kPa)	1.4	0.03	0.4
Residual matric suction	Ψ_r (kPa)	0.07	0.20	1.8
Residual volumetric water content	θ_r	0.04	0.13	0
Fredlund & Xing (1994)	a (kPa)	1.94	0.05	4.45
Fitting parameters	n	6.3	7.97	2.17
	m	0.87	0.47	70.69
Wetting curve				
Water-entry value	Ψ_w (kPa)	3.5	0.20	0.22
Volumetric water content at Ψ_w	θ_w	0.01	0.11	0
Fredlund & Xing (1994)	a (kPa)	1.81	0.56	0.18
Fitting parameters	n	3.19	0.21	5.1
	m	3.74	0.80	5.25

soil. Therefore, it can be inferred that the growth of root resulted in an increase in the saturated water content and AEV of the soil.

Saturated and unsaturated consolidated drained (CD) triaxial tests (Fredlund and Rahardjo, 1993) were per-

formed to obtain shear strength parameters of soils without vegetation and soils with vegetations. Shear strength properties are shown in Table 7. Shear strength failure envelopes of the soil with Orange Jasmine roots and Vetiver grass roots are shown in Figs. 5 and 6, respectively. The

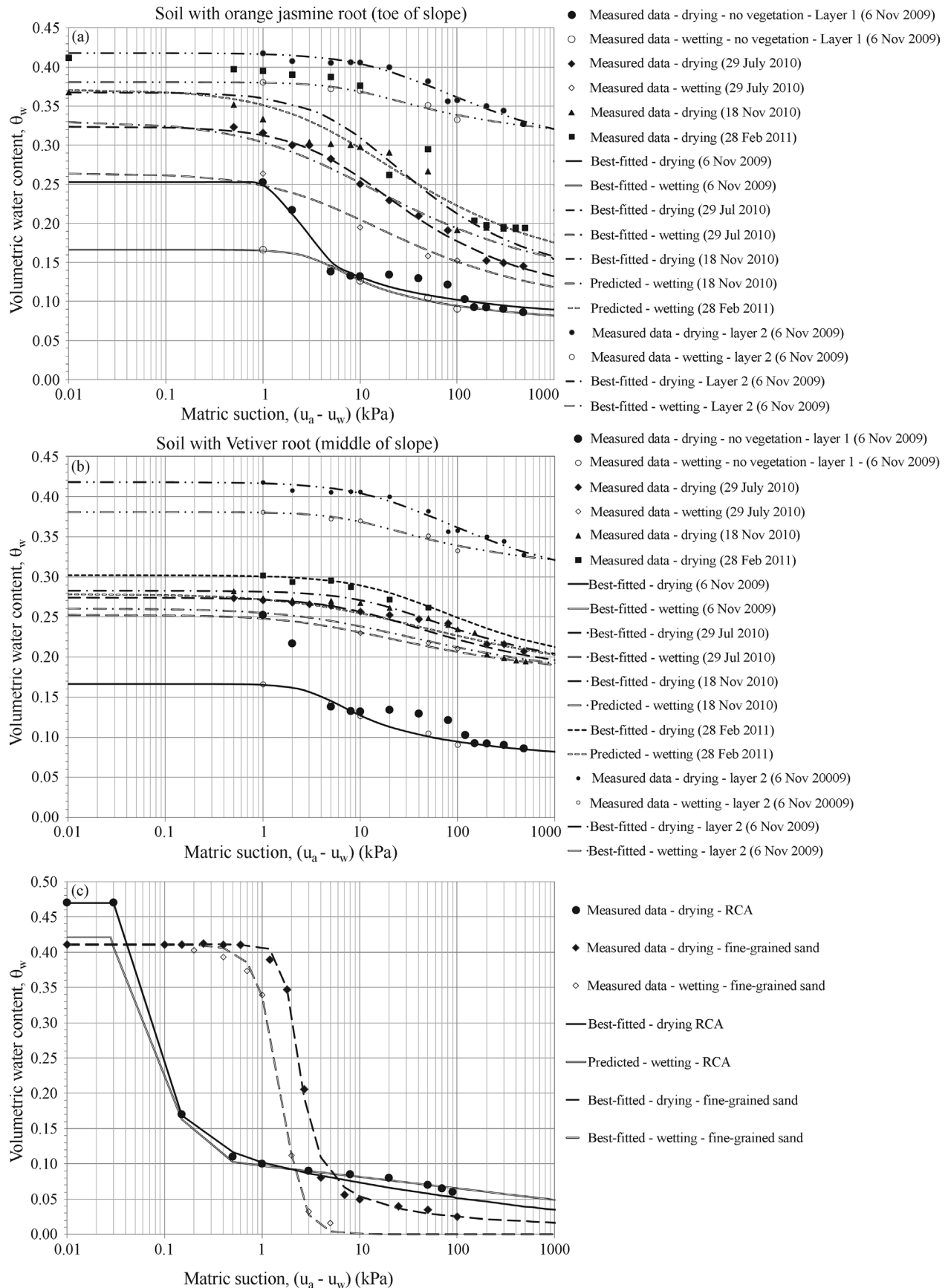


Figure 3 - SWCCs of the soils used in the study. (a) Soil with Orange Jasmine roots.

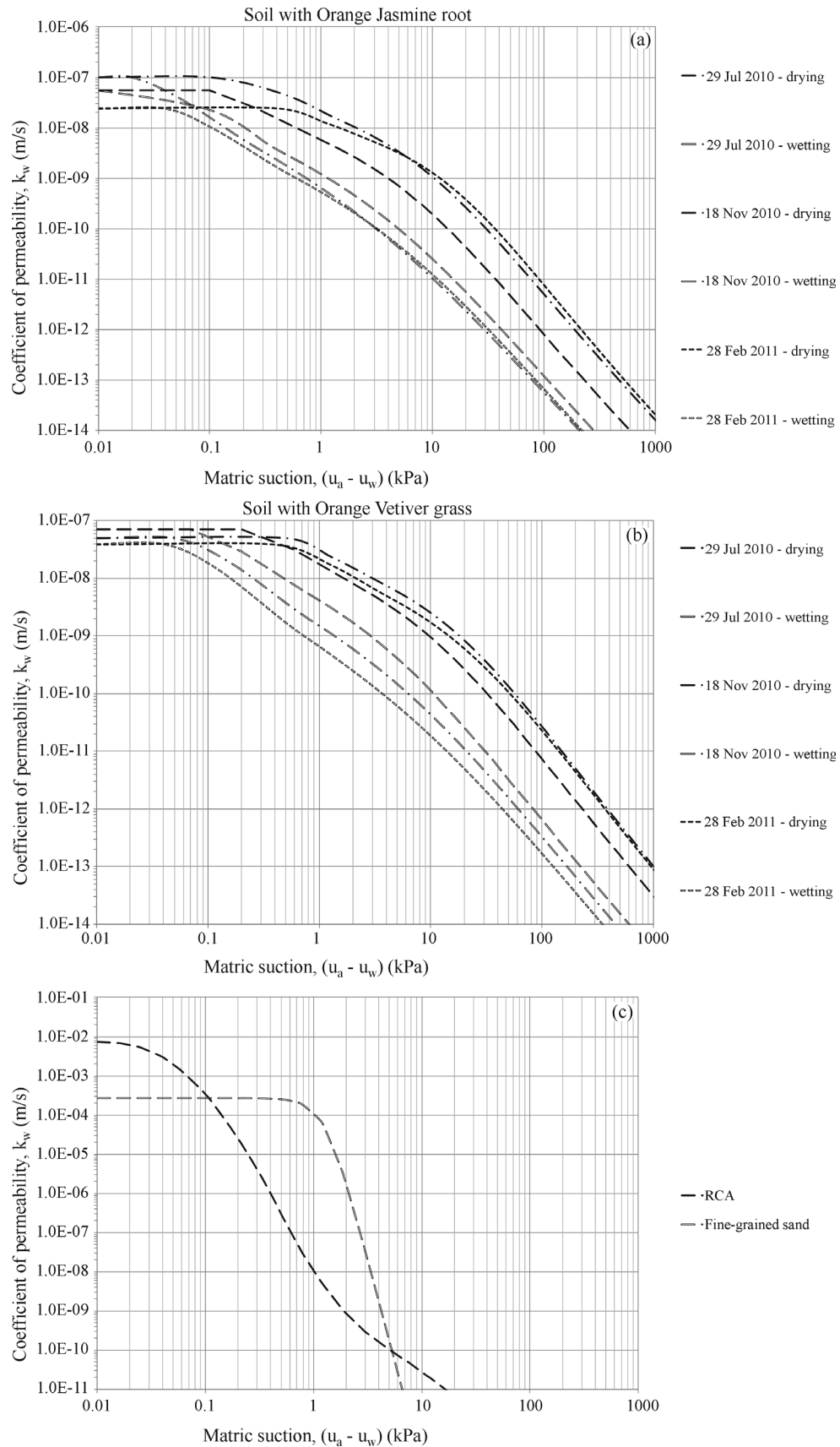


Figure 4 - Permeability functions of the soils used in the study. (a) Soil with Orange Jasmine roots. (b) Soil with Vetiver Grass roots. (c) CBS with RCA as the coarse-grained layer.

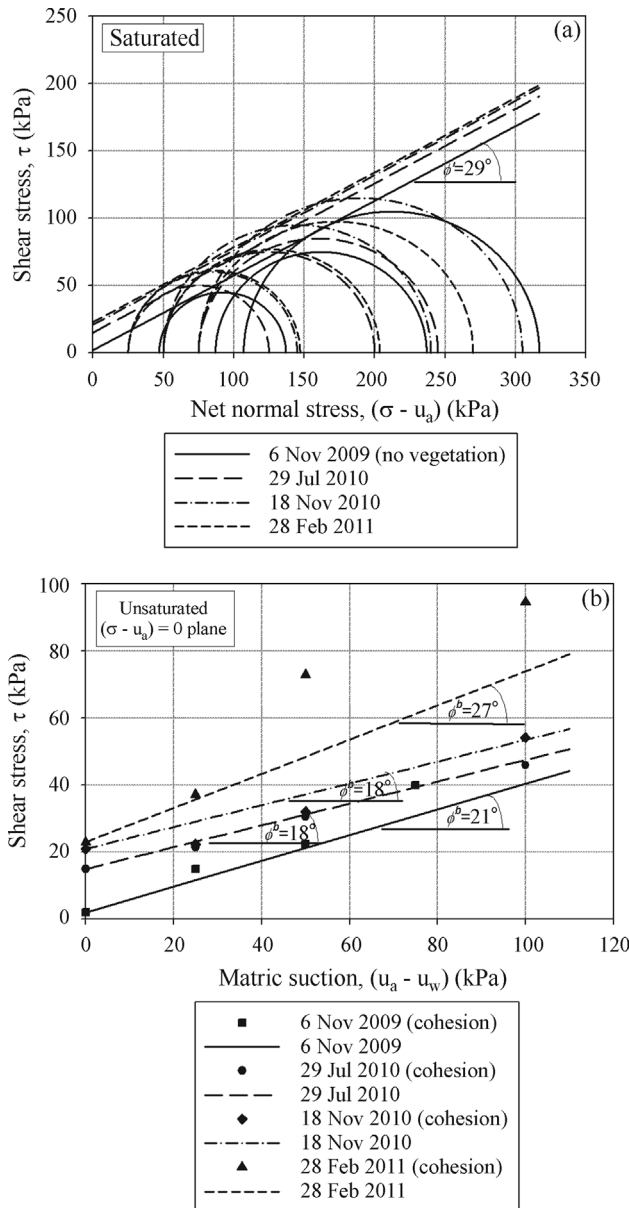


Figure 5 - Mohr-Coulomb failure envelopes of original soil and soil with Orange Jasmine roots: (a) at zero matric suction, (b) at matric suctions greater than zero and on $(\sigma - u_a) = 0$ plane.

shear strength envelope at zero matric suction (Figs. 5a and 6a) involves Mohr circles at failure and the envelope gives effective cohesion, c' and effective friction angle, ϕ' . The shear strength envelope at matric suctions greater than zero (Figs. 5b and 6b) was plotted on $(\sigma - u_a) = 0$ plane to obtain ϕ^b angle.

Comparison of shear strength parameters of the original soil (Layer 1) and the ones of the soils with Orange Jasmine roots and Vetiver grass roots in Figs. 5 and 6 and Table 7 indicates that the presence of Orange Jasmine and Vetiver grass roots increases the effective cohesion of soil. The ϕ^b angle of the soil with Orange Jasmine roots de-

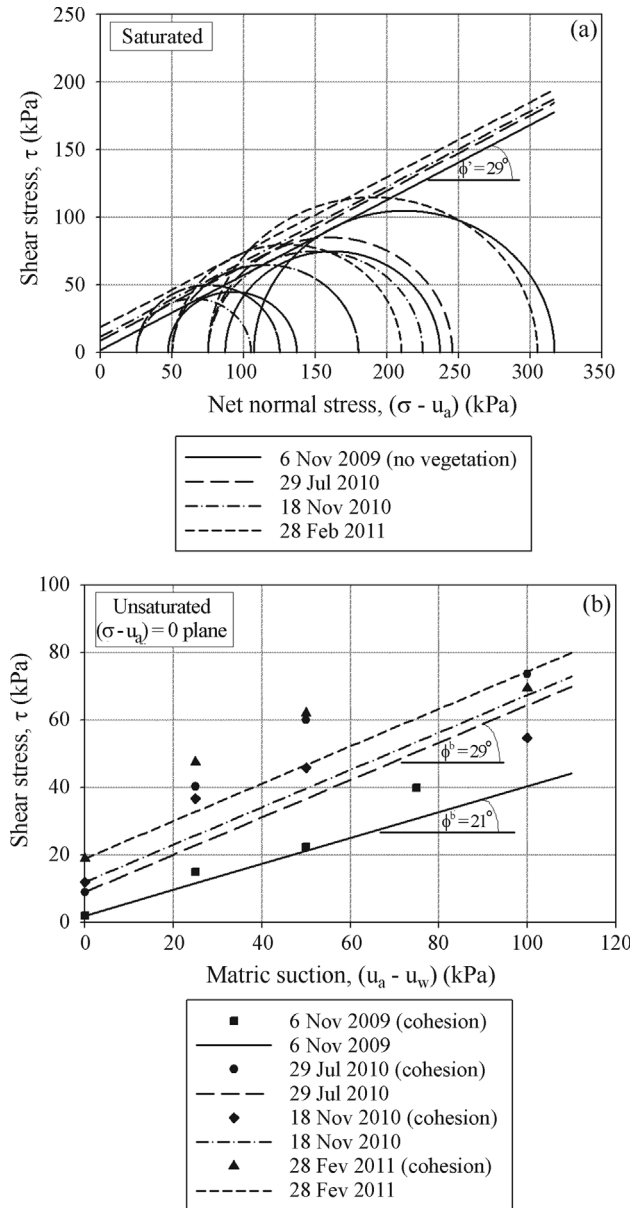


Figure 6 - Mohr-Coulomb failure envelopes of original soil and soil with Vetiver grass roots: (a) at zero matric suction, (b) at matric suctions greater than zero on $(\sigma - u_a) = 0$ plane.

creases from 21° to 18° and then increases to 27° , indicating that the ϕ^b angle of the soil with Orange Jasmine was relatively constant. The ϕ^b angle of the soil with Vetiver grass roots increases compare to the original soil.

5. Numerical Analyses

Numerical analyses were performed to investigate the effectiveness of CBS and vegetative slope covers in maintaining soil suction. Seepage and slope stability analyses were performed using the finite element software SEEP/W (GEO-SLOPE International Ltd. 2007a) and SLOPE/W (GEO-SLOPE International Ltd. 2007b), respectively.

Table 7 - Shear strength properties of the soils used in the study.

(a) Soils without vegetation.

Description	Symbol (unit)	Soils	
		Layer 1	Layer 2
Unit weight	γ (kN/m ³)	15.5	18.5
Effective cohesion	c' (kPa)	2	5
Effective friction angle	ϕ' (°)	29	37
	ϕ^b (°)	21	18

(b) Soils with Orange Jasmine roots.

Description	Symbol (unit)	Soil with Orange Jasmine root		
		29 Jul 2010	18 Nov 2010	28 Feb 2011
Unit weight	γ (kN/m ³)	16.3	19.8	20.2
Effective cohesion	c' (kPa)	15	21	23
Effective friction angle	ϕ' (°)	29	29	29
	ϕ^b (°)	18	18	27

(c) Soils with Vetiver grass roots.

Description	Symbol (unit)	Soil with Vetiver Grass root		
		29 Jul 2010	18 Nov 2010	28 Feb 2011
Unit weight	γ (kN/m ³)	16.5	19.5	20.4
Effective cohesion	c' (kPa)	9	12	19
Effective friction angle	ϕ' (°)	29	29	29
	ϕ^b (°)	29	29	29

(d) CBS.

Description	Symbol (unit)	Soils	
		Fine-grained layer	Coarse-grained layer (RCA)
Unit weight	γ (kN/m ³)	18	20
Effective cohesion	c' (kPa)	3.5	0
Effective friction angle	ϕ' (°)	44	49
	ϕ^b (°)	30	49

5.1 Slope geometries and boundary conditions

The boundary conditions (BC) for the numerical analyses are shown in Fig. 2. The boundaries were set as no flow boundaries at the bottom and as nodal flux, Q , equals to zero along the sides above water table. Constant head, H , was applied along the sides below water table. The actual rainfall was applied to the slope surface as a flux boundary, q . Ponding was not allowed to occur as water will run off the slope. Rainfalls at two time periods (the first time period represented the conditions prior to, during, and after the low intensity rainfall which occurred on 6 July 2010, named the period of low rainfall intensity while the second time period represented the conditions prior to, during, and after the high intensity rainfall which occurred on 25 November 2010, named the period of high rainfall intensity) were selected for the analyses (Figs. 7e and 8). Details of each of the rainfall events are shown in Fig. 8. The initial condition was based on the initial water table as measured using piezometers and pore-water pressure measurements from tensiometers (Figs. 7a to 7d).

Transient seepage analyses were performed for these two time periods. The results of numerical analyses were then compared with data obtained from field measurements. Analyses were performed for the original slope, slope with Orange Jasmine, slope with Vetiver grass, and slope with CBS. In the analyses for slope with Orange Jasmine and slope with Vetiver grass, SWCC and permeability function on 29 July 2010 were used for the

seepage analysis of the period of low intensity rainfall whereas SWCC and permeability function on 18 November 2010 were used for the seepage analysis of the period of high intensity rainfall. The results of numerical analyses and data obtained from field measurements for each slope section were compared to evaluate the effectiveness of slope cover in maintaining soil suction in the slope especially during rainfall.

5.2 Seepage analyses

Results of the numerical analyses for the original slope, the slope with Orange Jasmine, the slope with Vetiver grass, and the slope with CBS within the period of low intensity rainfall are shown in Figs. 9 and 10. Results from field measurements are also shown together with results from numerical analyses. It is obvious from the field measurements as well as from the numerical analysis results (Figs. 9, 10, 11, and 12) that the presence of a sub layer with a lower saturated permeability, k_s , caused a higher increase in the pore-water pressure in this lower permeability layer as compared to the soil layer located above this layer. The numerical analyses showed good agreement with the data obtained from field measurements. Generally, the performances of the different slope covers in maintaining matric suction are essentially similar during the period of low intensity rainfall.

Results of the numerical analyses for the original slope, the slope with Orange Jasmine, the slope with Vetiver

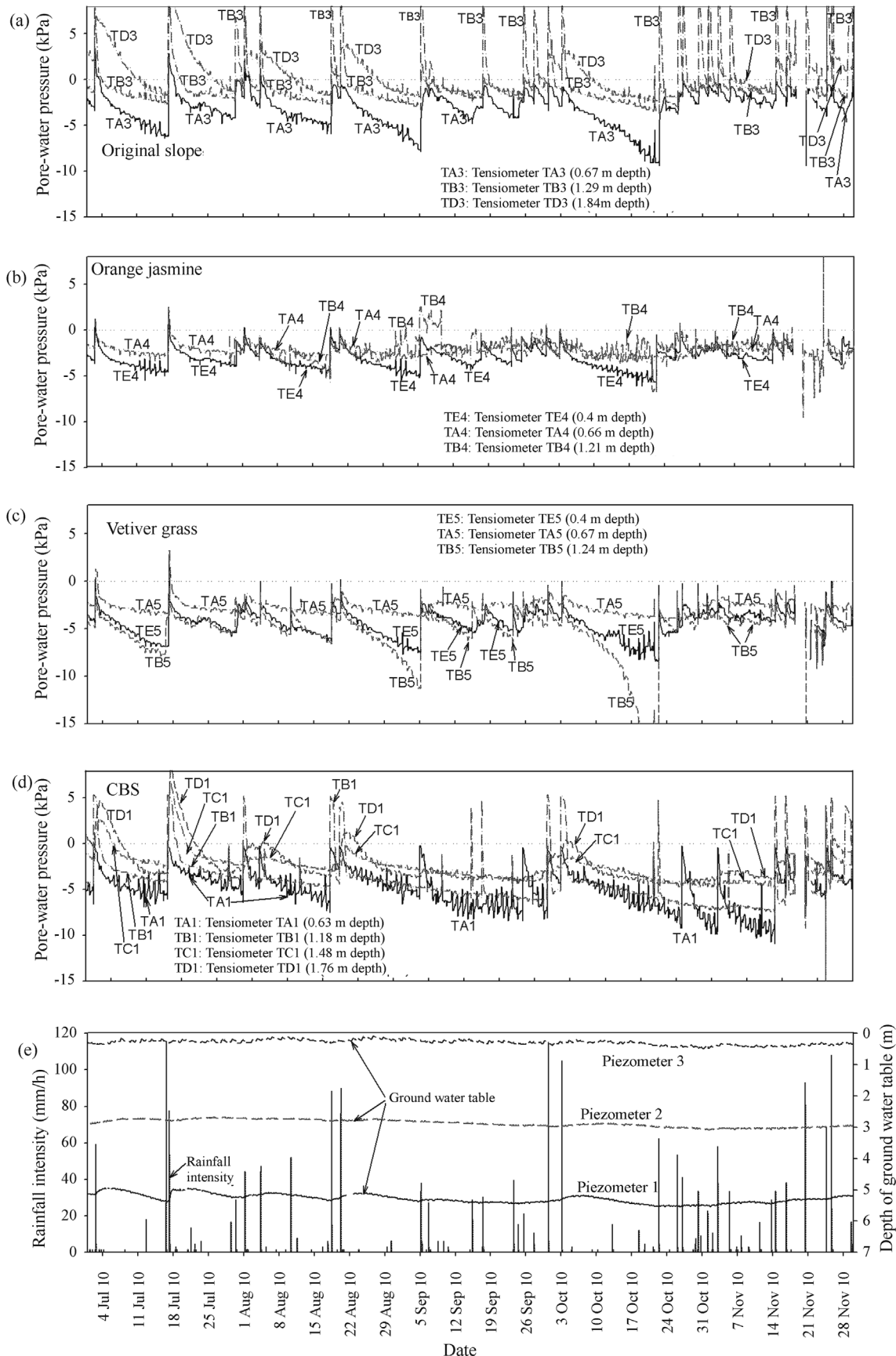


Figure 7 - Pore-water pressure, groundwater level, and daily rainfall vs. time.

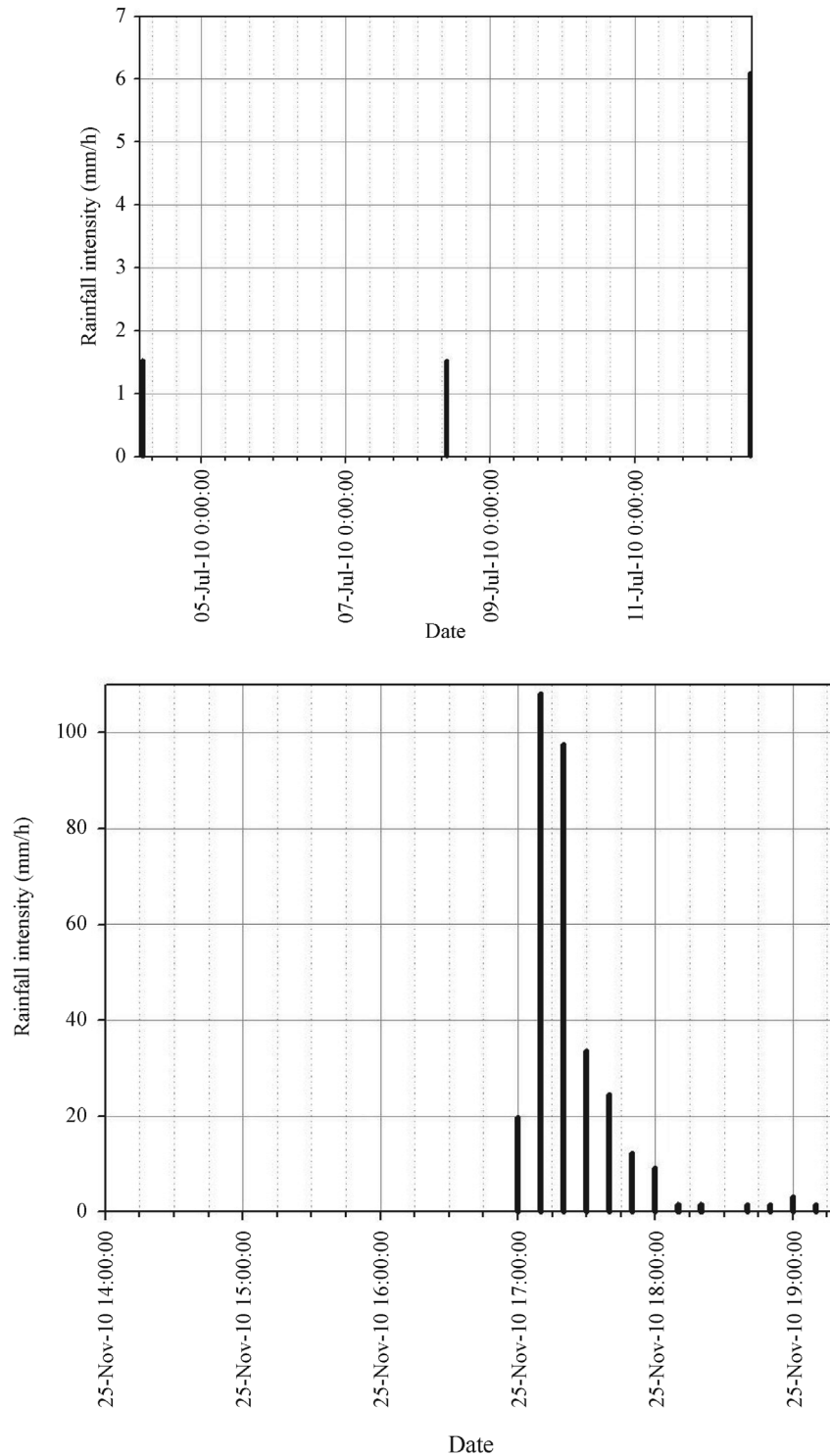


Figure 8 - Rainfall events used for the analyses. (a) Period of low intensity rainfall (prior to, during, and after 6 July 2010 rainfall event). (b) Period of high intensity rainfall (prior to, during, and after the 25 November 2010 rainfall event).

ver grass, and the slope with CBS at the period of high intensity rainfall are shown in Figs. 11 and 12. The performances of the different slope covers in maintaining matric suction are also essentially similar during the period of high intensity rainfall.

Both seepage analyses from the periods of low and high intensity rainfall showed that pore-water pressures in the slope sections with cover systems were always lower than those in the original slope without any cover system, illustrating the effective-

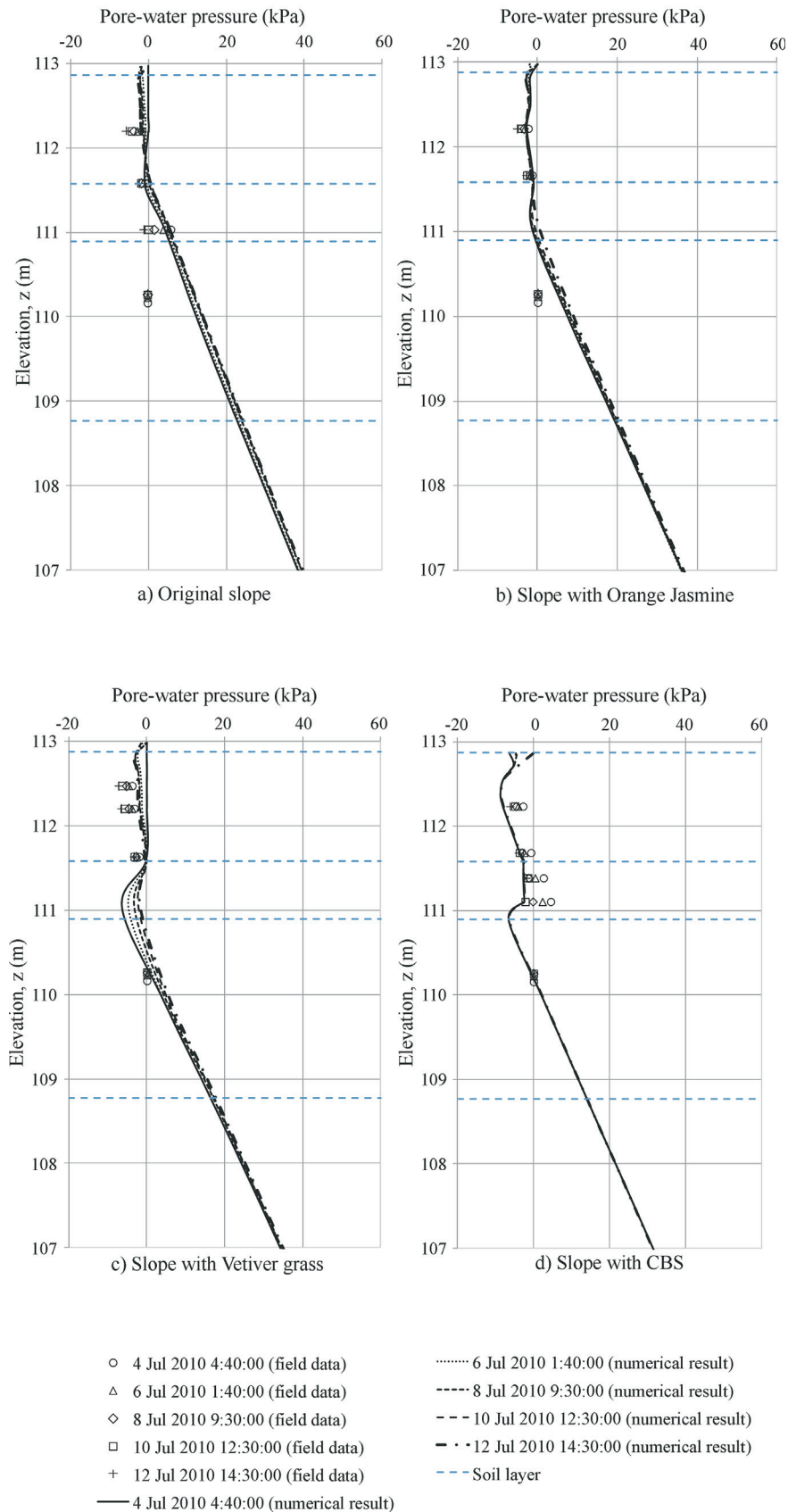


Figure 9 - Pore-water pressure profiles at each slope during the period of low intensity rainfall. (a) Original slope. (b) Slope with Orange Jasmine. (c) Slope with Vetiver grass. (d) Slope with CBS.

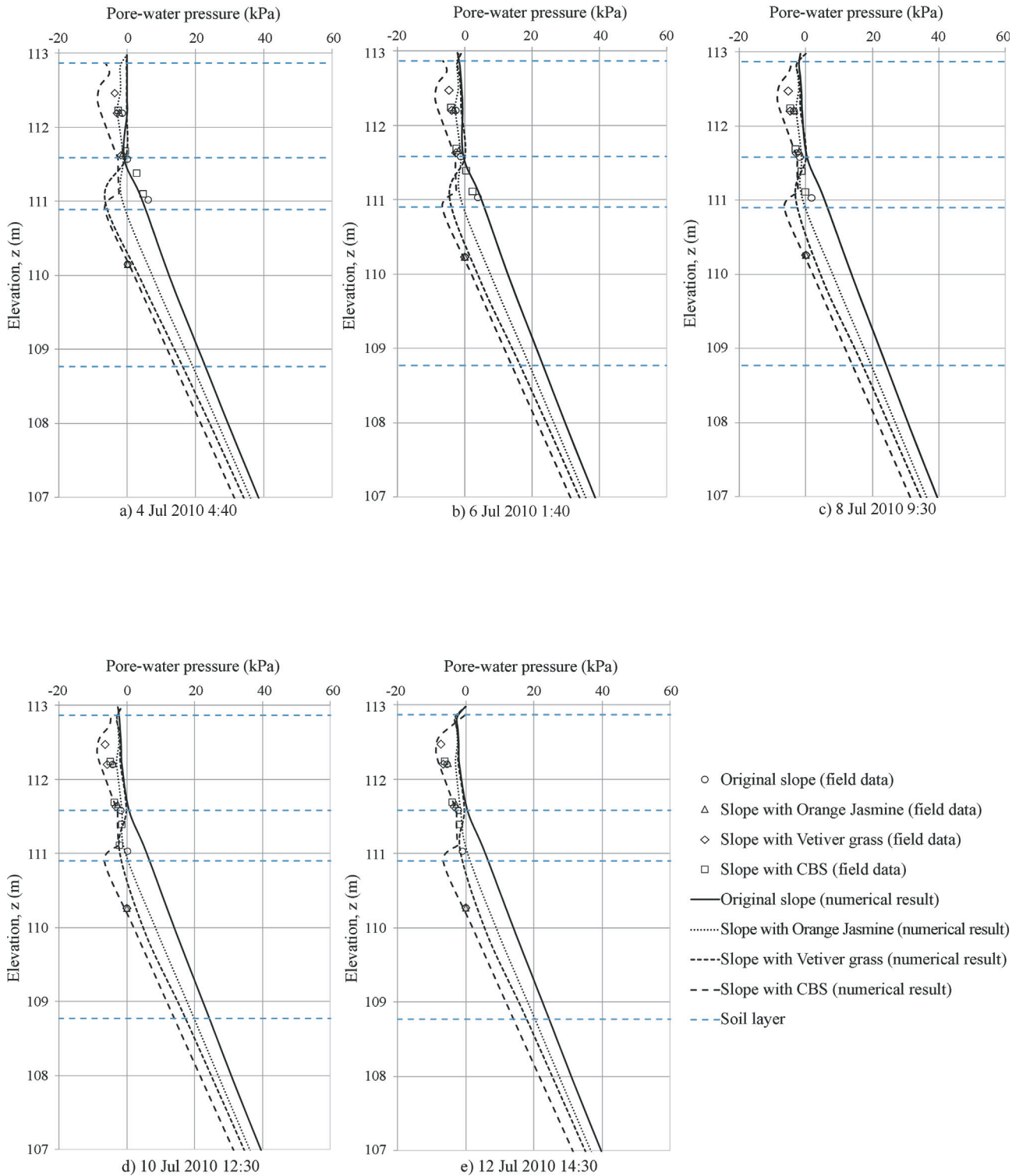


Figure 10 - Comparison of pore-water pressure profiles during the period of low intensity rainfall. (a) 4 Jul 2010 4:40. (b) 6 Jul 2010 1:40. (c) 8 Jul 2010 9:30. (d) 10 Jul 2010 12:30. (e) 12 Jul 2010 14:30.

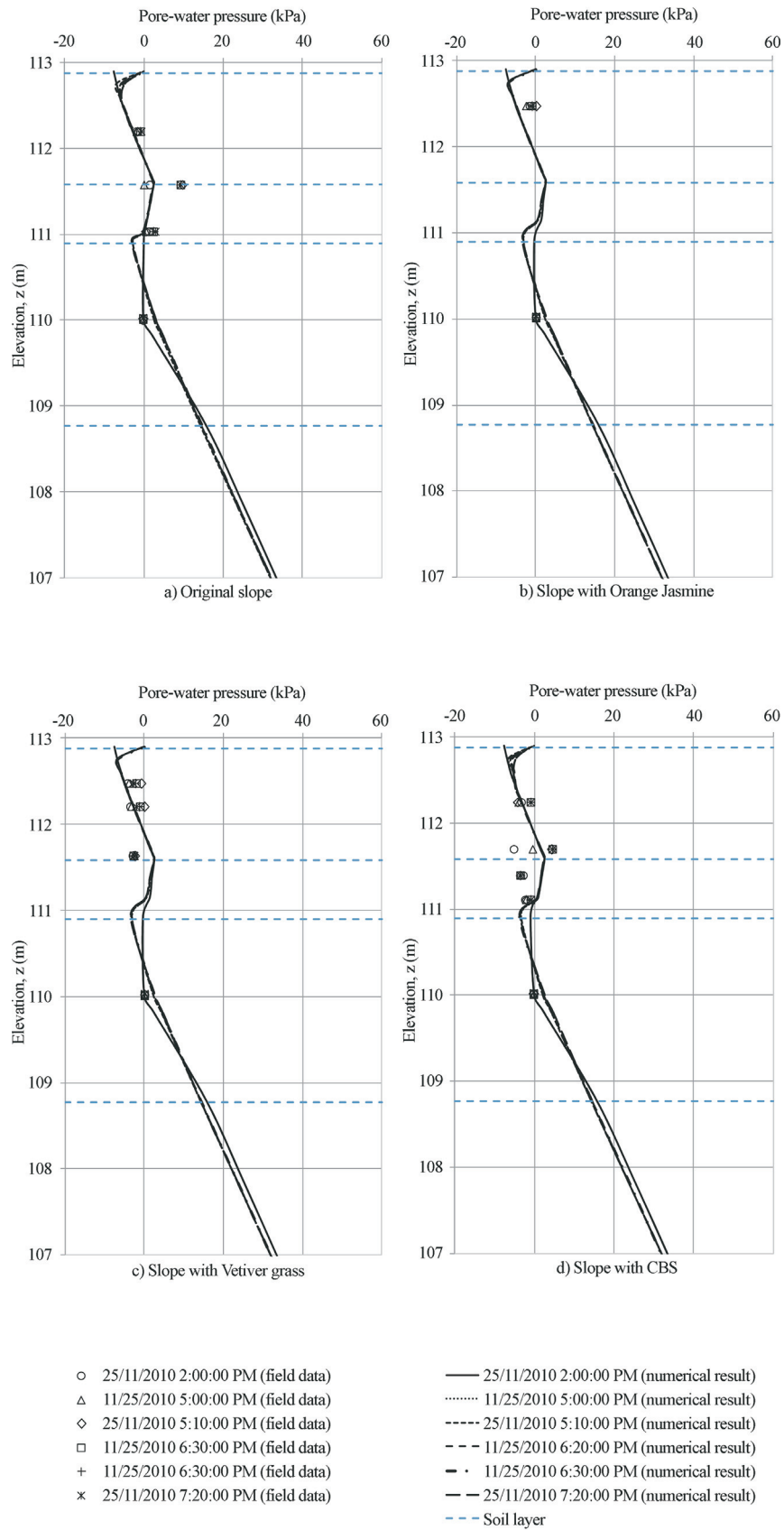


Figure 11 - Pore-water pressure profiles at each slope during the period of high intensity rainfall. (a) Original slope. (b) Slope with Orange Jasmine. (c) Slope with Vetiver grass. (d) Slope with CBS.

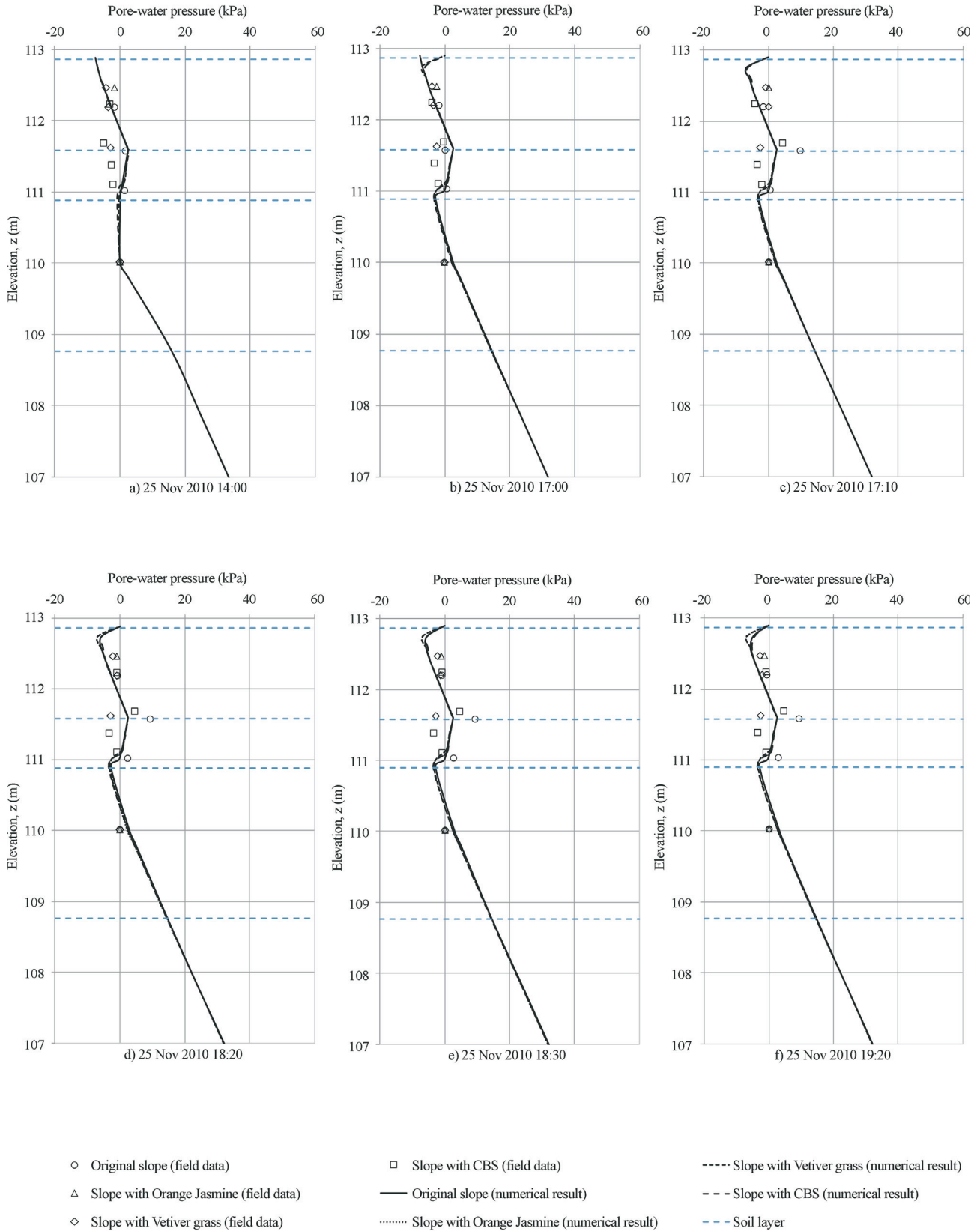


Figure 12 - Comparison of pore-water pressure profiles during the period of high intensity rainfall. (a) 25 Nov 2010 14:00. (b) 25 Nov 2010 17:00. (c) 25 Nov 2010 17:10. (d) 25 Nov 2010 18:20. (e) 25 Nov 2010 18:30. (f) 25 Nov 2010 19:20.

ness of cover system in maintaining soil suction in the slope during rainfall.

5.3 Slope stability analyses

Slope stability analyses were performed using Bishop simplified method by incorporating pore-water pressures at the periods of low and high intensity rainfall. Shear strength parameters used in the analyses are shown in Table 7. In the analyses for slope with Orange Jasmine and slope with Vetiver grass, the shear strengths on 29 July 2010 were used for the slope stability analyses of the period of low intensity rainfall whereas the shear strengths on 18 November 2010 were used for the slope stability analyses of the period of high intensity rainfall.

Variations of the factor of safety (FoS) of the different slopes during the period of low intensity rainfall are shown in Fig. 13. FoS of the slopes during the period of low intensity rainfall vary from 2.1 to 2.3. The small variation in FoS indicated that the performances of the different slope covers in maintaining matric suction in the slope were essentially similar.

Variations of FoS of the different slopes during the period of high intensity rainfall are shown in Fig. 14. FoS of the slopes during the period of high intensity rainfall vary from 2.0 to 2.1. The small variation in FoS indicated that the performances of the different slope covers in maintaining matric suction in the slope were essentially similar.

In addition to the above analyses, a stability analysis was performed using a maximum rainfall intensity of 533.2 mm/day that occurred continuously for 1 day based on a 25-year return period. This rainfall intensity is a maximum total amount of rainfall in a day of 533.2 mm that should be used in drainage system design in Singapore (PUB 2000). The effectiveness of the different slope covers experiencing this rainfall intensity was investigated through this analysis. The results are shown in Fig. 15.

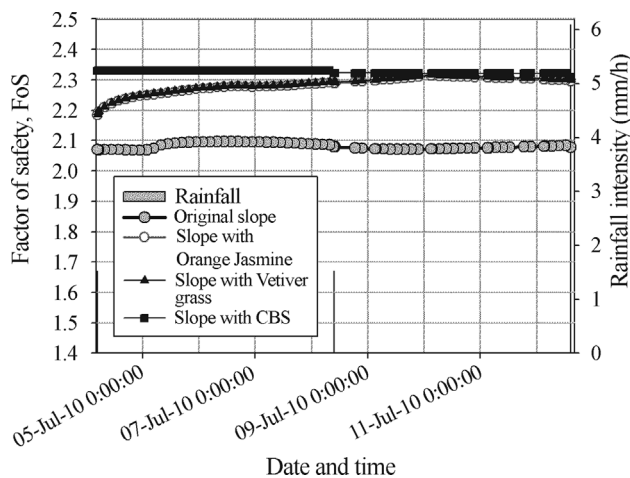


Figure 13 - Factor of safety variation during the period of the low intensity rainfall event on 6 July 2010.

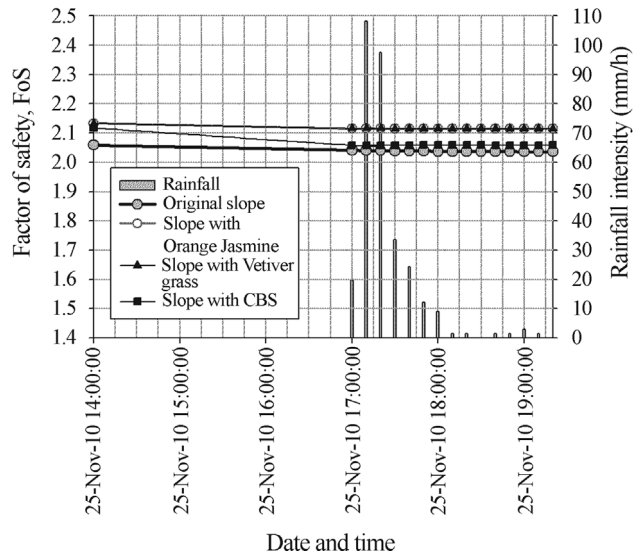


Figure 14 - Factor of safety variation during the period of the high intensity rainfall event on 25 November 2010.

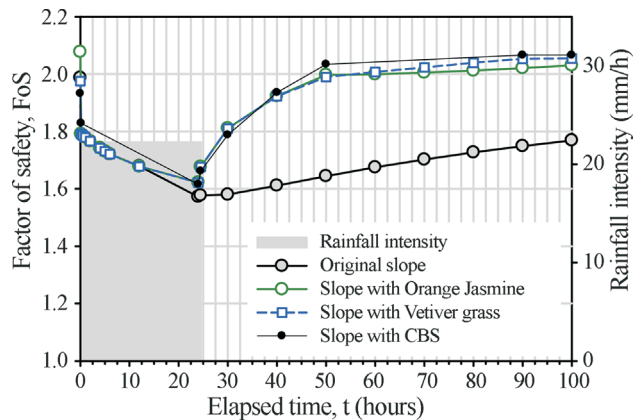


Figure 15 - Factor of safety variations during a high hypothetical rainfall intensity of 22.2 mm/h for 24 h.

The slopes had an initial FoS of around 2. After subjecting the slopes to the maximum daily rainfall, FoS of the slopes dropped to around 1.6. After the end of rainfall, FoS of the slopes with covers recovered faster than that of the original slope, indicating the effectiveness of the different cover systems in recovering FoS of the slopes after the maximum daily rainfall as compared to the original slope without cover. In addition, FoS of the slopes with slope covers were essentially similar throughout the study period.

6. Conclusions

Laboratory test results show that the presence of root increases shear strength of soils. The increase in shear strength is indicated by the increase in effective cohesion in both soils with Orange Jasmine roots and with Vetiver grass roots and by the increase in ϕ^b angle in the soil with

Vetiver grass roots. In addition to this, the presence of roots results in an increase in the saturated permeability and AEV of the soil.

Field monitoring results show that the slopes with slope covers can maintain negative pore-water pressures better than the original slope without cover. The amount of matric suction that can be maintained by the slope covers during the periods of low and high intensity rainfalls were similar for the slopes covered with Orange Jasmine, Vetiver grass, and CBS. As a result, FoS of slopes with the different covers were essentially similar during the low and high intensity rainfall periods. However, during the period of maximum intensity rainfall the slope covers resulted in a faster recovery of FoS of the slopes as compared to the original slope without the slope cover. In addition, FoS of the slopes with slope covers were essentially similar throughout the period of maximum intensity rainfall.

Acknowledgment

The work presented in this paper was supported by the Housing and Development Board and Nanyang Technological University, Singapore. Samwoh Pte Ltd provided the recycled concrete aggregate used in this study.

References

- Brand, E.W. (1992). Slope instability in tropical areas. In: Proc. 6th International Symposium on Landslides, Christchurch, New Zealand, pp. 2031-2051.
- Fredlund, D.G. & Rahardjo, H. (1993). Soil Mechanics for Unsaturated Soils. John Wiley & Sons Inc., New York, 517 p.
- Fredlund, D.G. & Xing, A. (1994). Equations for the soil-water characteristic curve. Canadian Geotechnical Journal, 31(4):521-532.
- Gasmo, J.M.; Rahardjo, H. & Leong, E.C. (2000). Infiltration effects on stability of a residual soil slope. Computers and Geotechnics, 26(2):145-165.
- GEO-SLOPE International Pte. Ltd. (2007a). SEEP/W User's Guide for Slope Stability Analysis. Geoslope International Ltd., Calgary, Alberta, Canada, 307 p.
- GEO-SLOPE International Pte. Ltd. (2007b). SLOPE/W User's Guide for Slope Stability Analysis. Geoslope International Ltd., Calgary, Alberta, Canada, 355 p.
- Grimshaw, R.G. (1994). Vetiver grass-Its use for slope and structure stabilization under tropical and semitropical conditions. In: Vegetation and Slopes. Institution of Civil Engineers, London, pp. 26-35.
- Khire, M.; Benson, C. & Bosscher, P. (2000). Capillary barriers: design variables and water balance. Journal of Geotechnical and Geoenvironmental Engineering, ASCE, 126(8):695-708.
- Krisdani, H.; Rahardjo, H. & Leong, E.C. (2008). Measurement of geotextilewater characteristic curve using capillary rise principle. Geosynthetics International, 15(2):86-94.
- Leong, E.C. & Rahardjo, H. (1997). A review on soil-water characteristic curve equations. ASCE Journal of Geotechnical and Geoenvironmental Engineering, 123(12):1106-1117.
- Morel-Seytoux, H.J. (1994). Steady-state effectiveness of a capillary barrier on a sloping interface. In: Proc. 14th Hydrology Days Conference, Fort Collins, pp. 5-8.
- Morel-Seytoux, H.J. (1993). Dynamic perspective on the capillary barrier effect at the interface of an upper fine layer with a lower coarse layer. In: Proc. of Engineering Hydrology, San Francisco, pp. 467-472.
- Morris, C.E. & Stormont, J.C. (1997a). Capillary barriers and subtitle D covers: Estimating equivalency. Journal of Environmental Engineering, ASCE, 123(1):3-10.
- Morris, C.E. & Stormont, J.C. (1997b). Closure to "Capillary barriers and subtitle D covers: estimating equivalency" by Carl E. Morris and John C. Stormont. Journal of Environmental Engineering, ASCE, 123(1):3-10.
- National Research Council (1993). Vetiver Grass: A Thin Green Line Against Erosion. National Academy Press, Washington DC, 188 p.
- Pham, H.; Fredlund, D.G. & Barbour, S.L. (2005). A study of hysteresis models for soil-water characteristic curves. Canadian Geotechnical Journal, 42(6):1548-1568.
- Pitts, J. (1985). An Investigation of Slope Stability on the NTU Campus, Singapore. Applied Research Project RPI/83. Nanyang Technological Institute, Singapore.
- PUB (2000). Code of Practice on Surface Water Drainage. Public Utilities Board, Singapore, 63 pp.
- Ross, B. (1990). The diversion capacity of capillary barriers. Water Resources Research, 26(10):2625-2629.
- Steenhuis, T.S.; Parlange, J.-Y. & Kung, K.-J. (1991). Comment on "The Diversion Capacity of Capillary Barriers" by Benjamin Ross. Water Resources Research, 27(8):2155-2156.
- Stormont, J.C. (1996). The effectiveness of two capillary barriers on a 10% slope. Geotechnical and Geological Engineering, 14(4):243-267.
- Styczen, M.E. & Morgan, R.P.C. (1995). Engineering properties of vegetation. In: R.P.C. Morgan and R.J. Rickson (eds) Slope Stabilization and Erosion Control. E & FN Spon, London, pp. 5-58.
- Tami, D.; Rahardjo, H.; Leong, E.C. & Fredlund, D.G. (2004a). A physical model for sloping capillary barriers. Geotechnical Testing Journal, 27(2):173-183.
- Tami, D.; Rahardjo, H.; Leong, E.-C. & Fredlund, D.G. (2004b). Design and laboratory verification of a physical model of sloping capillary barrier. Canadian Geotechnical Journal, 41(5):814-830.
- Tan, S.B.; Tan, S.L.; Lim, T.L. & Yang, K.S. (1987). Landslides problems and their control in Singapore. In: Proc. 9th Southeast Asian Geotechnical Conference, Bangkok, Thailand, v. 1, pp. 25-36.

- TenCate (2011). TenCate Polyfelt TS Nonwoven Geotextiles. TenCate Geosynthetics Asia Sdn. Bhd. Selangor Darul Ehsan, Malaysia, 8 pp.
- Truong, P. & Gawander, J.S. (1996). Back from the future: do's and don'ts after 50 years of Vetiver utilisation in Fiji. Proc. First International Conference on Vetiver. Office of the Royal Development Projects Board, Bangkok, pp. 12-17.
- Tsaparas, I.; Rahardjo, H.; Toll, D.G. & Leong, E.C. (2002). Controlling parameters for rainfall-induced landslides. *Computers and Geotechnics*, 29(1):1-27.
- World Bank (1995). Vetiver Grass for Soil and Water Conservation. Technical Paper No. 273. RG Grimshaw (ed), Washington DC, 281 p.
- Yang, H.; Rahardjo, H.; Leong, E.C. & Fredlund, D.G. (2004b). A study of infiltration on three sand capillary barriers. *Canadian Geotechnical Journal*, 41(4):629-643.

Influence of Poisson's Ratio on the Stress vs. Settlement Behavior of Shallow Foundations in Unsaturated Fine-Grained Soils

W.T. Oh, S.K. Vanapalli

Abstract. Poisson's ratio is typically assumed to be constant for both saturated and unsaturated soils. However, the back-calculated Poisson's ratio using the relationship between elastic and shear modulus (*i.e.* the equation for homogeneous, isotropic and linear elastic continuum) published in the literature showed that the Poisson's ratio is not constant but decreases with the degree of saturation (or increasing suction). In the present study, more focused investigations are undertaken to study the influence of Poisson's ratio on the stress vs. settlement (SVS) behaviour of shallow foundations in an unsaturated fine-grained (UFG) soil. The FEA are carried out using the software, SIGMA/W (GeoStudio 2007) to better understand the SVS behavior taking account of the influence of Poisson's ratio for different matric suction values and compared with the model footing tests conducted in an UFG soil. Several suggestions are made with respect to the influence of Poisson's ratio on the SVS behavior of shallow foundations in the UFG soils based on the results of this study.

Keywords: unsaturated soil, poisson's ratio, stress vs. settlement, shallow foundation, finite element analysis.

1. Introduction

In recent years, significant advancements were made in the area of geotechnical engineering applications extending the mechanics of unsaturated soils for the shallow foundations (Ausilio & Conte 1999, Costa *et al.*, 2003, Cerato & Lutenegeger 2006, Oh & Vanapalli 2013a), deep foundations (Weaver & Grandi 2009, Vanapalli & Taylan 2012), and heave analysis (Chao *et al.*, 2001), etc.. However, laboratory or field studies on the unsaturated soils are time-consuming, cumbersome, and require elaborate testing equipment. Due to this reason, more and more studies on the unsaturated soils are directed to Finite Element Analysis (hereafter referred to as FEA), which can be attributed to the recent advancements with respect to several semi-empirical or constitutive models for unsaturated soils (Georgiadis *et al.*, 2003, Vu & Fredlund 2006, Wejrungsikul *et al.*, 2011, Oh & Vanapalli 2011a,b, Adem & Vanapalli 2013, Gallipoli *et al.*, 2013). In the present study, an attempt is made to estimate the stress vs. settlement (hereafter referred to as SVS) behavior of a model footing (*i.e.* shallow foundation) in unsaturated fine-grained (hereafter referred to as UFG) soils using the FEA extending mechanics of unsaturated soils.

The bearing capacity and settlement are two key parameters in the design of shallow foundations. However, it is commonly acknowledged that the design of shallow foundations is typically governed by settlement behavior rather than the bearing capacity. Mohamed & Vanapalli (2006) carried out model footing ($B \times L = 100 \text{ mm} \times 100 \text{ mm}$ and $150 \text{ mm} \times 150 \text{ mm}$) tests in a sandy soil for

four different average matric suction values (*i.e.* 0, 2, 4 and 6 kPa). Based on their experimental results, Vanapalli & Mohamed (2007) proposed a semi-empirical model to estimate the variation of bearing capacity of coarse-grained soils with respect to matric suction. However, the SVS behaviours from the model footing test results showed that the matric suction has significant influence on not only bearing capacity but also on the initial tangent elastic modulus, E_t . In other words, the reliable estimation of elastic settlement in unsaturated soils can be obtained by considering the variation of initial tangent elastic modulus with respect to matric suction. By extending this concept, Oh *et al.* (2009) proposed a semi-empirical model that can be used to estimate the variation of initial tangent elastic modulus with respect to matric suction for coarse-grained soils below shallow foundations. This model uses two fitting parameters, α and β and the Soil-Water Characteristic Curve (hereafter referred to as SWCC). Vanapalli & Oh (2010) extended this model to fine-grained soils with Plasticity Index, I_p values less than 16% and showed that fitting parameter, α is a function of I_p . This model can be effectively used to estimate elastic settlement of unsaturated soils below shallow foundations; however, there is limitation to identify stress ranges corresponding to elastic settlement. To overcome this disadvantage, Oh & Vanapalli (2011a) proposed two methods to predict the variation of the SVS behavior of shallow foundations located on the surface of coarse-grained soils. In the first method, the SVS behavior was idealized using two straight lines, which represent elastic and perfectly plastic behaviour, respectively. These two

Won Taek Oh, Ph.D., Department of Civil Engineering, University of New Brunswick, Fredericton, Canada. e-mail: woh@unb.ca.

Sai K. Vanapalli, Ph.D., Department of Civil Engineering, University of Ottawa, Ottawa, Ontario, Canada. e-mail: vanapall@eng.uottawa.ca.

Invited Article, no discussion.

straight lines were established extending the concepts proposed by Oh *et al.* (2009) and Vanapalli & Mohamed (2007) to predict the initial tangent modulus of subgrade reaction based on initial tangent elastic modulus and bearing capacity with respect to matric suction, respectively. In the second method, the FEA was carried out also using elastic - perfectly plastic model with Mohr-Coulomb yield criterion (Chen & Zhang 1991). In the FEA, the soil profile was assumed to be a single layer with average matric suction value (*i.e.* constant total and apparent cohesion and initial tangent elastic modulus). The second method (*i.e.* FEA) has been successfully used to simulate the SVS behavior of in-situ footing ($B \times L = 1 \text{ m} \times 1 \text{ m}$) load test results in unsaturated sand (Oh & Vanapalli 2011b, 2012). The studies by Oh & Vanapalli (2011b, 2012) show that the SVS behaviour of shallow foundation in unsaturated soils can be reliably estimated when the FEA is carried out using the elastic modulus function (*i.e.* variation of elastic modulus with respect to the matric suction). This is because the FEA based on elastic - perfectly plastic model is mainly influenced by the elastic modulus and the Poisson's ratio, ν . Oh & Vanapalli (2012) investigated the influence of the Poisson's ratio on the SVS behavior of shallow foundation by conducting the FEA for different ν values. The estimated SVS behavior were relatively close to each other for the ν values used in the analysis (*i.e.* $\nu = 0.1, 0.2, 0.3, 0.4$ and 0.495). However, better comparison between the measured and the estimated SVS behaviour was obtained for the ν values of 0.2 and 0.3 , which are more reasonable for sands.

In the present study, more focused investigations are undertaken to study the influence of Poisson's ratio on the SVS behaviour of shallow foundations in unsaturated fine-grained soils. The FEA are performed using the SIGMA/W (GeoStudio 2007) for the model footing tests results (Oh & Vanapalli 2013b) in UFG soils. The elastic - perfectly plastic model was used for the FEA and the SVS behavior estimated taking account of the influence of suction with different values of Poisson's ratio are compared with those from the model footing tests. Based on the results of these studies several suggestions are made with respect to the influence of Poisson's ratio on the SVS behavior for shallow foundations in the UFG soils.

2. Model Footing test in Unsaturated Fine-Grained Soil

Oh & Vanapalli (2013b) conducted a series of model footing tests on a statically compacted glacial till using specially designed equipment (Fig. 1). The tests were performed for five different average matric suction values (*i.e.* $0, 55, 100, 160,$ and 205 kPa). The value of matric suction at the center of gravity of the matric suction distribution diagram from 0 to $1.5B$ ($B =$ width of foundation) depth region was considered as the average matric suction. $1.5B$ is the depth in which the stress below a shallow foundation is pre-

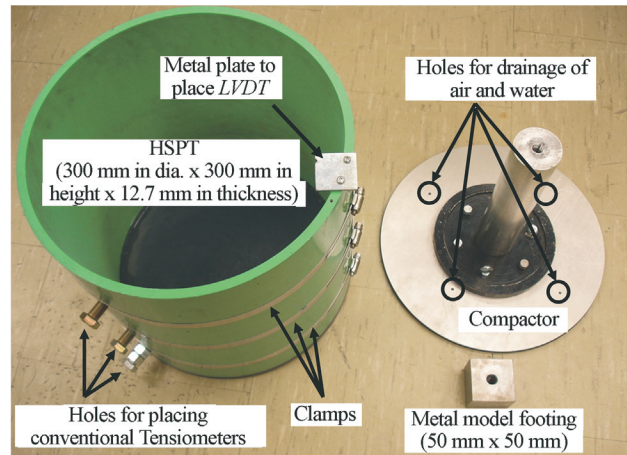


Figure 1 - Equipments used in the study for conducting model footing tests (Oh & Vanapalli, 2013b).

dominant (Agarwal & Rana 1987, Vanapalli & Mohamed 2007, Oh *et al.*, 2009, Oh & Vanapalli 2011a,b). The matric suction distribution diagrams with depth for different average matric suction values were obtained based on the SWCC (Fig. 2) using water contents measured along with depth. The SWCC was measured using pressure plate technique. Figure 3 and Fig. 4 show the model footing test setup and the SVS behaviors for five different matric suction values. The bearing capacity values were determined using a graphical method (*i.e.* stress corresponding to the intersection of elastic and plastic line on the SVS behavior).

3. Finite Element Analysis

Oh & Vanapalli (2011) suggested that the FEA can be effectively used to simulate the SVS behavior of shallow foundations on unsaturated soils using an elastic - perfectly plastic model with the Mohr-Coulomb yield criterion. In the present study, commercial FEA software, SIGMA/W (GeoStudio 2007) is used to simulate the SVS of the model

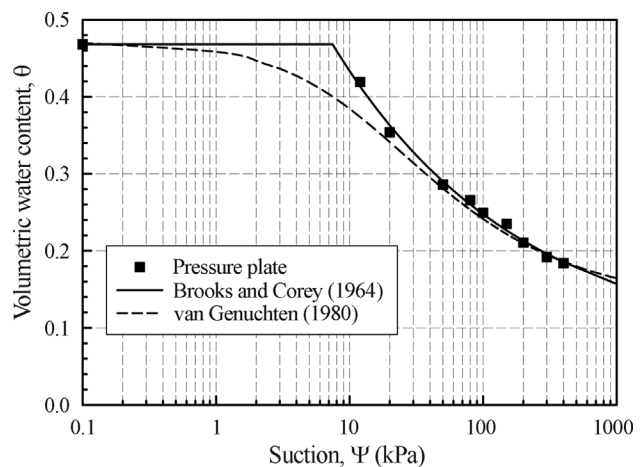


Figure 2 - Soil-water characteristic curve measured using pressure plate technique (modified after Oh & Vanapalli, 2013b).

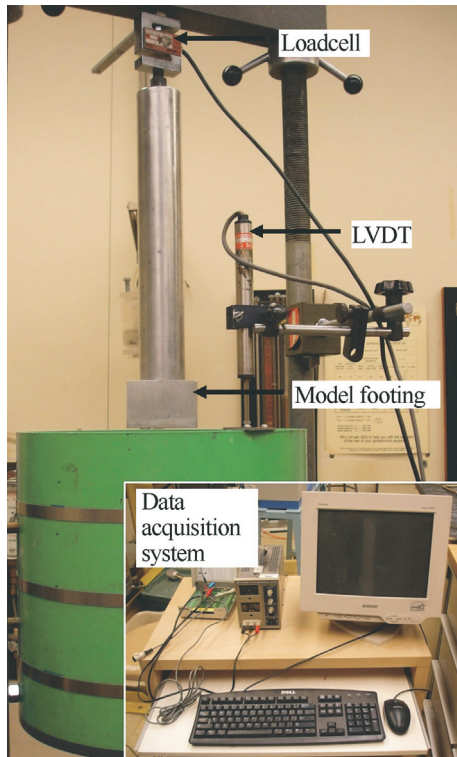


Figure 3 - Equipment set-up for conducting model footing tests (Oh & Vanapalli, 2013b).

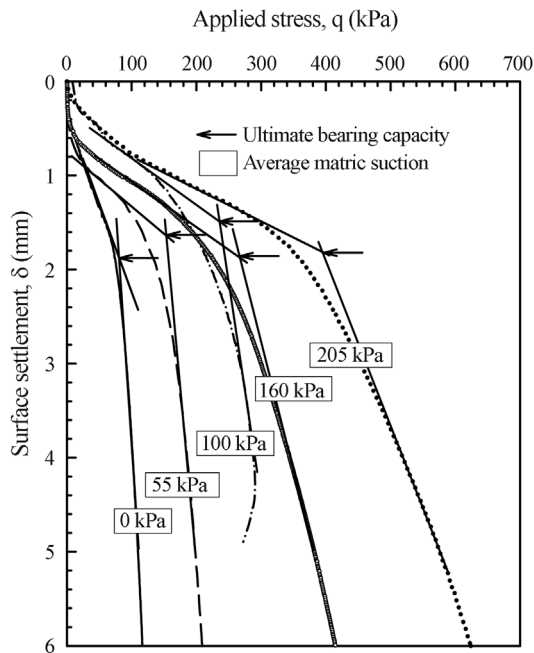


Figure 4 - Bearing capacity test results (modified after Oh & Vanapalli, 2013b).

footing test results by Oh & Vanapalli (2013b). The main input parameters required for the elastic - perfectly plastic model are cohesion and internal friction angle, initial tangent elastic modulus, and Poisson's ratio.

3.1. Cohesion and internal friction angle

Oh & Vanapalli (2013b) suggested that the bearing capacity of unsaturated soils should be estimated considering soil type and drainage condition. Based on this concept, they proposed two approaches, Modified Effective Stress Approach (MESA) and Modified Total Stress Approach (MTSA) for unsaturated coarse- and fine-grained soils, respectively. In the case of unsaturated coarse-grained soils, (i) both the pore-air and the pore-water in soils are in drained condition during the loading stages and (ii) the general failure can be expected for relatively high density coarse-grained soils. In other words, the bearing capacity of unsaturated coarse-grained soils can be reliably estimated extending effective stress approach using effective shear strength parameters, c' and ϕ' for saturated condition (*i.e.* MESA, Vanapalli & Mohamed 2007).

$$q_{ult(unsat)} = [c' + (u_a - u_w)_b (1 - S^{\psi_{BC}} \tan \phi') + (u_a - u_w)_{AVR} S^{\psi_{BC}} \tan \phi'] N_c \xi_c + 0.5 B \gamma N_\gamma \xi_\gamma \quad (1)$$

where $q_{ult(unsat)}$ = ultimate bearing capacity of unsaturated soils, $(u_a - u_w)_b$ = air-entry value, $(u_a - u_w)_{AVR}$ = average matric suction value, S = degree of saturation, γ = soil unit weight, ψ_{BC} = fitting parameter with respect to bearing capacity ($\psi_{BC} = 1$ for coarse-grained soils), B = width of footing, N_c , N_γ = bearing capacity factor from Terzaghi (1943) and Kumbhokjar (1993), respectively, and $\xi_c = \left[1.0 + \left(\frac{N_q}{N_c} \right) \left(\frac{B}{L} \right) \right]$, $\xi_\gamma = \left[1.0 - 0.4 \left(\frac{B}{L} \right) \right]$ = shape factors from Vesic (1973).

In SIGMA/W (2007), the influence of matric suction on the cohesion is considered using Eq. 2 (Vanapalli *et al.*, 1996). A constant value of effective internal friction angle, ϕ' can be used in the FEA as ϕ' is not influenced by matric suction (Vanapalli *et al.*, 1996, Wang *et al.*, 2002, Nishimura *et al.*, 2007).

$$c = c' + (u_a - u_w) \left[\left(\frac{\theta_w - \theta_r}{\theta_s - \theta_r} \right) \tan \phi' \right] \quad (2)$$

where c = total cohesion, c' , ϕ' = effective cohesion and internal friction angle, respectively, $(u_a - u_w)$ = matric suction, θ_w = volumetric water content, θ_s = saturated volumetric water content, and θ_r = residual volumetric water content

On the other hand, the behavior of the UFG soils below footings can be interpreted using the punching shear failure mechanism (Oloo 1994, Schnaid *et al.*, 1995, Consoli *et al.*, 1998, Costa *et al.*, 2003, Rojas *et al.*, 2007). For punching shear failure condition, the slip surfaces below footings are typically not extended to the ground surface but instead restricted to vertical planes and no heave is observed on the surface of the soil as shown in Fig. 5. This characteristic behaviour indicates that the bearing capacity

of the UFG soils is governed by the compressibility of the soil below a footing (*i.e.* soil A-A'-B-B' in Fig. 5; hereafter referred to as soil block). When the soil block, A-A'-B-B' is compressed due to the stress applied by a footing the soil around the soil block acts as confining pressure. In other words, the bearing capacity of the UFG soils can be represented as a function of a compressive strength of the soil block. A reasonable assumption can be made with respect to the pore-air to be under drained condition while the pore-water is under undrained condition during the loading stages of model footings or in-situ plate load tests in the UFG soils. This means that the pore-air is equal to atmospheric pressure and the water content in the soil is constant throughout the loading stage. Among the various methods available for estimating the shear strength of unsaturated soils, the constant water content (CW) test is regarded as the most reasonable technique for simulating this loading and drainage condition (Rahardjo *et al.*, 2004; Infante Sedano *et al.*, 2007). The CW test is however time-consuming and needs elaborate testing equipments. Hence, the unconfined compressive shear strength for unsaturated fine-grained soils can be used instead of the conventional CW test results. The use of unconfined compression test results can be justified based on the following facts and reasonable assumptions.

- (i) The drainage condition in unconfined compression tests for unsaturated fine-grained soils is the same as the CW test (*i.e.* pore-air pressure is atmospheric pressure and the water content is constant throughout the test).
- (ii) The shear strength increases with increasing confining pressure for the same matric suction values for CW test (Rahardjo *et al.*, 2004). Therefore, the shear strength obtained from the unconfined compression tests typically provides conservative estimates.

Based on this discussion, Oh & Vanapalli (2013b) suggested that the bearing capacity of UFG soils can be estimated using Eq. 3 extending the total stress approach (*i.e.* MTSA).

$$q_{ult(unsat)} = \left[\frac{q_u(unsat)}{2} \right] \left[1 + 0.2 \left(\frac{B}{L} \right) \right] N_{unsat} \quad (3)$$

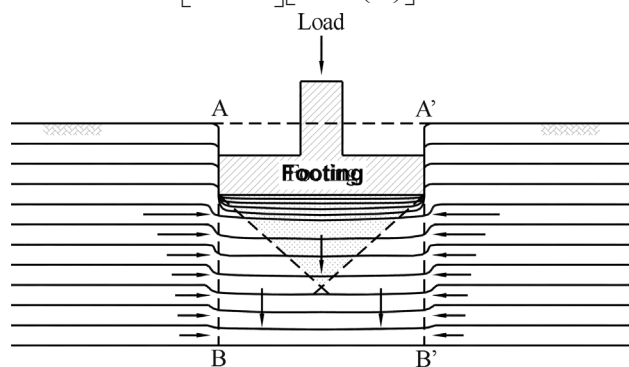


Figure 5 - Punching shear failure mechanism in unsaturated fine-grained soils below a footing (modified after Oh & Vanapalli, 2013b).

where $q_{ult(unsat)}$ = ultimate bearing capacity of unsaturated fine-grained soil, $q_u(unsat)$ = unconfined compressive strength for unsaturated fine-grained soil, B, L = width and length of foundation, and N_{unsat} = bearing capacity factor N_c for the UFG soil.

3.2. Initial tangent elastic modulus

The initial tangent elastic modulus, E_i from plate load (or model footing) test can be calculated using Eq. 4 (Fig. 6).

$$E_i = \frac{(1-\nu^2)}{\left(\frac{\Delta\delta}{\Delta q} \right)} I_w B = k_{is} (1-\nu^2) I_w B \quad (4)$$

where E_i = initial tangent elastic modulus, ν = Poisson's ratio (*i.e.* $\nu = 0.3$ for coarse-grained soils), $\Delta q, \Delta\delta$ = applied stress and displacement in elastic range, respectively, k_{is} = initial tangent subgrade reaction modulus ($= \Delta\delta/\Delta q$), B = width of footing, and I_w = influence factor (*i.e.* 0.88 for square plate)

In the case of FEA, the influence of ν on the SVS behavior is included as an input parameter. In addition, if the analysis is conducted as axisymmetric condition the influence of I_w on the SVS behavior can be considered by using equivalent area. Hence, Oh & Vanapalli (2011a) proposed the Eq. 5 to calculate the E_i for the FEA.

$$E_i = \frac{15B}{\left(\frac{\Delta\delta}{\Delta q} \right)} = \frac{\Delta q}{\left(\frac{\Delta\delta}{15B} \right)} \quad (5)$$

3.3. Poisson's ratio

The elastic (E) and shear (G) modulus of soils are two key parameters that are required in the evaluation of the immediate settlement and dynamic response behavior respectively of geotechnical structures in engineering practice. If

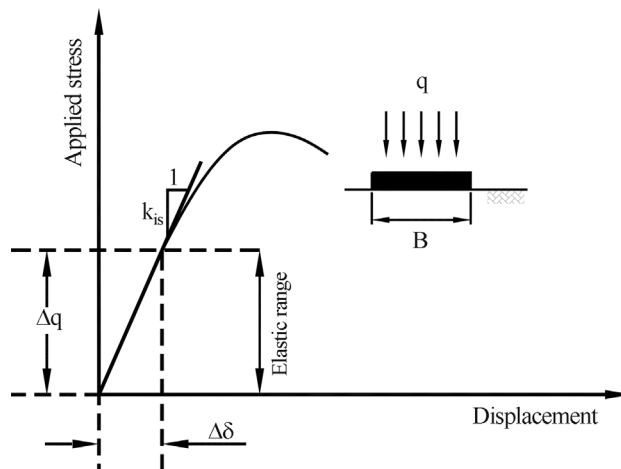


Figure 6 - Typical stress vs. settlement behavior from plate load test (Oh & Vanapalli, 2011).

a soil is assumed to be homogeneous, isotropic and linear elastic continuum the Poisson's ratio can be calculated using the relationship between the E and the G . The Poisson's ratio, ν is typically assumed to be constant in the numerical modelling studies of both saturated and unsaturated soils. Such an assumption is reasonable for coarse-grained soils since the change in mean effective stress and associated volume change due to the wetting and drying cycles is negligible. However, in the case of fine-grained soils, the drying and wetting cycles contribute to significant volume changes in soils, which results in different compressibility characteristics with respect to the degree of saturation. In other words, the mathematical relationship between the E and the G that were originally developed for homogeneous, isotropic and linear elastic continuum may not applicable for the E and the G values for unsaturated soils.

The $E_{\max} - G_{\max}$, and $G_{\max} - M_{\max}$, and $M_{\max} - E_{\max}$ relationship for homogeneous, isotropic, and linear elastic continuum are given in Eqs. 6, 7, and 8, respectively.

$$E_{\max} = 2G_{\max}(1 + \nu) \quad (6)$$

$$G_{\max} = \frac{(1 - 2\nu)}{2(1 - \nu)} M_{\max} \quad (7)$$

$$M_{\max} = \frac{(1 - \nu)}{(1 + \nu)(1 - 2\nu)} E_{\max} \quad (8)$$

where E_{\max} = maximum elastic modulus, G_{\max} = Maximum shear modulus and M_{\max} = maximum constraint modulus (*i.e.* E , G and M at small strain)

Equation 6 and Eq. 7 can be extended to E_{\max} , G_{\max} , and M_{\max} values measured for unsaturated soils as shown in Eq. 9 and Eq. 10, respectively.

$$E_{\max(unsat)} = 2G_{\max(unsat)}(1 + \nu) \quad (9)$$

$$G_{\max} = \frac{(1 - 2\nu)}{2(1 - \nu)} M_{\max} \quad (10)$$

where $E_{\max(unsat)}$, $G_{\max(unsat)}$, and $M_{\max(unsat)} = E_{\max}$, G_{\max} , and M_{\max} for unsaturated condition, respectively

To check the validity of Eq. 9 and Eq. 10, Oh & Vanapalli (2012) reanalyzed the $E_{\max(unsat)}$, $G_{\max(unsat)}$, and $M_{\max(unsat)}$ values measured with the bender element test technique for different degree of saturation values (Mendoza *et al.*, 2005, Alramahi *et al.*, 2010).

Figure 7 shows the variation of back-calculated ν with respect to degree of saturation for the data by Mendoza *et al.* (2005). The negative ν and greater than 0.5 values were ignored since they are not realistic. A trend line is drawn assuming $\nu = 0.1$ representing the relatively dry condition, which was also supported by Lee & Santamarina (2005). In the case of bender element test results by Mendoza *et al.* (2005), the Poisson's ratio values are relatively high with the values between 0.5 and 0.35 in the boundary effect zone, which indicates that the soil specimens were close to undrained condition. The Poisson's ratio values in

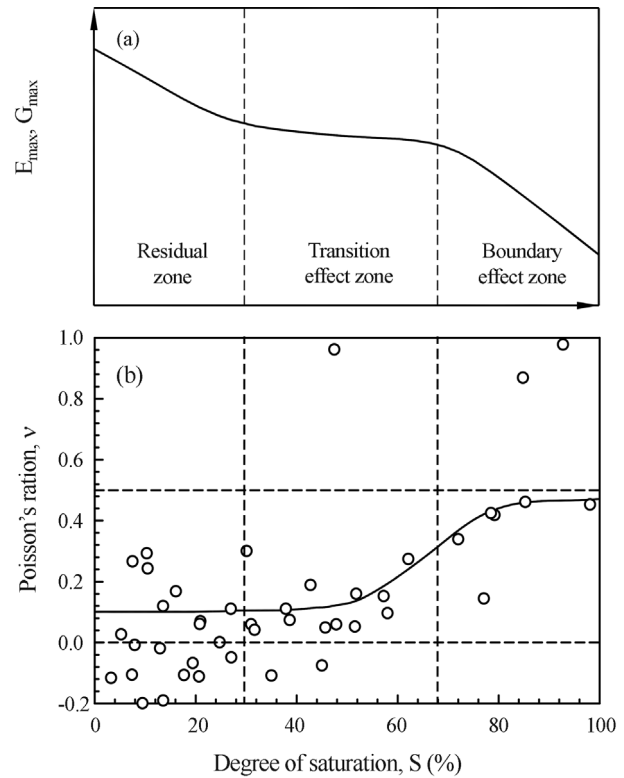


Figure 7 - a) Degree of saturation versus maximum elastic and shear modulus relationship and (b) back-calculated Poisson's ratio with respect to degree of saturation (data from Mendoza *et al.*, 2005) (Oh & Vanapalli, 2012).

the range of 0.35 and 0.1 typically fall in the transition effect zone. In residual zone, the Poisson's ratio gradually converges to a relatively constant value of 0.1.

Figure 8(a) and (b) show the variation of back-calculated ν values with respect to degree of saturation for clay-slurry pore and silt-slurry pore, respectively for the data provided by Alramahi *et al.* (2010). The behavior shown in Fig. 8(a) (*i.e.* clay-slurry pore) is similar to that shown in Fig. 7(b); however, this behavior is not observed for the silt-slurry pore specimen (*i.e.* Fig. 8(b)). The difference in the back-calculated ν values between the saturated (*i.e.* $S = 100\%$) and the dry (*i.e.* $S = 0\%$) conditions for clay specimen (Mendoza *et al.*, 2005) and clay- and silt-slurry pore specimens (Alramahi *et al.*, 2010) are found to be 0.4, 0.04, and 0.02 respectively. This fact indicates that the variation of Poisson's ratio with respect to degree of saturation is more predominant for finer soil materials.

The results in Fig. 7 and Fig. 8 indicates that the Poisson's ratio can be expressed as a function of degree of saturation (*i.e.* $f(S)$; Eq. 11 and Eq. 12). Figure 7 and Fig. 8(a) also show that the variation of Poisson's ratio with respect to degree of saturation is similar to that of SWCC. In other words, the SWCC can be used as a tool to estimate the variation of Poisson's ratio with respect to degree of saturation.

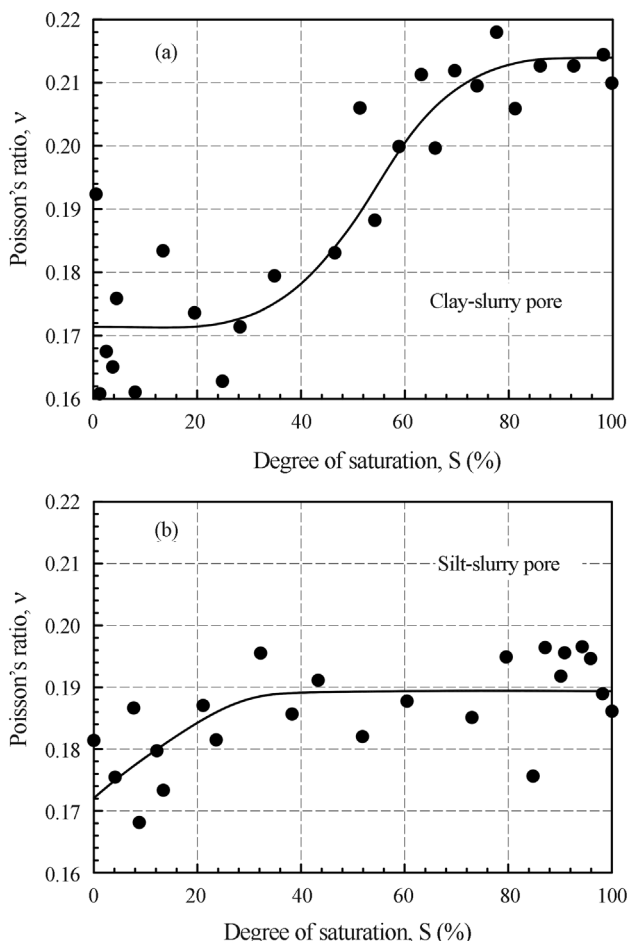


Figure 8 - Back-calculated Poisson’s ratio with respect to degree of saturation for (a) clay-slurry pore and (b) silt-slurry pore (data from Alramahi *et al.*, 2010) Oh & Vanapalli, 2012).

$$v^* = \left[\frac{E_{\max(unsat)}}{2G_{\max(unsat)}} \right] - 1 = f(S) \tag{11}$$

$$v^* = \left[\frac{M_{\max(unsat)} - 2G_{\max(unsat)}}{2(M_{\max(unsat)} - G_{\max(unsat)})} \right] = f(S) \tag{12}$$

where v^* = Poisson’s ratio of unsaturated soils, which is a function of degree of saturation

4. Analysis Results

4.1. Soil properties boundary conditions used in the FEA

In the present study, the model footing test results in UFG soils as detailed in Section 2 are used. Hence, the FEA for each average matric suction value was carried out using the half unconfined compressive strength as total cohesion for five different v values (*i.e.* 0.1, 0.2, 0.3, 0.4, and 0.495). Figure 9 shows meshes along with boundary conditions used in the analysis. Model footing was considered as a material with extremely high elastic modulus and shear

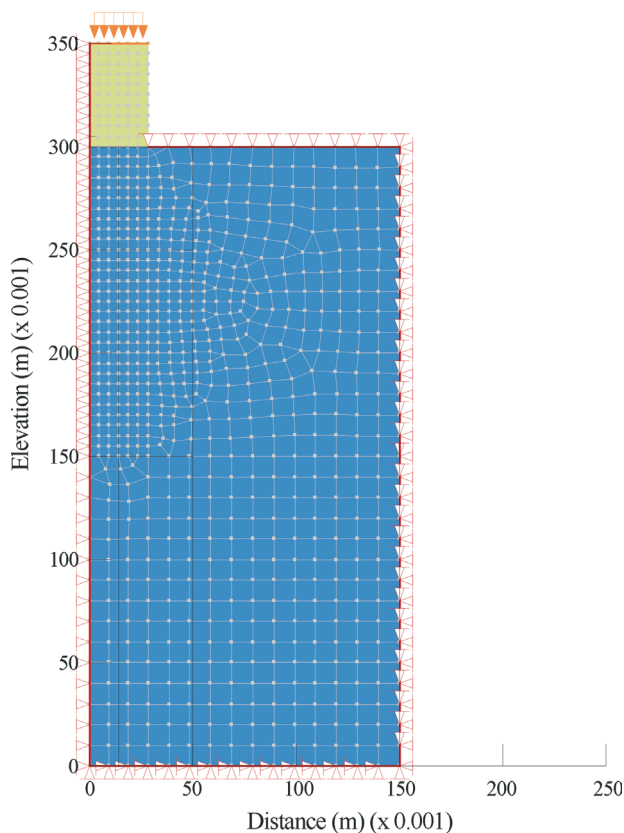


Figure 9 - Meshes and boundary condition used in the FEA.

strength parameters in the FEA. Analyses were performed as axisymmetric condition. The ‘y-displacement fixed’ boundary was assigned on the surface of the compacted soils to simulate ‘no heave (*i.e.* punching failure mechanism’ as discussed in Section 3) condition.

4.2. Comparison between the measured and estimated stress vs. settlement behaviors

Figure 10 shows the comparisons between the measured SVS behaviors and those estimated using the FEA for five different Poisson’s ratio values. Reasonable comparisons were observed between the measured and the estimated SVS behaviors regardless of Poisson’s ratio; however, best comparisons were achieved for low Poisson’s ratio values (*i.e.* less than 0.3). This good comparison also indicates that the MTSA can be successfully extended to the simulation of the SVS behavior of shallow foundations in UFG soils.

5. Summary and Conclusions

In the present study, the influence of Poisson’s ratio on the stress vs. settlement (SVS) behavior of a model footing in an unsaturated fine-grained (UFG) soil is investigated. The conclusions obtained from the research can be summarized as below.

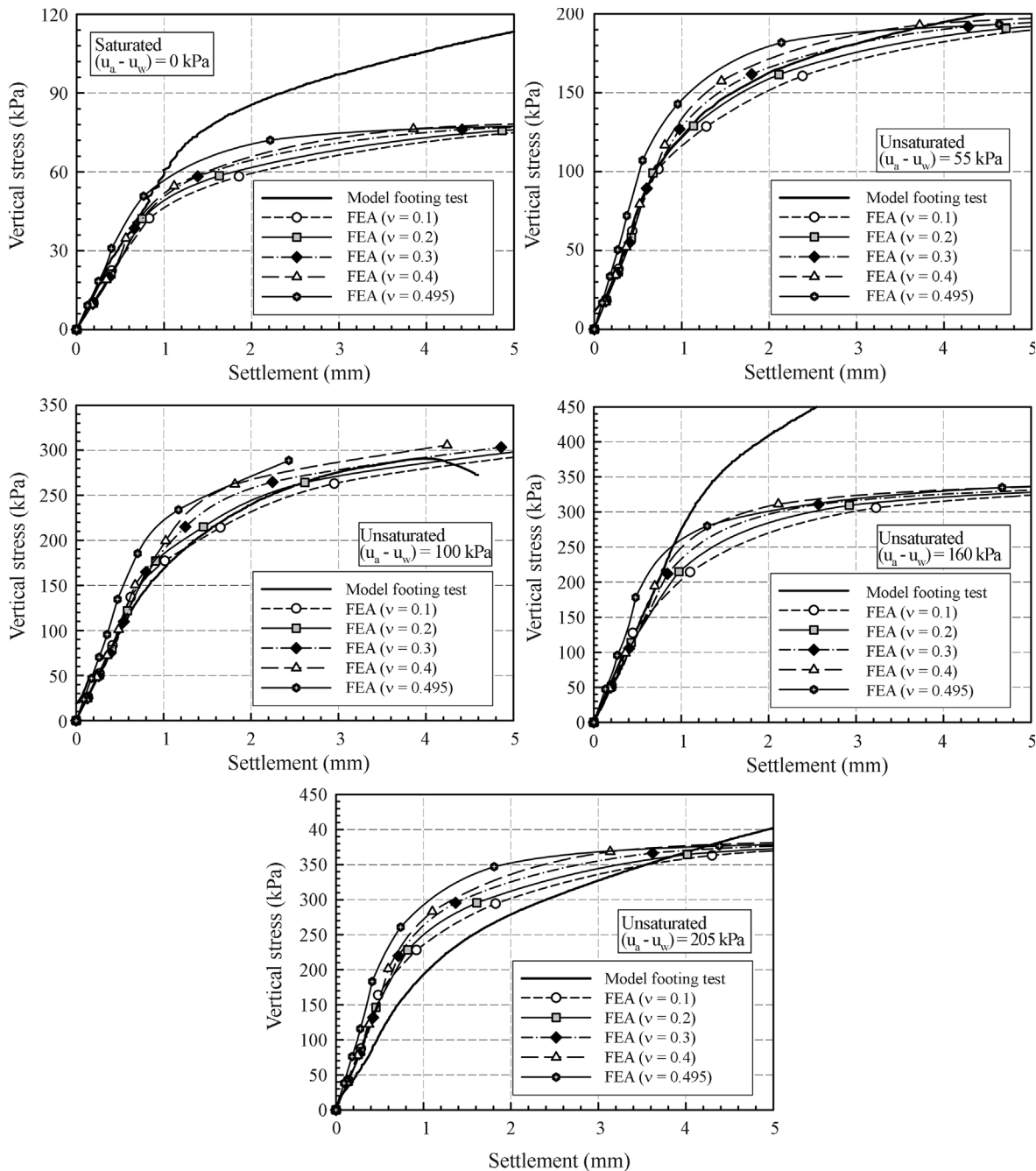


Figure 10 - Comparison between measured SVS behaviors and those estimated using the FEA for different Poisson's ratio.

1. The stress vs. settlement behavior of a model footing can be reliably estimated using the Finite Element Analysis (FEA) extending Modified Total Stress Approach (MTSA).
2. There was good comparison between the measured SVS behaviors and those estimated using the FEA with the Poisson's ratio values in the range of 0.1 and 0.3.
3. Poisson's ratio is not constant, but varies with respect to degree of saturation. In other words, there is a strong relationship between Poisson's ratio and the SWCC. Hence, it is necessary to conduct more studies on vari-

ous types of unsaturated soils (including expansive soils) to develop a semi-empirical model to estimate the variation of Poisson's ratio with respect to degree of saturation using SWCC.

References

Adem, H.H. & Vanapalli, S.K. (2013). Constitutive modeling approach for estimating the *I-D* heave with respect to time for expansive soils. *International Journal of Geotechnical Engineering*, 7(2):199-204.

- Agarwal, K.B. & Rana, M.K. (1987). Effect of ground water on settlement of footing in sand. Proc. 9th European Conference on Soil Mechanics and Foundation Engineering, Dublin, pp. 751-754.
- Aframahi, B.; Alshibli, K.A. & Fratta, D. (2010). Effect of fine particle migration on the small-strain stiffness of unsaturated soils. *Journal of Geotechnical and Geoenvironmental Engineering*, 136(4):620-628.
- Ausilio, E. & Conte, E. (1999). Settlement rate of foundations on unsaturated soils. *Canadian Geotechnical Journal*, 36(5):940-946.
- Cerato, A.B. & Lutenegeger, A.J. (2006). Bearing capacity of square and circular footings on a finite layer of granular soil underlain by a rigid base. *Journal of Geotechnical and Geoenvironmental Engineering*, 132(11):1496-1501.
- Chao, K.C.; Neslon, J.D. & Overton, D.D. (2011). Factors influencing design of deep foundations on expansive soils. Proc. 5th Asia Pacific Conference on Unsaturated soils, Pattaya, Thailand, v. 2, pp. 829-834.
- Chen, W.F. & Zhang, H. (1991). Structural plasticity: Theory, problems, and CAE software. Springer-Verlag.
- Consoli, N.C.; Schnaid, F. & Milititsky, J. (1998). Interpretation of plate load tests on residual soil site. *Journal of Geotechnical and Geoenvironmental Engineering*, 124(9):857-867.
- Costa, Y.D.; Cintra, J.C. & Zornberg J.C. (2003). Influence of matric suction on the results of plate load tests performed on a lateritic soil deposit. *Geotechnical Testing journal*, 26(2):219-226.
- Gallipoli, T.; Sanchez, M. & Sheeler, S. (2013). Rainfall-induced differential settlements of foundations on heterogeneous unsaturated soils. *Géotechnique*, 63(15):1346-1355.
- Georgiadis, K.; Potts, D.M. & Zdravkovic, L. (2003). The influence of partial soil saturation pile behaviour. *Géotechnique*, 53(1):11-25.
- Infante Sedano, J.A.; Vanapalli, S.K. & Garga, V.K. (2007). Modified ring shear apparatus for unsaturated soils testing. *Geotechnical Testing Journal*, 30(1):1-12.
- Kumbhokjar, A.S. (1993). Numerical evaluation of Terzaghi's N_γ . *Journal of Geotechnical Engineering, ASCE*, 119(3):598-607.
- Lee, J-S & Santamarina, J.C. (2005). Bender elements: Performance and signal interpretation. *Journal of Geotechnical and Geoenvironmental Engineering*, 131(9):1063-1070.
- Mendoza, C.E.; Colmenares, J.E. & Merchán, V.E. (2005). Stiffness of an unsaturated compacted clayey soil at very small strains. Proc. of Int. Symp. on Advanced Experimental Unsaturated Soil Mechanics, Ternto, pp. 199-204.
- Mohamed, F.M.O. & Vanapalli, S.K. (2006). Laboratory investigations for the measurement of the bearing capacity of an unsaturated coarse-grained soil. Proc. 59th Canadian Geotechnical Conference, Vancouver, pp. 219-226.
- Nishimura, T.; Toyota, H.; Vanapalli, S.K. & Oh, W.T. (2007). Evaluation of critical state parameters for an unsaturated soil. Proc. 60th Canadian Geotechnical conference, Ottawa, Ontario, pp. 1029-1036.
- Oh, W.T.; Vanapalli, S.K. & Puppala, A.J. (2009). Semi-empirical model for the prediction of modulus of elasticity for unsaturated soils. *Canadian Geotechnical Journal*, 48(6):903-914.
- Oh, W.T. & Vanapalli, S.K. (2011a). Modelling the applied vertical stress and settlement relationship of shallow foundations in saturated and unsaturated sands. *Canadian Geotechnical Journal*, 48(3):425-438.
- Oh, W.T. & Vanapalli, S.K. (2011b). Modelling the stress vs. displacement behavior of shallow foundations in unsaturated coarse-grained soils. Proc. 5th Int. Symp. on Deformation Characteristics of Geomaterials, Seoul, South Korea, pp. 821-828.
- Oh, W.T. & Vanapalli, S.K. (2012). Modelling the settlement behaviour of in-situ shallow foundations in unsaturated sands. Proc. Geo-Congress 2012, ASCE, pp. 2542-2551.
- Oh, W.T. & Vanapalli, S.K. (2013a). Scale effect of plate load tests in unsaturated soils. *International Journal of Geomate*, 4(2):585-594.
- Oh, W.T. & Vanapalli, S.K. (2013b). Interpreting the bearing capacity of unsaturated fine-grained soils using modified effective and total stress approaches. *International Journal of Geomechanics*. (Accepted for publication)
- Oloo, S.Y.; Fredlund, D.G. & Gan, J.K-M. (1997). Bearing capacity of unpaved roads. *Canadian Geotechnical Journal*, 34(3):398-407.
- Rahardjo, H.; Heng, O.B. & Leong, E.C. (2004). Shear strength of a compacted residual soil from consolidated drained and the constant water content tests. *Canadian Geotechnical Journal*, 41(3):1-16.
- Rojas, J.C.; Salinas, L.M. & Seja, C. (2007). Plate-load tests on an unsaturated lean clay. Proc. 2nd Int. Conf. on Unsaturated Soils, Weimar, pp. 445-452.
- Schnaid, F.; Consoli, N.C.; Cumdani, R. & Milititsky, J. (1995). Load-settlement response of shallow foundations in structured unsaturated soils. Proc. 1st Int. Conf. on Unsaturated Soils, Paris, pp. 999-1004.
- Terzaghi, K. (1943). *Theoretical Soil Mechanics*. John Wiley and Sons, New York, 510 p.
- Vanapalli, S.K.; Fredlund, D.G.; Pufahl, D.E. & Clifton, A.W. (1996). Model for the prediction of shear strength with respect to soil suction. *Canadian Geotechnical Journal*, 33(3):379-392.
- Vanapalli, S.K. & Mohamed, F.M.O. (2007). Bearing capacity of model footings in unsaturated soils. Proc. Int. Conf. From Experimental Evidence towards Numerical

- Modeling of Unsaturated Soil, Weimar, Germany, pp. 483-493.
- Vanapalli, S.K. & Oh, W.T. (2009). A model for predicting the modulus of elasticity of unsaturated soils using the soil-water characteristic curves. *International Journal of Geotechnical Engineering*, 4(4):425-433.
- Vanapalli, S.K. & Taylan, Z.N. (2012). Design of single pile foundations using the mechanics of unsaturated soils. *International Journal of Geomate, Construction Materials and Environment*, 2(1):197-204.
- Vesic A.B. (1973). Analysis of ultimate loads of shallow foundations. *Journal of the Soil Mechanics and Foundation Division, ASCE* 99(1):45-73.
- Vu, H.Q. & Fredlund, D.G. (2006). Challenges to modeling heave in expansive soils. *Canadian Geotechnical Journal*, 43:1249-1272.
- Wang, Q.; Pufahl, D.E. & Fredlund, D.G. (2002). A study of critical state on an unsaturated silty soil. *Canadian Geotechnical Journal*, 39(1):213-218.
- Weaver, T. & Grandi, O. (2009). Lateral load analysis of deep foundations in unsaturated soils. contemporary topics in *in situ* testing, analysis, and reliability of foundations. *Geotechnical Special Publications*, 186:552-559.
- Wejrungsikul, T.; Puppala, A.J.; Williammee, R.S.; Rutanaporamakul, Jr. P. & Hoyos, L.R. (2011). Inclined load capacities of drilled shafts in unsaturated soil environments. *Proc. 5th Asia Pacific Conference on Unsaturated soils, Pattaya, Thailand*, v. 2, pp. 817-822.

Statistical Assessment of Hydraulic Properties of Unsaturated Soils

G.F.N. Gitirana Jr., D.G. Fredlund

Abstract. The availability of statistical values for soil parameters is essential in reliability-based geotechnical design and sensitivity analysis. Unfortunately, there are few statistical studies available about unsaturated soil parameters. The primary objective of this paper is to present a methodology for the statistical assessment of hydraulic properties of unsaturated soil and to present the results of a statistical study carried out using a large database of soil properties. Two fundamental unsaturated soil properties are considered; namely, the soil-water characteristic curve (SWCC) and the hydraulic conductivity function. Appropriate nonlinear functions and fitting parameters with well-defined and unique physical and/or geometrical meanings were adopted. The main contribution of this article is the establishment of central tendency measures, standard deviations, and correlation coefficients for the unsaturated soil parameters, considering soil datasets grouped according to soil texture. It was determined based on the analyses results that the air-entry value, primary SWCC slope, residual SWCC slope, saturated hydraulic conductivity, and hydraulic conductivity function slope could be well described using lognormal probability density functions. Finally, general guidelines are provided regarding the statistical values to be adopted for the unsaturated soil properties studied.

Keywords: unsaturated soils, soil-water characteristic curve, hydraulic conductivity, statistics, coefficient of variation, correlation coefficient.

1. Introduction

The analysis of unsaturated soil problems can be significantly enhanced and rationalized if the uncertainty associated with the soil properties is addressed through probabilistic analysis. Unfortunately, probabilistic analyses require the knowledge of statistical measures for the input properties involved. The availability of statistical data on unsaturated soil properties benefits a wide range of geotechnical and geoenvironmental problems. Unsaturated/saturated seepage analysis, contaminant transport, and cover/barrier design are some of the major fields that can take advantage of statistical data on unsaturated soil properties. Other areas of application also relevant are those that involve thermal and hydro-mechanical problems.

The main statistical measures required in probabilistic analyses are the central tendency values, standard deviations (or coefficients of variation), and the correlation matrix for the input variables. Typical, representative values for the coefficients of variation and correlation coefficients are often used for the assessment of soil properties in engineering practice. The adoption of a range of typical values is often preferable because it is not feasible to test a large number of soil samples to characterize a particular site (Whitman, 1984; Harr, 1987; Duncan, 2000). Typical central tendency values are also useful but are usually only recommended for preliminary analyses. Numerous studies can be found in the literature suggesting typical coefficients of

variation for saturated soil parameters (see references in Table 1). Typical values for correlation coefficients and central tendencies can also be found for saturated soil parameters. Unfortunately, there is limited number of studies presenting statistical assessments for unsaturated soil parameters.

The primary objective of this paper is to present the results of a statistical study carried out using 186 datasets of soil-water characteristic curves and hydraulic conductivity functions. Normality, central tendency measurements, property uncertainty, and correlations coefficients were investigated. The study was directed toward the establishment of guidelines about the typical values expected for different textural groups.

2. Background

A review of descriptive statistics applied to geotechnical engineering problems was presented by Ladd (1983). Unbiased estimators can be used for the mean of a random variable, standard deviation, correlation coefficient between two random variables, and autocorrelation coefficient as a function of distance. Most statistical assessment studies found in the geotechnical literature, such as the study by Ladd (1983), deal with the uncertainty of saturated soil parameters. The coefficient of variation, COV, is commonly used as a measure of uncertainty (Harr, 1987). Contrary to the standard deviation, the coefficient of variation can often be assumed to be independent of the magnitude of

Gilson de F. N. Gitirana Jr., PhD., Escola de Engenharia Civil e Ambiental, Universidade Federal de Goias, 74605-220 Goiania, GO, Brazil. e-mail: gilsongitirana@gmail.com.

Delwyn G. Fredlund, PhD., Golder Associates Ltd., 1721 - 8th Street East, Saskatoon, S7H 0T4 SK, Canada. e-mail: del_fredlund@golder.com.

Invited Article, no discussion.

Table 1 - Compilation of coefficients of variation found in the literature for saturated soil parameters.

Property	Coefficient of variation COV	Source
Porosity, n	10%	Shultze (1971)
Void ratio, e	10-20%	Krahn & Fredlund (1983)
Unit weight, γ_{sat}	3-7%	Hammitt (1966), Kulhawy (1992), Tan <i>et al.</i> (1993)
Friction angle, ϕ'	7-12%	Shultze (1971), Lacasse & Nadim (1997), Duncan (2000), Phoon & Kulhawy (1999a)
Friction angle, $\tan(\phi')$	5-25%	Lumb (1966), Tan <i>et al.</i> (1993)
Cohesion, c'	10-50%	Fredlund & Dahlman (1971), Harr (1987), Kulhawy (1992), Tan <i>et al.</i> (1993), Lacasse & Nadim (1997), Phoon & Kulhawy (1999a), Duncan (2000)
Undrained strength, S_u	50-80%	Krahn & Fredlund (1983), Phoon & Kulhawy (1999a)
Saturated water coefficient of permeability, k_{sat}	68-90%	Nielsen <i>et al.</i> (1973), Duncan (2000)
Unsaturated water coefficient of permeability, k	130-240%	Nielsen <i>et al.</i> (1973), Benson <i>et al.</i> (1999)
Preconsolidation pressure, σ'_p	10-35%	Padilla & Vanmarcke (1974), Lacasse & Nadim (1997), Duncan (2000)
Compression index, C_c	10-37%	Lumb (1966), Padilla & Vanmarcke (1974), Krahn & Fredlund (1983), Kulhawy (1992), Duncan (2000)

the variable. One shortcoming is that the equation defining COV breaks down when the mean value approaches zero.

Uncertainty of soil parameters can be due to several factors. Whitman (1984) identified four sources of parameter uncertainty; namely, (i) inherent spatial variability; (ii) random testing errors; (iii) statistical error due to a finite number of samples; and (iv) measurement bias. Spatial variability and random testing errors are characterized as scatter in the data. Data scatter averages over large soil volumes and its contribution to parameter uncertainty decreases as the volume of the problem increases. The other two sources of variability are systematic errors that do not average out over the soil volume and have a significant influence on overall uncertainty.

Phoon & Kulhawy (1999a, 1999b) presented a detailed conceptual description where the sources of soil property uncertainty were divided into inherent variability, measurement variability, and estimation model uncertainty. In addition, an extensive literature review was conducted to collect information required to determine typical inherent soil variability, scales of spatial fluctuation, measurement error variability, and transformation uncertainty. The authors observed that the COV of inherent variability for sand is higher than that for clays. Phoon & Kulhawy (1999a) also observed that index parameters present lower values of COV when compared to the COV of shear strength parameters and soil modulus. Unsaturated soil properties were not addressed by their study.

Dai & Wang (1992) and Duncan (2000) indicate that the *three-sigma rule* provides a useful approximation for the coefficients of variation of geotechnical properties.

Since 99.73% of all values of a normally distributed parameter fall within three standard deviations of the mean value, the following equation can be used to estimate the coefficient of variation of a parameter:

$$\text{COV}[x] = \frac{1}{E[x]} \frac{\text{HCV} - \text{LCV}}{6} \quad (1)$$

where $E[x]$ is the mean value of the parameter x , HCV is the highest conceivable value, and LCV is the lowest conceivable value of the parameter x .

There is a tendency to estimate ranges of conceivable values that are smaller than the real ranges. Duncan (2000) observed that with practice and experience the subjective estimation exercise becomes more accurate. It was also suggested that “an effort should be made to make the range of conceivable values as wide as seemingly possible or even wider, to overcome the natural tendency to make the range too small.”

The three-sigma rule was conceived as a substitute to the application of conventional descriptive statistics on measured soil parameters. Conventional descriptive statistics are rarely used in geotechnical engineering practice because the number of samples and tests required to obtain values of statistical significance is prohibitive for most projects. The cost of the tests and the time available are simply too great. Other alternative often adopted is the use of published values of typical coefficients of variation obtained from past studies.

Table 1 presents a compilation of some values of coefficient of variation from published data. The ranges presented envelop values provided from several sources. The

information available in the literature enables the application of reliability-based design into geotechnical practice. It is interesting to note that cohesion, undrained strength and permeability present considerably higher COVs. The COV of porosity and void ratio found in the literature are of particular interest to the present study, since the range of published values can be compared with the value presented herein.

Unsaturated soil properties are generally defined as nonlinear functions of the stress state variables. The nonlinear characteristics of such soil properties require a somewhat more elaborate procedure for statistical assessment than that adopted for saturated soil properties. Confidence bands are often used in the statistical characterization of functions (Bates & Watts, 1988). This was the approach used in the statistical characterization of the SWCC by Mishra *et al.* (1989) and Zapata *et al.* (2000). Both authors were able to establish typical ranges of variability expected for SWCCs. Unfortunately, such an approach is not convenient for reliability analysis. Reliability analyses can be more easily undertaken if property variability is characterized in terms of the variability of a finite and relatively small number of curve parameters. A small number of authors, such as Meyer *et al.* (1997), Rawls *et al.* (1998), Faulkner *et al.* (2003) and Phoon *et al.* (2010), have presented statistical and probabilistic studies regarding some of the hydraulic properties of unsaturated soils. Unfortunately, these studies are based on specific fitting functions whose parameters have little or no physical meaning and are not independently related to individual shape features of the unsaturated soil property functions.

3. Methodology for the Statistical Assessment of Unsaturated Soil Properties

The statistical assessment of unsaturated soil properties requires the establishment of an appropriate methodology regarding the selection of data and analysis procedure. This section presents the criteria established for data selection and data grouping, the fitting equation that have been used in this study, and the fitting procedure adopted.

3.1. Soil properties studied and criteria for selection of data records

The properties studied in this paper are for the soil-water characteristic curve, SWCC, and the hydraulic conductivity function. Data records were sampled from a soils database (SoilVision Systems, 2005). Only drying curves were used in the present study, as those are the most commonly measured and found in the literature.

Other unsaturated soil properties such as the vapor conductivity, thermal properties, and shear strength were not analyzed in this paper due to the limited availability of data at the present time. However, these unsaturated soil properties can be visualized as variables dependent on the soil-water characteristic curve. There are numerous predic-

tive models available based on the SWCC. Consequently, the statistical study presented herein for the SWCC becomes useful for the assessment of other unsaturated soil properties. A complete statistical assessment of all unsaturated soil properties would also require studies on the uncertainties associated with the predictive models.

The term hydraulic conductivity function is used herein to denote the relationship between the hydraulic conductivity and soil suction. The hydraulic conductivity function can also be treated as a property dependent on the SWCC. Huang *et al.* (1998) presents a review of several hydraulic conductivity prediction methods. However, the relatively large amount of directly measured hydraulic conductivity data available provided an opportunity for the independent analysis presented in this study.

A total of 186 soil records were sampled from the SoilVision database. The number of sampled records was limited by the number of available “complete” soil records. To be considered “complete”, a soil record was required to have a grain-size distribution, the soil porosity, n , the drying soil-water characteristic curve, the saturated hydraulic conductivity, and the hydraulic conductivity function. The porosity data provided an indication of total water storage. The grain-size distribution was required for the classification of each soil sample and grouping the soil data with respect to texture.

3.2. Fitting equations and corresponding soil parameters

The soil-water characteristic curve and the hydraulic conductivity function can be described using various equations (Fredlund and Xing 1994) whose soil parameters can be treated as best-fit parameters obtained using a nonlinear fitting algorithm. Unfortunately, unsaturated soil property functions have often been defined using functions whose fitting-parameters have limited physical significance and are somewhat interrelated. For instance, for most SWCC equations it is possible to obtain similar fitting with completely different sets of parameters (Gitirana Jr. & Fredlund, 2004). In other words, the set of best-fit parameters do not appear to be unique. Consequently, it becomes difficult to perform a meaningful statistical analysis on such parameters. In order to overcome these difficulties, it is suggested herein that it is better to use soil property functions defined by mathematically independent and preferably meaningful soil parameters.

3.2.1. Soil-water characteristic curve equation

The soil-water characteristic curve datasets were fitted using the unimodal equations proposed by Gitirana Jr. & Fredlund (2004). Two equations were used herein; namely, the unimodal equation with two bending points and the unimodal equation with one bending point. The unimodal equation with two bending points can be written as follows:

$$S = \frac{S_1 - S_2}{1 + \left(\frac{\Psi}{\sqrt{\Psi_b \Psi_{res}}} \right)^d} + S_2 \quad (2)$$

$$S_i = \frac{\tan \theta_i (1 + r_i^2) \ln \left(\frac{\Psi}{\Psi_i^a} \right)}{1 + r_i^2 \tan^2 \theta_i} + (-1)^i \cdot \frac{1 + \tan^2 \theta_i}{1 - r_i^2 \tan^2 \theta_i} \cdot \sqrt{r_i^2 \ln^2 \left(\frac{\Psi}{\Psi_i^a} \right) + \frac{a^2 (1 - r_i^2 \tan^2 \theta_i)}{1 + \tan^2 \theta_i}} + S_i^a \quad (3)$$

where $i = 1, 2$; $\theta_i = -(\lambda_{i-1} + \lambda_i)/2$; $r_i = \tan((\lambda_{i-1} - \lambda_i)/2)$; $\lambda_0 = 0$; $\lambda_i = \arctan[(S_i^a - S_{i+1}^a) / (\ln(\Psi_{i+1}^a / \Psi_i^a))]$; $S_1^a = 1$; $S_2^a = S_{res}$; $S_3^a = 0$; $\Psi_1^a = \Psi_b$; $\Psi_2^a = \Psi_{res}$; $\Psi_3^a = 10^6$; $d = 2 \exp(1/\ln(\Psi_{res}/\Psi_b))$; Ψ = soil suction; and a is a parameter controlling the curve sharpness at the two bending points.

The unimodal equation with one bending point can be obtained directly from Eq. 3, making $S = S_1$, $\theta_1 = -\lambda/2$, $r_1 = \tan(\lambda/2)$, and $\lambda = \arctan[1/(\ln(10^6/\Psi_b))]$.

According to Eq. 2, a SWCC with two bending points can be defined using four parameters; namely, Ψ_b = air-entry value; Ψ_{res} = residual suction; S_{res} = residual degree of saturation; and the sharpness parameter, a . These four parameters correspond to the number of shape features of a typical SWCC (see Fig. 1). Figure 1 also shows that two shape features define a SWCC with one bending point; namely, Ψ_b and a . Each one of these soil parameters have a physical meaning (Gitirana Jr. & Fredlund, 2004).

Other SWCC parameters are defined in Fig. 1; namely, λ_d , the primary drainage slope; and λ_{res} , the residual drainage slope. The primary and residual drainage slopes can be calculated as follows:

$$\lambda_d = \frac{1 - S_{res}}{\log_{10} \left(\frac{\Psi_{res}}{\Psi_b} \right)} \quad (4)$$

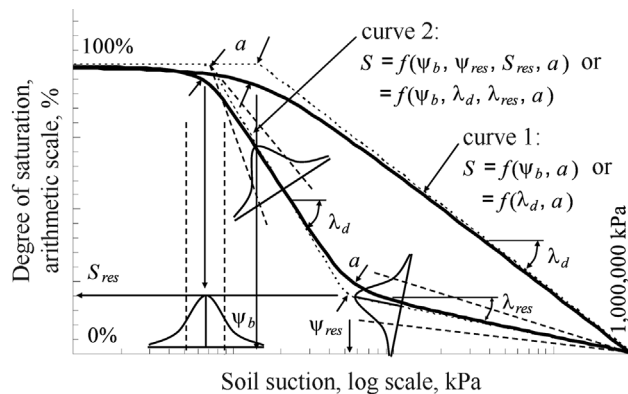


Figure 1 - Idealization of a unimodal soil-water characteristic curve with one and two bending points.

$$\lambda_{res} = \frac{S_{res}}{\log_{10} \left(\frac{1,000,000}{\Psi_{res}} \right)} \quad (5)$$

The primary drainage slope, λ_d , is influenced by the distribution of the pore-sizes. Uniform pore-size distributions result in steeper primary drainage slopes.

Four parameters should be used to describe the SWCC because the curve has four distinct shape features. The use of a number of parameters lower than four would impose restrictions to the SWCC shape. The set of parameters Ψ_b , λ_d , λ_{res} , and a was deemed to be appropriate for this study. For instance, difficulties in probabilistic analyses would arise for estimate points (or random realizations) of Ψ_b greater than Ψ_{res} , a combination of parameters that is physically inadmissible. The use of constraints to prevent $\Psi_b > \Psi_{res}$ is mathematically cumbersome and, as a result, Ψ_{res} and S_{res} were replaced by λ_d and λ_{res} .

Most sampled SWCC datasets show curves with two bending points (*e.g.*, curve 2 in Fig. 1). However, most clay soils have SWCCs with only one bending point and do not present a distinguishable residual point (*e.g.*, curve 1 in Fig. 1). As a result, all clay datasets were fitted using the unimodal equation with one bending point, while other soil types were fitted using an equation with two-bending points.

Gitirana Jr. & Fredlund (2004) show that the parameter a slightly improves the fitting capabilities of the equation. However, the physical meaning of a is not as clear and as significant as the physical meaning of the other three SWCC parameters. Therefore, fixed values were adopted for a , based on the observation that a good fit could be obtained for the absolute majority of data when using the chosen values. A value of a equals to 0.075 was selected for all Sands, 0.050 was selected for Loams, and 0.025 was selected for Clays.

3.2.2. Hydraulic conductivity function

The hydraulic conductivity function datasets were fitted using a bi-linear function on a log vs. log plot (see Fig. 2). The bi-linear shape was found to fit reasonably well most experimental curves. The first portion of the curve is defined using a constant value equal to the saturated hydraulic conductivity, k_{sat} . The value of k_{sat} was not treated as a fitting parameter but as an independently measured value. The second portion of the curve was assumed to be defined by a constant slope, η . The following bi-linear equation was used (Brooks & Corey, 1964):

$$\begin{aligned} k &= k_{sat} & \text{for } \Psi \leq \Psi_{bk} \\ k &= k_{sat} \left[\frac{\Psi_{bk}}{\Psi} \right]^n & \text{for } \Psi > \Psi_{bk} \end{aligned} \quad (6)$$

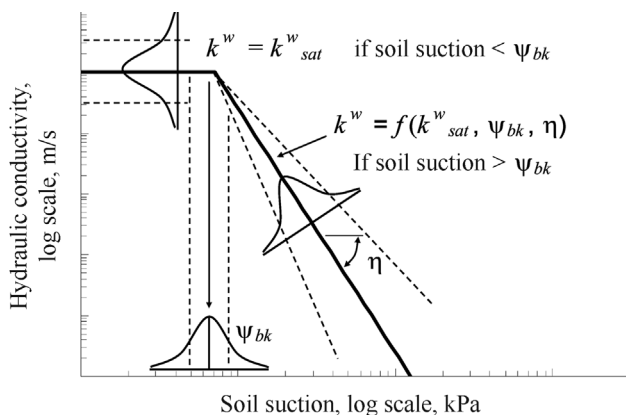


Figure 2 - Idealization of a hydraulic conductivity function.

where k = hydraulic conductivity; k_{sat} = saturated hydraulic conductivity; ψ_{bk} = break point of the hydraulic conductivity function; η = slope of the hydraulic conductivity function.

In theory, the break point, ψ_{bk} , corresponds to the air-entry value, ψ_b . However, it was found that the air-entry value obtained from the SWCC fitting does not always match the break point observed in the hydraulic conductivity function. The use of ψ_{bk} equal to ψ_b would compromise the fitting capability of Eq. 6. As a result, the fitting of the hydraulic conductivity function was made independently of the soil-water characteristic curve fit (i.e., the air-entry value from the SWCC was not used for the hydraulic conductivity function).

3.3. Fitting procedure and statistical representation of unsaturated soil property functions

The following soil parameters were statistically assessed, in order to completely define the SWCC and hydraulic conductivity function: ψ_b , λ_d , λ_{res} , k_{sat} , ψ_{bk} , and η . The data records sampled from the SoilVision database were first imported into a spreadsheet. The fitting of the SWCCs and hydraulic conductivity functions was performed by minimizing the sum of the squared residuals between the experimental data and the fitting curve. The nonlinear minimization solver available in MS Excel® was utilized. The nonlinear fitting application appeared to perform well provided that the initial guess was sufficiently close to the final best-fit parameter. Other minimization techniques are available and some of these have been described by Fredlund & Xing (1994).

Figures 1 and 2 illustrate the manner in which the soil-water characteristic curve and the hydraulic conductivity function can be statistically described based on the statistical characterization of the soil parameters ψ_b , λ_d , λ_{res} , k_{sat} , ψ_{bk} , and η . Each soil parameter was considered as a random variable with a frequency distribution characterized based on statistical descriptive measures, as traditionally done for other soil properties.

3.4. Soil grouping based on the USDA textural classification system

The 186 soil records sampled from the SoilVision database are diverse soils with distinct characteristics. Ideally, the statistical assessment of individual “soil groups” is preferable (Fredlund & Dahlgren, 1971) even though the definition of the term “soil group” is not totally precise. To address that concern, the sampled records were grouped according to their textural characteristics. The separation of soil types is an attempt to group soils with similar engineering behavior, even though soil behavior depends on many other characteristics.

Two of the commonly used soil classification systems are the USDA system (Soil Survey Staff, 1975) and the Unified Soil Classification System, USCS, (ASTM, 1993). The USCS system is generally preferred in geotechnical engineering. However, the number of “complete” records in the SoilVision database where Atterberg limits are presented is small. As a result, the USDA system has been adopted herein.

Figure 3 presents the textural diagram used in the USDA soil classification system (Soil Survey Staff, 1975) along with the textural characteristics of the data records sampled. The percentages of sand, silt and clay plotted in Fig. 3 were defined using the following particle size, x , intervals: Clay: $x < 0.002$ mm; Silt: $0.002 \leq x < 0.05$ mm; Sand: $0.05 \leq x < 2$ mm; and Coarse material: $2 \leq x < 300$ mm.

Three main groups are identified in Fig. 3; namely, sands (Sa), loams (L), and clays (C). The silt and silty fractions (Si) are placed within the loam fraction. The number of sampled records pertaining to each soil group is 62, making a total of 186 sampled records. Each of the three main soil groups is subdivided into a number of subgroups (Sa ,

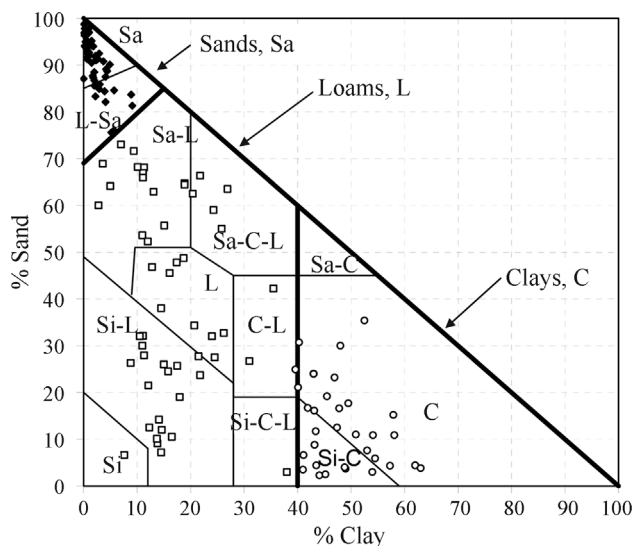


Figure 3 - Sampled soil records classified according to the USDA classification system.

L-Sa, Sa-L, Sa-C-L, L, Si-L, Si, C-L, Si-C-L, Sa-C, Si-C, and *C*).

4. Results and Discussion of Normality Tests

Normality tests were performed on the soil parameters and on the natural logarithm of most soil parameters in order to determine whether normal or lognormal density functions reasonably represent each unsaturated soil parameter. Normality tests were performed with the aid of Minitab 13 (Minitab Inc., 2000). Minitab has three hypothesis tests available for testing normality; namely, Anderson-Darling test; Ryan-Joiner test; and Kolmogorov-Smirnov test. D’Augustino & Stevens (1986) present detailed descriptions and comparisons of these tests for normality. The Anderson-Darling test has relatively superior power for detecting non-normality and was selected. The null hypothesis for the Anderson-Darling test is “*H0: data follow a normal distribution*”. The results of the normality tests are presented in terms of *p*-values. *P*-values represent the probability of making a *type 1 error*, which is “rejecting the null hypothesis when it is true.” A cut-off value often used was 5%, which means “reject the null hypothesis when the *p*-value is less than 5%” (D’Augustino and Stevens 1986).

Sampled records were grouped according to the USDA classification system, as presented in Fig. 3. For the normality tests the analyses were carried out following three distinct procedures: a) considering all the sampled records as one single group; b) assembling the data using the three main groups of soils (*i.e.*, *Sa, L,* and *C*); and c) assembling the data using the smaller soils subgroups indicated in Fig. 3. The soil subgroups *Si, C-L, Si-C-L,* and *Sa-C* could not be analyzed because of the relatively small number of sample records in those subgroups.

Figure 4 present the results of the normality tests in terms of *p*-values. Dashed lines indicate the threshold of 5%, below which normality is unlikely. Figure 4 shows that most parameters and soil groups deviate to some extent from a normal distribution. This is particularly true for ψ_b , λ_d , λ_{res} , k_{sat} , ψ_{bk} , and η . When the logarithm of ψ_b , λ_d , λ_{res} , k_{sat} , ψ_{bk} , and η were tested the parameters were closer to being normally distributed (*i.e.*, larger *p*-values). Based on the results presented in Fig. 4, it was concluded that the parameters ψ_b , λ_d , λ_{res} , k_{sat} , ψ_{bk} , and η can be considered log normally distributed while *n* is reasonably described using a normal distribution.

The effect to the normality tests of grouping soil data into textural classes can be clearly observed in Fig. 4. None of the parameters were found to be normally or log normally distributed when all sampled records were analyzed as a single soil. The more detailed soil textural classification (Fig. 4b) appears to produce parameter distributions that are better described by normal and lognormal distributions.

5. Results and Discussion of Descriptive Statistics Analysis

Tables 2 and 3 present descriptive statistical parameters obtained for the three main soil groups; namely, sands (*Sa*), loams (*L*), and clays (*C*). The minimum and maximum values are presented along with measures of central tendency and the standard deviation. Three measures of central tendency were calculated; namely, the median, the mean, and the global best-fit parameters. The global best-fit parameters were obtained by assembling in the same plot all the datasets pertaining to a given soil group.

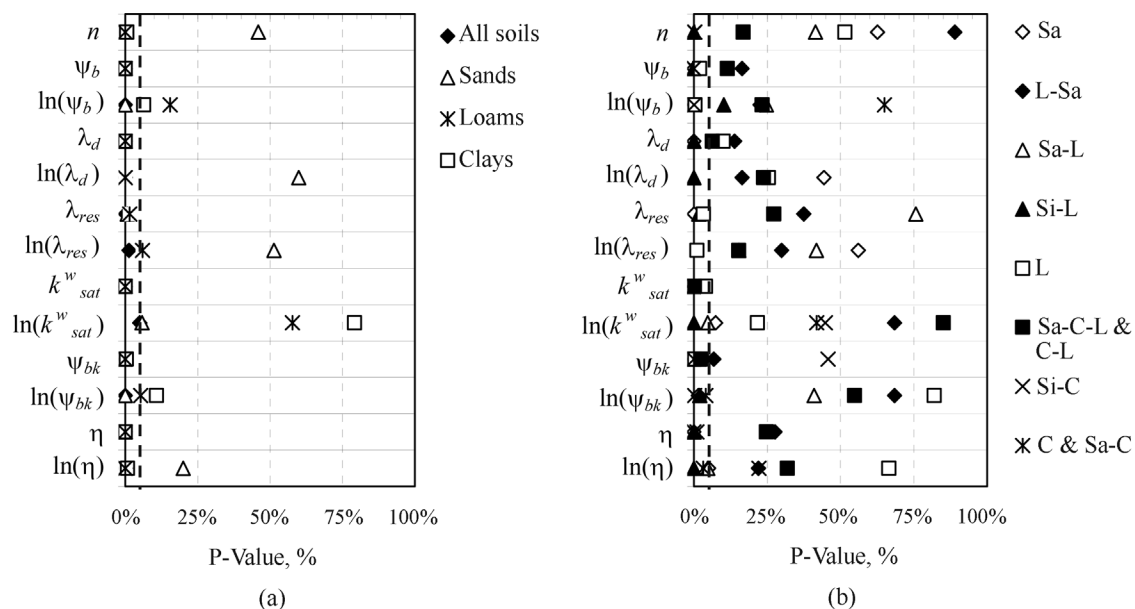


Figure 4 - Normality tests: *p*-values for all soil parameters considering (a) the three main soil groups and (b) all soil subgroups.

Table 4 presents a summary of the coefficients of variation, COV, obtained from the statistical analyses. Two main measures are usually considered in the quantification of uncertainty; namely, the standard deviation, SD, and the coefficient of variation. The standard deviation of a random variable is strongly influenced by the mean values and depends on the units of the variable. The coefficient of variation tends to offer a means of normal-

Table 2 - Descriptive statistics for unsaturated soils properties ($a = 0.075$ for sands, 0.050 for loams, and 0.025 for clays).

Group	Measure	n	ψ_b (kPa)	λ_d	λ_{res}	k_{sat} (m/s)	ψ_{bk} (kPa)	η
Sands	Min	0.297	0.183	0.405	0.019	3.8×10^{-7}	0.100	1.288
	Max	0.570	12.00	4.228	0.126	3.50×10^{-4}	7.239	10.500
	Median	0.409	2.438	1.178	0.044	1.82×10^{-5}	1.585	3.484
	Mean	0.410	2.937	1.446	0.047	3.88×10^{-5}	1.874	4.037
	Global best-fit	—	1.64	0.844	0.049	7.06×10^{-6}	1.550	3.107
	Std. Dev.	0.055	2.050	0.880	0.021	6.34×10^{-5}	1.582	2.141
Loams	Min	0.378	0.054	0.177	0.038	3.49×10^{-8}	0.040	1.027
	Max	0.715	40.000	2.471	0.144	1.33×10^{-4}	10.000	7.657
	Median	0.471	2.697	0.371	0.087	3.23×10^{-6}	1.000	2.057
	Mean	0.501	4.398	0.633	0.090	1.42×10^{-5}	2.032	2.792
	Global best-fit	—	1.351	0.334	0.103	3.14×10^{-6}	0.830	1.954
	Std. Dev.	0.085	6.190	0.571	0.025	2.50×10^{-5}	2.261	1.624
Clays	Min	0.351	0.500	—	—	5.42×10^{-10}	0.030	1.094
	Max	0.790	4932.4	—	—	5.88×10^{-6}	6.000	4.933
	Median	0.544	2.11	—	—	1.17×10^{-7}	2.078	2.000
	Mean	0.534	91.4	—	—	5.51×10^{-7}	2.363	2.095
	Global best-fit	—	2.505	—	—	1.39×10^{-6}	0.179	1.571
	Std. Dev.	0.100	626.1	—	—	1.16×10^{-6}	1.614	0.791

Table 3 - Descriptive statistics for the natural logarithm of unsaturated soil properties ($a = 0.075$ for sands, 0.050 for loams, and 0.025 for clays).

Group	Measure	$\ln(\psi_b)$ ln(kPa)	$\ln(\lambda_d)$	$\ln(\lambda_{res})$	$\ln(k_{sat})$ ln(m/s)	$\ln(\psi_{bk})$ ln(kPa)	$\ln(\eta)$
Sands	Min	-1.701	-0.904	-3.968	-14.78	-2.303	0.253
	Max	2.485	1.442	-2.068	-7.96	1.979	2.351
	Median	0.891	0.163	-3.119	-10.91	0.461	1.248
	Mean	0.856	0.198	-3.141	-11.34	0.119	1.268
	Std. Dev.	0.733	0.592	0.430	1.736	1.180	0.506
	Loams	Min	-2.914	-1.734	-3.270	-17.17	-3.219
Max		3.689	0.905	-1.940	-8.92	2.303	2.036
Median		0.992	-0.991	-2.446	-12.64	0.000	0.721
Mean		0.927	-0.737	-2.445	-12.58	-0.047	0.895
Std. Dev.		1.090	0.689	0.291	1.870	1.391	0.492
Clays		Min	-1.049	—	—	-21.34	-3.507
	Max	8.504	—	—	-12.04	1.792	1.596
	Median	0.743	—	—	-15.96	0.731	0.693
	Mean	0.999	—	—	-16.03	0.527	0.682
	Std. Dev.	2.064	—	—	2.053	0.992	0.331

Table 4 - Coefficients of variation for unsaturated soil properties.

Group	Sub-group	Records	n	$\ln(\psi_b)$	$\ln(\lambda_d)$	$\ln(\lambda_{res})$	$\ln(k_{sat})$	$\ln(\psi_{bk})$	$\ln(\eta)$
All	—	186	20.2	151.6	294.4	18.1	20.6	608.8	53.7
Sands	All	62	13.5	85.6	299.3	13.7	15.3	988.7	39.9
	<i>Sa</i>	53	12.7	92.1	279.9	13.9	15.4	5439.9	43.0
	<i>L-Sa</i>	9	13.7	53.2	655.6	8.5	15.3	111.3	14.4
Loams	All	62	17.1	117.6	93.5	11.9	14.9	2962.5	55.0
	<i>Sa-L</i>	15	11.3	105.5	74.5	10.2	13.6	539.3	60.3
	<i>Si-L</i>	27	13.5	74.3	133.2	11.4	15.7	365.4	57.7
	<i>L</i>	12	18.0	684.0	49.6	8.9	13.5	177.2	33.3
	<i>Sa-C-L & C-L</i>	8	16.3	149.2	101.0	12.2	14.3	937.3	55.3
Clays	All	62	18.7	206.6	—	—	12.8	188.2	48.6
	<i>Si-C</i>	22	26.3	125.5	—	—	10.4	76.5	52.2
	<i>Sa-C & C</i>	40	13.4	295.2	—	—	13.3	369.2	44.7

izing the standard variation with respect to the mean value. The coefficient of variation is unitless and has been traditionally used for characterizing geotechnical parameter uncertainty.

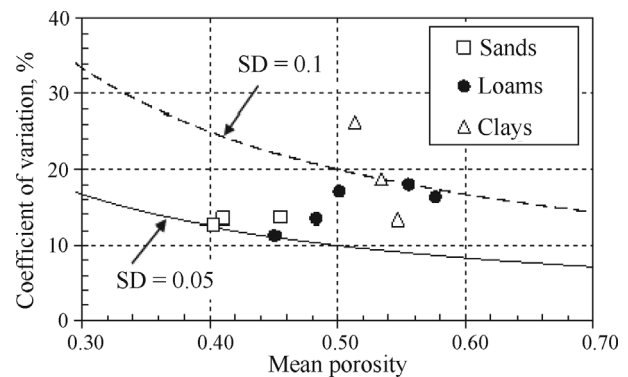
It was shown in the previous section that the parameters ψ_b , λ_d , λ_{res} , k_{sat} , ψ_{bk} , and η can be better analyzed in terms of natural logarithm. Therefore, values of COV are presented for the natural logarithms of all soil parameters, with exception of porosity, which was not considered log normally distributed. The coefficients of variations for n , $\ln(\psi_b)$, $\ln(\lambda_d)$, $\ln(\lambda_{res})$, $\ln(k_{sat})$, $\ln(\psi_{bk})$, and $\ln(\eta)$ are presented for each USDA group. Some neighboring groups with a reduced number of records where joined, as indicated. The data summarized in Tables 2-4 will be discussed in the following sections.

5.1. Porosity

The mean value of porosity, n , is 0.410 for sands, 0.501 for loams, and 0.534 for clays. The median values obtained do not differ considerably from the mean. Both the mean and median values appear to provide a reasonable measure of the central tendency for porosity. The minimum, maximum, median, and mean porosities increase for finer-grained soils, as expected.

The standard deviations and coefficients of variation increase for finer-grained soils. The coefficients of variation of porosity were 13.5% for sands, 17.1% for loams, and 18.7% for clays. The values previously reported in the literature show COVs for porosity varying from 10% to 20%. The results obtained herein suggest that the variability of the soil records studied may be slightly higher than that of soil records obtained from a single location or soil formation.

Figure 5 presents a plot of mean values of porosity vs. the computed coefficients of variation. Each data point corresponds to a distinct soil group gathered from the sampled

**Figure 5** - Mean vs. the coefficient of variation of the soil porosity, n .

soil records. The two lines surrounding the data points correspond to constant values of standard deviation, as indicated. One outlier was ignored. The data points plotted in Fig. 5 indicate that the COV for porosity show little variation with the mean value, as is often assumed. Although some of the results presented for porosity may appear obvious, the availability of statistical data in the literature allows comparisons that serve as verifications of the validity of the results obtained.

5.2. Air-entry value

The mean air-entry value was 2.9 kPa for sands, 4.4 kPa for loams, and 91.4 kPa for clays. The median values of ψ_b are considerably lower than the mean values, indicating positive skewness in the frequency distribution. However, the mean and median values of $\ln(\psi_b)$ are in reasonable agreement. This observation supports previous observations indicating the log normality of ψ_b .

The global best-fit values of ψ_b appear to be in poor agreement with the mean values of ψ_b and in better agree-

ment with the median values of ψ_b . The best-fit air-entry value is also in better agreement with the exponential of the mean values of $\ln(\psi_b)$. In other words, the mean values of $\ln(\psi_b)$ appear to be the best measurement of central tendency associated with ψ_b . The data for the air-entry value obtained from the hydraulic conductivity function lead to the same findings

The maximum and mean air-entry values increased for finer grained soils, as expected. The minimum and median values do not appear to show the same increasing trend. It appears that there are some factors other than the relationship between pore-size distribution and texture that influence the air-entry value. Soil structure, for instance, would appear to have a particularly important effect in the air-entry value of clay soils. Therefore, the values of ψ_b of clay soils can vary over a relatively large range and not always be higher than those of sand and loam soils.

Figure 6 presents a comparison of ψ_{bk} and ψ_b . In theory, the values of ψ_{bk} should be similar to the values of ψ_b . This tendency is in part confirmed by Fig. 6, with numerous data points near the 1:1 line. However, dispersion is observed and the values of ψ_{bk} tend to be lower than the values of ψ_b . This trend may be expected for soils that undergo substantial volume changes. Volume changes may cause a decrease in the hydraulic conductivity (Huang *et al.*, 1998). Consequently, a false break point in the hydraulic conductivity function may appear at a value of soil suction slightly below the value of ψ_b obtained from the SWCC.

The coefficients of variation obtained for the natural logarithm of the air entry values obtained from the SWCC, $\ln(\psi_b)$, were 85.6% for sands, 117.6% for loams, and 206.6% for clays. The coefficients of variation of the air entry values measured on the permeability functions, $\ln(\psi_{bk})$, seem unreasonably high. The COV of $\ln(\psi_{bk})$ is 989% for sands, 2962% for loams, and 188.2% for clays. The high values of COV of $\ln(\psi_b)$ and remarkably high values of COV of $\ln(\psi_{bk})$ are due to fact that some of the mean values of $\ln(\psi_b)$ and $\ln(\psi_{bk})$ are significantly close to 0 ln(kPa). The

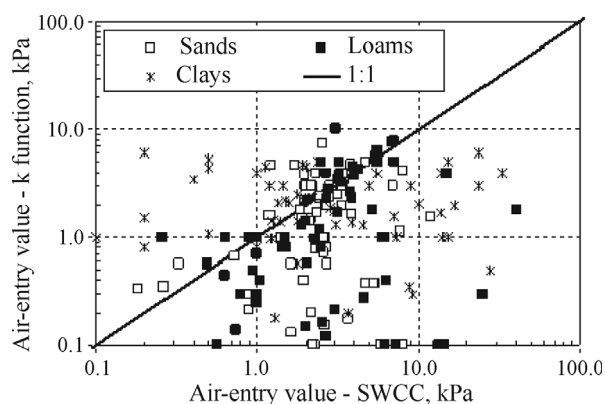


Figure 6 - Air-entry values obtained by best-fit of the soil-water characteristic curves and the hydraulic conductivity functions.

values of COV are highly sensitive to small changes in the mean value when the mean value is between -1 and 1 ln(kPa) and close to 0 ln(kPa). The sensitivity of COV to small mean values becomes obvious by examining its mathematical definition.

Figure 7 presents a plot of absolute values for the mean $\ln(\psi_b)$ and $\ln(\psi_{bk})$ vs. the computed COVs. Each data point corresponds to a distinct soil group gathered from the sampled soil records. The two lines surrounding the data points correspond to constant values of SD equal to 0.8 ln(kPa) and 2.1 ln(kPa). Figure 7 shows that most data points are located between COV values of 75% and 125%. However, when the mean values of $\ln(\psi_b)$ and $\ln(\psi_{bk})$ fall between -0.5 and 0.5 ln(kPa) and approach 0 ln(kPa), significantly higher values of COV are obtained.

The coefficients of variation for $\ln(\psi_b)$ and $\ln(\psi_{bk})$ show a clear trend with soil texture. The values of COV of $\ln(\psi_b)$ and $\ln(\psi_{bk})$ increase for fine-grained soils. This result is anticipated since sands are known to have air entry values varying over a smaller range of soil suctions while loams and clays have air-entry values varying over a wider range.

In summary, the results obtained herein suggest that COV values between 75% and 125% can be adopted in cases where the mean values of $\ln(\psi_b)$ or $\ln(\psi_{bk})$ are not within the -0.5 to 0.5 ln(kPa) range. When the mean values of $\ln(\psi_b)$ or $\ln(\psi_{bk})$ are within the -0.5 to 0.5 ln(kPa) range, the COV values should be abandoned and the parameter uncertainty should be defined using a standard deviations between 0.8 and 2.1 ln(kPa).

5.3. Primary drainage slope

The mean values obtained for the primary drainage slope, λ_a , were 1.446 for sands and 0.633 for loams. Primary drainage slope values for the SWCC of clay soils are not reported, since those soils were described using two parameters, ψ_b and a . As observer for the air-entry value, the mean values of λ_d for sands and loams disagreed with the median values, indicating non symmetric frequency distri-

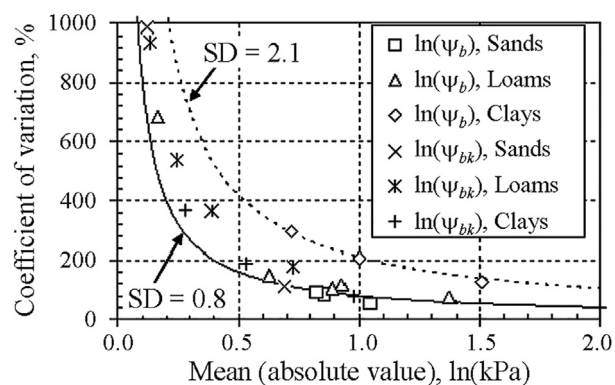


Figure 7 - Mean vs. the coefficient of variation of the natural logarithm of air-entry value obtained from the SWCC and from the k function, $\ln(\psi_b)$ and $\ln(\psi_{bk})$, ln(kPa).

butions. The closer agreement between the mean and median values of $\ln(\lambda_d)$ corroborates previous observations indicating the log normality of λ_d . It can also be observed that the values of λ_d for sands are higher than those of loams, as expected. Loam soils tend to have broader pore-size distributions than sands as reflected in the grain-size distributions.

The variability of the primary drainage slope was analyzed in the same manner as the previous parameters. The coefficient of variation of $\ln(\lambda_d)$ was 299.3% for sands and 93.5% for loams. The COV of $\ln(\lambda_d)$ of loams is significantly lower than that of sands. This result does not reflect the wider grain-size distribution for loams and the narrower variation in grain-size distribution for sands. In fact, the results once again are influenced by low mean values of $\ln(\lambda_d)$ that approach zero. Figure 8 presents a plot of mean values of $\ln(\lambda_d)$ vs. the computed COVs. The two lines plotted correspond to constant values of SD that encompass all the data points. The loam data points are closer to the maximum standard deviation line.

The results obtained herein suggest that a COV value between 75 and 100% can be adopted in cases where the mean values of $\ln(\lambda_d)$ are not within the -0.5 to +0.5 range. In cases where the mean values of $\ln(\lambda_d)$ are within the -0.5 to +0.5 range, the COV values suggested above should be abandoned and the parameter variability should be established using a range of standard deviations between 0.45 and 0.80.

5.4. Residual drainage slope

The mean values for the residual drainage slope, λ_{res} , were 0.047 for sands and 0.090 for loams. The comparison between mean, median and global best-fit values of λ_{res} and $\ln(\lambda_{res})$ suggest once again the log normality of λ_{res} . It can also be observed that the values of λ_{res} for sands were significantly lower than those of loams. This result was expected, since the smaller pores found in loam soils are capable of holding water up to relatively high soil suctions.

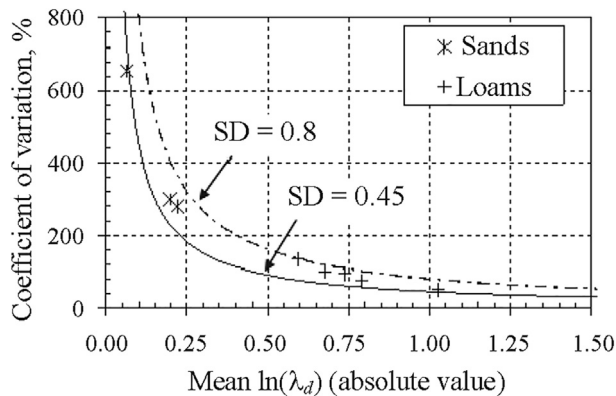


Figure 8 - Mean vs. the coefficient of variation of the natural logarithm of the primary drainage slope, $\ln(\lambda_d)$.

The coefficient of variation of $\ln(\lambda_{res})$ is 13.7% for sands and 11.9% for loams. The COV of $\ln(\lambda_{res})$ for loam soils was slightly lower than that of sands. The mean values of $\ln(\lambda_{res})$ did not have a significant effect on the COV values since they did not fall within the -0.5 and 0.5 range. Figure 9 presents a plot of mean values of $\ln(\lambda_{res})$ vs. the computed COVs. The two lines plotted correspond to constant SD values of 0.20 and 0.45. The sand data points are closer to a SD value of 0.45 but have higher mean values. Most data points are located between COV values of 8 and 12%.

The results obtained herein suggest that a COV value between 8 and 12% can be adopted. Nevertheless, the mean values of $\ln(\lambda_{res})$ should be verified. When the mean values of $\ln(\lambda_{res})$ are within the -0.5-0.5 range, the COV values suggested above should be abandoned and the parameter variability should fall within a SD range between 0.2 and 0.45.

5.5. Saturated hydraulic conductivity

Central tendency measures of the saturated hydraulic conductivity, k_{sat} , can be misleading because its frequency distribution is positively skewed and its values may vary over several orders of magnitude. Just as with other previous parameters, statistical moments of the natural logarithm of the property are more meaningful and easier to interpret.

The values of k_{sat} and $\ln(k_{sat})$ decreased for finer grained soils, as obviously expected. The mean values of $\ln(k_{sat})$ are -11.3 for sands, -12.6 for loams, and -16.0 for clays. The corresponding exponential values are $k_{sat} = 1.23 \times 10^{-5}$ m/s for sands, $k_{sat} = 3.37 \times 10^{-6}$ m/s for loams, and $k_{sat} = 1.09 \times 10^{-7}$ m/s for clays.

The variability of the saturated hydraulic conductivity was analyzed using the natural logarithm transformation. The coefficients of variation of $\ln(k_{sat})$ were 15.3% for sands, 14.9% for loams, and 12.8% for clays. Apparently, the COV of $\ln(k_{sat})$ slightly decrease for fine-grained soils. Figure 10 presents a plot of mean values of $\ln(k_{sat})$ vs. the

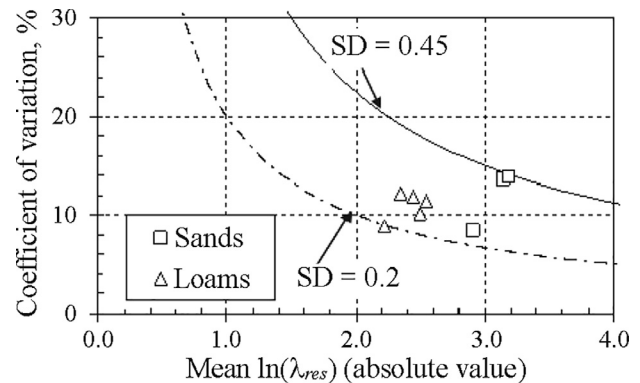


Figure 9 - Mean vs. the coefficient of variation of the natural logarithm of the residual drainage slope, $\ln(\lambda_{res})$.

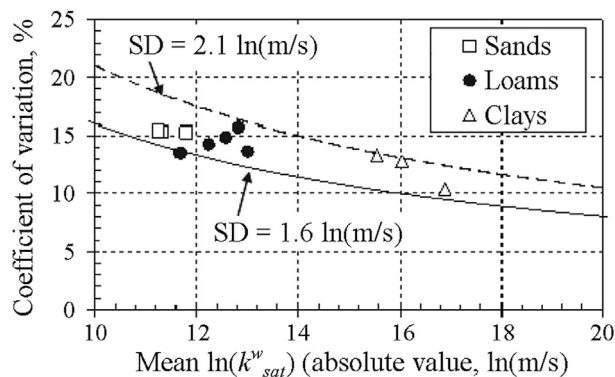


Figure 10 - Mean vs. the coefficient of variation of the natural logarithm of the saturated hydraulic conductivity, $\ln(k_{sat})$, $\ln(\text{m/s})$.

computed COVs, in the same fashion as done for the previous parameters. The sand data points are closer to the maximum SD line, equal to $2.1 \ln(\text{m/s})$. The data points plotted in Fig. 10 indicate that the measures of COV of $\ln(k_{sat})$ appear to show little variation with the mean values. Therefore, results presented herein suggest that a value of COV of $\ln(k_{sat})$ between 13 and 16% is representative.

5.6. Hydraulic conductivity function slope

The mean values of the hydraulic conductivity function slope, η , were 4.037 for sands, 2.792 for loams, and 2.095 for clays. The values of η for sands are higher than those of loams and clays, as expected. This trend was observed for the minimum, maximum, median, mean values, and global best-fit values.

The coefficients of variation of $\ln(\eta)$ are 39.9% for sands, 55.0% for loams, and 48.6% for clays. The COV of $\ln(\eta)$ does not show any clear relationship with soil texture, though it appears to slightly increase for fine-grained soils. Figure 11 presents a plot of mean values of $\ln(\eta)$ vs. computed COVs. The two lines shown correspond to constant SD values of 0.28 and 0.58. One outlier was ignored. Most data points are within a COV range between 40 and 55%. The data points plotted in Fig. 11 do not indicate any clear

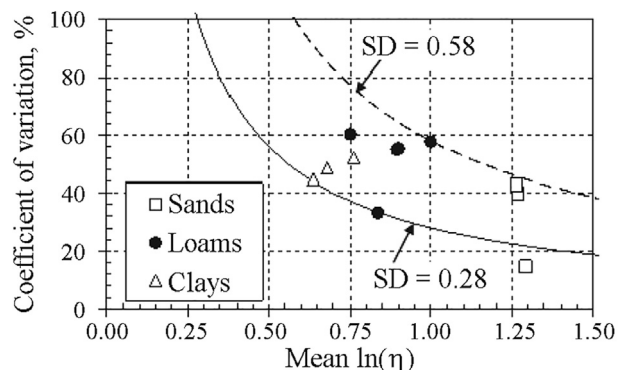


Figure 11 - Mean vs. the coefficient of variation of the natural logarithm of the hydraulic conductivity function slope, $\ln(\eta)$.

relationship between the COV measures for $\ln(\eta)$ and the mean values. The results obtained herein suggest that COV values of $\ln(\eta)$ should be between 40 and 55%.

6. Correlation Coefficients Between Unsaturated Soil Parameters

The correlation coefficient, ρ , between each pair of unsaturated soil parameters was determined with the aid of Minitab 13 (Minitab Inc., 2000). The parameters studied were n , $\ln(\psi_b)$, $\ln(\lambda_d)$, $\ln(\psi_{res})$, $\ln(k_{sat})$, $\ln(\lambda_{bk})$, and $\ln(\eta)$. A two-tailed correlation test was applied. The null hypothesis of the test performed was H_0 : correlation coefficient of zero. P -values were computed to represent the probability of making a *type 1 error*, which is “rejecting the null hypothesis when it is true.” The smaller the P -value, the higher the likelihood that the parameters are correlated. The cut-off value used was 5%, that is, the null hypothesis was rejected when the p -value was less than 5%.

Table 5 presents the results of the correlation analyses. The correlation coefficients are presented for all pairs of variables. Some correlation coefficients are accompanied by a star (*), which indicates that the p -value obtained was less than 5%.

The correlation coefficients presented in Table 5 were calculated considering all data records as a single group and also considering the three soil groups (*Sa*, *L*, and *C*) individually. The p -values tended to decrease when the data records were considered as a single group, except in a few cases. An increase in the number of data points generally results in a decrease in the uncertainty associated with a *type 1 error*.

Porosity did not present substantial correlation with any parameter, with exception of the parameter $\ln(\lambda_{res})$. The correlation coefficient between n and $\ln(\lambda_{res})$ did not have a p -value lower than 5% for all soil groups. Similarly, the variable $\ln(\lambda_{res})$ did not present substantial correlation with any other parameter with the exception of the aforementioned correlation with porosity and some mild correlation with $\ln(\psi_b)$.

Noteworthy correlations involving the air-entry value were found when considering both $\ln(\psi_b)$ and $\ln(\psi_{bk})$. While $\ln(\psi_b)$ presented considerable correlations with the SWCC-related parameters, $\ln(\psi_{bk})$ showed significant correlations with the parameters related to the k function. The parameters $\ln(\psi_b)$ and $\ln(\lambda_d)$ presented correlation coefficients that varied from +0.374 to +0.587. This significantly positive correlation indicates that soils with larger air-entry value tend to be the same soils that have “poorly graded” pore-size distributions. The parameters $\ln(\psi_b)$ and $\ln(\lambda_{res})$ presented correlation coefficients that varied from +0.211 to +0.281. This correlation was not as anticipated since there would appear to be little physical meaning for a relationship between the air-entry value and the residual drainage slope.

Table 5 - Correlation matrix for unsaturated soil properties.

Parameter	Group	<i>n</i>	$\ln(\psi_b)$	$\ln(\lambda_d)$	$\ln(\lambda_{res})$	$\ln(k_{sat})$	$\ln(\psi_{bk})$	$\ln(\eta)$
<i>n</i>	All soils	1						
	Sands	1						
	Loams	1						
	Clays	1						
$\ln(\psi_b)$	All soils	-0.147*	1					
	Sands	-0.079	1					
	Loams	-0.096	1					
	Clays	-0.282*	1					
$\ln(\lambda_d)$	All soils	-0.311*	0.374*	1				
	Sands	0.084	0.587*	1				
	Loams	-0.032	0.443*	1				
	Clays	—	—	—				
$\ln(\lambda_{res})$	All soils	0.534*	0.211*	-0.399*	1			
	Sands	0.354*	0.270*	0.096	1			
	Loams	0.227	0.281*	-0.080	1			
	Clays	—	—	—	—			
$\ln(k_{sat})$	All soils	-0.210*	-0.216*	0.354*	-0.233*	1		
	Sands	0.193	-0.276*	0.234	-0.086	1		
	Loams	0.249	-0.174	0.192	0.095	1		
	Clays	0.228	-0.347*	—	—	1		
$\ln(\psi_{bk})$	All soils	0.078	0.140	0.373*	-0.041	-0.408*	1	
	Sands	0.073	0.187	0.127	0.141	-0.427*	1	
	Loams	0.012	0.320*	0.626*	-0.167	-0.275*	1	
	Clays	0.032	0.023	—	—	-0.630*	1	
$\ln(\eta)$	All soils	-0.151*	0.025	0.675*	-0.227*	0.393*	0.500*	1
	Sands	0.092	0.083	0.365*	0.105	0.057	0.755*	1
	Loams	0.079	0.228	0.847*	-0.095	0.280*	0.700*	1
	Clays	0.300*	-0.084	—	—	0.023	0.338*	1

symmetric

Note: (*) indicates the correlation coefficients for which the *p*-value is less than 5%.

The parameters $\ln(\psi_{bk})$ and $\ln(k_{sat})$ presented moderate to high correlation coefficients that varied from -0.275 to -0.630. The negative correlation between $\ln(\psi_b)$ and $\ln(k_{sat})$ was also expected since the same factors that cause higher air-entry values are responsible for lower values of k_{sat} , such as larger fractions of fines. The parameters $\ln(\psi_{bk})$ and $\ln(\eta)$ presented correlation coefficients that varied from +0.338 to +0.755.

Finally, the parameters $\ln(\eta)$ and $\ln(\lambda_d)$ presented high degrees of correlation that varied from +0.365 to +0.847. The high degree of positive correlation was as anticipated. Several mechanistic models of prediction for the hydraulic conductivity function indicate that the slope of

the *k* function increases with increasing values of λ_d (e.g., Brooks & Corey, 1964).

7. Summary of Suggested Typical Values

The information presented and interpreted in the previous sections is summarized in a convenient manner in Tables 6-8. Table 6 presents a summary of the mean values for the unsaturated soil parameters *n*, $\ln(\psi_b)$, $\ln(\lambda_d)$, $\ln(\lambda_{res})$, $\ln(k_{sat})$, and $\ln(\eta)$ along with the exponential value of all variables, except for porosity. Independent best estimates for mean air-entry values are suggested for $\ln(\psi_b)$ and $\ln(\psi_{bk})$. The values presented in Table 6 are suggested as the best measures of central tendency for each main soil group.

Porosity can be considered normally distributed and all the remaining parameters presented in Table 6 can be assumed to be log normally distributed. It is important to point out that the similar mean values of air-entry value for different textural classes are explained by an increase in COV and range of values for finer grained soils. As a result, the mean values of the entire population remain relatively low. The wide variation of air-entry values for finer-grained soils can be attributed, for example, to the importance of fabric to the pore-size distribution.

Table 7 presents a summary of the coefficients of variation for the unsaturated soil parameters n , $\ln(\psi_b)$, $\ln(\lambda_d)$, $\ln(\lambda_{res})$, $\ln(k_{sat})$, and $\ln(\eta)$. The values of $\ln(\psi_b)$ were established by combining the results obtained for $\ln(\psi_b)$ and $\ln(\psi_{bk})$. General ranges for all soil types are presented along with specific information for each main soil group, Sa , L , and C .

Some ranges for the coefficient of variation suggested in Table 7 are not applicable when the mean value of the parameter is within the range -0.5 and 0.5. In these cases the standard deviation values provided in Table 7 can be adopted.

Table 8 presents a summary of the correlation coefficients for pairs for the following unsaturated soil parameters, n , $\ln(\psi_b)$, $\ln(\lambda_d)$, $\ln(\lambda_{res})$, $\ln(k_{sat})$, and $\ln(\eta)$. The correlation coefficients associated with the air-entry value were established by combining the results obtained for $\ln(\psi_b)$ and $\ln(\psi_{bk})$. Average values applicable to all soil types were established. The values presented in Table 8 are suggested as general guideline values applicable for any soil type.

8. Concluding Remarks

This paper presented a comprehensive statistical study of hydraulic properties of unsaturated soil. The primary objective was to present approximate uncertainty values that could be used in probabilistic geotechnical analyses. The property functions studied were the soil-water characteristic curve and the hydraulic conductivity function. The statistical study was based on a large database of soils. The study was undertaken considering three soil groups based on the USDA textural classification system; namely, sands, loams, and clays.

A methodology was developed for the statistical assessment of unsaturated soil property functions. Appropriate nonlinear unsaturated soil property equations and fitting

Table 6 - Mean values for unsaturated soil properties by soil group.

Group	Sands	Loams	Clays
n	0.410	0.500	0.534
$\ln(\psi_b)$, $\ln(\text{kPa})$	0.856 (2.35)	0.927 (2.53)	0.999 (2.71)
$\ln(\lambda_d)$	0.198 (1.219)	-0.737 (0.478)	—
$\ln(\lambda_{res})$	-3.141 (0.043)	-2.445 (0.087)	—
$\ln(k_{sat})$, $\ln(\text{m/s})$	-11.34 (1.19×10^{-5})	-12.58 (3.44×10^{-6})	-16.03 (1.09×10^{-7})
$\ln(\psi_{bk})$, $\ln(\text{kPa})$	0.119 (1.13)	-0.047 (0.95)	0.527 (1.69)
$\ln(\eta)$	1.268 (3.554)	0.895 (2.447)	0.682 (1.978)

Note: Values between brackets indicate the exponential of the variable.

Table 7 - Coefficients of variation and standard deviations of unsaturated soil properties.

Soil parameter	General ranges for all soils of the Coefficient of Variation (COV) and Standard Deviation (SD)	Coefficient of variation		
		Sands	Loams	Clays
n	COV = 13-19%	13%	17%	19%
$\ln(\psi_b)$	COV = 75-205% for $-0.5 > E[\ln(\psi_b)] > 0.5 \ln(\text{kPa})$ otherwise, $SD = 0.8-2.1 \ln(\text{kPa})$	85%	115%	205%
$\ln(\lambda_d)$	COV = 75-100% for $-0.5 > E[\ln(\lambda_d)] > 0.5$ otherwise, $SD = 0.45-0.80$	100%	90%	—
$\ln(\lambda_{res})$	COV = 8-14% for $-0.5 > E[\ln(\lambda_{res})] > 0.5$ otherwise, $SD = 0.20-0.45$	14%	12%	—
$\ln(k_{sat})$	COV = 13-16%	16%	15%	13%
$\ln(\eta)$	COV = 40-55%	40%	55%	50%

Table 8 - Correlation matrix for unsaturated soil properties.

Parameter	n	$\ln(\psi_b)$	$\ln(\lambda_d)$	$\ln(\lambda_{res})$	$\ln(k_{sat})$	$\ln(\eta)$
n	1					
$\ln(\psi_b)$	0	1			<i>symmetric</i>	
$\ln(\lambda_d)$	0	0.45	1			
$\ln(\lambda_{res})$	0	0.25	0	1		
$\ln(k_{sat})$	0	-0.40	0	0	1	
$\ln(\eta)$	0	0	0.60	0	0.60	1

parameters were described. All equation parameter were shown to have a clearly defined feature on the soil property function and the equation parameters were mathematically independent. The Gitirana Jr. & Fredlund (2004) soil-water characteristic curve equation was used and a bilinear equation was adopted for hydraulic conductivity. The soil parameters studied are: n , ψ_b , λ_d , λ_{res} , k_{sat} , ψ_{bk} , and η .

Normality tests showed that unsaturated soil parameters can be considered to be log normally distributed. Various central tendency measures were evaluated. The mean values of the natural logarithm of the soil parameters provided the best central tendency measure. Uncertainty measures were presented in terms of standard deviations and coefficients of variation. Fairly constant coefficients of variations were determined for various soil groups. However, some unsaturated soil parameters have mean values that may fall within a -0.5 to 0.5 range, making the coefficient of variation a poor measure of uncertainty. A combination of standard deviation and coefficient of variation values were proposed for these parameters.

Correlation matrices were determined considering the three selected soil groups as well as considering all datasets as one large soil group. Correlations involving the air-entry value were found considering both $\ln(\psi_b)$ and $\ln(\psi_{bk})$. While $\ln(\psi_b)$ presented considerable correlations with the SWCC-related parameters, $\ln(\psi_{bk})$ showed significant correlations with the parameters related to the k function. The parameters $\ln(\psi_{bk})$ and $\ln(k_{sat})$ presented moderate to high negative correlations, as anticipated. The pairs $\ln(\psi_{bk}) - \ln(\eta)$, $\ln(\eta) - \ln(\lambda_d)$, and $\ln(\eta) - \ln(k_{sat})$ presented moderate to strong positive correlation.

The coefficients of variation and standard deviations presented herein include diverse sources of uncertainty. Individual sources of parameter variability could not be assessed. Nevertheless, the presented standard deviations and coefficients of variations serve as a general indication and as a first approximation. The information presented herein can be refined in future studies as further data is collected and analyzed.

Acknowledgments

The authors would like to thank the “Conselho Nacional de Desenvolvimento Científico e Tecnológico - CNPq”, Brazil, Canadian Pacific Railway, Saskatchewan Highways and Transportation, and NSERC for financial support.

References

- ASTM D 2487-93 (1993). Standard Classification of Soils for Engineering Purposes (Unified Soil Classification System).
- Bates, D. & Watts, D. (1988). Nonlinear Regression Analysis and its Applications. John Wiley & Sons, New York, United States of America.
- Benson, C.H.; Daniel, D.E. & Boutwell, G.P. (1999). Field performance of compacted clay liners. Journal of Geotechnical and Geoenvironmental Engineering, ASCE, 125(5):390-403.
- Brooks, R.H. & Corey, A.T. (1964). Hydraulic properties of porous media. Hydrology. Paper No. 3, Colorado State University, Fort Collins, Colorado, 27 p.
- Dai, S.-H. & Wang, M.-O. (1992). Reliability Analysis in Engineering Applications. Van Nostrand Reinhold, New York.
- D’Augustino, R.B. & Stevens, M.A. (1986). Goodness-of-Fit Techniques. Marcel Dekker Inc., New York, 576 p.
- Duncan, M. (2000). Factors of safety and reliability in geotechnical engineering. Journal of Geotechnical and Geoenvironmental Engineering, ASCE, 126(4):307-316.
- Faulkner, B.R.; Lyon, W.G.; Khan, F.A. & Chattopadhyay, S. (2003). Modeling leaching of viruses by the Monte Carlo method. Water Research, 37(19):4719-4729.
- Fredlund, D.G. & Dahlman, A.E. (1971). Statistical geotechnical properties of glacial lake Edmonton sediments. Proc. 1st International Conference on Applications of Statistics and Probability to Soil and Structural Engineering, Hong Kong, pp. 204-228.
- Fredlund, D.G. & Xing, A. (1994). Equations for the soil-water characteristic curve. Canadian Geotechnical Journal, 31(4):533-546.

- Gitirana Jr., G.F.N. & Fredlund, D.G. (2004). Soil-water characteristic curve equation with independent properties. *Journal of Geotechnical and Geoenvironmental Engineering*, ASCE, 130(2):209-212.
- Hammitt, G.M. (1966). Statistical analysis of data from a comparative laboratory test program sponsored by ACIL. Miscellaneous Paper 4-785, U.S. Army Engineering Waterways Experiment Station, Corps of Engineers.
- Harr, M.E. (1987). *Reliability-Based Design in Civil Engineering*. John Wiley and Sons, New York, 291 p.
- Huang, S.; Barbour, S.L. & Fredlund, D.G. (1998). Development and verification of a coefficient of permeability function for a deformable unsaturated soil. *Canadian Geotechnical Journal*, 35(3):411-425.
- Krahn, J. & Fredlund, D.G. (1983). Variability in the engineering properties of natural soil deposits. Proc. 4th International Conference on Applications of Statistics and Probability in Soil and Structural Engineering, Florence, Italy, pp. 1017-1029.
- Kulhawy, F.H. (1992). On the evaluation of soil properties. ASCE Geotech. Special Publication 31, Reston, pp. 95-115.
- Lacasse, S. & Nadim, F. (1997). Uncertainties in Characterizing Soil Properties. Publication No. 201, Norwegian Geotechnical Institute, Oslo, Norway, pp. 49-75.
- Ladd, C.C. (1983). Geotechnical exploration in clay deposits with emphasis on recent advances in laboratory and in situ testing and analysis of data scatter. *Journal of Civil and Hydraulic Engineering*, Taiwan, 10(3):3-35.
- Lumb, P. (1966). The variability of natural soils. *Canadian Geotechnical Journal*, 3(2):74-97.
- Meyer, P.D.; Rockhold, M.L. & Gee, G.W. (1997). Uncertainty analyses of infiltration and subsurface flow and transport for SDMP sites. NUREG/CR-6565. U.S. NRC.
- Minitab Inc. (2000). *Minitab User's Manual*, Version 13. Copyright 2000. Minitab Inc. State College, PA.
- Mishra, S.; Parker, L.C. & Singhal, N. (1989). Estimation of soil hydraulic properties and their uncertainty from particle size distribution data. *Journal of Hydrology*, 108(1):1-18.
- Nielsen, D.R.; Biggar, J.W. & Erh, K.T. (1973). Spatial variability of field-measured soil-water properties. *Hilgardia*, 42(7):215-260.
- Padilla, J.D. & Vanmarcke, E.H. (1974). Settlement of structures on shallow foundations: A probabilistic analysis. Res. Rep. R74-9, MIT, Cambridge, Mass.
- Phoon, K.-K. & Kulhawy, F.H. (1999a). Characterization of geotechnical variability. *Canadian Geotechnical Journal*, 36(4):612-624.
- Phoon, K.-K. & Kulhawy, F.H. (1999b). Evaluation of geotechnical property variability. *Canadian Geotechnical Journal*, 36(4):625-639.
- Phoon, K.-K.; Santoso, A. & Quek, S.-T. (2010). Probabilistic analysis of soil-water characteristic curves. *Journal of Geotechnical and Geoenvironmental Engineering*, ASCE, 136(3):445-455.
- Rawls, W.J.; Gimenez, R. & Grossman, R. (1998). Use of soil texture, bulk density, and slope of the water retention curve to predict saturated hydraulic conductivity. *Trans ASAE*. 41(4):983-988.
- Schultze, E. (1971). Frequency distributions and correlations of soil properties. Proc. First International Conference on Applications of Statistics and Probabilistic in Soil and Structure Engineering, Hong Kong. pp. 371-387.
- Soil Survey Staff (1975). *Soil Taxonomy: A Basic System of Soil Classification for Making and Interpreting Surveys*. 2nd Ed. USDA-SCS Agriculture Handbook, U.S. Gov. Print. Office, Washington, D.C., 869 p.
- SoilVision Systems (2005). *SoilVision User's Guide - A Knowledge-based System for Geotechnical Engineers*. Version 4.0. Saskatoon, SK, , 149 p.
- Tan, C.P.; Donald, I.B. & Melchers, R.E. (1993). Probabilistic slip circle analysis of earth and rockfill dams. Proc. Conference on Probabilistic Methods in Geotechnical Engineering, Canberra, pp. 281-288.
- Whitman, R.V. (1984). Evaluating calculated risk in geotechnical engineering. *ASCE Geotechnical Engineer Journal*. 110(2):145-189.
- Zapata, C.E.; Houston, W.N.; Houston, S.L. & Walsh, K.D. (2000). Soil-water characteristic curve variability. Shackelford, C.D., Houston S.L., & Chang N.-Y. (eds), *Advances in Unsaturated Geotechnics*, ASCE, Geotechnical Institute Geotechnical Special Publication No. 99, August 5-8, 2000, pp. 84-124.

List of Symbols

- COV: coefficient of variation
 E : mean
 HCV : highest conceivable value
 k : hydraulic conductivity
 k_{sat} : saturated hydraulic conductivity
 LCV : lowest conceivable value
 n : porosity
 SD : standard deviation
 S : degree of saturation
 S_{res} : residual degree of saturation
 η : slope of the hydraulic conductivity function
 λ_d : primary drainage slope
 λ_{res} : residual drainage slope
 ρ : correlation coefficient
 ψ : soil suction
 ψ_b : air-entry value
 ψ_{bk} : break point of the hydraulic conductivity function
 ψ_{res} : residual suction

Numerical Modeling of Unsaturated Soils Problems

M.D. Fredlund

Abstract. Numerical modeling (finite element analyses) of saturated-unsaturated soils problems generally involves the solution of linear or nonlinear partial differential equations, PDEs. The soil properties for unsaturated soils usually take on a functional form that subsequently requires an iterative procedure to obtain a solution. Special numerical solution techniques are helpful (and in some cases necessary) in order to have confidence that the results of the numerical solution are accurate. The dynamic upgrade of the finite element mesh (and time steps) during the iterative solution process have proven to be of significant value in ensuring the proper convergence of the numerical solution. The unsaturated soil property functions are usually obtained through use of estimation procedures based on the measurement of the soil-water characteristic curve, SWCC. One or more estimation procedures have been proposed in the research literature for soil property functions for each physical process of interest in unsaturated soil mechanics. The numerical modeller must be aware of the relationship between the estimated soil property functions and the solution technique. Boundary conditions required when solving unsaturated soils problems often involve the assessment of moisture and thermal flux conditions computed from meteorological records. There are conditions and requirements that must be quantifiable when solving unsaturated soils problems. The estimation of the unsaturated soil property functions makes the solution of unsaturated soils problems more complex than those of saturated soils.

Keywords: numerical modeling, unsaturated soil mechanics, partial differential equations, finite element analysis, adaptive mesh refinement.

1. Introduction

There are several distinct differences between the modeling saturated soil mechanics problems and unsaturated soils problems (or saturated-unsaturated soils problems). This paper describes the differences between these two classes of problems and illustrates numerical modeling techniques that have been found to perform well when modeling problems involving unsaturated soils. The boundaries for unsaturated soil mechanics problems often involve the assessment of moisture (and thermal) fluxes that are related to climatic conditions. Solving unsaturated soils problems with realistic moisture flux boundary conditions has proven to be challenging (Fredlund & Stianson, 2011). Ground surface, moisture flux boundary conditions constitute another common difference between solving saturated and unsaturated soils problems.

Numerical modeling of most saturated soils problems is quite straight forward because the soil properties can generally be assumed to be constant values. For example, transient water seepage problems may require the designation of the hydraulic conductivity, k_w (coefficient of permeability), and the water storage coefficient of volume change, m_v . Similarly, other saturated soils problems also have soil properties that can be input as constant values. In other words, saturated soil modeling generally involves the input of fixed, designated soil properties. Unsaturated soils problems, on the other hand, generally involve the designation of soil properties that have the form of mathematical functions. Consequently, numerical modeling solutions be-

come nonlinear and require an iterative procedure to obtain a solution. Stated another way, *saturated soil mechanics* can be viewed as *linear soil mechanics* problems with constant soil properties while *unsaturated soil mechanics* can be viewed as *nonlinear soil mechanics* problems.

One of the challenges in solving unsaturated soil mechanics problems is related to obtaining solutions that have converged to the “correct solution”. This is particularly important when solving transient field problems where the solution from one time step affects subsequent mass balance calculations. Fortunately, computing techniques such as “automatic mesh refinement”, AMF, have been developed to ensure that the solution of nonlinear partial differential equations can indeed converge to a “correct solution”.

2. Theoretical Differences in Formulations Between Saturated Soils and Unsaturated Soils

Any physical process involving soils can be formulated as a boundary-value problem within a continuum mechanics framework. The procedure starts with the selection of a representative elemental volume, REV, to which the conservative laws of physics are applied (*e.g.*, conservation of mass and/or conservation of energy). The physical laws of behaviour for the process under consideration are then substituted into the conservative field equations. The physical laws of behaviour will either include soil properties with constant values or mathematical functions that describe the manner in which the soil properties vary with re-

spect to another variable that is part of the solution. Soil properties for problems involving unsaturated soils generally fall into the latter category (*i.e.*, mathematical functions). The end result is a nonlinear (or possibly a linear) partial differential equation that needs to be solved through use of a numerical modeling technique.

It is generally possible to formulate the behaviour of *unsaturated soil* processes in such a way that *saturated soil* processes are also embraced. The *unsaturated soil* formulations constitute a more general formulation and the *saturated soil* case becomes a special case that is simpler to solve. Consequently, a single generalized formulation can be used for solving problems involving *saturated-unsaturated soil* systems.

The primary difference between saturated soil numerical modeling and unsaturated soil numerical modeling lies in the fact that the unsaturated soil properties are in the form of a mathematical function that contains one of the variables for which a solution is being sought. Consequently, an assumed value must first be selected for the unsaturated soil properties. Once a solution is obtained for the primary variables being solved for, a check must be made to ensure that the correct unsaturated soil properties were used in obtaining the solution. If the correct unsaturated soil properties were not used in the solution, the soil properties must be up-dated and the solution repeated. This procedure sets up an iterative technique that may continue for 10 s and even 100 s of iterations. In the end, the solution may not be a “correct solution” unless certain conditions have been met during the iterative solution procedure. Special mesh refinement techniques (*e.g.*, AMR) have proven to be particularly useful in not only ensuring convergence but also ensuring convergence to an accurate (or correct) solution.

3. Moisture Flux Boundary Conditions

The ground surface forms the uppermost boundary when solving many unsaturated soils problems. In some unsaturated soils cases it is possible to apply a hydraulic head or pressure boundary condition at the ground surface, however, in most situations it is more realistic to apply a moisture flux boundary condition based on climatic conditions. Rainfall (and snowfall) can be applied as a downward moisture flux at the ground surface. In the absence of precipitation, an upward moisture flux can be applied to represent evaporation (or evapotranspiration). A decision must also be made with regard to whether or not evaporation should be applied during rainfall conditions. It appears that the most commonly used assumption is to have the two processes (*i.e.*, precipitation and evaporation) occur simultaneously. Figure 1 shows the components associated with calculating water balance at the ground surface. Each component of moisture movement must be evaluated, however, there is an interaction between components such as rainfall (intensity) and runoff.

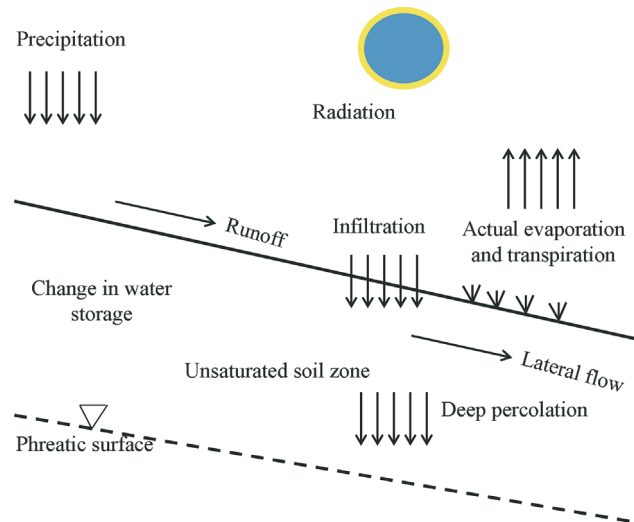


Figure 1 - Primary moisture components of a typical near-ground-surface geotechnical engineering problem (Fredlund & Stianson, 2011).

Meteorological stations commonly monitor precipitation on a daily basis. The daily precipitation records are valuable but it is the intensity of rainfall records that are of greatest significance in evaluating the interaction between infiltration and runoff. Figure 2 shows a typical weather station record of daily precipitation and the cumulative rainfall at a particular site in Canada. The graph shows that most of the rainfall occurs during the spring and fall seasons. The simulation of transient infiltration conditions requires the usage of short time steps often in the order of minutes. Consequently, assumptions are required regarding the rainfall duration (and therefore, the average rainfall intensity). The infiltration of moisture is closely related to rainfall intensity and the permeability of the near-ground-surface soils.

In northern climates such as found in Canada, additional assumptions must be made with regard to the snow sublimation, snowmelt and spring runoff. Figure 3 illustrates how each year can be subdivided into periods of varying degrees of moisture movement activity. For example, the period from point 1 to point 2 (or 3), can be referred to as the inactive period. The period from point 3 to 4, is the snowmelt period with significant activity. The snowmelt period is followed by the active growing period. Assumptions regarding “how best to handle” each season of the year have been addressed in the literature (Stianson & Fredlund, 2011).

Evaporation of moisture from the ground surface is closely related to net radiation conditions (temperature) and wind speed at ground surface. There are two terms commonly associated with the calculation of evaporation moisture fluxes; namely, potential evaporation, PE, and actual evaporation, AE. The physical processes associated

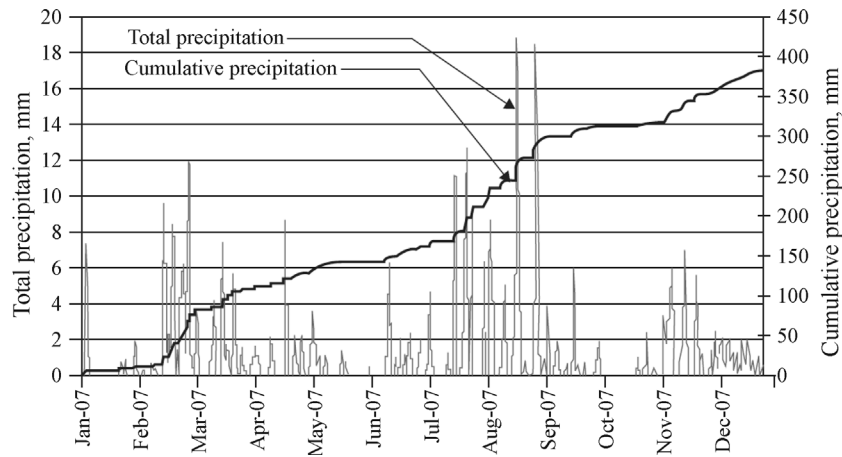


Figure 2 - Typical weather station record showing daily precipitation and cumulative rainfall at a particular site in Canada.

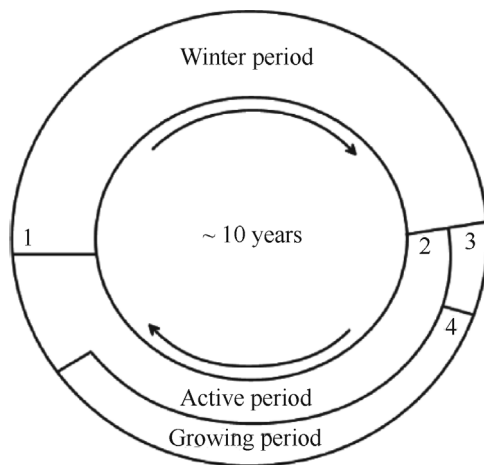


Figure 3 - Typical climatic periods of the year in cold climates (Fredlund & Stianson, 2011).

with the PE term are quite well-known and the PE term can be calculated based on above-ground-surface conditions. Potential evaporation, PE, is dependent upon the vapour pressure gradient at ground surface, assuming there is an ample supply of water in the soil surface. Vapour pressure gradient is mainly a function of net radiation reaching the ground surface and the effect of “mixing” or wind turbulence at the ground surface. PE corresponds to the evaporation that occurs from a water saturated soil surface.

Actual evaporation, AE, is the moisture flux that is required for most numerical modeling scenarios. In addition to the effects of net radiation and “mixing”, AE is also a function of the affinity of the ground surface soils for water (*i.e.*, total suction) (Wilson *et al.*, 1994). Total suction combines the effect of negative pore-water pressures (*i.e.*, matric suction) and osmotic suction (*i.e.*, effect of salts in the pore-water). There are other mechanisms that also significantly affect AE (Tran, 2013). For example, most of the salts in the pore-water are left behind to collect on the soil

surface when water evaporates from a soil surface. The salt crust corresponds to a saturated salt solution with a high osmotic suction and a corresponding reduction in the evaporation rate.

In coarse-grained soils there is another factor affecting actual evaporation referred to as the “canopy effect”. The canopy effect is usually associated with the vegetative cover on ground surface, however, desaturation of the soils near ground surface tends to produce another type of canopy effect (Tran, 2013). Most moisture movement occurs in the form of water vapour once the soil near ground surface dries to near residual water content conditions. At this point, water movement through evaporation is extremely slow.

Potential evaporation from a soil surface can be computed independent of the soil properties and a moisture flow model. The calculation of PE is relatively simple in comparison to the calculation for AE. The calculation of actual evaporative flux has proven to be a challenge in agriculture-related disciplines and geotechnical engineering. The calculation of actual evaporation requires that heat flow and moisture flow partial differential equations be combined and solved in either a coupled or uncoupled manner. The solution for AE is also undertaken in conjunction with the solution of the saturated-unsaturated moisture flow model for soil near ground surface.

Recent numerical computations of actual evaporation from sand columns show that it is possible to obtain reasonably reliable results provided the primary physical processes are taken into consideration (Fredlund *et al.*, 2011; Tran, 2013). In particular, it is necessary to include a “canopy-type” effect when the water content of a relatively coarse material (*e.g.*, sand) reduces to near residual water content conditions. The effect of salts in the pore-water and salt accumulation at the soil surface also affect the rate of evaporation from ground surface. The canopy effect and salts in the pore-water reduce actual evaporation from a soil surface by reducing the vapor pressure gradient at the soil

surface. Figure 4 shows measured evaporation rates from a sand column (Wilson, 1990) along with a comparison with numerical simulations undertaken by Fredlund *et al.* (2011) and Tran (2013). The numerical simulations were performed using several procedures available in the SVFlux - FlexPDEs software from SoilVision Systems Ltd.

4. Finite Element Numerical Modeling

The finite element numerical modeling procedure became available for usage as an engineering analysis tool after computers became available for rapidly solving large matrices of equations. Mainframe computers began to be used for numerical modeling in the late 1960s and in a matter of about one decade the computing power of these computers was available on desktop and laptop computers.

Seepage analyses were one of the first numerical solutions to find their way into geotechnical engineering practice. These problems had one degree of freedom at each node and many problems could be solved using head boundary conditions and zero flux boundary conditions (*i.e.*, impervious boundaries). Solutions involving moisture flux boundary condition problems would prove to be considerably more challenging because of the need to combine heat and moisture partial differential equation solutions in order to calculate actual evaporation from ground surface.

Original finite element solutions in the 1960s involved the manual design of a finite element mesh that covered a cross-section of the soil continuum. Each element needed to be numbered. This exercise was followed by the

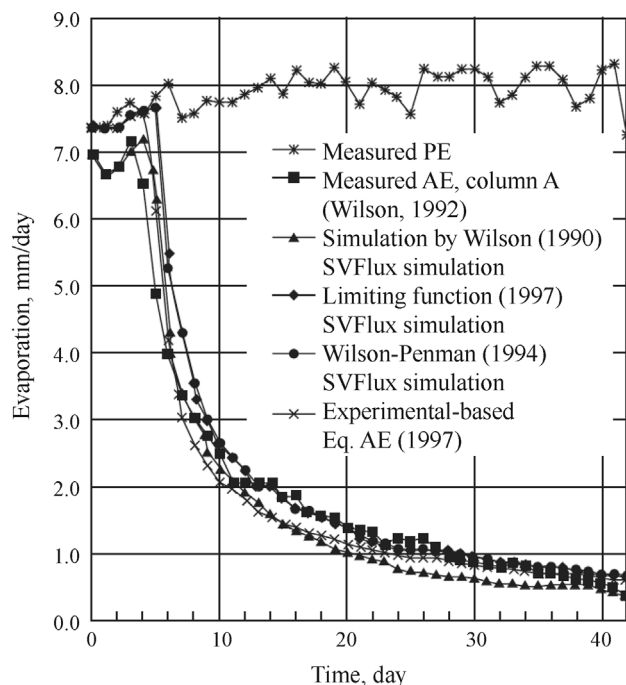


Figure 4 - Comparison of measured evaporation rates to predicted evaporation rates using coupled moisture movement models (Fredlund *et al.*, 2012).

numbering of the nodes around each element in a counter-clockwise manner. The time-consuming process of preparing a finite element mesh was later made easy through the use of the automatic design and numbering of elements and nodes comprising a finite element mesh.

The geotechnical engineer was aware that smaller elements needed to be used in regions where the hydraulic gradients were greater; however, there appeared to be no fixed rules with regard to the exact size of the small elements relative to the remainder of the finite element mesh. In other words, the design of the finite element mesh was largely a trial and error exercise. The relative sizes of elements throughout the soil continuum became of increased importance as attempts were made to solve nonlinear problems involving unsaturated soils. Unsaturated soils often had hydraulic conductivity values that could range over several orders of magnitude depending upon the suction in the soil.

The solution of unsaturated soils problems involved the solution of nonlinear partial differential seepage equations. Convergence to an accurate solution required that the finite element mesh be designed in a manner that met certain criteria for convergence. Research in the mathematics and computing science disciplines discovered that it was possible to design the finite element mesh in such a way that convergence was ensured (Oberkampf *et al.*, 1995; Reddy, 2006; Roache, 2009). The methodology for the design of the finite element mesh resulted in removing the tedious and challenging task of designing a finite element mesh from the geotechnical engineer to the mathematician. The finite element design technique became known as “automatic adaptive mesh refinement”.

The finite element mesh could be designed at the start of solving the problem and then changed, as necessary, as the solution moved towards convergence. For transient problems this meant that the finite element mesh could be changed from one time step to another time step, and also within each time step. The time steps could also be altered to assist in solving convergence issues. Finite element codes for solving geotechnical engineering problems can presently be categorized as: i.) manual mesh design codes, ii.) semi-automatic (or user-controlled) mesh design and iii.) automatic and adaptive mesh refinement, AMR, codes. Semi-automatic mesh generation codes have proven to be time-consuming and are quite often error-prone. Difficulties are most often encountered in situations where the mesh requires varying levels of change from one location to another location.

4.1. Automatic adaptive mesh refinement, AMR

The use of fully-automatic and adaptive mesh refinement codes are particularly useful in solving problems involving unsaturated soils. Two automatic adaptive mesh refinement, AMR, models are used in this paper to illustrate how converged solutions can be obtained with the assis-

tance of automatic adaptive mesh refinement. The automated adaptive mesh refinement can reduce modeling time as well as errors during the modeling process. The AMR solutions were performed using the SVFlux - FlexPDE software. The AMR results are discussed in the contexts of the solutions for a series of seepage problems published by Chapuis (2012) using a user-controlled mesh design.

4.2. Types of errors that occur in finite element analysis

The mathematical type of errors that can be introduced into a finite element solution of a differential equation can be attributed to three basic sources (Reddy, 2006):

1. Domain approximation errors which are due to an approximation of actual domain,
2. Quadrature and finite arithmetic errors which are errors associated with the numerical evaluation of integrals and the numerical computations on the computer,
3. Approximation errors which are due to the approximation of the solution through interpolation functions.

The above list does not give consideration to errors in programming, and differences between the numerical model and the characterization of other physical processes (Oberkampf *et al.*, 1995; Roache, 2009).

4.3. Convergence of the solution

The primary question that needs to be addressed when undertaking numerical modeling is, “How well does the model approximate the physical processes being studied and how well does the solution approach an accurate solution?” The answer to this question presumes that there is such a thing as an accurate solution to the problem. Studies involving interpolation theory can assist in understanding the meaning of an accurate solution to the problem.

4.4. Finite element adaptive mesh refinement, AMR

An adaptive mesh refinement, AMR, procedure measures the adequacy of the mesh during every iterative solution and refines the mesh wherever the estimated error is deemed to be too large. The mesh is refined and solution continues to iterate towards a solution until a user-defined “error tolerance” is achieved. The most common convergence criterion to use involves prescribing a total limit of the estimated error computed for the energy norm. Often this estimated energy norm error is specified to not exceed a specified percentage of the total norm of the solution. An adaptive mesh refinement procedure is used between iterations to reduce the estimated errors. This procedure is repeated until a solution has been obtained. The procedure is referred to as “adaptive” since the process depends on previous results at all stages.

There are various procedures for the refinement of the finite element solution. The refinement procedures can be broadly placed into two categories (Zienkiewicz *et al.*, 2005).

1. The h -refinement involves the ongoing usage of the same class of element while the size of the element is changed. In some locations the elements will be made larger while in other locations the elements will be made smaller. The intent is to provide the maximum efficiency in reaching the desired solution,
2. The p -refinement involves the ongoing usage of the same element size while there is a simple hierarchical increase in the order of the polynomial used in the definition of the elements.

It is sometimes useful to divide the above categories into sub-classes since the h -refinement can be applied in different ways. There are three typical h -refinement methods that can be described as follows:

1. Element subdivision can be used if the existing elements show too large an estimated error. The elements are simply divided into smaller elements while keeping the original element geometry boundaries intact,
2. Mesh regeneration (*i.e.*, re-meshing) can be performed on the basis of a given solution. In this case, a new element size is predicted in all the domains and a new mesh is generated,
3. r -refinement involves keeping the total number of nodes constant while adjusting the position of the nodes to obtain an optimal approximation. This method may be difficult to use in practice and is therefore not the preferred procedure.

The p -refinement subclasses can be described as follows:

1. The polynomial order of each element is increased uniformly throughout the entire domain,
2. The polynomial order is increased locally while using hierarchical refinement.

Occasionally it is possible to combine the h - and p -refinements and in this case the procedure is referred to as the hp -refinement. The element size and the polynomial degree, p are both altered when using the hp -refinement procedure.

5. Nonlinearity of the Unsaturated Material Properties

The nonlinearity of the partial differential equations that need to be solved for unsaturated soils is related to the nonlinear soil property functions that define the unsaturated soil properties. The nonlinearity in unsaturated soil properties result from significant changes in the degree of saturation of the soil as a particular physical process is simulated. The degree of saturation is primarily related to changes in soil suction.

Hydraulic properties such as the coefficient of permeability and water storage of a soil can be computed as a function of matric suction in the range of suctions from zero to about 1500 kPa. The relationship between soil suction and the amount of water in the soil (*e.g.*, volumetric water content and degree of saturation) has given rise to a series

of estimation procedures that can be used to approximate the unsaturated soil property functions.

The rate of actual evaporation from a soil, on the other hand, is related to the total suction of the soil (*i.e.*, matric suction plus osmotic suction).

6. Prominent Role of the Soil-Water Characteristic Curve, SWCC

The direct laboratory measurement of unsaturated soil property functions has proven to be too costly for most engineering projects. However, a variety of estimation procedures have been proposed and found to be of reasonable accuracy for most geotechnical engineering problems. The estimation procedures are based on the saturated soil properties along with information gleaned from the soil-water characteristic curve, SWCC. Various mathematical procedures have been applied to the SWCC (*e.g.*, various forms of integration along the SWCC, differentiation of the SWCC, and direct use of the SWCC equation), to obtain the desired unsaturated soil property functions.

It appears that the unsaturated soil property functions associated with every physical process common to geotechnical engineering are quite nonlinear in form. Each unsaturated soil property function has been found to be related to the soil-water characteristic curve, SWCC. There is a drying and a wetting SWCC and as a result the unsaturated soil property functions are hysteretic. The geotechnical engineer must either use the drying SWCC or an approximation of the wetting and drying SWCCs to determine a suitable approximation of unsaturated soil properties.

Figure 5 shows typical drying and wetting branches of the soil-water characteristic curve, SWCC, for a sand soil. Water storage in a soil is defined as the change in the volume of water in the soil for a particular change in soil suction. Consequently, the SWCC (*i.e.*, drying or wetting

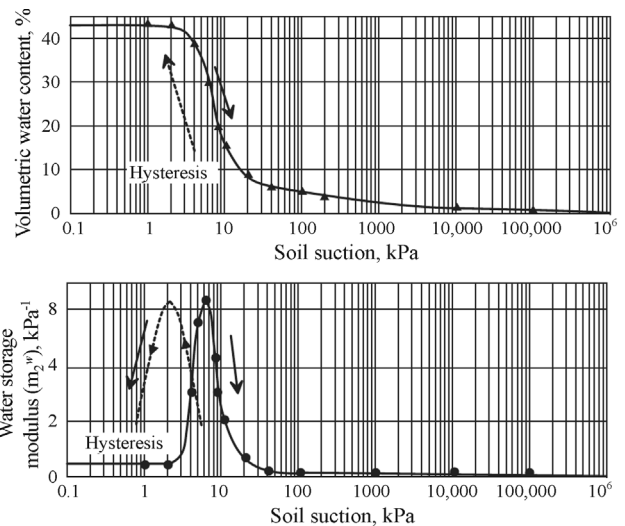


Figure 5 - Typical drying and wetting branches of the soil-water characteristic curve, SWCC, for a sand soil along with the corresponding water storage functions.

branches of volumetric water content vs. soil suction), can be differentiated to obtain the water storage function.

The hydraulic conductivity (or permeability) function can be estimated by starting with the saturated coefficient of permeability and integrating along the SWCC. Several integration procedures have been proposed and as a result there are several procedures for estimating the permeability function (Fredlund *et al.*, 2012).

Figure 6 shows a water permeability function estimated for the sand soil with the drying SWCC shown in Fig. 5. At high soil suctions (*i.e.*, approaching residual suction and beyond) the flow of liquid water become small and moisture movement is essentially through water vapor flow.

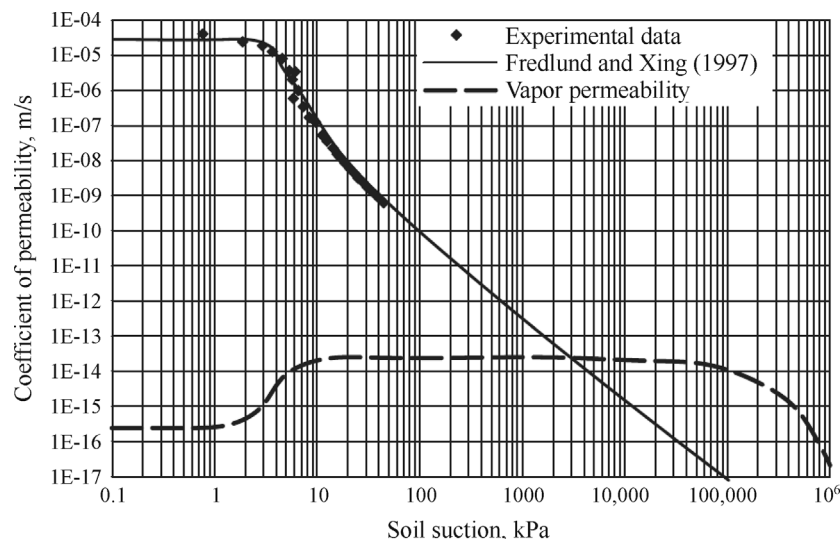


Figure 6 - Water permeability function estimated from the saturated coefficient of permeability and the soil-water characteristic curve.

7. Examples of Unsaturated Soils Problems

Partial differential equations can be written to describe a wide range of physical processes that may be encountered in geotechnical engineering practice. The partial differential equations are nonlinear in character when an unsaturated soil is involved. Water flow through an unsaturated soil is used to illustrate how nonlinear partial differential equations can be solved to answer question asked of practicing geotechnical engineers.

The partial differential equation for water flow through an unsaturated soil can be written as follows (Fredlund *et al.*, 2012).

$$k_w \frac{\partial^2 h_w}{\partial x^2} + \frac{\partial k_w}{\partial x} \frac{\partial h_w}{\partial x} + k_w \frac{\partial^2 h_w}{\partial y^2} + \frac{\partial k_w}{\partial y} \frac{\partial h_w}{\partial y} = m_w^2 \rho_w g \frac{\partial h_w}{\partial t} \quad (1)$$

where h_w = hydraulic head (m), k_w = coefficient of permeability (m/s), m_w^2 = water storage coefficient, (1/kPa), ρ_w = density of water, g = acceleration due to gravity, (m/s²), t = time (s) and x , y = x -coordinate and y -coordinate, respectively.

Equation 1 describes the physical process of water flow through a two-dimensional, unsaturated soil continuum. The equation applies for transient flow as well as steady state flow. The right-hand side of Eq. 1 becomes zero in the case of steady-state flow. The equation also applies for saturated soils. The difficulty in solving the partial differential equation arises when the soil is unsaturated because in this case there are three unknowns in this single equation; namely, h_w , k_w , and m_w^2 . It is necessary to make use of two unsaturated soil property functions to render the problem determinate. A converged solution is obtained through use of an iterative process involving estimated values and repeated solutions. It is the adaptive mesh refinement, AMR, technique that assists in obtaining convergence to the “correct” solution.

Partial differential equations can also be written for other physical processes. The partial differential equation for air flow has similarities to the water flow equation with the exception that the permeate fluid is compressible and the unit weight is small. The air phase properties required when solving transient problems consists of: i.) the air permeability function, ii.) the air storage function, and iii.) the air compressibility function. In addition, the properties of air are quite sensitive to changes in temperature and as a result it might be necessary to combine heat and air flow partial differential equations when solving some engineering problems.

The heat flow partial differential equation for saturated-unsaturated soils requires soil property functions for: i.) the thermal conductivity function, and ii.) the heat storage function. Water can exist in three possible phases and

as a result latent heat of fusion must also be taken into account when phase change is considered. The thermal properties are a function of the degree of saturation of the soil; however, many thermal conductivity problems can be solved through use of selected constants for the thermal properties. In other words, “coupling” between heat and moisture flow may not be required in some situations.

Stress analyses involving unsaturated soils also take on the form of partial differential equations for both saturated and unsaturated soils. There are two degrees of freedom at each node for a two-dimensional analysis. The stress analysis is often decoupled from the pore-fluid analysis; however, this may not be appropriate in some cases.

There are numerous other physical processes in saturated-unsaturated soil systems that can be described in the form of a partial differential equation. For example, chemicals move through the pore fluid system through the physical processes of advection, diffusion and adsorption. Advection flow can involve a coupling between pore fluid flow and chemical transport.

Unsaturated soils are generally encountered near ground surface in the region where several physical processes may overlap. Consequently, the combining of more than one process can be necessary to provide an adequate geotechnical engineering solution. Combining two or more physical processes can either be performed in a “coupled” or “uncoupled” manner. Modeling the combination of more than one physical process is presently an area of intensive research both in unsaturated soil mechanics as well as in other engineering disciplines.

7.1. Use of water seepage analysis for unsaturated soils

The flow of water through a homogeneous earth-fill dam is used as an example to illustrate the manner in which unsaturated soil properties are input in order to obtain a solution. Also illustrated is the type of output information that is typically shown in graphical form.

The soil-water characteristic curve, SWCC, must be known in order to estimate the unsaturated soil property functions (Fig. 7). The assumption is made that the soil does not undergo significant volume change as soil suction is increased. The solution of a steady-state type analysis only requires that the permeability function be known for the soil.

The permeability function is computed using an integration process along the SWCC, starting at the saturated coefficient of permeability (Fredlund *et al.*, 2012; Fig. 8). The solution of a transient type analysis requires that the water storage function for the soil also be known (*i.e.*, water storage vs. soil suction). The water storage function is obtained by differentiating the SWCC (Fig. 9).

The results of a transient analysis are shown by raising the water level along the upstream side of the reservoir of the dam from zero to 10 m. Figure 10a shows the automatically generated finite element mesh along with the

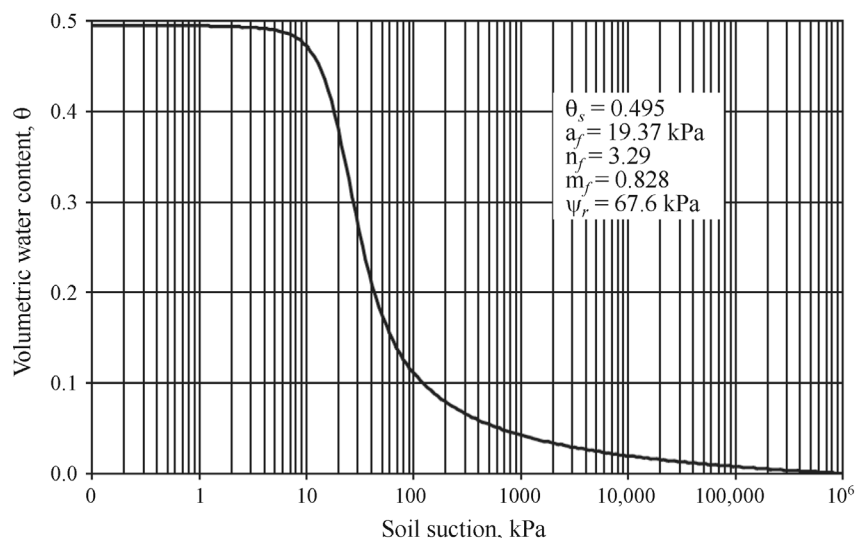


Figure 7 - Soil-water characteristic curve used to compute the unsaturated soil property functions for the example problem.

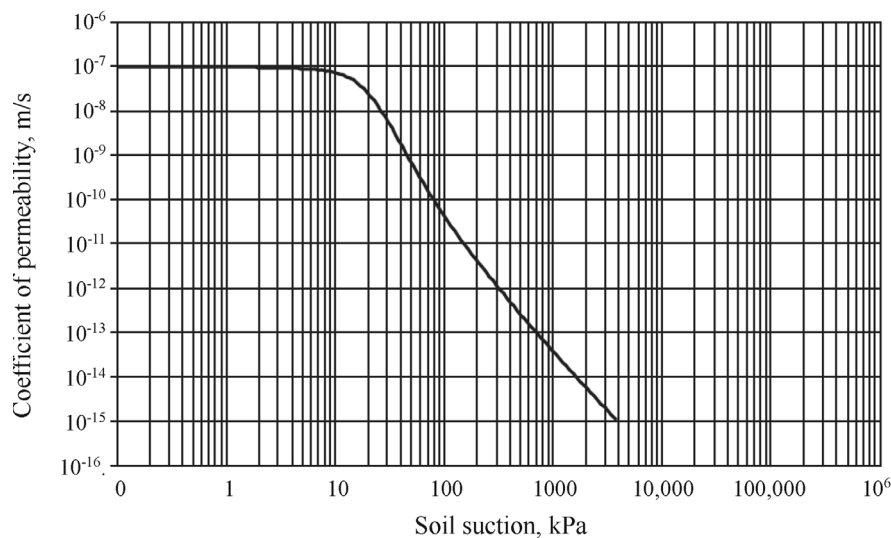


Figure 8 - Computed permeability function for the example problem.

head contours illustrating the dissipation of the head across the dam after 25 days. The finite element mesh is automatically refined in regions of higher hydraulic gradient to ensure convergence to an accurate solution.

Figure 10b shows the same hydraulic head contours along with velocity vectors. The closeness of the head contours and the congestion of the velocity vectors are indicative of the high degree of nonlinearity of the unsaturated soil properties. It can be observed that the water velocity vectors move across the phreatic line (*i.e.*, the line of zero pore-water pressure). Also noteworthy is the manner in which the head contours smoothly extend across the phreatic line to ground surface.

If the transient seepage analysis is extended for an elapsed time of 1500 days, the solution approaches that of a steady-state analysis where the water storage function is

not required as input information. Figure 11a shows the automatically generated finite element mesh along with the hydraulic head contours corresponding to an elapsed time of 1500 days. Figure 11b shows the hydraulic head contours along with velocity vectors. Once again there is some movement of water across the phreatic surface. In other words, the phreatic line does not constitute an uppermost flow line of seepage.

One further saturated-unsaturated seepage analysis is shown where the cross-section of a dam consisting of two materials, a shell with a low permeability core that does not extend to the surface of the dam. The results of a steady-state analysis of the dam are shown in Figs. 12a and 12b. Figure 12a shows the close spacing of the head contours across the core of the dam. Figure 12b shows the velocity vectors with water moving over-top of the low permeability

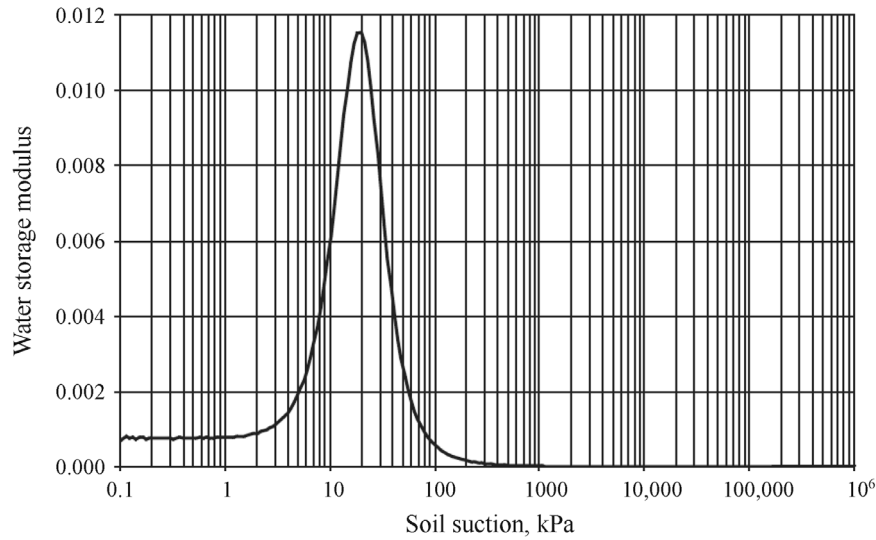


Figure 9 - Computed water storage function for the example problem.

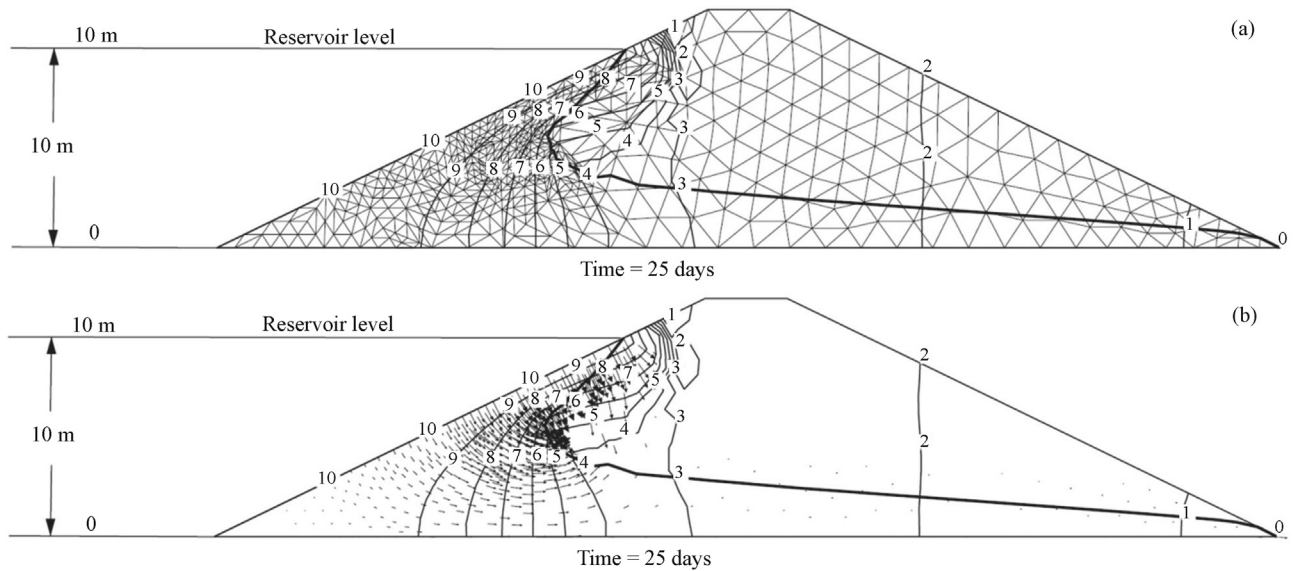


Figure 10 - a) Finite element mesh and hydraulic heads after the reservoir level was raised for 25 days. b) Velocity vectors and hydraulic heads after the reservoir level was raised for 25 days.

core through a syphon effect. The results indicate that it is easier for the water to flow upward through the unsaturated soil rather than to flow through the lower permeability core material. The siphon phenomenon was one of the early unsaturated soils that intrigued geotechnical engineers but is now readily explainable through use of saturated-unsaturated seepage analysis (Terzghi, 1943).

8. Use of Automatic Adaptive Mesh Refinement for Saturated Seepage Examples

Automatic adaptive mesh generation and refinement can also be used to advantage when modeling saturated-unsaturated seepage problems. Two example problems in-

volving seepage through a saturated soil were analyzed by Chapuis (2012). These examples are re-analyzed taking advantage of automatic mesh generation and refinement. The example problems were solved using automatic mesh refinement, AMR, programmed in the SVFlux - FlexPDE finite element code.

8.1. Cut-off example

The geometry of the model dam analyzed is shown in Fig. 13. The dam has a partial cut-off wall and the soil has a saturated coefficient of permeability of 8.13×10^{-3} m/day.

Chapuis (2012) obtained converged solutions using a uniform mesh with an element size of 0.5 m. Figure 13

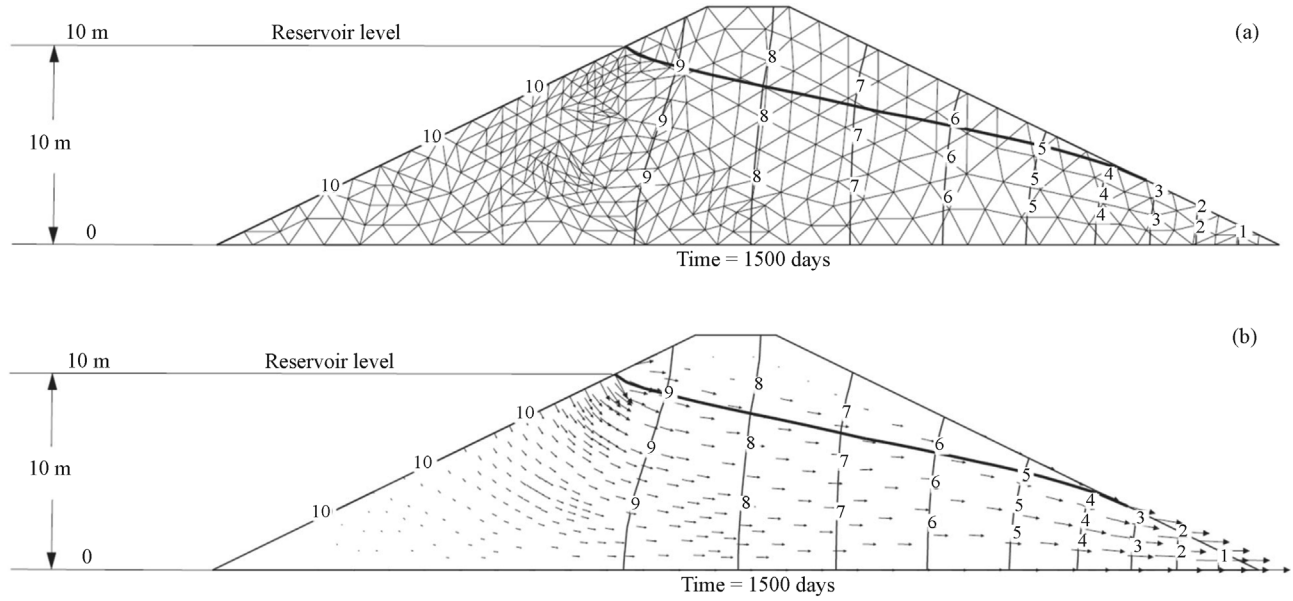


Figure 11 - a) Finite element mesh and hydraulic heads after the reservoir level was raised for 1500 days. b) Velocity vectors and hydraulic heads after the reservoir level was raised for 1500 days.

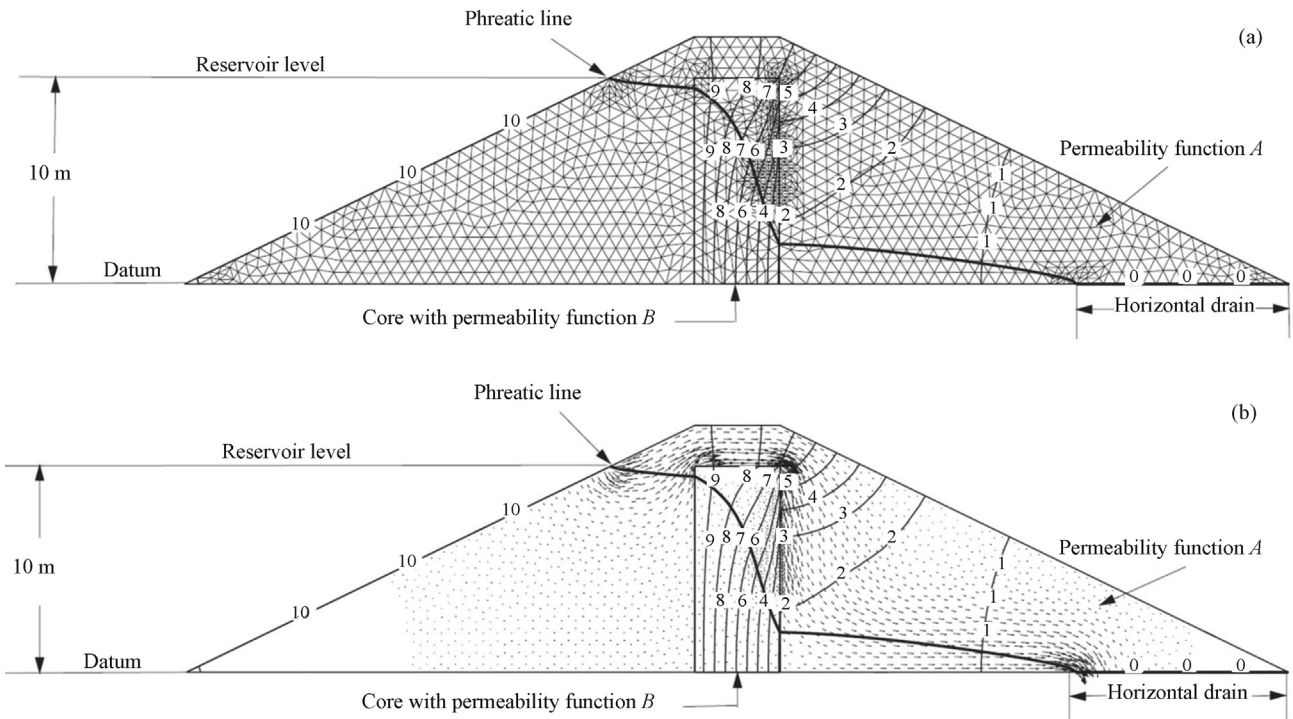


Figure 12 - a) Finite element mesh and hydraulic heads under steady state conditions. b) Velocity vectors and hydraulic heads under steady state conditions.

shows that the converged solution obtained when using the automatic adaptive mesh refinement has larger elements in most parts of the analyzed domain. The exception is around the cut-off wall where the finite element sizes are significantly smaller than the overall average element size. For the

mesh shown in Fig. 13, the calculated flow rate was $6.82 \times 10^{-7} \text{ m}^3/\text{s}$ using the automatic mesh refinement code of SVFlux - FlexPDE. A comparison of seepage rate results obtained when using manually-controlled mesh and the automatic-controlled adaptive mesh are shown in Fig. 14. The

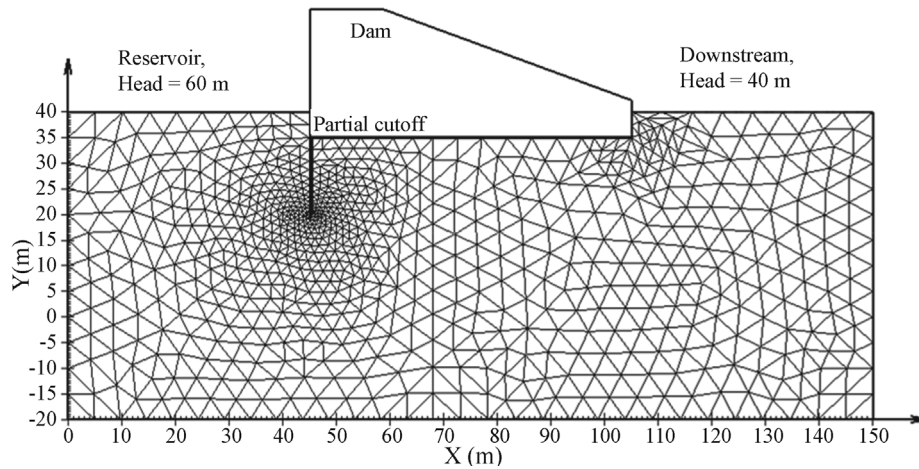


Figure 13 - Partial cut-off wall model geometry with mesh generated using the automatic adaptive mesh generator.

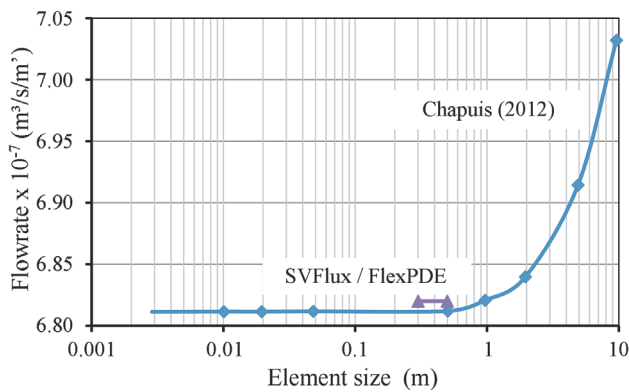


Figure 14 - Converged leakage flow-rate for the cut-off example.

automatic adaptive mesh refinement technique required considerably less computer time to obtain an accurate solution.

8.2. Confined aquifer example

The geometry of the second example problem is presented in Fig. 15. The pumping well is in a confined aquifer with a saturated coefficient of permeability of 4.0×10^{-4} m/s.

Figure 15 shows the model geometry with the finite element mesh generated using the adaptive generator.

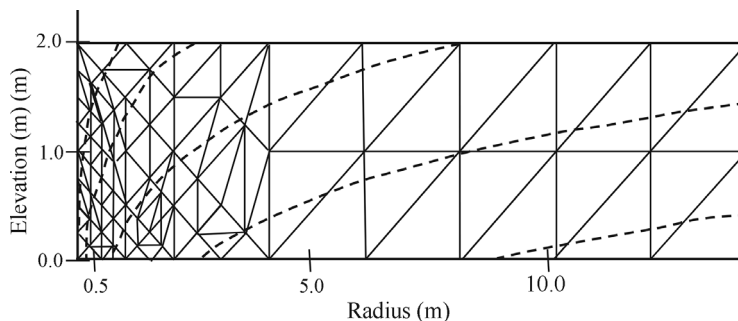


Figure 15 - Pumping well in a confined aquifer.

There are some triangular elements that have angles larger than 90 degrees and this is not the preferred shape for calculation purposes. The problem is axisymmetric with a radius of 600 m. The converged solution when using a uniform mesh occurred with an element size of 0.1 m (Chapuis, 2012). The same problem was solved using automatic mesh refinement in the SVFlux - FlexPDE code. The converged solution obtained using the automatic adaptive mesh has larger elements in most parts of the analyzed domain with the exception of the region around the pumping well where the element size is significantly smaller. For the mesh presented in Fig. 15 the computed flow-rate was 369.2 m³/day.

Figure 16 shows a comparison of the flow-rate obtained when the mesh was manually-controlled and when the mesh was automatically generated using adaptive mesh refinement. Figure 17 shows a comparison of the total head calculated at the well.

The results from the reported study indicate that the use of a finer mesh does not necessarily provide a more accurate solution. The primary concern is that the calculated result can be in error if the finite element mesh is not sufficiently refined. The results obtained when using automatic adaptive mesh refinement procedure can have larger elements over most parts of the domain while the accuracy of the solution remains preserved.

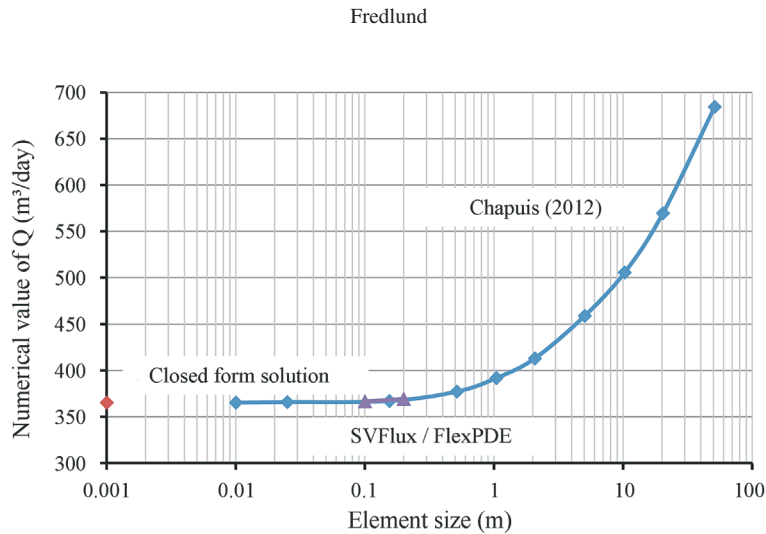


Figure 16 - Converged numerical flow-rates.

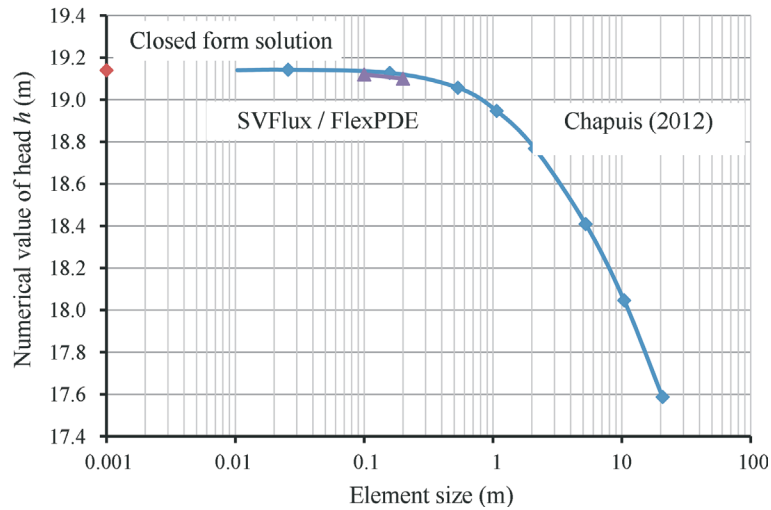


Figure 17 - Converged total heads at a radius, r equal to 20.15 m.

9. Conclusions

There are distinct differences in the manner in which saturated and unsaturated soils problems are solved. Unsaturated soils problems generally require the solution of a nonlinear partial differential equation because of the nonlinear nature of the soil properties. Automatic mesh refinement techniques developed in recent years for the solution of nonlinear partial differential equations are useful in ensuring that an accurate solution is obtained when unsaturated soils problems are analyzed.

One of the valuable assets of the automatic mesh refinement technique is the assurance that convergence requirements have been satisfied when solving unsaturated soils problems. The optimized mesh (*i.e.*, use of locally finer and coarser elements) means fewer equations need to be solved and at the same time the accuracy of the solution is assured. Finite element computer codes have proven to be a valuable tool for solving the nonlinear partial differen-

tial equations associated with unsaturated soils. Computers have also been useful in performing the calculations associated with the estimation of unsaturated soil property functions. Geotechnical engineers can now think in terms of simultaneously solving the saturated and unsaturated soil zones.

References

- Akin, J.E. (2005). Finite Element Analysis with Error Estimators: An Introduction to the FEM and Adaptive Error Analysis for Engineering Students. Elsevier Butterworth-Heinemann, Oxford, 512 p.
- Chapuis, R.P. (2012). Influence of element size in numerical studies of seepage: Small-scale details, Geotechnical News, 30(1): 32-35.
- Fredlund, D.G. & Rahardjo, H. (1993). Soil Mechanics for Unsaturated Soils. John Wiley & Sons, New York, 517 p.

- Fredlund, D.G.; Rahardjo, H. & Fredlund, M.D. (2012). *Unsaturated Soil Mechanics in Engineering Practice*. John Wiley & Sons, New York, 926 p.
- Fredlund, D.G. & Stianson, J. (2011). Utilization of weather station data for the assessment of ground surface moisture fluxes. *Proc. Fifth Asia-Pacific Conference on Unsaturated Soils*, Payatta, Thailand, pp. 1-18.
- Fredlund, M.D. (2012). *SVFlux User's Manual*. SoilVision Systems Ltd. Saskatoon, Canada, 112 p.
- Fredlund, M.D.; Zhang, J.M.; Tran, D. & Fredlund, D.G. (2011). Coupling heat and moisture flow for the computation of actual evaporation. *Proc. Canadian Geotechnical Conference and Fifth Pan-American Conference*, Toronto, Paper 1058.
- Oberkampf, W.L.; Blottner, F.G. & Aeschliman, D.P. (1995). Methodology for computational fluid dynamics code verification/validation. *Proc. AIAA Fluid Dynamics Conference*, San Diego, Paper 95-2226.
- Petrovic, I. & Fredlund, M.D. (2012). Benefits of adaptive mesh refinement. *Geotechnical News*, 30(4): 37-40.
- Reddy, J.N. (2006). *An Introduction to the Finite Element Method*. McGraw-Hill, Boston, 784 p.
- Roache P.J. (2009). *Fundamentals of Verification and Validation*. Hermosa Publishers, Socorro, 648 p.
- Terzaghi, K. (1943). *Theoretical Soil Mechanics*. Wiley, New York, 510 p.
- Tran, Dat Tien Quoc (2013). *Re-Visitation of Actual Evaporation Theories*. Ph.D. Thesis, University of Alberta, Edmonton, 420 p.
- Wilson, G.W. (1990). *Soil Evaporative Fluxes for Geotechnical Engineering Problems*. PhD Thesis, Department of Civil and Geological Engineering, University of Saskatchewan, 464 p.
- Wilson, G.W.; Fredlund, D.G. & Barbour, S.L. (1994). Coupled soil-atmospheric modeling for soil evaporation, *Canadian Geotechnical Journal*, 31(2):151-161.
- Zienkiewicz, O.C.; Taylor, R.L. & Zhu, J.Z. (2005) *The Finite Element Method: Its Basis and Fundamentals*. Elsevier Butterworth-Heinemann, Oxford, 752 p.

SOILS and ROCKS

An International Journal of Geotechnical and Geoenvironmental Engineering

Publication of

ABMS - Brazilian Association for Soil Mechanics and Geotechnical Engineering

SPG - Portuguese Geotechnical Society

Volume 39, N. 1, January-April 2015

Author index

Cordão Neto, M.P.	29	Lins, C.	19
Fredlund, D.G.	3, 81, 97	Mascarenha, M.M.A.	29
G.F.N. Gitirana Jr.,	81	Oh, W.T.	71
Gomes, I.	19	Rahardjo, H.	51
Guimarães, L.	19	Sheng, D.	41
Krisnanto, S.	51	Silva, M.T.M.G.	29
Leong, E.C.	51	Silva, N.	19
Lima, A.	19	Vanapalli, S.K.	71



COBA

GEOLOGY AND GEOTECHNICS

Hydrogeology • Engineering Geology • Rock Mechanics • Soil Mechanics • Foundations and Retaining Structures • Underground Works • Embankments and Slope Stability
Environmental Geotechnics • Geotechnical Mapping



- Water Resources Planning and Management
- Hydraulic Undertakings
- Electrical Power Generation and Transmission
- Water Supply Systems and Pluvial and Wastewater Systems
- Agriculture and Rural Development
- Road, Railway and Airway Infrastructures
- Environment
- Geotechnical Structures
- Cartography and Cadastre
- Safety Control and Work Rehabilitation
- Project Management and Construction Supervision



PORTUGAL

CENTER AND SOUTH REGION
Av. 5 de Outubro, 323
1649-011 LISBOA
Tel.: (351) 210125000, (351) 217925000
Fax: (351) 217970348
E-mail: coba@coba.pt
www.coba.pt

Av. Marquês de Tomar, 9, 6.
1050-152 LISBOA
Tel.: (351) 217925000
Fax: (351) 213537492

NORTH REGION

Rua Mouzinho de Albuquerque, 744, 1.
4450-203 MATOSINHOS
Tel.: (351) 229380421
Fax: (351) 229373648
E-mail: engico@engico.pt

ANGOLA

Praceta Farinha Leitão, edifício nº 27, 27-A - 2º Dto
Bairro do Maculusso, LUANDA
Tel./Fax: (244) 222338 513
Cell: (244) 923317541
E-mail: coba-angola@netcabo.co.ao

MOZAMBIQUE

Pestana Rovuma Hotel. Centro de Escritórios.
Rua da Sé nº114. Piso 3, MAPUTO
Tel./Fax: (258) 21 328 813
Cell: (258) 82 409 9605
E-mail: coba.mz@tdm.co.mz

ALGERIA

09, Rue des Frères Hocine
El Biar - 16606, ARGEL
Tel.: (213) 21 922802
Fax: (213) 21 922802
E-mail: coba.alger@gmail.com

BRAZIL

Rio de Janeiro
COBA Ltd. - Rua Bela 1128
São Cristóvão
20930-380 Rio de Janeiro RJ
Tel.: (55 21) 351 50 101
Fax: (55 21) 258 01 026

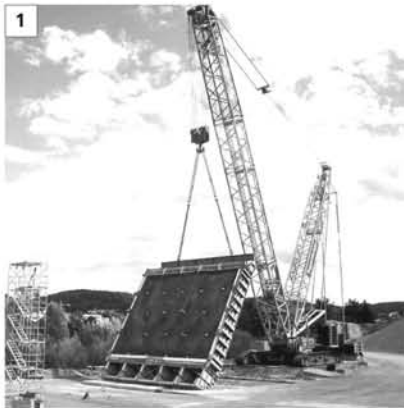
Fortaleza

Av. Senador Virgílio Távora 1701, Sala 403
Aldeota - Fortaleza CEP 60170 - 251
Tel.: (55 85) 3261 17 38
Fax: (55 85) 3261 50 83
E-mail: coba@esc-te.com.br

UNITED ARAB EMIRATES

Corniche Road - Corniche Tower - 5th Floor - 5B
P. O. Box 38360 ABU DHABI
Tel.: (971) 2 627 0088
Fax: (971) 2 627 0087

1. TECCO® SYSTEM³ teste em escala real, Suíça, outubro 2012
2. TECCO® SYSTEM³ instalação, B462, Alemanha
3. Ângulo máximo de inclinação de 85° durante o teste de campo



TECCO® SYSTEM³ – Seu talude estabilizado

... validado por teste em escala real com inclinação do talude de até 85°.

A malha de aço de alta resistência TECCO®, as placas de ancoragem e garras de conexão TECCO®, juntas, estabilizaram com sucesso 230 toneladas de cascalho com 85° de inclinação em um ensaio em escala real.

- moldura de teste com dimensões 10 x 12 x 1.2m
- espaçamento dos grapmos 2.5m x 2.5m, utilizando Gewi 28mm

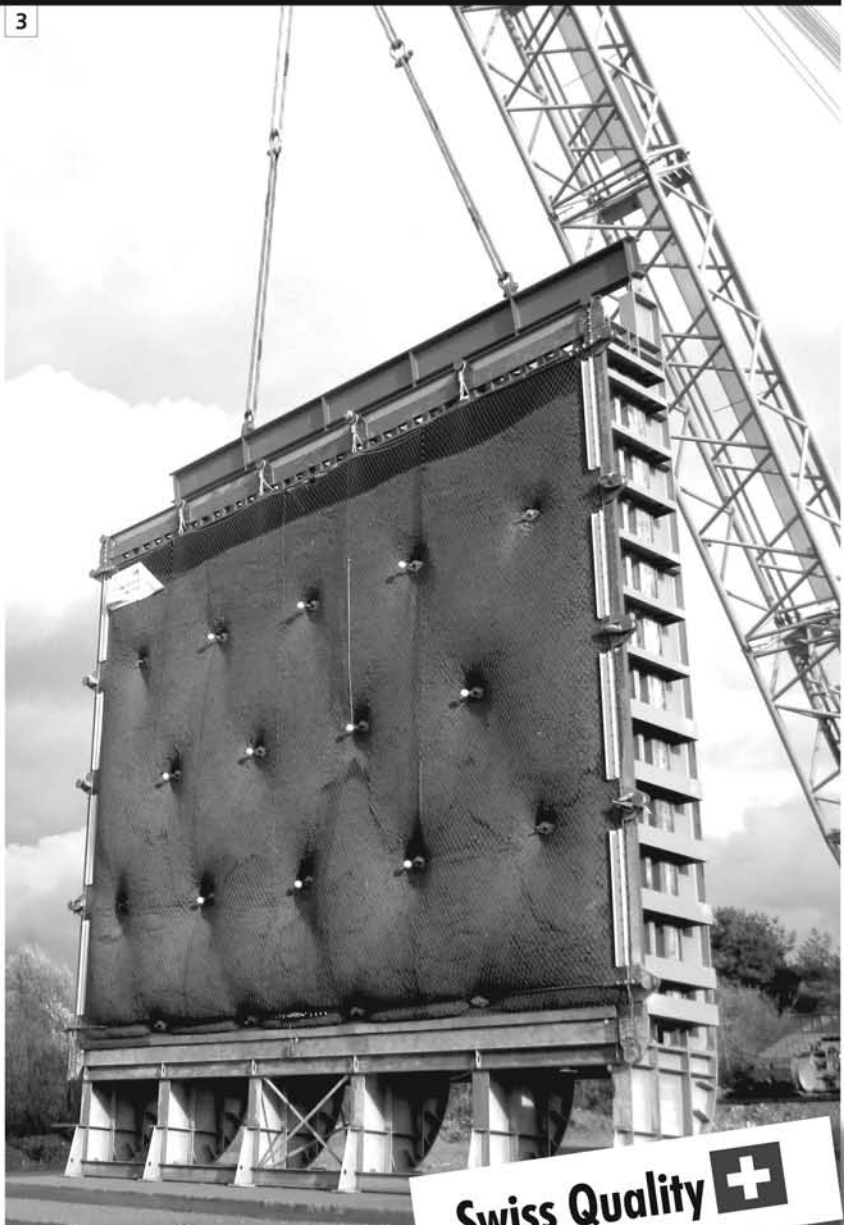
Para um estudo preliminar de solução de estabilização ou de riscos de desastres naturais nas obras em que você atua, entre em contato conosco através do e-mail info@geobrugg.com



Assista ou escaneie nosso filme com instalação TECCO® em www.geobrugg.com/slopes



Geobrugg AG, Geohazard Solutions
Rua Visconde de Pirajá, 82 sl.606
Ipanema - Rio de Janeiro • 22410-003
Fone: +55 21 3624.1449
Cel: +55 21 99979.1288
www.geobrugg.com



Swiss Quality 

SPECIALISTS IN GEOTECHNICAL IN-SITU TESTS AND INSTRUMENTATION

GEOTECHNICAL SERVICES (onshore and offshore)

■ IN-SITU TESTS

Seismic CPT
Cone Penetration Testing Undrained-CPTu (cordless system)
Vane Shear Testing (electrical apparatus)
Pressuremeter Testing (Menard)
Flat Dilatometer Test-DMT (Machetti)
Standard Penetration Test-SPT-T

■ INSTRUMENTATION

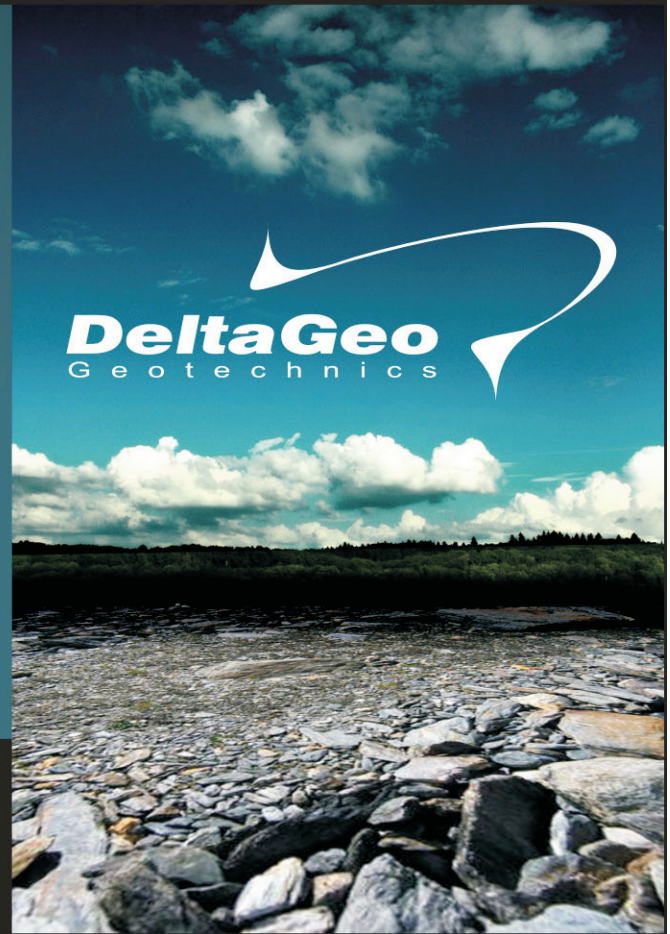
Instrumentation, installation and direct import
Routine Monitoring
Operation and Maintenance
Engineering analyses
Consultancy, design & geotechnical engineering services

■ SAMPLING

Soil sampling and monitoring
Groundwater sampling and monitoring
Field and laboratory testing

■ ENVIRONMENTAL

Environmental Services
Soil and groundwater sampling and monitoring
Field and laboratory testing

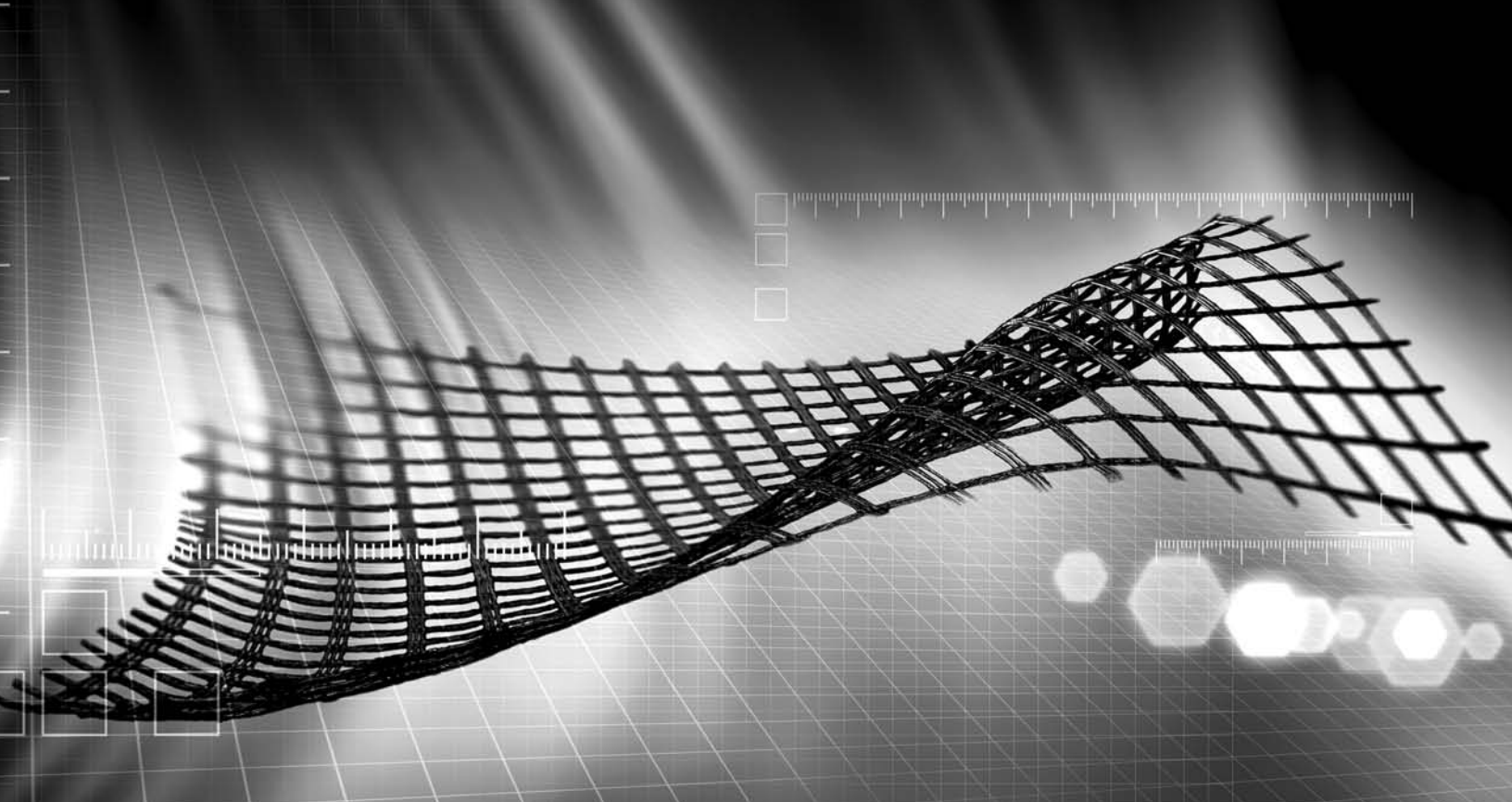


0800 979 3436

São Paulo: +55 11 8133 6030

Minas Gerais: +55 31 8563 2520 / 8619 6469

www.deltageo.com.br deltageo@deltageo.com.br



A strong, lasting connection.

With a history of over 150 years of pioneering in geosynthetics, we strive to create solutions for the most diverse engineering challenges.

Our business areas:



Earthworks and Foundations



Environmental Engineering



Roads and Pavements



Hydraulic Engineering

Talk to HUESKER Brasil:
www.HUESKER.com.br
HUESKER@HUESKER.com.br
+55 (12) 3903 9300

Follow HUESKER Brasil in social media:



HUESKER
Ideen. Ingenieure. Innovationen.



Reinforced Soil Walls Terramesh®



Gabions Retaining Walls

GREAT GEOTECHNICAL WORKS REQUIRES GREAT SOLUTIONS



Waterproofing of Reservoirs, Lakes and Channels



Dynamic rockfall barriers

BRASIL

Phone: 55 (11) 4525-5000
Fax: 55 (11) 4599-4275
info@br.maccaferri.com
www.maccaferri.com/br

PORTUGAL

Phone: (351) 218 968 282
Fax: (351) 218 968 078
info@es.maccaferri.com
www.maccaferri.com/es

MACCAFERRI

Engineering a better solution



Geotechnic and Rehabilitation

TEIXEIRA DUARTE
ENGENHARIA E CONSTRUÇÕES, S.A.

- **Head Office**
Lagoas Park – Edifício 2
2740-265 Porto Salvo - Portugal
Tel.: [+351] 217 912 300
Fax: [+351] 217 941 120/21/26
- **Algeria**
Parc Miremont – Rua A, Nº136 - Bouzareah
16000 Alger
Tel.: [+213] 219 362 83
Fax: [+213] 219 365 66
- **Spain**
Avenida Alberto Alcocer, nº24 – 7º C
28036 Madrid
Tel.: [+34] 915 550 903
Fax: [+34] 915 972 834
- **Angola**
Alameda Manuel Van Dunen 316/320 - A
Caixa Postal 2857 - Luanda
Tel.: [+34] 915 550 903
Fax: [+34] 915 972 834
- **Brazil**
Rua Iguatemi, nº488 – 14º - Conj. 1401
CEP 01451 - 010 - Itaim Bibi - São Paulo
Tel.: [+55] 112 144 5700
Fax: [+55] 112 144 5704
- **Mozambique**
Avenida Julyus Nyerere, 130 – R/C
Maputo
Tel.: [+258] 214 914 01
Fax: [+258] 214 914 00



GEOLOGY - GEOTECHNICS - SUPERVISION OF GEOTECHNICAL WORKS



EMBANKMENT DAMS - UNDERGROUND WORKS - RETAINING STRUCTURES



SPECIAL FOUNDATIONS - SOIL IMPROVEMENT - GEOMATERIALS

CENOR Consultores, S. A.

PORTUGAL | ANGOLA | ALGERIA | BRAZIL | CAPE VERDE | COLOMBIA
MALAWI | MOROCCO | MOZAMBIQUE | EAST TIMOR | VENEZUELA

Rua das Vigias, 2. Piso 1 | Parque das Nações | 1990-506 LISBOA. PORTUGAL
T. +351.218 437 300 | F. +351.218 437 301 | E. cenor@cenor.pt



MARCA
DE QUALIDADE
CONFORME O QUE SE ENcontra

ISO 9001
ISO 14001
OHSAS 18001
BUREAU VERITAS
Certificação





- > **Prospecção Geotécnica**
Site Investigation
- > **Consultoria Geotécnica**
Geotechnical Consultancy
- > **Obras Geotécnicas**
Ground Treatment-Construction Services
- > **Controlo e Observação**
Field Instrumentation Services and Monitoring Services
- > **Laboratório de Mecânica de Solos**
Soil and Rock Mechanics Laboratory

Certificada ISO 9001 por



Geocontrole



Parque Oriente, Bloco 4, EN10
2699-501 Bobadela LRS
Tel. 21 995 80 00
Fax. 21 995 80 01
e.mail: mail@geocontrole.pt
www.geocontrole.pt


Geocontrole
Geotecnia e Estruturas de Fundação SA

Instructions for Submission of Manuscripts

Category of the Papers

Soils and Rocks is the international scientific journal edited by the Brazilian Association for Soil Mechanics and Geotechnical Engineering (ABMS) and the Portuguese Geotechnical Society (SPG). The aim of the journal is to publish (in English) original research and technical works on all geotechnical branches.

According to its content the accepted paper is classified in one of the following categories: Article paper, Technical Note, Case Study or Discussion. An article paper is an extensive and conclusive dissertation about a geotechnical topic. A paper is considered as a technical note if it gives a short description of ongoing studies, comprising partial results and/or particular aspects of the investigation. A case study is a report of unusual problems found during the design, construction or the performance of geotechnical projects. A case study is also considered as the report of an unusual solution given to an ordinary problem. The discussions about published papers, case studies and technical notes are made in the Discussions Section.

When submitting a manuscript for review, the authors should indicate the category of the manuscript, and is also understood that they:

- assume full responsibility for the contents and accuracy of the information in the paper;
- assure that the paper has not been previously published, and is not being submitted to any other periodical for publication.

Manuscript Instructions

Manuscripts must be written in English. The text is to be typed in a word processor (preferably MS Word), **single column**, using ISO A4 page size, left, right, top, and bottom margins of 25 mm, Times New Roman 12 font, and line spacing of 1.5. All lines and pages should be numbered. The text should be written in the third person.

The first page of the manuscript must include the title of the paper followed by the names of the authors with the abbreviation of the most relevant academic title. The affiliation, address and e-mail must appear below each author's name. An abstract of 200 words follows after the author's names. A list with up to six keywords at the end of the abstract is required.

Although variations on the sequence and title of each section are possible, it is suggested that the text contains the following sections: Introduction, Material and Methods, Results, Discussions, Conclusions, Acknowledgements, References and List of Symbols. A brief description of each section is given next.

Introduction: This section should indicate the state of the art of the problem under evaluation, a description of the problem and the methods undertaken. The objective of the work should be clearly presented at the end of the section.

Materials and Methods: This section should include all information needed to the reproduction of the presented work by other researchers.

Results: In this section the data of the investigation should be presented in a clear and concise way. Figures and tables should not repeat the same information.

Discussion: The analyses of the results should be described in this section.

Conclusions: The content of this section should be based on the data and on the discussions presented.

Acknowledgements: If necessary, concise acknowledgements should be presented in this section.

References: References to other published sources must be made in the text by the last name(s) of the author(s), followed by the year of publication, similarly to one of the two possibilities below:

...while Silva and Pereira (1987) observed that resistance depended on soil density... or It was observed that resistance depended on soil density (Silva and Pereira, 1987).

In the case of three or more authors, the reduced format must be used, e.g.: Silva *et al.* (1982) or (Silva *et al.*, 1982). Two or more citations belonging to the same author(s) and published in the same year are to be distinguished with small letters, e.g.: (Silva, 1975a, b, c.). Standards must be cited in the text by the initials of the entity and the year of publication, e.g.: ABNT (1996), ASTM (2003).

Full references shall be listed alphabetically at the end of the text by the first author's last name. Several references belonging to the same author shall be cited chronologically. Some examples are listed next:

Papers: Bishop, A.W. & Blight, G.E. (1963). Some aspects of effective stress in saturated and unsaturated soils. *Geotechnique*, 13(2):177-197.

Books: Lambe, T.W & Whitman, R.V. (1979). *Soil Mechanics*, SI Version. John Wiley & Sons, New York, 553 p.

Book with editors: Sharma, H.D.; Dukes, M.T. & Olsen, D.M. (1990). Field measurements of dynamic moduli and Poisson's ratios of refuse and underlying soils at a landfill site. Landva, A. & Knowles, G.D. (eds), *Geotechnics of Waste Fills - Theory and Practice*, American Society for Testing and Materials - STP 1070, Philadelphia, pp. 57-70.

Proceedings (printed matter or CD-ROM): Jamiolkowski, M.; Ladd, C.C.; Germaine, J.T. & Lancellotta, R. (1985). New developments in field and laboratory testing of soils. Proc. 11th Int. Conf. on Soil Mech. and Found. Engn., ISSMFE, San Francisco, v. 1, pp. 57-153. (specify if CD ROM).

Thesis and dissertations: Lee, K.L. (1965). *Triaxial Compressive Strength of Saturated Sands Under Seismic Loading Conditions*. PhD Dissertation, Department of Civil Engineering, University of California, Berkeley, 521 p.

Standards: ASTM (2003). *Standard Test Method for Particle Size Analysis of Soils - D 422-63*. ASTM International, West Conshohocken, Pennsylvania, USA, 8 p.

Internet references: Soils and Rocks available at <http://www.abms.com.br> and downloaded on August 6th 2003.

On line first publications must also bring the digital object identifier (DOI) at the end.

Figures shall be either computer generated or drawn with India ink on tracing paper. Computer generated figures must be accompanied by the corresponding digital file (.tif, .jpg, .pcx, etc.). All figures (graphs, line drawings, photographs, etc.) shall be numbered consecutively and have a caption consisting of the figure number and a brief title or description of the figure. This number should be used when referring to the figure in text. Photographs should be black and white, sharp, high contrasted and printed on glossy paper.

Tables shall be numbered consecutively in Arabic and have a caption consisting of the table number and a brief title. This number should be used when referring to the table in the text. Units should be indicated in the first line of the table, below the title of each column. Acronyms should be avoided. When applicable, the units should come right below the corresponding column heading. Additional comments can be placed as footnotes.

Equations shall appear isolated in a single line of the text. Numbers identifying equations must be flushed with the right margin. International System (SI) units must be used. The definitions of the symbols used in the

equations must appear in the List of Symbols. It is recommended that the symbols used are in accordance with Lexicon in 8 Languages, ISSMFE (1981) and the ISRM List of Symbols.

The text of the submitted manuscript (including figures, tables and references) intended to be published as an article paper or a case history should not contain more than 30 pages, formatted according to the instructions mentioned above. Technical notes and discussions should have no more than 15 and 8 pages, respectively. Longer manuscripts may be exceptionally accepted if the authors provide proper explanation for the need of the required extra space in a cover letter.

Discussion

Discussions must be written in English. The first page of a discussion should contain:

The title of the paper under discussion;

Name of the author(s) of the discussion, followed by their position, affiliation, address and e-mail. The author(s) of the discussion should refer to himself (herself/themselves) as the reader(s) and to the author(s) of the paper as the author(s).

Figures, tables and equations should be numbered following the same sequence of the original paper. All instructions previously mentioned for the preparation of article papers, case studies and technical notes also apply to the preparation of discussions.

Editorial Review

Each paper will be evaluated by reviewers selected by the editors according to the subject of the paper. The authors will be informed about the results of the review process. If the paper is accepted, the authors will be required to submit a version of the revised manuscript with the suggested modifications. If the manuscript is rejected for publication, the authors will be informed about the reasons for rejection. In any situation comprising modification of the original text, classification of the manuscript in a category different from that proposed by the authors, or rejection, the authors can reply presenting their reasons for disagreeing with the reviewer comments.

Submission

The author(s) must upload a digital file of the manuscript to the Soils and Rocks website.

Follow Up

The online management system will provide a password to the corresponding author, which will enable him/her to follow the reviewing process of the submitted manuscript at the Soils and Rocks website.

Volume 39, N. 1, January-April 2016

Table of Contents

ARTICLES

<i>State Variables in Saturated-Unsaturated Soil Mechanics</i> D.G. Fredlund	3
<i>Numerical and Experimental Analysis of Horizontal Stress Changes and Soil Collapse During Chemical Dissolution in a Modified Oedometer Cell</i> C. Lins, N. Silva, L. Guimarães, A. Lima, I. Gomes	19
<i>Alternative Method for Analysing Hydromechanical Behaviour of Unsaturated Soils</i> M.M.A. Mascarenha, M.P. Cordão Neto, M.T.M.G. Silva	29
<i>Recent Developments and Limitations of the SFG Model</i> D. Sheng	41
<i>Effectiveness of Capillary Barrier and Vegetative Slope Covers in Maintaining Soil Suction</i> H. Rahardjo, S. Krisnanto, E.C. Leong	51
<i>Influence of Poisson's Ratio on the Stress vs. Settlement Behavior of Shallow Foundations in Unsaturated Fine-Grained Soils</i> W.T. Oh, S.K. Vanapalli	71
<i>Statistical Assessment of Hydraulic Properties of Unsaturated Soils</i> G.F.N. Gitirana Jr., D.G. Fredlund	81
<i>Numerical Modeling of Unsaturated Soils Problems</i> M.D. Fredlund	97